

Magmatic / Hydrothermal Interactions at Fast Spreading  
Mid-Ocean Ridges:  
Implications on the Dynamics of the Axial Melt Lens

Von der  
NATURWISSENSCHAFTLICHEN FAKULTÄT  
DER GOTTFRIED WILHELM LEIBNIZ UNIVERSITÄT HANNOVER

und der  
UNIVERSITE DE MONTPELLIER 2  
U.F.R. DES SCIENCES DE MONTPELLIER

Zur Erlangung des Grades  
**Doktor der Naturwissenschaften, Dr. rer. nat.**

**und**  
**Docteur en Geosciences**

genehmigte Dissertation  
von

MASTER mention Sciences de la Terre

**Lydéric France**

geboren am 16.06.1983 in St. Etienne, Frankreich

2010

**Referent:** Jürgen Koepke  
**Korreferent:** Benoit Ildéfonse  
**Tag der Promotion:** 08/12/2009



## **ERKLÄRUNG ZUR DISSERTATION**

Hierdurch erkläre ich, dass ich meine Dissertation mit dem Titel

Magmatic / Hydrothermal Interactions at fast spreading Mid-Ocean Ridges: Implications on the Dynamics of the axial Melt Lens

selbständig verfasst und die benutzten Hilfsmittel und Quellen sowie gegebenenfalls die zu Hilfeleistungen herangezogenen Institutionen vollständig angegeben habe.

Die Dissertation wurde nicht schon als Masterarbeit, Diplomarbeit oder andere Prüfungsarbeit verwendet.

Montpellier, den 16. 10.2009

Lydéric France

## **BEMERKUNG**

Die vorliegende Dissertation wurde in Englisch verfasst, die als mehrteilige Publikation veröffentlicht werden soll:

Teil 1. France, L., B. Ildefonse, and J. Koepke: Interactions between magma and hydrothermal system in Oman ophiolite and in IODP Hole 1256D: Fossilization of a dynamic melt lens at fast spreading ridges. *Geochem. Geophys. Geosyst.*, in press.

Teil 2. France, L., J. Koepke, B. Ildefonse, S. B. Cichy, and F. Deschamps: Hydrous partial melting in the sheeted dike complex at fast spreading ridges: Experiments and nature. Submitted to "Contributions to Mineralogy and Petrology".

Teil 3. France, L., B. Ildefonse, J. Koepke, C. J. MacLeod, and M. Godard: Melting the hydrothermally altered sheeted dike complex: an experimental / trace elements study. To be submitted to "Geology"



Il faut toujours penser par soi-même. Ne rien apprendre par cœur, mais tout redécouvrir et, en tous cas, ne rien accepter qui ne soit prouvé. Ne rien négliger de ce qui est concevable ou imaginable.

A. Einstein

Si vous trouvez que l'éducation coûte cher, essayez l'ignorance!

Abraham Lincoln



# Abstract

The transition between the small melt lens observed on top of fast spreading ridge magma chambers and the overlying sheeted dike complex marks the interface between magma and the hydrothermal convective system. The ~50 meters thick melt lens is believed to feed at least part of the upper and lower crust. Constraining processes occurring within the melt lens and its interactions with the surrounding rocks, fluids, and melts is therefore crucial for our understanding of fast spreading ridge accretion processes, and of oceanic crust composition.

This PhD work is based on field, petrographic, and geochemical observations of rocks originated at the base of the sheeted dike complex, in the Oman ophiolite and at IODP Site 1256 of the equatorial Pacific, coupled with an experimental study. It provides new constraints on processes that occur at the magma / hydrothermal system transition in oceanic crust formed at fast spreading ridges.

In the Oman Ophiolite, and in the Cocos plate (IODP Hole 1256D), the base of the sheeted dike complex is truncated by intrusive isotropic gabbros, and therefore reheated and recrystallized to the "granoblastic dikes" under temperatures up to 1030°C. Granoblastic dikes are former dikes now composed of microgabbro and microgabbro-norite that display well equilibrated, fine-grained metamorphic textures. Xenoliths of granoblastic microgabbros and microgabbro-norites derived from the granoblastic dikes are commonly observed in the horizon of isotropic gabbro that underlies the sheeted dike complex. Some xenoliths of gabbro are also observed. The isotropic gabbro horizon is about 100 meters thick, highly heterogeneous and composed of varytextured gabbros. The isotropic gabbros locally contain granoblastic patches attesting of strong assimilation of the base of the sheeted dike complex. All the observed features can be explained by upward migrations of the melt lens. The occurrence of several assimilation features (xenoliths and granoblastic patches) in the isotropic gabbro horizon supports the hypothesis that this horizon represents the fossilization of the upper melt lens when its volume decrease and / or when moving off axis. Several cycles of upward and downward migrations of the melt lens roof can occur successively, and only the highest level can be recorded. Identified vertical migrations of the melt lens are associated to timescales  $\leq 10,000$  years.

The experimental study was designed to simulate experimentally the effect of partial melting of hydrothermally altered sheeted dikes. The results show that melting starts at 850°C, largely below the maximum equilibrium temperatures recorded in the granoblastic



dikes. The peculiar composition of the residual experimental assemblage (e.g., low Al and Ti contents in clinopyroxenes), matches the composition of granoblastic dikes and related xenoliths, implying that the granoblastic lithologies can be regarded as residues after an hydrous partial melting event.

Oceanic plagiogranites are commonly observed close the base of the sheeted dike complex, locally intruding the granoblastic dikes. The composition of the experimental melts generated at temperatures below 1000°C, is similar to that of typical natural oceanic plagiogranites from this horizon, implying that these are formed by anatexis of hydrous partial melting of granoblastic dikes. The trace element composition of experimental melts has been determined and confirms the anatectic origin of the natural oceanic plagiogranites and the residual origin of granoblastic dikes and related xenoliths. The melt formed during the hydrous partial melting of previously hydrothermally altered sheeted dikes represents the main contaminant for primitive MORBs at fast spreading ridges, and the precise evaluation of its composition by experimental means is very valuable for future detailed geochemical modeling on the variety of MORB compositions.

The upper axial melt lens at fast spreading mid-ocean ridges is herein described as a dynamic system that can migrate vertically, and which fossilizes when moving off-axis. On the first order, the melt supply from the underlying main magma chamber, the occurrence of eruptions, and the vigor of the hydrothermal convecting system regulate its position. Vertical migrations of its top imply a contamination of the melt lens by silicic hydrous melts formed during partial melting and by hydrothermal fluids recycled through assimilation.

**Key-words:** fast-spreading ridges; melt-lens; base of the sheeted-dike complex.

# Zusammenfassung

An schnell-spreizenden ozeanischen Rückensystemen befindet sich zwischen den Basalten der Ober- und den Gabbros der Unterkruste am Übergang zwischen dem hydrothermalen und magmatischen konvektiven System, die etwa 50 m dicke "axiale Schmelzlinse". Nach gängigen Vorstellungen werden von dieser nur etwa 50 Meter mächtigen Kammer, die nahezu vollständig mit MORB-Schmelze gefüllt ist, große Anteile der ozeanischen Kruste aufgebaut. Das Verstehen der magmatischen Prozesse in der Schmelzlinse, sowie ihre Wechselwirkung mit den auflagernden Sheeted Dikes und mit vom Meerwasser abzuleitenden Fluiden ist wesentlich für das Verständnis der Geodynamik der Krustenakkretion an schnell-spreizenden ozeanischen Rückensystemen und ist auch Ziel der vorliegenden Dissertation. Sie basiert auf geländebezogenen, petrographischen und geochemischen Untersuchungen an Gesteinen vom Gabbro / Dike - Übergang vom Oman-Ophiolith und von der IODP-Bohrung 1256 vom ostpazifischen Rücken, in Verbindung mit einer experimentellen Studie.

In beiden Vorkommen wird die Basis der Sheeted Dikes durch Intrusionen von isotropen Gabbros abgeschnitten, die auch eine Rekristallisation der Basalte zu den "Granoblastischen Dikes" bewirkte (mikogranulare Gabbros und Gabbronorite; oft mit granoblastischen, metamorphen Gefügen), wobei Gleichgewichtstemperaturen bis zu 1030°C ermittelt wurden. Xenolithe, die genetisch von den Granoblastischen Dikes abgeleitet werden können, sind in dem unter den Sheeted Dikes liegenden Horizont der isotropen Gabbros weit verbreitet. Diese Gabbros sind lithologisch äußerst heterogen zusammengesetzt und weisen zahlreiche Domänen von ehemaligen Granoblastischen Dikes auf, die darauf hindeuten, dass die Assimilation von vormals hydrothermal alterierten Sheeted Dikes durch MORB der Schmelzlinse ein signifikanter und weit verbreiteter Prozess ist.

Alle Natur-Beobachtungen zusammengenommen implizieren, dass die axiale Schmelzlinse eine sehr dynamische Struktur ist, die vertikal zu wandern vermag. Die weite Verbreitung von Assimilationsstrukturen im isotropen Gabbro (Xenolithe und granoblastische Domänen), unterstützen ein Modell, dass der isotrope Gabbro der fossilisierten Schmelzlinse entspricht, nach einer Phase der Entleerung und Bewegung in eine "off-axis" - Position. Dabei sind mehrere Zyklen von Aufwärts- und Abwärtsbewegungen denkbar, wobei nur der "Hochstand" später als petrologischer Record aufgefunden werden kann. Die Zyklizität dieser Prozesse kann auf  $\leq 10,000$  Jahre abgeschätzt werden.

Eine experimentelle Studie wurde durchgeführt, um den Prozess des Aufschmelzens von hydrothermal alterniertem Dike-Material am Top der axialen Schmelzlinse experimentell zu simulieren (Druck: 100 MPa). Erste Schmelze tritt bei Temperaturen von 850°C auf, also deutlich unter den maximalen Äquilibration-Temperaturen für die Granoblastischen Dikes. Der Vergleich der Zusammensetzungen der residualen experimentellen Mineralvergesellschaftungen (insbesondere die niedrigen Al- und Ti-Gehalte im Klinopyroxen) mit denen der entsprechenden granoblastischen Dikes und entsprechender Xenolithe, weist darauf hin, dass die granoblastischen Lithologien insgesamt als residuale Paragenesen nach einem partiellen Aufschmelzvorgang angesehen werden können. Die gute Übereinstimmung der Zusammensetzung der experimentellen Schmelzen mit der von typischen ozeanischen Plagiograniten, die in den natürlichen Vorkommen an der Basis des Sheeted Dike Komplexes beobachtet werden können und lokal die Granoblastischen Dikes intrudieren, macht ein Modell sehr wahrscheinlich, dass die ozeanischen Plagiograniten als Aufschmelzprodukte der hydrothermal alterierten Dikes angesehen werden können. Charakteristische Spurenelementmuster für die experimentellen Schmelzen, die erstmalig mittels In-situ-Methode ermittelt wurden, unterstützen das Modell der anatektischen Plagiogranite und residualen Granoblastische Lithologien.

Die plagiogranitischen Schmelze, die beim Aufwärtswandern der axialen Schmelzlinse entstehen, wurde als Haupt-Kontaminator für MORB-Basalte von schnell-spreizenden Rücken identifiziert; die experimentelle Evaluierung ihrer Haupt- und Spurenelement- Zusammensetzung kann als wichtige Referenz für zukünftige geochemische Modellrechnungen zur MORB-Kontamination angesehen werden.

Die vorliegende Studie charakterisiert die axiale Schmelzlinse als ein sehr dynamisches System, das sich aufwärts- und abwärtsgerichtet bewegen kann, und fossilisiert, wenn es von der "on-axis"- in die "off-axis" - Position wandert. Die vertikale Position wird durch Schmelzversorgung durch die darunter liegende axiale Magmenkammer, die Häufigkeit von Füllung und Entleerung (Eruptionen), und durch die Aktivität des hydrothermalen Kühlungssystems kontrolliert. Die vertikale Migrationen impliziert eine Kontamination der primitiven MORB-Schmelzen an schnell-spreizenden Rücken, sowohl durch anatektische, wasserhaltige SiO<sub>2</sub>-reiche Schmelzen, als auch durch Assimilation / Recycling der residualen granoblastischen Lithologien incl. der durch Interaktion mit meerwasser-bezogenen Fluide hervorgerufenen integrativen Alterationsgeochemie.

**Schlagwörter:** Schnell-spreizende ozeanische Spreizungszonen; Schmelz-Linse; Basis des Sheeted-Dike-Komplexes.

# Résumé

La transition entre la petite lentille magmatique observée au sommet des chambres magmatiques des dorsales à expansion rapide, et le complexe filonien situé au dessus marque l'interface entre le magma et le système hydrothermal. Au moins une partie de la croûte océanique supérieure et inférieure trouve son origine dans cette lentille magmatique épaisse d'environ 50 mètres. La détermination des processus se produisant au sein de cette lentille magmatique, et ses interactions avec les roches, fluides et magmas l'entourant est donc crucial pour comprendre les processus d'accrétion au niveau des dorsales rapides, et la composition de la croûte océanique.

Ce travail de thèse est basé sur des observations de terrain, sur une étude pétrographique et géochimique des roches formées à la base du complexe filonien dans l'ophiolite d'Oman et au niveau du Site IODP 1256 situé dans le Pacifique équatorial, ainsi que sur une étude expérimentale. De nouvelles contraintes sont apportées sur les processus se produisant à la transition magma / système hydrothermal dans la croûte océanique formée au niveau des dorsales à expansion rapide.

Dans l'ophiolite d'Oman et au niveau de la plaque Cocos (puits IODP 1256D), l'intrusion de gabbros isotropes dans la base du complexe filonien a provoqué son réchauffement et sa recristallisation en « dikes granoblastiques » jusqu'à des températures de 1030°C. Les dikes granoblastiques sont des anciens dikes maintenant composés de microgabbro et de microgabbronorites qui montrent des textures métamorphiques équi-granulaires à grain fins. Des xénolites de microgabbro et de microgabbronorite à texture granoblastique dérivées des dikes granoblastiques sont souvent observées dans le niveau de gabbros isotropes qui est présent à la base du complexe filonien. Des xénolites de gabbros sont aussi observées. Le niveau de gabbros isotropes mesure environ 100 mètres d'épaisseur, il est très hétérogène et composé de gabbros à texture variable. Les gabbros isotropes contiennent localement des patches granoblastiques attestant d'une assimilation importante de la base du complexe filonien au sein de la lentille magmatique. Toutes les caractéristiques observées peuvent être expliquées par des migrations verticales vers le haut de la lentille magmatique. Les nombreuses évidences d'assimilation (xénolites et patches granoblastiques) dans le niveau des gabbros isotropes appuient l'hypothèse que ce niveau représente la fossilisation de la lentille magmatique supérieure lorsque son volume décroît et / ou lorsqu'elle se déplace hors axe. De nombreux cycles de migrations vers le haut et vers le bas du sommet de la lentille magmatiques peuvent se produire successivement, mais seul le plus

haut niveau atteint sera enregistré. Les migrations verticales identifiées sont associées à des échelles de temps  $\leq 10\,000$  ans.

L'étude expérimentale a consisté à simuler expérimentalement l'effet de la fusion partielle du complexe filonien préalablement hydrothermalisé. Les résultats montrent que la fusion commence à 850°C, une température nettement plus basse que les plus hautes enregistrées dans les dikes granoblastiques. La composition particulière de l'assemblage résiduel expérimental (e.g., les faibles teneurs en Al et en Ti des clinopyroxènes), est similaire à la composition des dikes et xénolites granoblastiques et atteste de leur origine résiduelle.

Des plagiogranites océaniques sont couramment observés à proximité de la base du complexe filonien et intrudent localement les dikes granoblastiques. La composition des liquides expérimentaux formés à des températures inférieures à 1000°C est similaire à celle de ces plagiogranites océaniques, ceci implique par conséquent une origine anatectique pour ces plagiogranites océaniques. La composition en éléments trace des liquides expérimentaux a été déterminée et confirme l'origine anatectique de ces plagiogranites océaniques naturels et l'origine résiduelle des dikes et xénolites granoblastiques. Le liquide formé lors de la fusion partielle hydratée de complexe filonien préalablement hydrothermalisé représente le principal contaminant pour les MORBs primitifs émis au niveau des dorsales rapides. La détermination précise de sa composition est une référence très utile pour les futures études géochimiques détaillées des MORBs.

La lentille magmatique supérieure observée au niveau des dorsales médio-océaniques à expansion rapide est ici décrite comme un système dynamique qui peut migrer verticalement, et qui est fossilisée lorsqu'elle se déplace hors axe. Au premier ordre, l'apport magmatique depuis la chambre magmatique principale située en dessous, l'occurrence d'éruptions, et la vigueur de l'activité hydrothermale régulent sa position. Les migrations verticales de son sommet impliquent la contamination de la lentille magmatique par les liquides hydratés et riches en silice formés lors de la fusion partielle, et par des fluides hydrothermaux recyclés lors de l'assimilation.

**Mots-clés:** dorsale océanique à expansion rapide; lentille magmatique; base du complexe filonien





# Table of contents

Introduction .....	11
Chapter I. Magmatic accretion at fast spreading ridges .....	17
I.1. Architecture of oceanic crust at fast spreading ridges.....	19
I.1.a. General structure .....	19
I.1.b. Magma chamber models .....	21
I.1.c. Ridge segmentation .....	24
I.2. The upper melt lens, a key horizon .....	24
I.2.a. Structure .....	24
I.2.b. Melt storage, composition and delivery .....	28
I.3. The melt lens and the root zone of the sheeted dike complex: relations and evolution	32
I.3.a. General presentation.....	32
I.3.b. Interaction processes .....	32
I.3.c. Geological settings .....	34
I.3.d. Lithostratigraphy .....	35
I.3.e. Conceptual models and implications.....	36
I.4. Key questions and hypotheses to be tested .....	41
Chapter II. “Magmatic / hydrothermal transition in IODP Hole 1256D” .....	43
II.1. Geological context.....	45
II.2. Petrology of the granoblastic microgabbro and gabbros.....	47
II.3. Mineral major element compositions .....	58
Chapter III. “Magmatic / hydrothermal interactions in the Oman ophiolite” .....	65
III.1. Visited areas .....	67
III.2. Lithostratigraphy .....	68
III.3. Interactions between magma and hydrothermal system in Oman ophiolite and in	
IODP Hole 1256D: fossilization of a dynamic melt lens at fast spreading ridges.....	76
III.3.a. Abstract .....	76
III.3.b. Introduction .....	77
III.3.c. Background .....	78
III.3.d. Field observations .....	80
III.3.d.1. The Wadi Gideah area.....	81
III.3.d.2. The Al Ahmadi Hills .....	87
III.3.e. IODP Hole 1256D .....	90
III.3.f. Mineral compositions and thermometry .....	93
III.3.f.1. Root zone lithologies and protodikes .....	93
III.3.f.2. Isotropic/foliated gabbros transition in Wadi Gideah .....	96
III.3.f.3. Foliated gabbros .....	96
III.3.f.4. Thermometry .....	96
III.3.g. Discussion .....	98
III.3.g.1. A dynamic melt lens.....	98
III.3.g.2. Stopping, assimilation and coarse-grained gabbros .....	101
III.3.g.3. Comparison with IODP Hole 1256D .....	103
III.3.g.4. A general model .....	104
III.3.g.5. Time scale constraints .....	106
III.3.h. Conclusions .....	109
III.4. Aswad area: further constrains on the model .....	111
III.5. Reheating of the Aswad sheeted dikes .....	117



III.6.	Conclusion.....	123
Chapter IV.	“Melting the hydrothermally altered sheeted dike complex: experimental study”	125
IV.1.	Introduction.....	126
IV.2.	Detailed experimental techniques.....	127
IV.2.a.	Sample preparation.....	127
IV.2.b.	Cold-seal pressure vessel.....	128
IV.2.c.	Internally heated pressure vessel.....	130
IV.3.	Hydrous partial melting in the sheeted dike complex at fast spreading ridges: Experiments and nature.....	132
IV.3.a.	Abstract.....	132
IV.3.b.	Introduction.....	133
IV.3.c.	Natural occurrences and previous experiments on hydrous partial melting of mafic rocks.....	134
IV.3.d.	Experimental and analytical techniques.....	136
IV.3.d.1.	Starting material.....	136
IV.3.d.2.	Experimental method.....	138
IV.3.d.3.	Analytical method.....	140
IV.3.e.	Experimental results.....	140
IV.3.e.1.	Attainment of equilibrium.....	140
IV.3.e.2.	Phase relations in the partial molten system.....	143
IV.3.e.3.	Prehnite break-down reaction.....	145
IV.3.e.4.	Phase compositions in the partial molten system.....	146
IV.3.f.	Discussion.....	149
IV.3.f.1.	Melt evolution: Origin of oceanic plagiogranites at the base of the Sheeted Dikes.....	149
IV.3.f.2.	Evolution of the residual minerals: formation of "granoblastic dikes" ..	151
IV.3.f.3.	MORB contamination at the base of the sheeted dikes.....	155
IV.3.g.	Conclusion.....	157
IV.4.	Mineral recrystallization during experiments: a preliminary study.....	157
IV.5.	Melting the hydrothermally altered sheeted dike complex: an experimental / trace elements study.....	162
IV.5.a.	Abstract.....	162
IV.5.b.	Introduction.....	163
IV.5.c.	Experimental and analytical techniques.....	165
IV.5.d.	Trace element contents.....	165
IV.5.e.	Discussion.....	167
IV.5.f.	DR 1: Analytical methods:.....	171
IV.5.g.	DR 2: Major element compositions.....	172
IV.5.h.	DR 3: Trace element compositions.....	172
IV.6.	Conclusion.....	172
Conclusion.....		175
References.....		181

# **Introduction**



## Introduction

Oceanic crust represents about two thirds of the Earth surface, and nearly half of it formed at fast-spreading mid-ocean ridges. The structure and composition of oceanic crust are constrained by off shore geophysical studies, and in-situ geological mapping and sampling (dredging and drilling), and ophiolitic complexes studies. Geophysical studies of fast-spreading ridges, primarily the East Pacific Rise (e.g., Sinton and Detrick, 1992), have shown that the ridge axis is composed of a magma chamber at depth, which is overlaid by a thin, narrow, and nearly continuous melt lens at its top, and of an upper lid formed by the sheeted dyke complex and the volcanics that seems to be injected from the axial melt lens (Figure 1). The upper melt lens is a key horizon in oceanic crust genesis, as it feeds at least part of the upper and lower crust. Understanding processes acting in and around the melt lens is therefore of major importance to precisely constrain the oceanic crust genesis at fast-spreading ridges. The upper melt lens is also the uppermost known nearly steady-state occurrence of melt at the ridge axis, and it corresponds to the sheeted dike / gabbro transition, where the magmatic system (that builds the crust) and the convecting hydrothermal one (that cools the crust) interact.

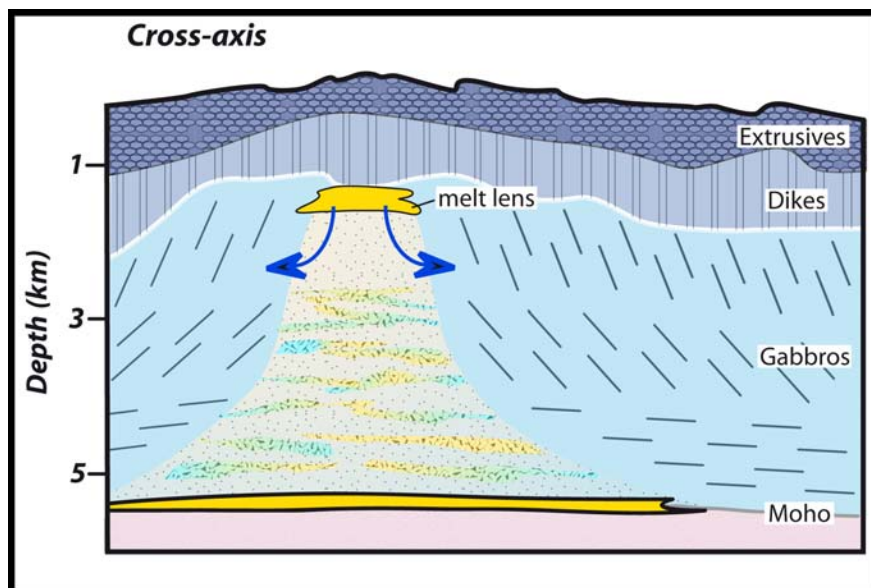


*Figure 1: Cross axis view of a ridge accreted at fast spreading centers (Modified from Sinton and Detrick, 1992, Nicolas and Boudier, 1995, Boudier et al., 1996; MacLeod and Yaouancq, 2000; and Nedimovic et al., 2005). A melt lens is present at the bottom of the upper crust and at the moho level. Gabbros are vertically foliated to the top and horizontally layered to the bottom. The mush underneath the upper melt lens is intruded by sills.*

Interactions between the magmatic and the hydrothermal systems can modify the composition of the melt lens and therefore influence the whole oceanic crust composition, in particular the mid-ocean ridge basalts (MORB) composition, which are the most accessible,

and therefore most commonly studied oceanic rocks. Several studies have focused on the root zone of the sheeted dike complex and have led to apparently contrasting models. Some authors have proposed that the melt lens is a steady state horizon (e.g., Nicolas et al., 2008), when others have proposed that it behaves as a dynamic horizon (e.g., Gillis, 2008). The origin of the isotropic gabbro horizon (~100-200m thick) below the sheeted dike complex is either attributed to the melt lens fossilization (e.g., MacLeod and Yaouancq, 2000) or to hydrous partial melting of the root zone of the sheeted dike complex (Nicolas et al., 2008). Hence the fundamental questions I have addressed in this work are: is the interface between the melt lens and the hydrothermal system a steady-state or a dynamic system? Is water incorporated to the melt, and if so through which process(es)? Does the isotropic gabbros represent the fossilization of part (or of all) of the melt lens?

In 2005, the Integrated Ocean Drilling Program (IODP) has drilled Hole 1256D on the Cocos plate, in an oceanic crust formed at the East Pacific Rise at a superfast spreading rate (> 20cm/y). For the first time, IODP Hole 1256D has sampled a complete, intact section of the upper oceanic crust (Wilson et al., 2006). It has reached the upper isotropic gabbros, sampling the contact between the sheeted dike complex and these gabbros. This drillhole gives us the first opportunity to compare this peculiar horizon in an intact portion of present-day oceanic crust with ophiolites and the derived "Penrose" model oceanic lithosphere generated at fast-spreading ridges. This comparison provides further constraints on the dynamic of this complex geological and petrological interface, and allows the elaboration of a common model for its evolution in time.

The main objective of this thesis was to identify processes acting at the gabbro / sheeted dike transition, and to identify the feedbacks between the magmatic and the hydrothermal systems in oceanic crust formed at fast-spreading ridges. Two complementary approaches have been implemented:

- ✘ **A compared field work, and petrological study** of IODP Hole 1256D and the Oman ophiolite was carried out. In the Oman ophiolite, two field-work campaigns have been realized (6 weeks during winter 2006-07 and 6 weeks during winter 2007-08). The isotropic gabbro horizon corresponding to the transition from the sheeted dike complex to the foliated gabbros has been studied in details in three areas of the southern massifs in the Oman ophiolite; ~10 other areas have been visited in other massifs to verify the widespread occurrence of the observed relations, hence the proposed model. IODP core 1256D has been

## Introduction

relogged and described in details during a visit in College Station in summer 2007. A petrological study of all samples (from Oman and IODP Hole 1256D) has been conducted, including mineral major element compositions of all lithologies. A comparison between the observations made in Oman and at IODP Site 1256 leads to the elaboration of a common coherent model for the interactions between the magmatic and the hydrothermal systems at fast spreading ridges.

- ✘ The approach based on natural rocks was complemented by an **experimental petrology study** that has been performed in the “Institut für Mineralogie” of the Leibniz University Hannover. The objective of this work was to reproduce the melting of the hydrothermally altered base of the sheeted dike complex under pressure, temperature, and redox conditions that match the natural processes. A natural altered dike from the Oman ophiolite has been used as starting material. The composition of the newly formed melt is compared with typical plagiogranitic rocks from oceanic lithosphere, and the coexisting experimental minerals to rocks associated to these oceanic plagiogranites. The trace element composition of the experimental melts is also studied for the first time.

The manuscript is organized in five chapters:

- I. A short overview of crustal accretion processes at fast spreading ridges, and a review of what is known to date about processes acting at the gabbro / sheeted dike transition is presented.
- II. The main lithologies recovered at the bottom of IODP Hole 1256D are described, and the major element composition of the mineral phases are documented.
- III. The sheeted dike / gabbro transition was studied in the Oman ophiolite and results are compared with IODP Hole 1256D. A general model integrating previously published models and new observations is proposed in an article published in *Geochemistry Geophysics Geosystems*.
- IV. An experimental study reproducing the melting of hydrothermally altered sheeted dikes is presented. The experimental method is precisely described, and the main results are presented in an article submitted to *Contributions to Mineralogy and Petrology*. A specific and innovative study of the trace element

concentration of the experimental products is also presented in an article that will be submitted to *Geology*.

- V. The conclusion summarizes the main results, and outlines some prospective directions of future research.

The appendix is divided in four parts:

- A. Other papers linked to this PhD work and used in the different chapters are presented.
- B. The dataset used in Chapters 2 and 4 is given.
- C. Abstract of other papers written during this PhD work are presented.
- D. Conference abstracts presented during my PhD work are presented.

## **Chapter I.**

# **Magmatic accretion at fast spreading ridges**





## I.1. Architecture of oceanic crust at fast spreading ridges

### I.1.a. General structure

For decades, scientists have explored oceanic crust to understand its structure, the way it is formed, and the processes that are active at the ridge axis. In April 1961, the Mohole project (Bascom, 1961) attempted to drill the whole oceanic crust down to the Moho (this has been reported in the *Life* magazine by John Steinbeck). The drillhole was situated to the west of the Mexico's Baja California and was the first scientific attempt to drill hard rocks. Although limited (only 13 meters of basalts have been recovered below the sediments), the success of drilling hard rocks was promising. The Penrose field conference (Conference Participants, 1972) has led to the elaboration of a consensual model for the oceanic crust structure. During this conference, the oceanic crust seismic models (e.g., Raitt, 1963; Shor et al., 1970) have been put in relation with the ophiolite structures and petrology (Figure I-1). The seismic model displays different layers that correspond to variable P wave velocities ( $V_p$  in km/s). The petrological model (ophiolitic model) is composed from the top to the bottom of the basalts (layer 2A), of the sheeted dike complex (layer 2B), of the gabbros (layer 3) and of the peridotites (layer 4).

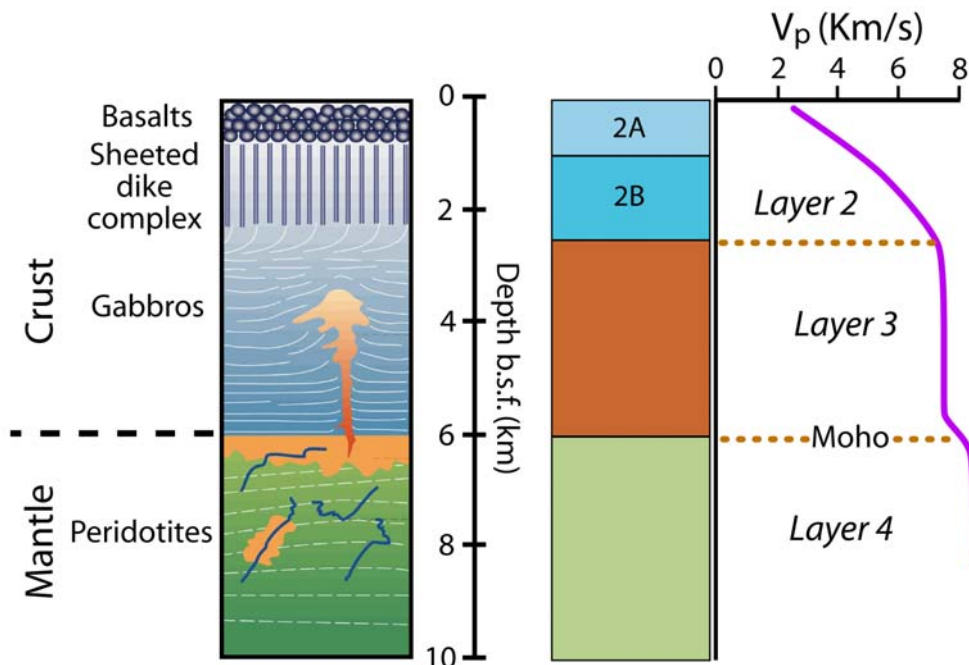


Figure I-1: Petrologic (or ophiolitic; left; after Nicolas et al., 1988) and seismicologic (right, Mével, 2003) models for oceanic crust formed at fast spreading centers. Vertical scale shows the depth below the sea floor (b.s.f.) in km. The layer 2A is believed to correspond to the pillow-lavas and lava-flows; the 2B to the sheeted dike complex; the layer 3 to the gabbro pile and the layer 4 to the mantle.

Drilling operations at site 504B (eastern equatorial pacific) have nevertheless reached the layer 3 within the sheeted dike complex horizon (Detrick et al., 1994; Alt et al., 1996) and the recent IODP Hole 1256D (Cocos plate) has reached the gabbros within the layer 2 (Teagle et al., 2006; Wilson et al., 2006). These observations support that parameters such as porosity and alteration are more important than the grain size or the rock type on the control of the location of layer 2 / 3 transition (Wilson et al., 2006).

Porosity is related to fracturing and alteration, and allows hydrothermal circulation, which is mainly concentrated in the upper crust. Recent geochemical and structural studies of the Oman ophiolite show that very high temperature fluids can reach the magma chamber margins in the lower crust (Bosch et al., 2004; Nicolas et al., 2003; Nicolas and Mainprice, 2005). The hydrothermal circulation is classically depicted across-axis, forming cells that are perpendicular to the ridge axis (e.g., Alt et al., 1986). These are believed to be represented by a recharge system with cold sea water injections, away from the ridge axis along off-axis faults, and by a discharge system that rise up to the surface after the reheating occurring close to the magma chamber (e.g., Alt et al., 1986; Lowell et al., 1995; Kelley et al. 2002; Fisher, 2003). At 9°50'N, beneath a well-studied hydrothermal vent field on the East Pacific Rise, microearthquakes hypocenter relocations using the double-difference algorithm (relative location errors are 50 m in average; Waldhauser and Ellsworth, 2000) have been performed (Figure I-2; Tolstoy et al., 2008).

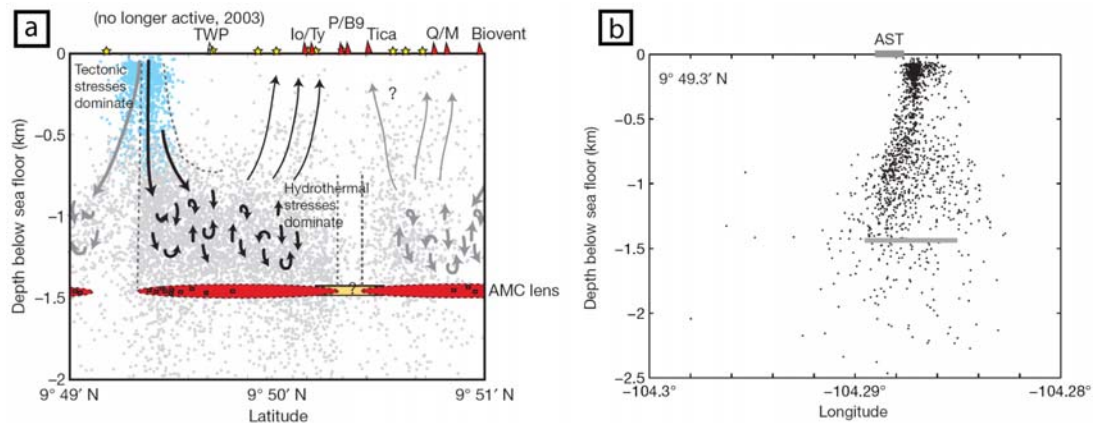


Figure I-2: a) Along axis cross section of the East Pacific Rise between 9°49'N and 9°51'N (Tolstoy et al., 2008). AMC: axial magma chamber or upper melt lens. The features of the best-defined hydrothermal cell are shown with black arrows, and the features inferred in adjacent cells are shown with grey arrows. Light blue dots illustrate the area where tectonic stresses are likely to dominate earthquake generation, creating a zone of permeability. Light grey dots illustrate where hydrothermal stresses probably dominate. Red triangles are high-temperature vents (with their associated names); yellow stars are low temperature vents. b) 200 m wide cross-axis section at 9°49.3'N; AST: axial summit trough; the grey line represents the melt lens reflector.

The hypocenters cluster in a vertical pipe-like zone (Figure I-2b), and in a band that lies directly above the melt lens (Figure I-2a). These data highlight that the convecting hydrothermal system forms along axis cells rather than cross axis ones (Figure I-2).

### I.1.b. Magma chamber models

In early models (Figure I-3), the organization of fast-spreading ridge magma chambers was envisioned as a large, mostly molten reservoir (e.g., Cann, 1974; Dewey and Kidd, 1977; Smewing, 1981; Pallister and Hopson, 1981; Casey and Karson, 1981; Nicolas et al., 1988).

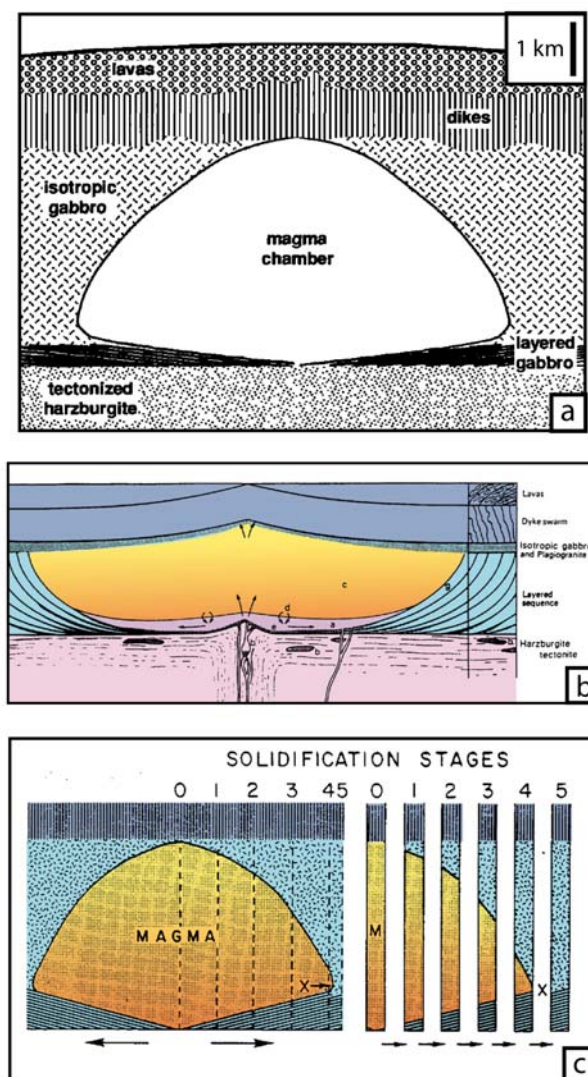


Figure I-3: Early models for the structure of the magma chamber (cross-axis views) that is represented by a large molten domain. a) Cann (1974) model; b) Smewing (1981) model [a]: magma input; [b]: olivine+spinel fractionation; [c]: main magma body; [d]: limited mixing with primary melts; [e]: olivine-rich cumulates; [g]: crystallization; c) Pallister and Hopson (1981) model: Solidification stages, X= sandwich horizon where downward crystallization from the roof and upward crystal accumulation from the floor converge.

In these models crystal fractionation is expected to produce the evolved composition of most of the mid-ocean ridge basalts (MORB; e.g., Bryan et al., 1976; Stolper, 1980; Grove and Bryan, 1983). Seismic reflection profiles (Morton and Sleep, 1985; Kent et al., 1990), multi-channel seismic imaging (Detrick et al., 1987), and tomographic studies of mid-ocean ridges (Toomey et al., 1989; Caress et al., 1992), and petrological studies of oceanic lithologies (e.g., Smewing, 1981; Browning, 1984; Langmuir et al., 1986; Bloomer et al., 1989; Sinton et al., 1991; Lamoureaux et al., 1999) have ruled out the large magma chamber model. The magmatic system is better represented by a thin and narrow, mostly liquid melt lens present at the base of the sheeted dike complex, and that overly a crystal-rich mush (Figure I-4). The size and structure of the melt lens has been further constrained by recent experiments at the East Pacific Rise (Singh et al., 1998; Kent et al., 2000) as outlined in section I.2.a. The presence of melt lenses close to the Moho has also been inferred from ocean bottom seismograph observations (Garmany, 1989), tomographic studies (Dunn et al., 2001), compliance studies (Crawford and Webb, 2002), multi-channel seismic data (Nedimovic et al., 2005), and three dimensional seismic reflection images (Singh et al., 2006). Recently, melt lenses within different levels of the lower crust (~850-900 m above, and at the Moho transition zone) have been observed through seismic reflection images (Figure I-4b; Canales et al., 2009).

These different melt lenses are expected to play a key role in controlling the crustal accretion. The upper melt lens is considered to be the source of the upper crust extrusives (sheeted dike complex and lavas). The different models for the formation of the lower crust which is typically composed of foliated and layered gabbros can be summarized in two end-members: (1) all the crystallization occurs in the shallow melt lens resulting in the subsidence of crystals in a “gabbro-glacier” building the lower crust (Figure I-5a; e.g., Henstock et al., 1993; Phipps Morgan and Chen, 1993; Quick and Denlinger, 1993); and (2) the lower crust crystallized mainly *in-situ* through injection of sills (Figure I-5c; Browning, 1982; Bedard et al., 1988; Gudmundsson, 1990; Kelemen et al., 1997; MacLeod and Yaouancq, 2000). An hybrid model of ductile flow resulting in subsidence from the shallow melt lens (Nicolas et al., 2009; see Appendix A1), with the occurrence of sill injections in the Moho transition zone (Kelemen et al., 1997) is also proposed (Figure I-5b; Boudier et al., 1996).

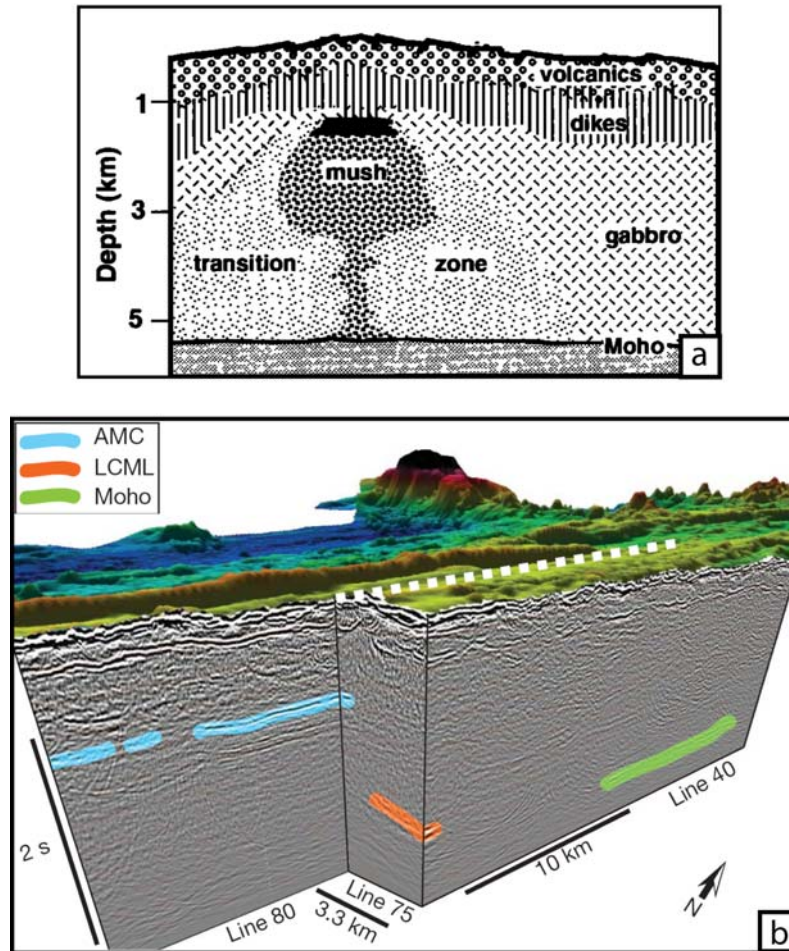


Figure I-4: a) Cross-axis view; the melt lens is restricted to a small domain at or close to, the sheeted dike base, it overlies a mush zone containing less than 20% of melt (Sinton and Detrick, 1992). b) Melt lenses are imaged at different levels of the crust (Canales et al., 2009): AMC=Axial magma chamber, it represents the melt lens depicted in a); LCML=Lower-crustal melt lens, and Moho the Moho melt lens. The section between the AMC and the Moho melt lens is considered to be mostly mushy (<20% melt according Lamoureux et al., 1999). The white dotted line represents the ridge axis.

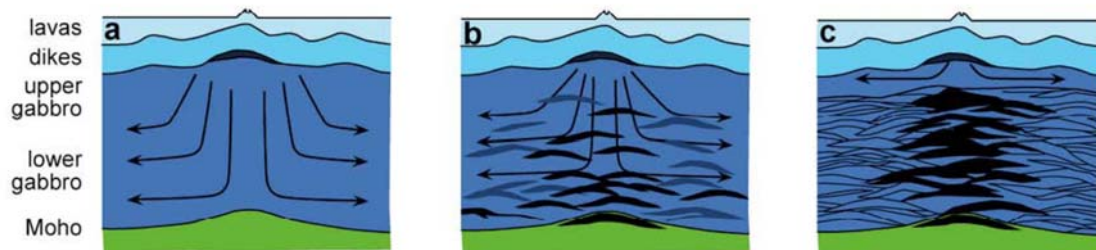


Figure I-5: Oceanic crust accretion models after Korenaga and Kelemen (1998) (B. Ildefonse personal com.). a) The “gabbro glacier” model: all the lower crust is crystallized through subsidence from the upper melt lens (e.g., Henstock et al., 1993; Phipps Morgan and Chen, 1993). b) Mixed model in which the lower crust is fed from the top through subsidence and from the bottom through sill injections (Boudier et al., 1996). c) The “sheeted sill” model in which most of the lower crust crystallize through sill injections (e.g., Kelemen et al., 1997; MacLeod and Yaouancq, 2000).

### **I.1.c. Ridge segmentation**

The ridge present at fast spreading centers is not a continuous feature (e.g., Macdonald et al., 1988); it is segmented at different scales. The largest scale segmentation is represented by the large transform faults that separate ridge segments; the transform offset is tens to hundreds of kilometers. These are believed to be originated from mantle heterogeneities. The second order segmentation is represented by the overlapping of oceanic spreading centers (OSC); these discontinuities offset the ridge by typically 5 to 20 kilometers and are believed to have a significant effect in the mantle. The third order segmentation is defined by changes in the volcanic morphology of the ridge axis and changes in its trend. It is inherited from shallow mantle melt distribution. The finest-scale segmentation is defined by offsets in axial summit trough, and is inferred to be induced by lateral dike intrusions. All these discontinuities are associated to variations in the physical properties and structure of the melt lens (Carbotte, 2008), and should be considered when studying the melt lens evolution.

## ***I.2. The upper melt lens, a key horizon***

As discussed in part I.1, the upper melt lens present at the axis of fast spreading ridges feeds most of the upper crust and at least part of the lower one. It is therefore a key horizon for understanding the genesis of the oceanic crust. Several processes or interactions can occur within the melt lens or at its boundaries with surrounding rocks, magmas and hydrothermal fluids. These processes can be fractional crystallization, magma mixing, assimilation of fresh and / or of hydrothermalized rocks, partial melting of the surrounding rocks, and hydration of the magma at different stages of the crystallization. These can occur jointly and at different levels in the melt lens. All these possible processes have the potential to influence the composition of the formed melt, in particular of the MORBs that are the most accessible and therefore most studied oceanic hard rocks for shedding light on the mantle and crustal magmatic processes. All processes operating within and around the upper melt lens have thus important implications on our understanding of the global ridge system, and should be precisely constrained.

### **I.2.a. Structure**

Morton and Sleep (1985) were the firsts to report the presence of a reflector at ~3500 m (below the ridge axis) depth, and interpret it as being related to an upper small melt lens at

the ridge axis at the top of a crystal mush containing a small percentage of melt. This melt lens is located at the bottom of the 2B layer representing the sheeted dike complex. Thermal structure at the axis, inferred from the tomographic study of Dunn et al. (2000), is in agreement with the presence of a small melt lens at the bottom of the sheeted dike complex (Figure I-6). Purdy et al. (1992) and Phipps Morgan and Chen (1993) have shown that the melt lens depth is proportional to the spreading rate; this has been recently confirmed in the Cocos plate where the first gabbros below the sheeted dike (considered as representing the melt lens) have been reached at relatively shallow depth (1157 meters below seafloor basement) by the IODP drilling operations performed at site 1256D (Figure I-7; Wilson et al., 2006). Along axis surveys along the East Pacific Rise show that the range of depth variation of the melt lens is about 1000 m, over tens to hundreds of km (e.g., Hooft et al., 1997; Figure I-8a).

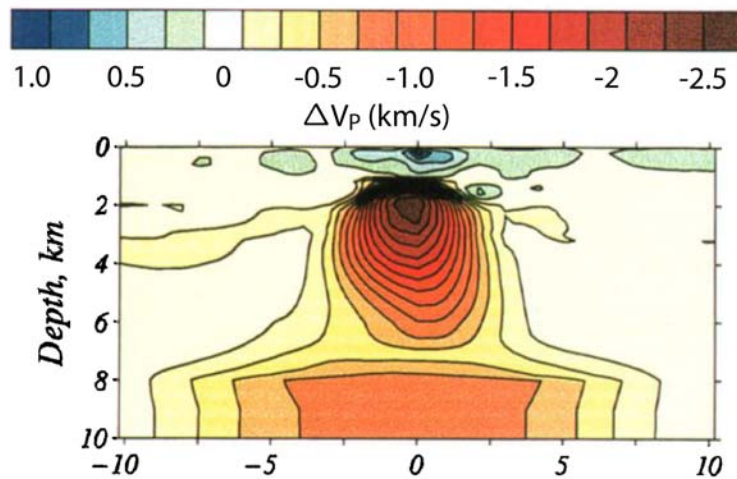


Figure I-6: Cross axis tomographic model of the East Pacific Rise at 9°31.74'N (Dunn et al., 2000). Velocity perturbations are calculated against a one dimensional velocity model.

Canales et al. (2005) have shown at the Juan de Fuca Ridge that the melt lens is present along axis over tens of km (Figure I-8b). The recent study of Canales et al. (2009), using higher resolution seismic reflection data, confirms the along axis continuity over several km of the narrow upper melt lens (Figure I-4b). Preliminary results of a recent multi-streamer 3D seismic reflection study of the 9°50' area of the East Pacific Rise show that the melt lens is divided into a series of discrete magma lens events that are continuous ~5-10 km (Carton et al., 2008; Carbotte, 2008). Cross-axis seismic reflection profiles beneath the East Pacific Rise at 9°30'N (Canales et al., 2005) show that the width of the melt lens ranges between 600 and 1700 m, which is in good agreement with the first estimates done by Kent et al. (1990). The



width of the melt lens is not correlated to depth variations (Figure I-8c). The erupted melt volume is not correlated to the melt lens depth but well correlated to its width (Bergmanis et al., 2007).

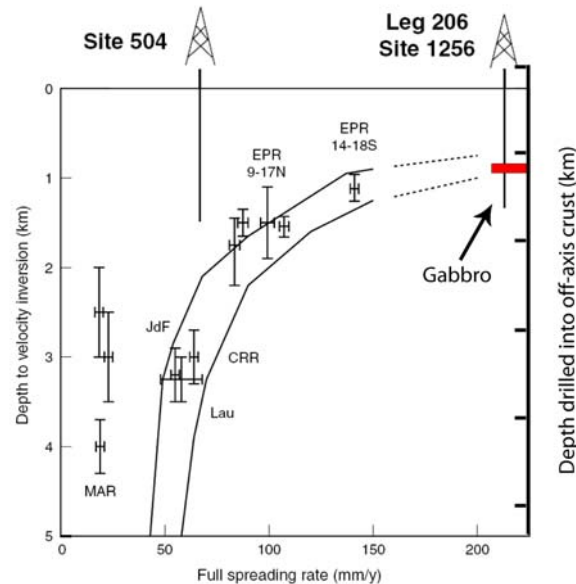


Figure I-7: Depth to the upper axial melt lens reflector against spreading rate (Wilson et al., 2006, after Purdy et al., 1992, and Carbotte et al., 1998). Two models of Phipps Morgan and Chen (1993) are shown (black lines) and extrapolated to higher spreading rates (dashed lines). The penetration of IODP Holes 504B and 1256D are added (black vertical lines) considering ~300 m of off-axis lavas for Hole 1256D (Wilson et al., 2006). The depth of the first gabbros encountered at IODP Hole 1256D fit well the extrapolations of the Phipps Morgan and Chen (1993) model. MAR=Mid Atlantic Ridge; JdF=Juan de Fuca Ridge; Lau=Valu Fa Ridge in Lau Basin; CRR=Costa Rica Rift; EPR=East Pacific Rise.

Collier and Singh (1997) have performed a detailed study of the top of the melt body beneath the East Pacific Rise at 9°40N, and have estimated the thickness of the narrow upper melt lens to be ~30 m. They also show that the melt lens contain less than 30% of crystals. Singh et al. (1998), using single-ship and two-ship multichannel seismic reflection profile near 14°S at the East Pacific Rise, both along- and across-axis, have shown that the melt lens is ~50 m thick, and that its internal properties change rapidly along axis, ranging from nearly pure melt (>90% of melt) to mush containing 40-60% of melt. Over the ~60 km of imaged melt lens, three 2-4 km long zones consist of, nearly pure melt, separated by 15-20 km long mushy zones. Singh et al. (1998) also noted that basaltic samples from the East Pacific Rise contain on average 7-10% of phenocrysts (Batiza and Niu, 1992), which suggest that eruptions originated in nearly pure melt lens segments. Singh et al. (1999) performed a full waveform inversion of the Singh et al. (1998) data, and showed that the ~50 m thick melt lens is underlain by a nearly solid floor (at least 100-150 m thick) and overlain by a 50-60 m thick

solid roof. They also showed that a low velocity zone (150-200 m thick) is present above the melt lens roof and may correspond to the base of the hydrothermal convecting system.

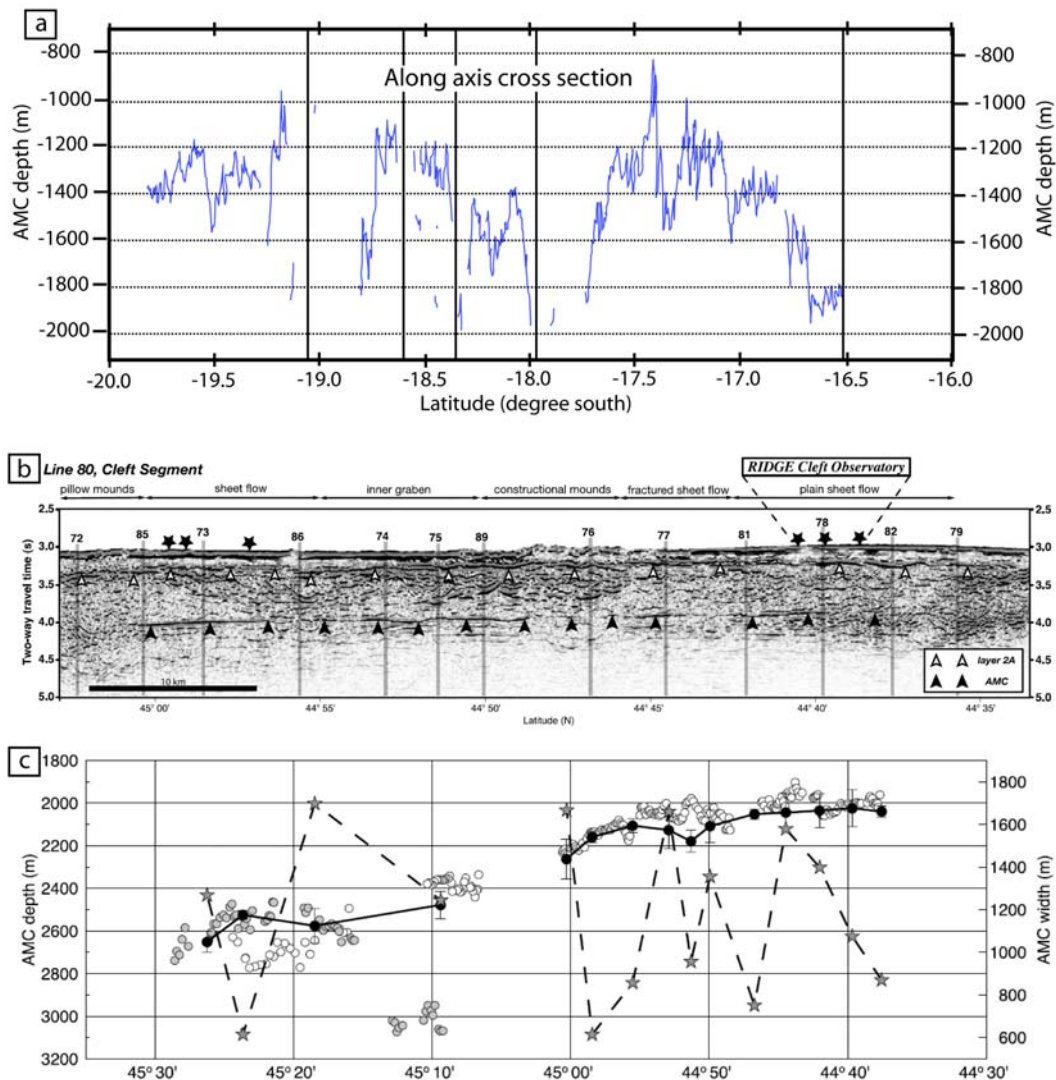


Figure I-8: Along axis imaging of the upper melt lens. a) Depth to the melt lens reflector along the East Pacific Rise between 16° and 20°S (Hooft et al., 1997). Vertical lines indicate the locations of overlapping spreading centers. b) Seismic reflection profile along the Juan de Fuca Ridge between 44°30N and 45°30N (Canales et al., 2005). Black arrows indicate the melt lens position (AMC); white arrows indicate the basement of layer 2A. Vertical black lines and associated numbers show the position of cross axis profiles shown in Canales et al. (2005). c) Melt lens depth (circles; left axis) and width (grey stars; right axis) vs. latitude along the Juan de Fuca Ridge between 44°30N and 45°30N (Canales et al., 2005). Solid line and solid circles correspond to the average melt lens depth estimated from cross-axis profiles. Open and grey circles correspond to two different along axis parallel segments.

Using the hydrothermal plume distribution along the South East Pacific Rise determined by Backer and Urabe (1996), and the mush – melt distribution from the same area proposed by Singh et al. (1998), Singh et al. (1999) proposed that hydrothermal plumes,

which correspond to the discharge part of the system, are associated to melt-rich segments of the axial melt lens. This is also in agreement with the recent study of the hydrothermal system at 9°50'N at the East Pacific Rise (Tolstoy et al., 2008), which shows that the hydrothermal recharge occurs in a location where no reflector is observed, and therefore no melt lens, is present (Figure I-2). These different results are summarized in Figure I-9 (Singh et al., 1999).

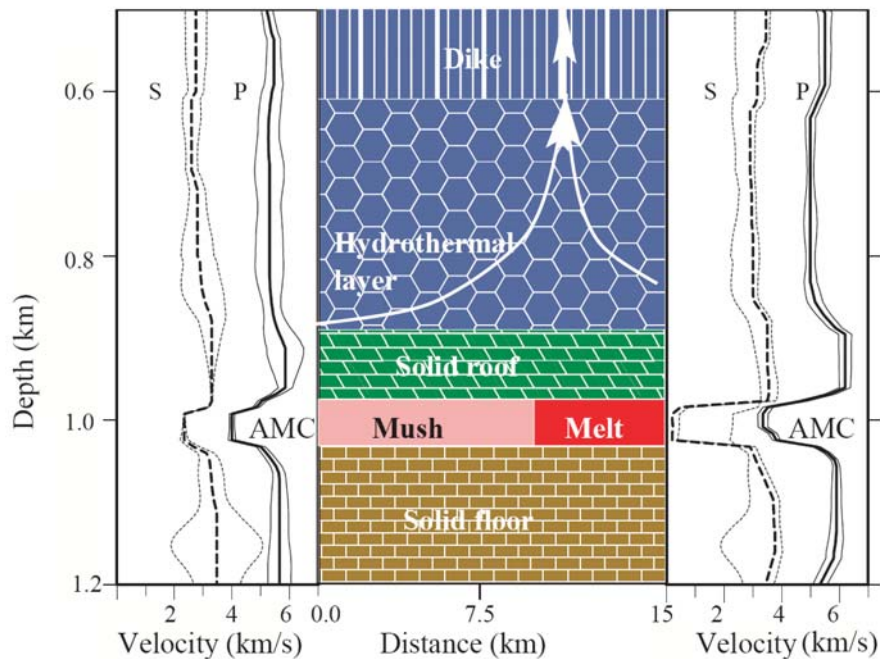


Figure I-9: Schematic along axis model of the melt lens area and associated velocity 1D models (Singh et al., 1999). The left model corresponds to the mush zones and the right one to the melt domains. Note that in melt domains, the S wave velocity is nearly zero at the melt lens depth. Hydrothermal discharge occurs above the melt domains.

### I.2.b. Melt storage, composition and delivery

The composition of the melt filling the melt lens is believed to be well represented by the compositions of the sheeted dike complex and the lava erupted on the sea floor (e.g., Sinton and Detrick, 1992), and is therefore similar to typical N-MORB. However, Natland and Dick (1996) proposed that differentiation that is believed to occur in the melt lens can produce iron-rich melts that are too dense to erupt, and that may lie on the melt lens floor. This hypothesis builds on the discovery of ferro-andesitic samples within the isotropic gabbro section below the sheeted dike at Hess Deep. Similar rocks have also been observed in the Oman ophiolite, but structural relationships suggest that they formed by differentiations at the melt lens margins (MacLeod and Yaouancq, 2000). These rocks therefore represent late processes occurring after the dike injections. Dike (and lava) composition is therefore

expected to represent an average composition of the melt lens, and the overall melt lens composition can be considered to be well represented by N-MORB. MacLeod and Yaouancq (2000) proposed that the varytextured gabbro horizon that underlies the sheeted dike complex represent the fossilized melt lens. Using the compositions and the proportions of the different lithologies forming this horizon, they have calculated an average composition that corresponds to typical MORB melts (with  $Mg\#=65$  where  $Mg\#=Mg/[Mg+Fe]$  and  $TiO_2=1.1wt\%$ ).

N-MORB melts represent evolved liquids regarding primitive mantle melts (e.g., Stolper, 1980) and must have fractionated before reaching the upper melt lens. Koga et al. (2001) noted that most of the clinopyroxenes in samples from the Moho transition zone in Oman (>90% of the samples) are equilibrated with MORB melts, and that mixing of various polybaric partial melts of mantle peridotite must have occurred at or below this zone to give the MORB signature. Determining the origin of the MORB composition is beyond the goals of this study. It is just worth noting here that the MORB composition appears to be consistent with channelized, reactive melt transport. For a given degree of partial melting (or a given amount of melt), this results in higher amounts of mineral consumption and higher amounts of newly formed olivine, compared to a melting reaction without channelization / fossilization (e.g., Kelemen et al., 1995; Asimow and Stolper, 1999; Lambart et al., 2009).

The MORB compositions follow the tholeiitic fractionation trend of increasing  $FeO_{total}$ ,  $Na_2O$ , and  $TiO_2$  and decreasing  $Al_2O_3$  and  $CaO$  with decreasing  $MgO$  (Klein and Langmuir, 1987; Klein et al., 1991). The major variations are attributed to differentiation processes occurring within the melt lens but some variations in composition can also be attributed to physical parameters such as the melt lens morphology and/or depth. For example, the  $MgO$  content of the erupted lavas at the East Pacific Rise,  $17^{\circ}30'S$ , is higher when the melt lens is deeper, and these most primitive lavas are less abundant and derived from narrower melt lens in contrast with more evolved lavas with lower  $MgO$  content (Bergmanis et al., 2007). Melt compositions are also correlated to the ridge axis water depth. Klein and Langmuir (1987) have shown that the  $Na_{8,0}$  (i.e., the  $Na_2O$  calculated value at 8 wt% of  $MgO$ , allowing to compare compositions that are not affected by fractional crystallization) increases with increasing water depth at the ridge axis.

Some MORB samples display high chlorine contents that are interpreted as indications of sea water contamination of the melt lens through assimilation of hydrothermally altered crustal rocks (e.g., Michael and Schilling, 1989; Michael and Cornell, 1998). The incorporation of sea water, hence of chlorine into MORB flows during their emplacement on

the seafloor is also possible (Soule et al., 2006). However, Cl incorporation during emplacement cannot account for the higher Cl/K ratio observed in fast spreading ridges MORB vs. slow spreading ridges MORB (Michael and Cornell, 1998), and assimilation effects as proposed by Michael and Cornell (1998) is likely to play a role. Nevertheless partly digested xenocrysts or amphibolite blocks are only rarely observed in MORB, and the Cl assimilation at the melt lens level is not well understood (Michael and Schilling, 1989). More recently, Coogan et al. (2003) have shown that assimilation processes do occur around the melt lens; this will be outlined in chapter I.3.

Significant differentiation is believed to occur occasionally in the melt lens; this is inferred from the occurrence of highly silicic rocks (>60 wt% SiO<sub>2</sub>) observed as lavas erupted on the seafloor (Fornari et al., 1983; Haase et al., 2005) and as plutonic rocks (oceanic plagiogranites) present at the sheeted dike base and in the gabbro unit (e.g., Pallister and Hopson, 1981). These silica-rich rocks can alternatively be generated by hydrous partial melting of mafic rocks (variously altered dikes and gabbros; e.g., Koepke et al., 2007). These two processes are not necessarily mutually exclusive, and may operate jointly (e.g., Pedersen and Malpas, 1984). The melt lens crystallization leading to differentiation is believed to be fast if no new magma injection occur (~50 years to crystallize a 50 m thick melt lens according to Singh et al., 1999). Constraining the timescales of magma replenishment and storage in the melt lens, and of magma supply is therefore a critical parameter. These are reviewed in detail together with the timescales for transfers from the mantle and for the melt lens dynamics in France et al. (2009a; section 6.5). Here, only a short overview of the timescale constrains for the replenishment time, residence time and eruptive events associated to the upper melt lens is given.

Using a mathematical model and basalt geochemical data, Rannou et al. (2006) have estimated the replenishment period of the melt lens to be ~750 years. Using the MORB major and trace elements composition, Rubin and Sinton (2007) proposed that this replenishment is achieved in less than 1000 years. Rannou et al. (2006) also proposed that the magma residence time in the melt lens is around 300 years, which is in agreement with the Rubin et al. (2005) study that proposed, using <sup>210</sup>Pb-<sup>226</sup>Ra-<sup>230</sup>Th radioactive disequilibria in samples from the East Pacific Rise, that the magma resides and mixes in the melt lens over periods of ~200-400 years. The eruptive events (or supply events) are believed to occur over periods of 10 to a few hundreds of years (Hooft et al., 1997; Sinton et al., 2002; Bergmanis et al., 2007).

***Do eruptive events have a significant influence on the melt lens structure and volume?*** Recent studies around 9°50'N at the East Pacific Rise seem to show that eruptions

do have an impact on the melt lens volume and on its melt proportion. Seismic measurements have been done in 1985 and 2008 in this area where two eruptions occur in 1991 and 2005-2006. Preliminary results from the recent multi-streamer reflection imaging experiment (Mutter et al., 2008), suggest that significant variations in the depth of the melt lens reflector have occurred between 1985 and 2008 at 9°50'N, below the location of the 2005-2006 eruption. No significant variation is observed at 9°30'N and 9°40'N, away from the eruption event. The reflectivity strength of the melt lens under the eruption locality is weaker than the one of the melt lens immediately to the North and South (Carton et al., 2008). This may indicate that a lower melt percentage is present in the melt lens that has fed the eruption.

***Are the erupted volumes significant comparable to the volume of the melt lens?***

Soule et al. (2007) have described lava flows over 18 km along axis at the East Pacific Rise, 9°50'N, and estimated the erupted volume of the 2005-2006 eruption to be  $\sim 22 \times 10^6 \text{ m}^3$ . They estimated that the dike feeding this eruption should be on average  $\sim 1$  m wide (which is the average thickness of sheeted dikes in the Oman ophiolite), 1.4 km high and 18 km long, and should be filled with  $\sim 25 \times 10^6 \text{ m}^3$  of magma. However, based on the studies of Singh et al. (1998; 1999) at the Southern East Pacific Rise, and on the preliminary results of Carton et al. (2008) at 9°50'N, the melt lens cannot be considered as a continuous melt horizon over 18 km. Singh et al. (1998) proposed that the melt lens containing nearly pure melt and that have the potential to feed eruptions are  $\sim 2$ -4 km long. The eruptible melt lens volume can be estimated by considering an average width of  $\sim 1000$ m (Bergmanis et al., 2007) and an average thickness of 40 m (30 m for Collier and Singh, 1997 and 50 m for Singh et al., 1999), i.e.,  $\sim 120 \times 10^6 \text{ m}^3$ . If we consider that the dike feeding the 2005-2006 eruption rooted in a  $\sim 2$ -4 km long melt lens rather than in a 18 km long melt lens, its volume can be considered to be  $\sim 4 \times 10^6 \text{ m}^3$  resulting in an total supplied volume of  $\sim 26 \times 10^6 \text{ m}^3$ . The supplied volume is therefore roughly one fifth of the eruptible melt lens volume. As the whole melt lens is probably not homogeneously involved in the eruption, some parts may have supplied even more magma; it is therefore expected that significant variations in the seismic properties of the melt lens can locally occur, and the variations in the depth of the axial melt lens observed by Mutter et al. (2008) are possibly linked to the eruption.

Lagabrielle and Cormier (1999), Lagabrielle et al. (2001) and Garel et al. (2002) have shown that periods of waning magma supply and of melt lens replenishment are associated to axial morphological variations. Along axis troughs interpreted as collapsed calderas (40-110m deep) may form when the melt supply of a previously inflated melt lens wanes or ceases. In contrast, the axial morphology is believed to be a broad, smooth dome structure when the

melt supply is higher. Along axis variations of the axial morphology are interpreted by Carbotte (2008) to represent the 4<sup>th</sup> order of fast spreading ridges segmentation; on each side of this 4<sup>th</sup> order discontinuity, geochemical compositions are different. This is consistent with Lagabrielle and Cormier (1999) who proposed that axial morphology variations correspond to differences in the magma supply. Hence, variations in basalt composition should be correlated with different axial morphologies. For example, Caroff et al. (1997) have shown that the presence of axial trough is associated to larger geochemical heterogeneities than in zones with dome-shaped axial morphology, and are associated to lavas enriched in rare-earth elements, deriving from melts that have evolved during periods of lesser replenishment.

### ***I.3. The melt lens and the root zone of the sheeted dike complex: relations and evolution***

#### **I.3.a. General presentation**

In this part, I discuss the available models for the melt lens evolution and for the evolution of the associated root zone of the sheeted dike complex. These zones are spatially associated, and correspond to the interface where the hydrothermal convecting system and the magmatic one are acting together. Several chemical and thermal exchanges can occur during the melts, fluids and rocks transfers. The thermal gradient ( $\sim 7^\circ/\text{m}$ ) is believed to be one of the highest nearly stable thermal gradients on earth (Nicolas et al., 2008; See Appendix A2). Although the foliated gabbros origin is discussed (Boudier et al., 1996; MacLeod and Yaouancq, 2000; Nicolas et al., 2009\_Appendix A1), in all models they represent the melt lens floor. I focus here on lithologies occurring above this horizon: *the isotropic gabbro horizon* and on the *base of the sheeted dike complex*.

#### **I.3.b. Interaction processes**

Several processes can operate in the melt lens, in the root zone of the sheeted dike complex and at the interface between them (Figure I-10). First of all, eruptions can occur (Figure I-10b), draining out some melt. Consequently, the axial morphology can be modified (Lagabrielle and Cormier, 1999). Crystallization at the melt lens margins (Figure I-10c) may occur when the magma supply decreases or when the thermal regime reaches lower temperatures; such a crystallization stage may lead to magma differentiation (e.g., MacLeod

and Yaouancq, 2000). New melt injections may come from the main, mushy magma chamber below the melt lens (Figure I-10d); this would result in magma mixing and melt lens replenishment. The replenishment can be associated to an inflation of the ridge axis morphology (Lagabrielle and Cormier, 1999) and to assimilation of the melt lens roof (Figure I-10e; e.g., Coogan et al., 2003). The melt lens roof is assumed to be hydrothermalized (see below) and its assimilation may account for the chlorine enrichment observed in some MORBs (Michael and Schilling, 1989; Coogan et al., 2003). As the melt lens feeds at least part of the lower crust through subsidence (Boudier et al., 1996; Nicolas et al., 2009), it may also account for the lower crust contamination documented by Coogan (2003). Some authors consider the melt lens to be a steady state horizon that cannot assimilate its roof (e.g., Nicolas et al., 2008). In this case, the chlorine enrichment / contamination may be explained by the incorporation of Cl-rich brine contained in the roof and / or wall rocks (Figure I-10e; e.g., Michael and Schilling, 1989; Michael and Cornell, 1998).

Even if the contamination mechanism is not fully understood, the incorporation of fluids and especially of water into the melt lens is very obvious. The addition of water to the melt lens, even at low concentrations, has strong implications. It lowers the melt viscosity (Giordano et al., 2008); lowers the solidus and liquidus temperatures (e.g., Berndt et al., 2005); increases the oxygen fugacity for a given hydrogen fugacity (Botcharnikov et al., 2005), and therefore stabilizes the Fe-Ti oxides (Berndt et al., 2005; Feig et al., 2006). The liquid line of descent is consequently modified and a differentiation trend characteristic of calc-alkaline series can be observed (Berndt et al., 2005). The mineral composition of erupted basalts can also be modified by water assimilation; as an example, the olivine and pyroxene Mg# and the An content of plagioclase are expected to increase (Kvassnes et al., 2004; Berndt et al., 2005; Feig et al., 2006; Koepke et al., 2009). High water activities in the melt lens due to assimilation also lowers the solidus temperature of rocks from the roof and the margins of the melt lens, with the potential to trigger hydrous partial melting and to incorporate the newly formed silicic melts into the melt lens. Such a partial melting event can occur either when fluids are transported into recently crystallized, still hot rocks (Nicolas et al., 2008) or when previously hydrothermally altered rocks are reheated.



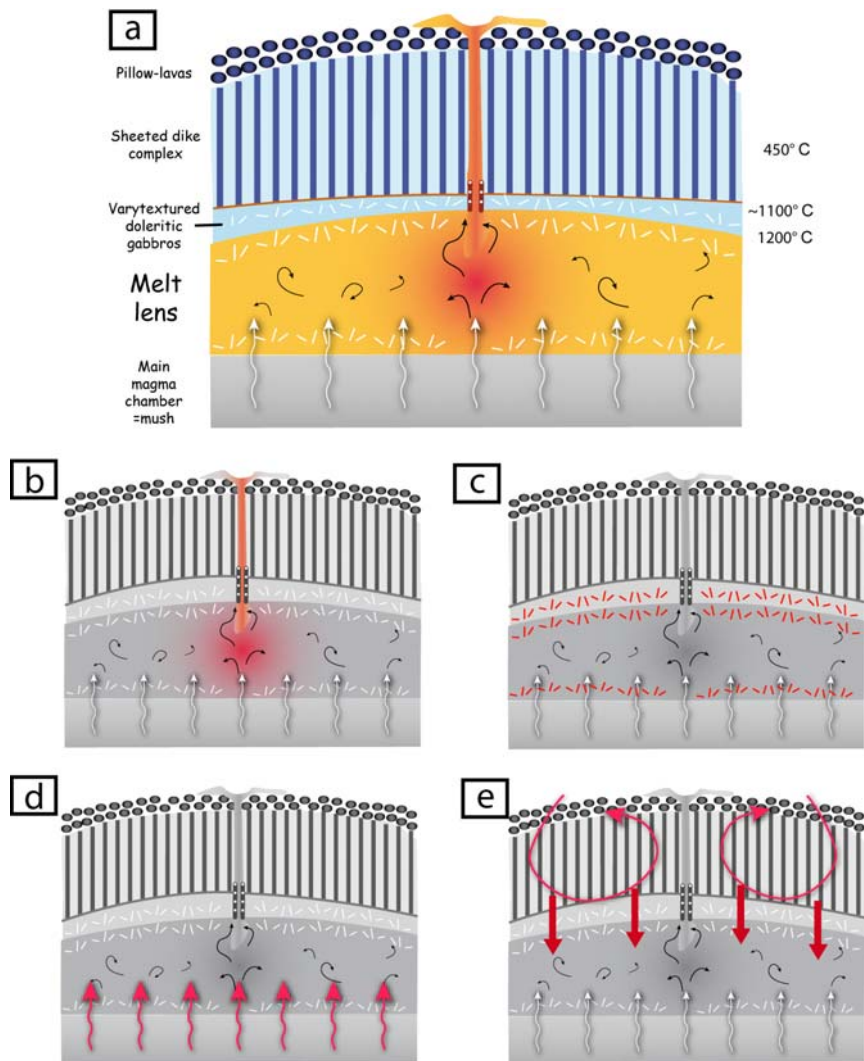


Figure I-10: Schematic cross-axis section showing the melt lens and the root of the sheeted dike complex (not to scale). a) General organization, lithologies and temperatures. After Nicolas et al. (2008). For details see Nicolas et al. (2008). b) Magma drained out during an eruption. c) Melt crystallization at the melt lens margins. d) New magma injection leading to partial or total replenishment of the melt lens. e) Hydrothermal circulation in the crust overlying the melt lens; fluids can be incorporated in the melt lens through assimilation of either hydrothermally altered rocks or brine.

### I.3.c. Geological settings

Depending on the geological setting, the melt lens (and associated base of the sheeted dike complex) structure, composition and evolution may vary. As an example, in back-arc systems the higher amount of water present in the melt will influence the crystallization sequence and the solidus and liquidus temperatures. The ridge segmentation can also influence the system, and ridge segments close to transform faults, or close to overlapping segments, may be disturbed by tectonics, allowing deep penetration of water. Boudier et al. (2000) have proposed that the occurrence of gabbronorites in areas of the Oman ophiolite that

are inferred to be located at the tip of propagating segments is related to high oxygen fugacities linked to melt hydration.

### I.3.d. Lithostratigraphy

Generally, the basalts forming the sheeted dike complex display intergranular, doleritic textures. The root of the sheeted dike complex has been first described in the Troodos ophiolite (Allen, 1975), and then in the Oman ophiolite (Rothery, 1983; Nicolas and Boudier, 1991; Nicolas et al., 2008). Dikes root into the isotropic upper gabbros (Figure I-11a), the chilled margins progressively disappear in gabbros and the center of dike roots is similar to the surrounding isotropic gabbros (Allen, 1975; Rothery, 1983).

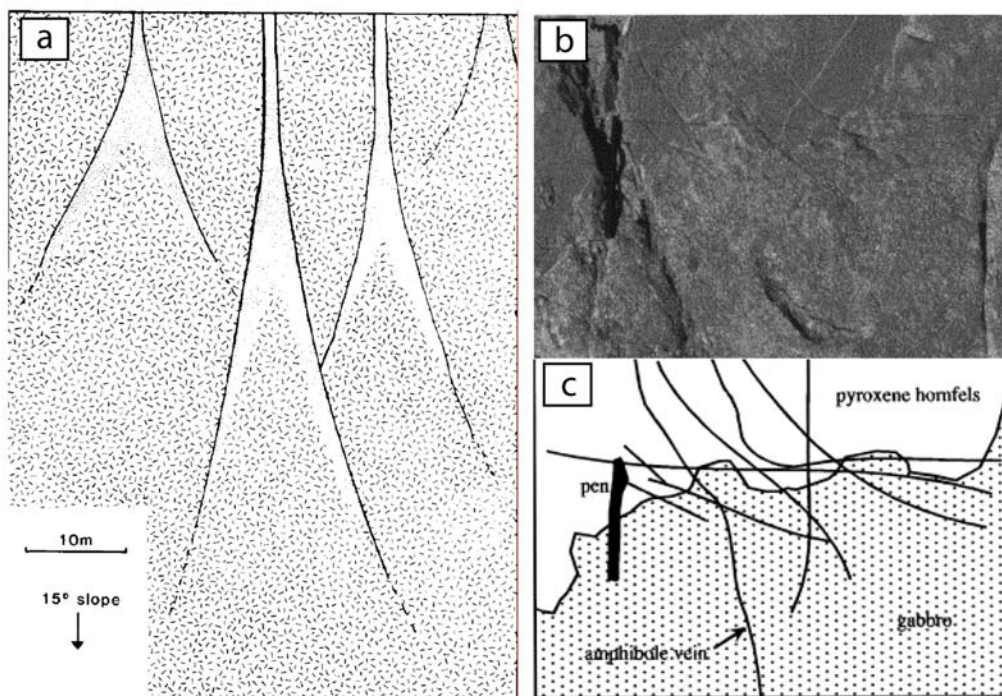


Figure I-11: a) Dikes rooting in the isotropic upper gabbros in the Oman ophiolite, line tone represents high-level gabbro, and dot tone represents doleritic textured microgabbro (Rothery, 1983). The center of the dike roots is similar to the surrounding isotropic gabbros. b-c) Outcrop photograph and sketch of the recrystallized base of the sheeted dike complex truncated by gabbros in the Troodos ophiolite (Gillis and Roberts, 1999).

Nicolas and Boudier (1991) and Nicolas et al. (2008) made similar general observations and describe further the nature of the dike roots. They show that these roots, called “protodikes”, display microgranular margins that have a well defined preferred crystallographic orientation, parallel to the dike margin, which records the upward magmatic flow. Dikes are sometimes crosscut by gabbro, diorite or plagiogranites injections (Figure

I-11b-c; Pallister and Hopson, 1981; Gillis and Roberts, 1999). They are then recrystallized and display microgranular textures ("granoblastic" textures in Wilson et al., 2006; Koepke et al., 2008; "hornfelsic" textures in Gillis and Roberts, 1999).

A thin (~100m) and complex horizon mainly composed of varytextured gabbros is present below the base of the sheeted dike complex (e.g., MacLeod and Yaouancq, 2000). The varytextured gabbro horizon is mainly composed of isotropic fine grained gabbros but also isotropic coarse grained gabbros (or pegmatitic gabbros) often with subophitic rock textures, diorites, and plagiogranites. Gabbros may be locally foliated (MacLeod and Yaouancq, 2000), and sometimes crosscut by late dikes.

Below the varytextured gabbro horizon, the gabbros display more equilibrated granular textures with a vertical foliation (Nicolas et al., 2009\_Appendix A1), these are believed to result either from subsidence from the floor of the melt lens (Nicolas et al., 2009\_Appendix A1) or from the upward moving melt that is believed to orientate crystals (MacLeod and Yaouancq, 2000).

### **I.3.e. Conceptual models and implications**

Since the discovery of the upper melt lens (Morton and Sleep, 1985; Detrick et al., 1987), its role in the oceanic crust accretion has been questioned. The geological setting (mid-ocean ridge, back-arc, propagator tip) is believed to influence the tectonics at or close to the ridge axis, and the water budget and should therefore affect the magmatic processes occurring in the melt lens (Nicolas et al., 2008\_Appendix A2).

Nicolas and Boudier (1991) proposed that, as a result of water ingress into the still hot, just crystallized upper gabbros, the latter can undergo hydrous partial melting and the newly formed melts can crystallize to gabbro-diorites. Such a wet anatexis is considered to occur in a steady state system, in which the melt lens is a stable horizon. Hooft et al. (1997) have shown at the Southern East Pacific Rise that the melt lens depth varies along axis, probably in response to variations in the magma supply from below or in response to variable hydrothermal cooling (Figure I-12). This model suggests that during periods of weak hydrothermal cooling, the melt lens migrates upward with the potential to trigger hydrous partial melting to the roof.

In the Troodos ophiolite, the base of the sheeted dike complex is intruded by gabbros and recrystallized to hornfelsic lithologies (Figure I-11b-c; Gillis and Roberts, 1999; Gillis, 2002). At the same structural level, the sheeted dikes can locally melt during the intrusion of

gabbroic mushes (Gillis and Coogan, 2002). Gillis and Coogan (2002) have attributed the gabbro intrusion in the Troodos ophiolite to upward movements of the melt lens, and the recrystallization of the base of the sheeted dike complex to contact metamorphism associated to this upward movement (Figure I-13).

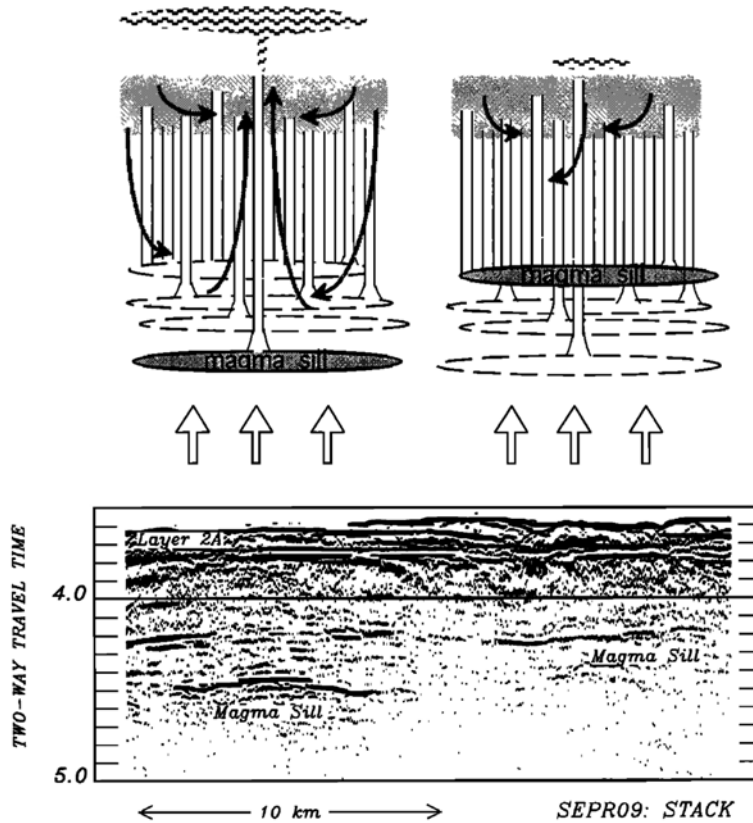


Figure I-12: Top: Cartoon showing two scenarios for the melt lens position depending on the strength of hydrothermal cooling. Bottom: along-axis seismic reflection profile (between 18°13'S and 18°02'S along the East Pacific Rise) illustrating apparent local depth variations of the magma sill (Hooft et al., 1997).

Intrusions of gabbroic rocks in gabbros and in the sheeted dike complex are known from the Oman ophiolite and according to Boudier et al. (2000) and Nicolas et al. (2000) only in areas of segment propagation. In such areas, a ridge segment is propagating in an older lithosphere (Figure I-14) with the potential to remobilize rocks that have been hydrothermally altered. According to Boudier et al. (2000) gabbroic injections occur while the main gabbro unit is still deforming as a magmatic mush; the occurrence of orthopyroxene is attributed to the water-rich conditions prevailing in these environments where there is active tectonics at or near the ridge axis (Boudier et al., 2000). Nicolas et al. (2008) postulated that intrusions of gabbroic rocks in the base of the sheeted dike base can only occur in these

peculiar areas that correspond to tips of propagating segments (Figure I-14), and cannot be considered as being representative of a "standard" mid-ocean ridge process. According to Yamasaki et al. (2006) gabbro-norites are rather related to a late magmatism stage that is probably related to the shallow subduction zone process occurring during the early obduction.

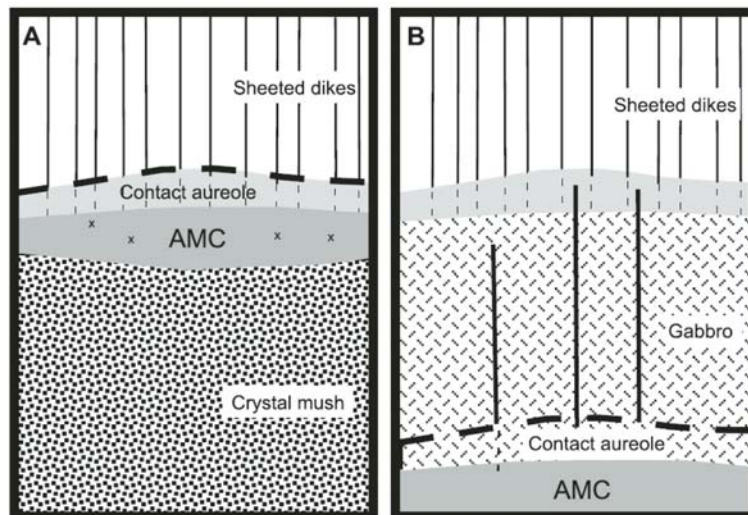


Figure I-13: Migrations of the melt lens can trigger recrystallization at its roof (Gillis (2008), as described in the Troodos ophiolite (Gillis and Roberts, 1999; Gillis, 2002). AMC= Axial Magma Chamber, i.e. the melt lens in this study; x= xenoliths.

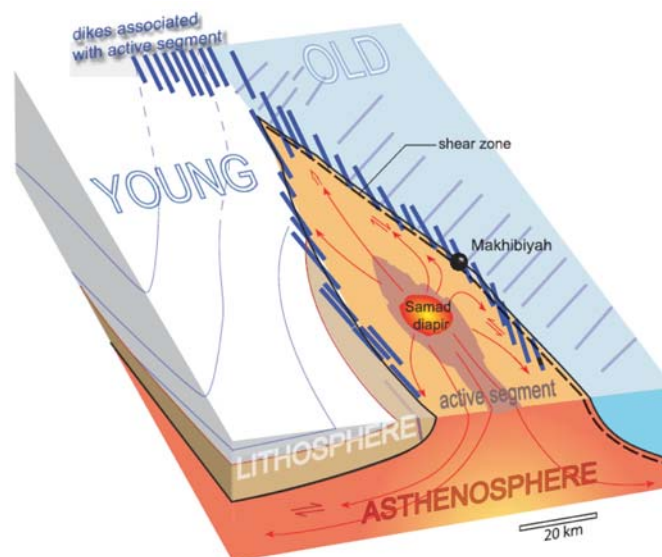


Figure I-14: Tip of a propagating segment that reopens an old domain (Nicolas and Boudier, 2008). Remobilization of hydrothermalized rocks is possible and tectonics at the ridge axis may result in the involvement of water in magmatic processes.

MacLeod and Yaouancq (2000) have studied the Abyad area in the Oman ophiolite, which is considered to be close to the tip of a propagating segment. Despite this peculiar

environment, they have described in this area a steady state system with nearly no gabbro intrusion in base of the sheeted dike.

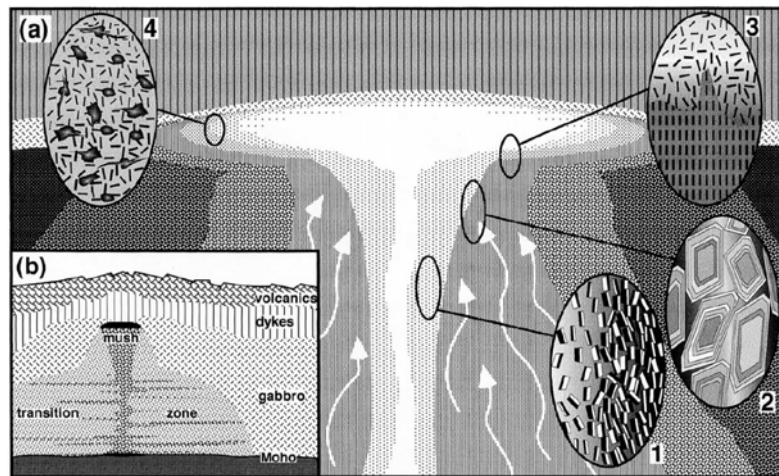


Figure I-15: Melt lens model from MacLeod and Yaouancq (2000). a) Focus on the melt lens and surrounding areas; b) Schematic section across the axis of a fast spreading ridge. In a), 1. shows the foliated gabbros; 2. shows the zoning observed in some plagioclase grains of the sub-melt lens region. 3. shows that some foliated gabbros can also be observed in the varytextured gabbro horizon and 4. proposes that at the melt lens margins some trapped melts can fractionate to form the Fe-Ti pegmatitic gabbro pockets observed in the varytextured gabbro horizon. In this model, MacLeod and Yaouancq (2000) interpret the varytextured gabbro horizon as the crystallized melt lens.

The occurrence of pegmatitic gabbros enriched in Fe-Ti (up to 4.4 wt % of  $\text{TiO}_2$ ) that can only be interpreted as fractionated melts under reducing condition has led MacLeod and Yaouancq (2000) to propose that the varytextured gabbro horizon represent the fossilized melt lens (Figure I-15). They therefore interpret these rocks, present as meter sized pockets in the isotropic gabbros, as trapped melts that have crystallized at the margins of the melt lens.

Coogan et al. (2003) combined geophysical results obtained at the East Pacific Rise with geochemical studies, and with field observations in the Troodos and Oman ophiolites to show that assimilation of roof fragments is common in the melt lens (Figure I-13). They propose that such a process can account for the chlorine enrichment observed in some MORB (Michael and Schilling, 1989). Nevertheless, they do not discuss the possibility of relating this process to tectonics related to segment propagation.

IODP Hole 1256D was drilled in an intact portion of oceanic crust in the Cocos plate formed at the EPR (Teagle et al., 2006), and is assumed to represent a regular ridge segment, away from mid-ocean ridge discontinuities. In this area, Wilson et al. (2006) described, at the base of the sheeted dike complex, truncated dikes with characteristic granoblastic textures

interpreted as reheated, contact-metamorphosed rocks. A detailed study of these granoblastic dikes (Koepke et al., 2008) shows an evolution of the recrystallization downward when approaching the isotropic gabbros, which are believed to intrude the base of the sheeted dike complex. This recrystallization is ascribed to reheating triggered by the melt lens upward migration. Gillis (2008) described similar hornfelsic lithologies present at the base of the sheeted dike complex and as xenoliths in the varytextured gabbro horizon of Pito Deep, Hess Deep, the Troodos ophiolite, and the Him area in the Oman ophiolite. She also ascribed these rocks to recrystallization in an environment of increasing temperature resulting from upward movements of the melt lens (Figure I-13). Gillis (2008) also proposed that the protodikes (Nicolas and Boudier, 1991) microgranular textures do not represent the dike roots but former dikes with chilled margins that have recrystallized during reheating events.

Following the renewed interest in the root zone of the sheeted dike complex triggered by the drilling of IODP Hole 1256D (Teagle et al., 2006), Nicolas et al. (2008) proposed a revised model that build on an older model of Nicolas and Boudier (1991), and is based on about 20 years of structural mapping of the Oman ophiolite, on recent observations, and on recent detailed mappings of selected area, away from discontinuities. It is briefly presented in this chapter, as the corresponding paper is presented in Appendix A2. The studied area is located in the well studied Sumail massif (Nicolas et al., 2000). The bottom-line is the confirmation that protodikes represent the dike roots, and in these areas situated away of ridge tectonics the melt lens is considered as a steady state horizon (Figure I-16). In this model, the steady state melt lens is not fossilized but pinches out at its margins where its roof meets its floor. The varytextured gabbro horizon hence does not represent the melt lens fossilization; most of it is interpreted as resulting from hydrous partial melting triggered by the ingression of hydrothermal fluids into the still hot, crystallized sheeted dike base. The fine grained isotropic gabbros are interpreted as representing protodikes cores and may be the only rocks of the varytextured gabbro horizon that are not originated in the hydrous partial melting of the dikes root zone. Based on these new results they questioned the origin of areas where gabbro intrusions in the sheeted dike base has been observed. Considering the presence of gabbro intrusions as product of ridge tectonic processes (Boudier et al., 2000), Nicolas et al. (2008) propose that nearly half the Oman ophiolite may have formed under the influence of ridge segmentation.

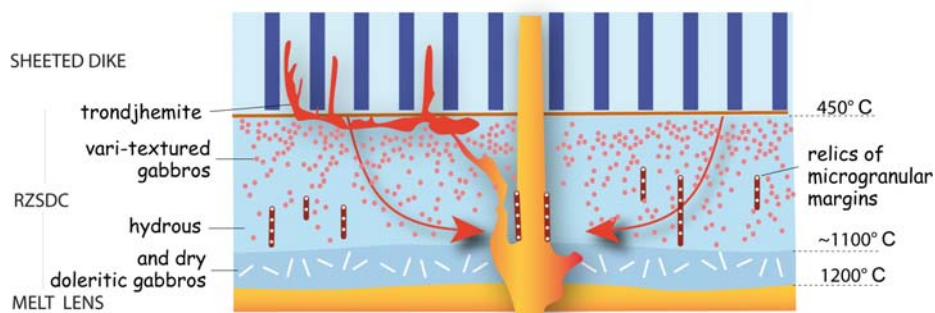


Figure I-16: Conceptual model for the root zone region (varytextured gabbro horizon) from Nicolas et al. (2008) presented in Figure I-10. The bottom of the injected dikes display microgranular margins (protodike) that evolve upward to a dike with chilled margins. The dry ophitic gabbro horizon (thickness <1m) is believed to represent the thermal boundary layer separating the magmatic system from the hydrothermal one. Most of the lithologies present in the root zone of the sheeted dike complex are believed to result from hydrous partial melting (red dots) of protodikes. Microgranular lenses are interpreted as relicts of protodikes after hydrous partial melting.

#### I.4. Key questions and hypotheses to be tested

In section I.3.e “Conceptual models and implications” I have presented several aspects dealing with the melt lens organization and evolution that are still debated. The key unresolved questions are:

- \*Is the melt lens fossilized off-axis?
- \*Do the varytextured gabbros represent the melt lens fossilization or the product of hydrous partial melting of the root zone lithologies?
- \*Is the melt lens a steady-state or a dynamic system?
- \*Does the geological context (e.g., tips of propagating segments) influence the processes occurring in and around the melt lens, and how?
- \*Does the partial melting of the dikes proposed in most published models results from a temperature increase or from a fluid ingress in still hot, recently crystallized rocks?
- \*What are the petrological and geochemical properties of the products of partial melting of hydrothermally altered dikes?
- \*How hydrous partial melting of the hydrothermally altered dikes can influence the composition of MORB?

The main objective of this PhD work was to try answering these questions by using field work, petrology on root zone lithologies, experimental petrology and geochemistry, and by comparing our results with the geophysical data at the mid-ocean ridge axis. Sr and O isotopic systems may be used to infer the effect of HT fluids, however these two isotopic



systems are the ones that are the most affected by low temperature hydrothermal alteration. Therefore the use of isotopes to discuss high temperature ( $>700^{\circ}\text{C}$ ) processes is hampered. Isotopic in-situ analyses of magmatic mineral cores may help to solve the problem of retrograde metamorphism; nevertheless I did not have access to such techniques.

## **Chapter II.**

# **“Magmatic / hydrothermal transition in IODP Hole 1256D”**



## II.1. Geological context

IODP Hole 1256D was recently drilled on the Cocos plate in a 15Ma old crust formed at the East Pacific Rise at superfast (full spreading rate > 20mm/year) spreading rate (Figure II-1; Teagle et al., 2006; Wilson et al., 2006). This drilling hole is of major relevance for this study as it is the first borehole which reached the sheeted dike / gabbro transition in an intact section of fast-spread oceanic crust (Figure II-2). The choice of superfast spread crust was motivated by the correlation between the depth of the melt lens and spreading rate (Figure I-7; Purdy et al., 1992; Phipps Morgan and Chen, 1993), hence the anticipation to reach the base of the sheeted dike at shallower depth (Wilson et al., 2006).

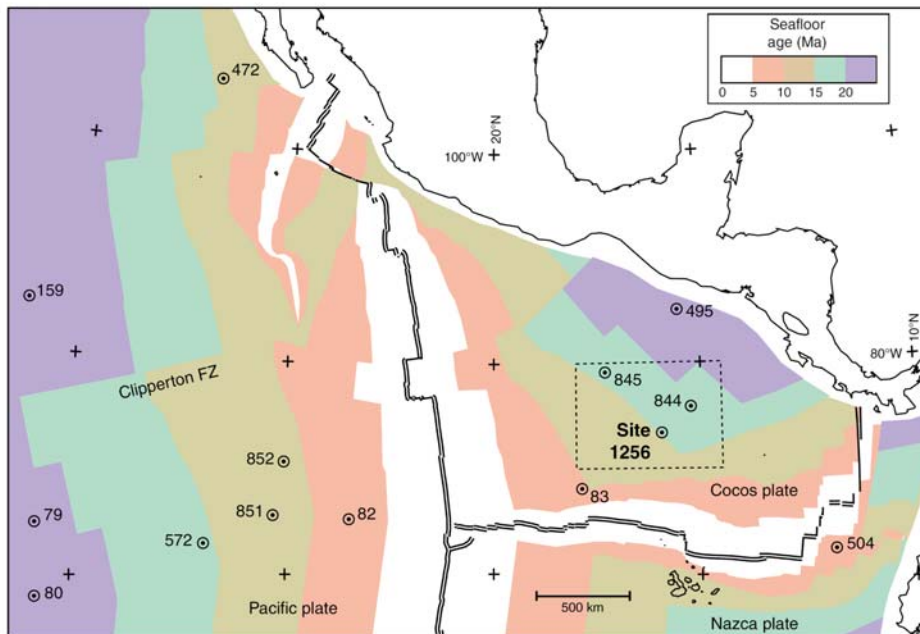


Figure II-1: Age map of the western Pacific seafloor (Teagle et al., 2006). IODP Site 1256 is located on the Cocos plate. Isochrons at 5 m.y. intervals are converted from magnetic anomaly identifications according to the timescale of Cande and Kent (1995). Other numbers correspond to earlier DSDP and ODP sites where the basement was drilled.

The uppermost part of the section recovered at Site 1256 is composed of ~100m lava interval (including a single flow ~75 m thick) that is considered to correspond to an off-axis lava pond (Wilson et al., 2006). In total, 284 m of sheeted and massive flow, and minor pillow flows are interpreted to correspond to off axis eruptions (Wilson et al., 2006). The sheeted and massive flow erupted at the ridge axis are then present from that depth down to 1004 mbsf (meters below sea floor; Figure II-2). 54 meters of mineralized breccias associated to subvertical intrusive contacts mark the transition zone to the relatively thin (~350 m thick) sheeted dike complex.

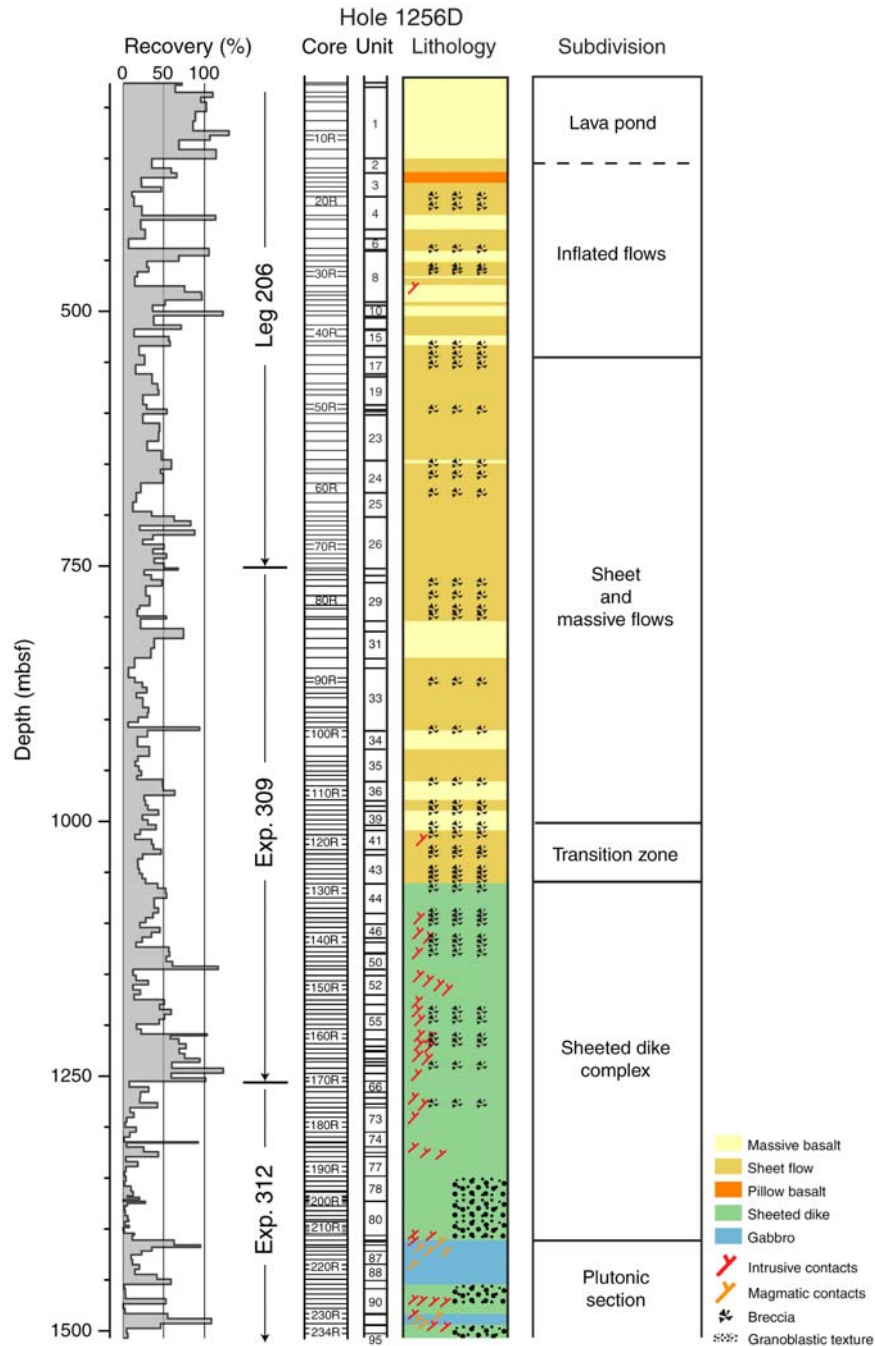


Figure II-2: Simplified igneous lithostratigraphy of IODP Core 1256D recovered during ODP Leg 206 and IODP Expeditions 309 and 312 (Teagle et al., 2006).

The sheeted dike complex is composed of massive basalts/diabases that locally display doleritic textures, and that are crosscut by subvertical dikes with brecciated and mineralized chilled margins. The alteration grade increases downhole from the lavas to the dikes. In lavas, alteration phases are mostly phyllosilicates and iron oxyhydroxides, attesting to temperatures < 150°C, whereas in dikes chlorite and other greenschist phases are observed indicating temperatures > 250°C. Downhole, in the sheeted dikes, the alteration intensity increases. Actinolite is the major alteration phase and is associated with magnesiohornblende, indicating

temperatures close to 400°C. In the lowermost dikes (from 1348 to 1407 mbsf), dikes are partially to pervasively recrystallized to granoblastic textures composed of plagioclase, clinopyroxene, orthopyroxene, oxides, and amphiboles that are interpreted to result from contact metamorphism (Wilson et al., 2006). A detailed petrological study of these granoblastic microgabbro dikes is proposed in Koepke et al. (2008). The base of the granoblastic microgabbro dikes is crosscut by a trondhjemitic dikelet (20 mm wide), and a quartz oxide diorite is described in the uppermost gabbros. At 1407 mbsf, the first gabbros are encountered (=1157 meters sub-basement [msb]=mbsf-sediment thickness); they intrude the granoblastic microgabbro dikes (Teagle et al., 2006). The gabbro horizon is complex and contains various gabbros types (gabbro, oxide-gabbros, olivine-gabbro, gabbro) of variable grain sizes (fine, medium and coarse grained), some xenoliths of granoblastic microgabbro representing recrystallized dikes, and a ~ 24 m thick screen of granoblastic microgabbro dikes (Wilson et al., 2006). The lowermost recovered sample is a diabase, presumably a dike, which displays a doleritic texture and contains actinolite and Ti-augite; it is interpreted as a late off axis dike (Wilson et al., 2006).

Below are described the granoblastic microgabbro dikes petrology (also described in Koepke et al., 2008), the gabbro horizon petrology, and the mineral compositions of these rocks. These data are compared with observations and data from the Oman ophiolite, and discussed in Chapter III.

## ***II.2. Petrology of the granoblastic microgabbro dikes and gabbros***

I describe hereafter the IODP Hole 1256D samples studied during this work. The Sheeted dikes / gabbro transition zone, down to the bottom of Hole 1256D, may be subdivided in 8 zones (Figure II-3):

- *zone 1* corresponds to the sheeted dike complex,
- *zone 2* corresponds to the granoblastic microgabbro dikes (~60 m thick),
- *zone 3* is the upper part of the gabbros, which display white patches (~5 m thick),
- *zone 4* is an interval that shows a close association of fine and coarse grained gabbros (~45 m thick); zones 3 and 4 correspond to the gabbro 1 interval in Wilson et al. (2006),
- *zone 5* is the granoblastic microgabbro horizon (24 m thick) interpreted as a screen of granoblastic microgabbro dikes (Wilson et al., 2006),

- zone 6 is the second gabbro section (~15 m thick),
- zone 7 correspond to the lower granoblastic microgabbronorites (lower dike screen after Wilson),
- zone 8 is the lowermost diabase, interpreted as an off-axis dike (Wilson et al., 2006).

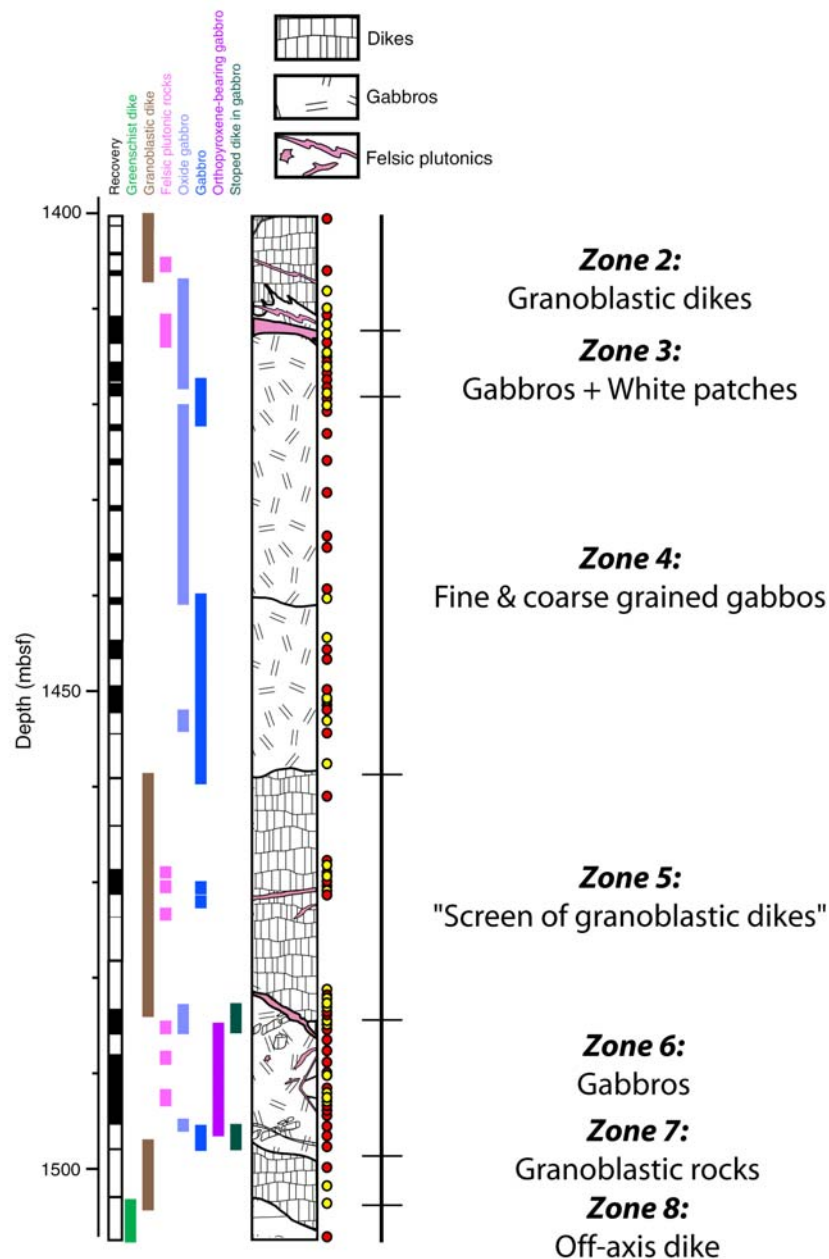


Figure II-3: Schematic lithostratigraphy of the bottom section of IODP Hole 1256D (after Teagle et al., 2006). Yellow and red dots indicate the locations of the studied samples (red: shipboard samples *C. Laverne* and *B. Ildefonse*; yellow: samples collected in College Station in August 2007).

The sheeted-dike complex displays in general an intergranular, doleritic texture, and contains various alteration phases such as actinolite (Figure II-4a); sub-vertical chilled margins are observed in some samples.

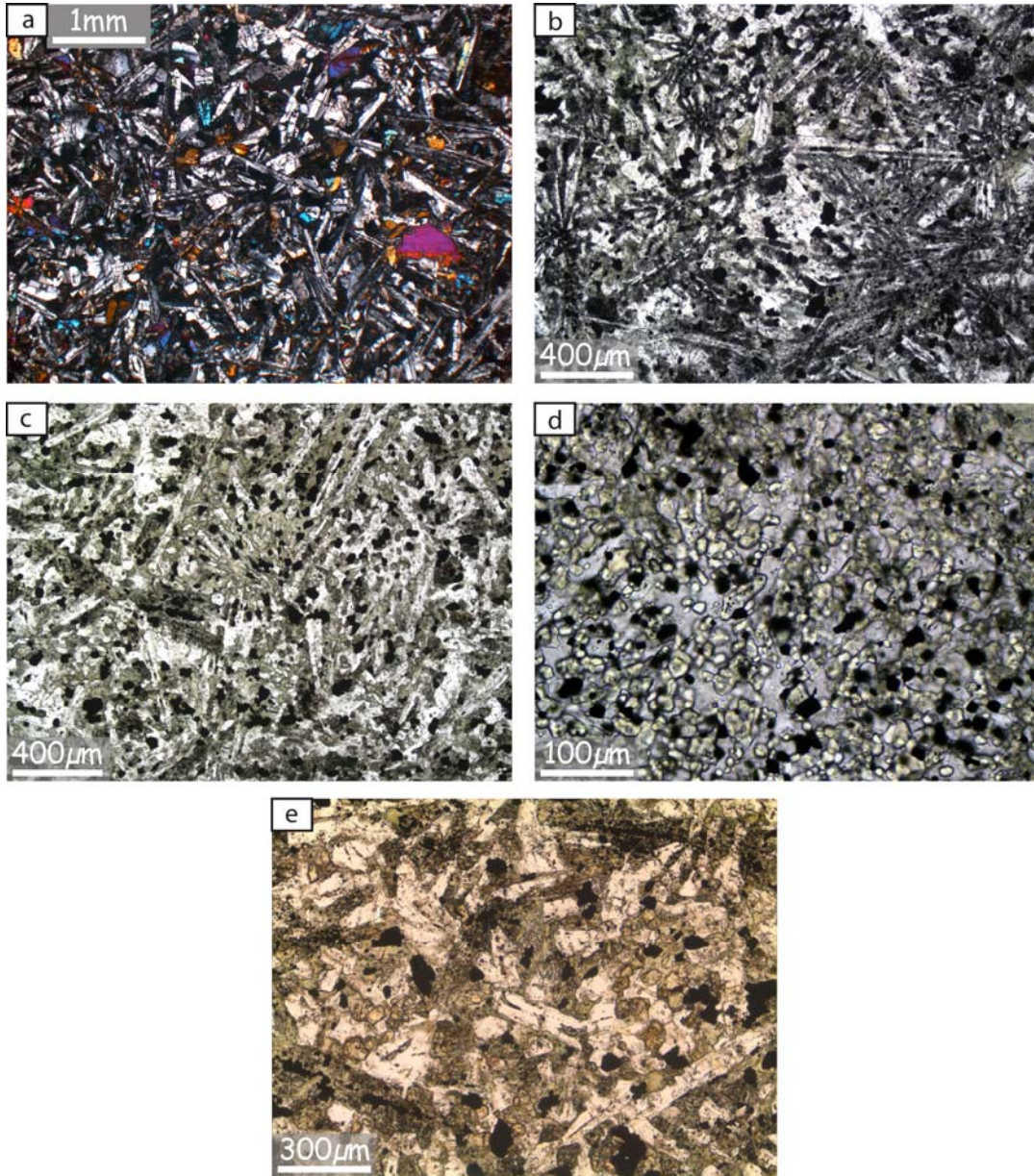


Figure II-4: Microphotographs of IODP Hole 1256D sheeted dike samples. a) diabase (zone 1; sample 176R-2\_3-7 (where 176 represents the core number, R2 the section number, 3 the top position in cm and 7 the bottom position in cm); cross-polarized light); b) weakly recrystallization in diabase ~150 m above the contact with gabbros (zone 1; sample 173R-2\_6-10; plane-polarized light); c) Stronger granoblastic recrystallization ~38 m above the contact with gabbros (zone 2, sample 198R-1\_45-49; plane-polarized light); d) Strong granoblastic recrystallization ~25 m above the contact with gabbros (zone 2, sample 205R-1\_10-14; plane-polarized light); e) Coarser grained recrystallized texture close to the contact with gabbro (~10 m above the contact), small pink granular grains are orthopyroxene (zone 2, sample 209R-1\_17-19; plane-polarized light). Microphotographs b-d are from IODP database (Teagle et al., 2006).



The granoblastic microgabbro dikes display a fine-grained recrystallized texture with increasing recrystallization downsection (Figure II-4b-d; Koepke et al., 2008). However, close to the base of the sheeted dike, some samples display coarser grained texture and seem to be less recrystallized (Figure II-4e). Such less recrystallized meta-dikes, close to the sheeted dike / gabbro transition may be opposed to the model in which the recrystallization is linked to a contact metamorphism event with heat supplied from the bottom (Wilson et al., 2006; Koepke et al., 2008). However, these coarser grained dikes containing orthopyroxene are also recrystallized, and the grain size may instead represent lateral variations in single dikes, the center of dikes being coarser grained than the chilled margins. ~1-2 m above the base of the sheeted dike complex, a small trondhjemitic dikelet (20 mm wide) is observed (Figure II-5a), and may be interpreted as resulting from local anatexis at the base of the sheeted dike complex (Koepke et al., 2008).

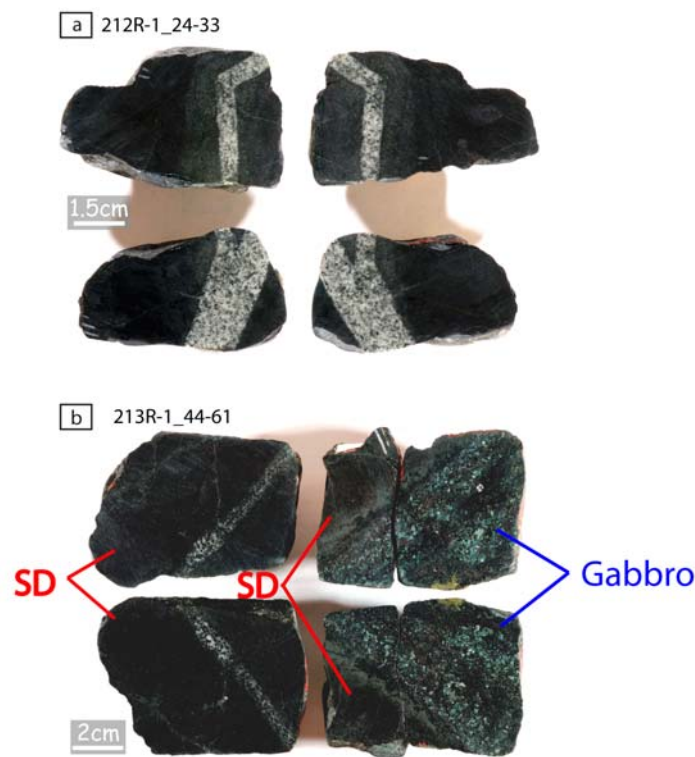


Figure II-5: Photographs of cores from IODP Hole 1256D (images are from the data base of Expedition 312 in Teagle et al., 2006). a) Trondhjemitic intrusion in the granoblastic microgabbro dikes close to the sheeted dike complex / gabbro transition (sample 212R-1\_24-33); b) Gabbroic dikelet (left pieces) in a granoblastic microgabbro dike ~4 cm above the contact with the first recovered gabbro (right pieces, sample 213R-1\_44-61).

The contact between the sheeted dike complex and gabbro (1407 mbsf) is sharp (Figure II-5b), and the grain size decreases in the gabbro toward the contact (Figure II-6), indicating the intrusive nature of the gabbro. This gabbro is composed of plagioclase (1-2 mm), heterogranular clinopyroxene (1-5 mm), oxides, actinolite, and locally olivine (Figure II-7a). 2-3 cm below the sheeted dike / gabbro contact, a small xenolith of granoblastic microgabbro is observed (Figure II-8a). Less than two meters below the contact, a quartz oxide diorite intrusion is observed. It is composed of primary and secondary amphibole (actinolite, and magnesiohornblende), plagioclase, quartz, ilmenite, magnetite and apatite, rutile, and sphene traces (Figure II-7b). Its whole rock composition (Teagle et al., 2006) is characteristic of evolved MORB obtained in differentiation experiments performed in a Fe-Ti MORB system (experiment Fe-21 in Toplis & Carroll, 1995).



Figure II-6: Whole thin section microphotograph (sample 213R-1\_52-55; cross-polarized light). The sample displays the contact between granoblastic microgabbro dikes and the first encountered gabbro. Note the decreasing grain size in the gabbro toward the contact.

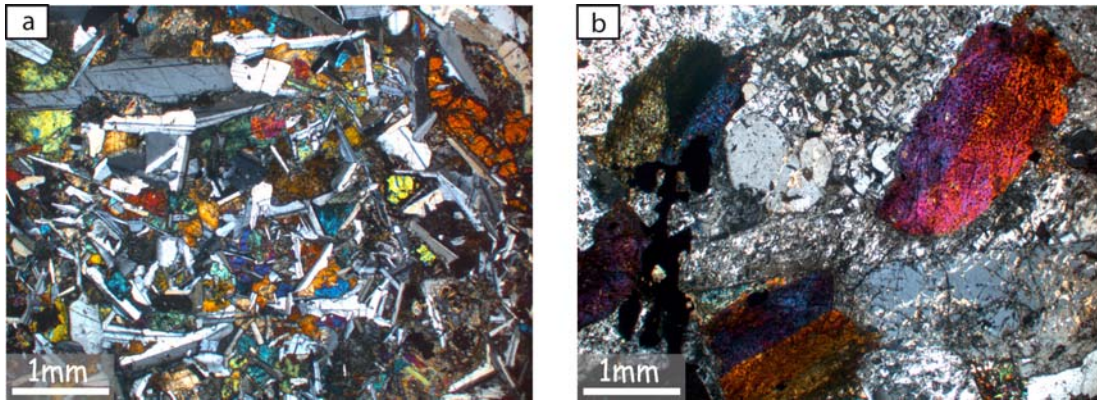


Figure II-7: Microphotographs of the upper plutonic rocks. a) First gabbro encountered below the contact with granoblastic microgabbro dikes (zone 3, sample 214R-1\_24-26; cross-polarized light). Minerals are plagioclase, clinopyroxene, oxides, olivine, and secondary actinolite. b) Quartz-oxide-diorite present in the plutonic rocks less than two meters below the contact with the recrystallized sheeted dike complex (zone 3, sample 214R-1\_43-47; cross-polarized light). Minerals primary and secondary amphibole (actinolite and magnesiohornblende), intergrowths of plagioclase and quartz, ilmenite, magnetite and some traces of apatite.

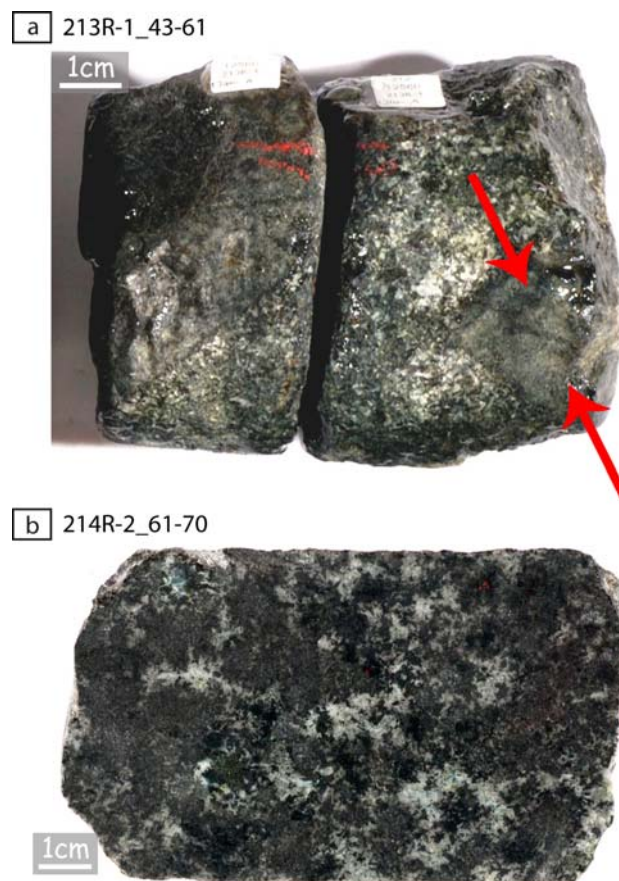


Figure II-8: Photographs of gabbro cores IODP Hole 1256D (images are from the data base of Expedition 312 in Teagle et al., 2006). a) Sharp contact between the granoblastic microgabbro dikes and the underlying gabbros; a xenolith with diffuse margins is present in the gabbros (red arrows; sample 213R-1\_43-61); b) Typical gabbro with white patches from zone 3. The white domains are highly altered zones (see text for further details; sample 214R-2\_61-70).

Below the quartz oxide diorite, gabbros (zone 3) display white patches that can make up to 35 % of the whole rock (Figure II-8b). These white patches are composed of actinolite, plagioclase, prehnite and pumpellyite and sometimes quartz (Figure II-9a), whereas the dark areas are gabbroic and composed of plagioclase (0.4 to 2 mm), large poikilitic clinopyroxene (up to 1.5 cm), ilmenite, magnetite, and rare olivine (Figure II-9b). Teagle et al. (2006) proposed that the white areas represent a second magmatic episode (an evolved melt composition is required to account for the assemblage plagioclase + quartz). However, these zones do not display sharp contacts with the surrounding gabbro and are more strongly altered at low temperature than the surrounding gabbros (presence of prehnite and pumpellyite; Figure II-9a). In gabbro hand specimens of ophiolites and oceanic crust, white color of plagioclases is usually associated to a high grade of low temperature alteration. A low temperature alteration overprinting the plagioclase rich zones representing a second magmatic episode (Teagle et al., 2006) is therefore expected for the white patches of zone 3. The white patches disappear progressively downward and the transition to zone 4 is not well defined.

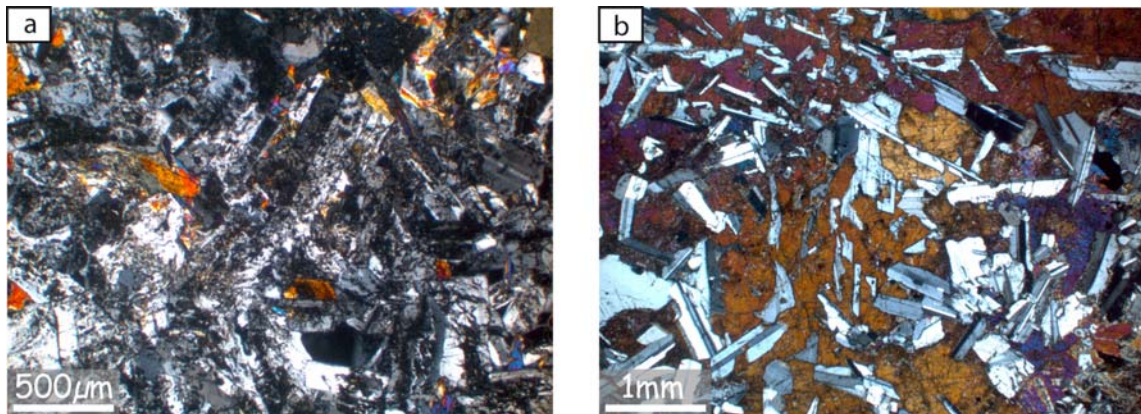
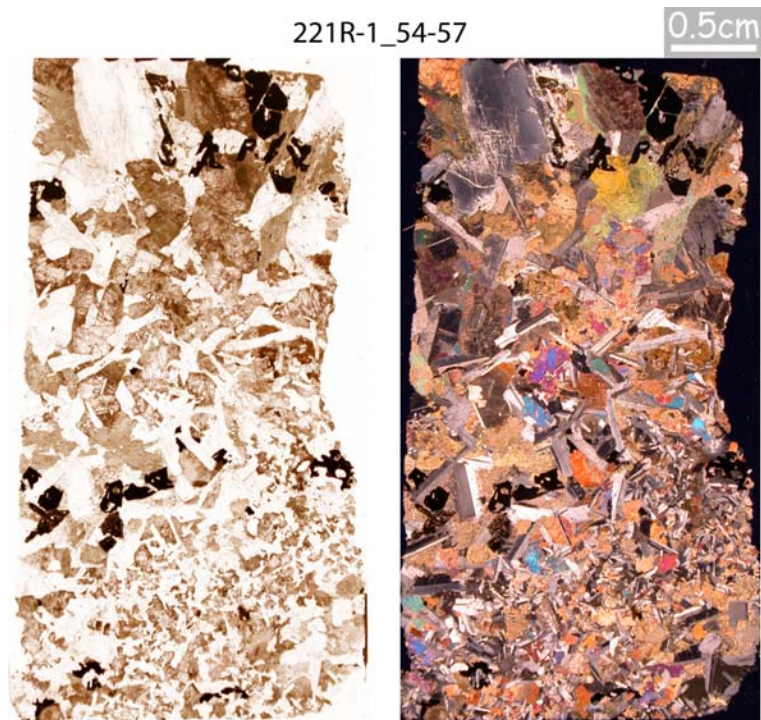


Figure II-9: Microphotographs (cross-polarized light) of sample 215R-1\_20-23 from zone 3 (gabbro with white patches). a) White patches domains composed of plagioclase, prehnite, pumpellyite, actinolite and sometimes quartz; b) gabbro is composed of plagioclase, poecilitic-clinopyroxene, ilmenite, magnetite and rare olivine.

Zone 4 is composed of varytextured gabbros (Figure II-10); some are fine grained (1-3 mm) and others coarse grained (0.5-1 cm). The coarse grained gabbros represent less than 30 % of zone 4 and the contact between fine- and coarse-grained gabbros is usually diffuse (Figure II-11).



*Figure II-10: Photograph of core 223R-2\_43-55 from IODP Hole 1256D (zone 4). Fine and coarse grained gabbroic domains are observed (image is from the data base of Expedition 312 in Teagle et al., 2006).*



*Figure II-11: Whole thin section microphotograph of sample 221R-1\_54-57 (zone 4; left: plane-polarized light; right: cross-polarized light). The transition from fine grained gabbro to coarse grained gabbro is continuous.*

The fine-grained gabbro is composed of plagioclase, slightly poikilitic clinopyroxene, oxides and rare olivine that can be associated to orthopyroxene close to coarser grained domains (Figure II-12a). Coarse grained areas are composed of plagioclase, orthopyroxene, clinopyroxene and oxides (Figure II-12b). Sparse, centimeter sized xenoliths of granoblastic microgabbro are observed in the lowermost few meters of zone 4; these xenoliths are similar to zone 5 (see below) and rimmed by coarse-grained gabbro. The lowermost sample of zone 4 (sample 224R-1\_7-9) is composite and contains domains with poikilitic clinopyroxene

associated with plagioclase and secondary amphiboles (actinolite, and magnesiohornblende), and domains with quartz and plagioclases intergrowths associated with oxides and apatite (Figure II-12c-d).

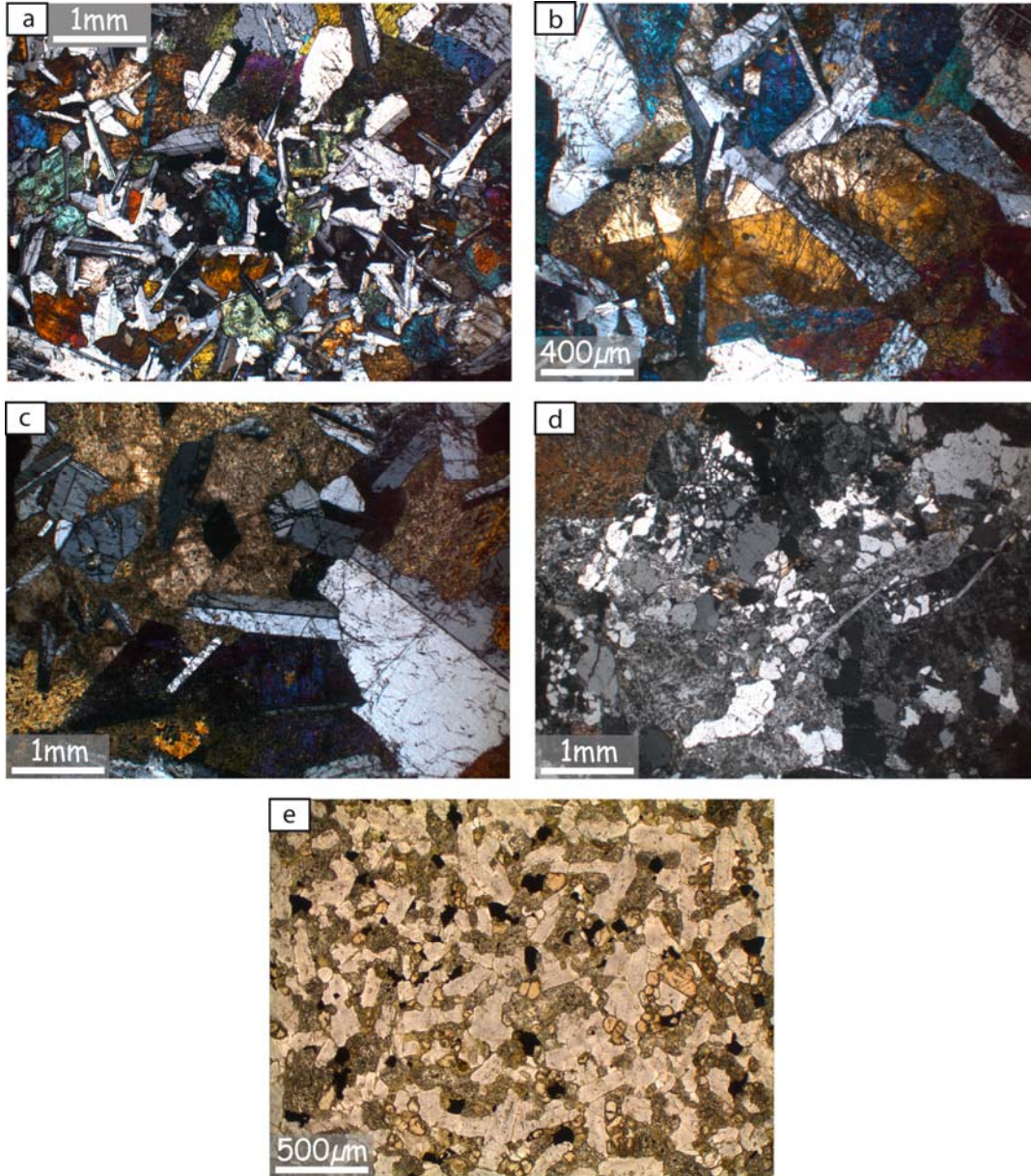


Figure II-12: Microphotographs of IODP Hole 1256D samples. a) Fine-grained gabbro from zone 4 composed of plagioclase, clinopyroxene, oxides, secondary actinolite and rare olivine (not visible on picture; cross-polarized light; sample 218R-1\_46-49); b) coarse-grained gabbro from zone 4 composed of plagioclase, clinopyroxene, secondary actinolite and rare orthopyroxene (not visible on picture; cross-polarized light; sample 220R-1\_18-18); c) domain with poikilitic clinopyroxene in the lowermost sample of zone 4 (cross-polarized light, sample 224R-1\_7-9); d) domain with quartz-plagioclase intergrowths associated to oxide and apatite in the lowermost sample of zone 4 (cross-polarized light, sample 224R-1\_7-9); e) granoblastic microgabbro sample from zone 5 composed of plagioclase, clinopyroxene, orthopyroxene (pink), oxides, and secondary actinolite (plane-polarized light, sample 227R-1\_30-34).

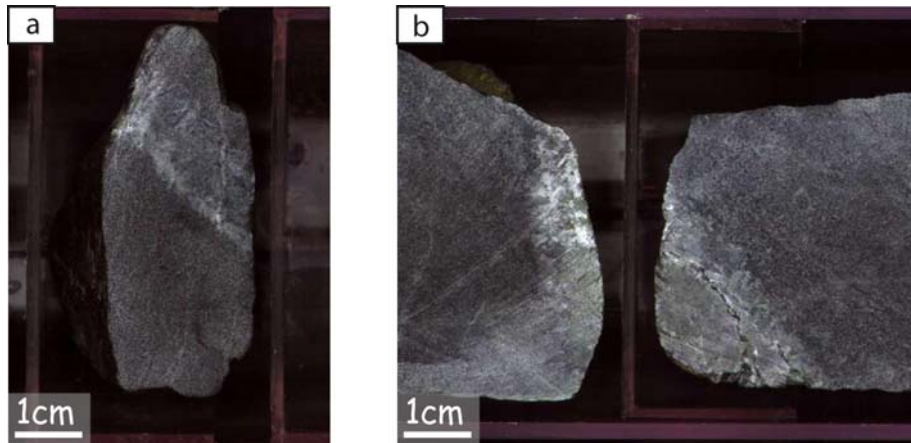


Figure II-13: Photographs of cores from IODP Hole 1256D displaying leucocratic intrusions within the “screen of granoblastic microgabbro dikes” (zone 5; images are from the data base of Expedition 312 in Teagle et al., 2006). a) Sharp contact (Sample 227R-1\_12-15); b), diffuse contact (sample 227R-2\_8-17).

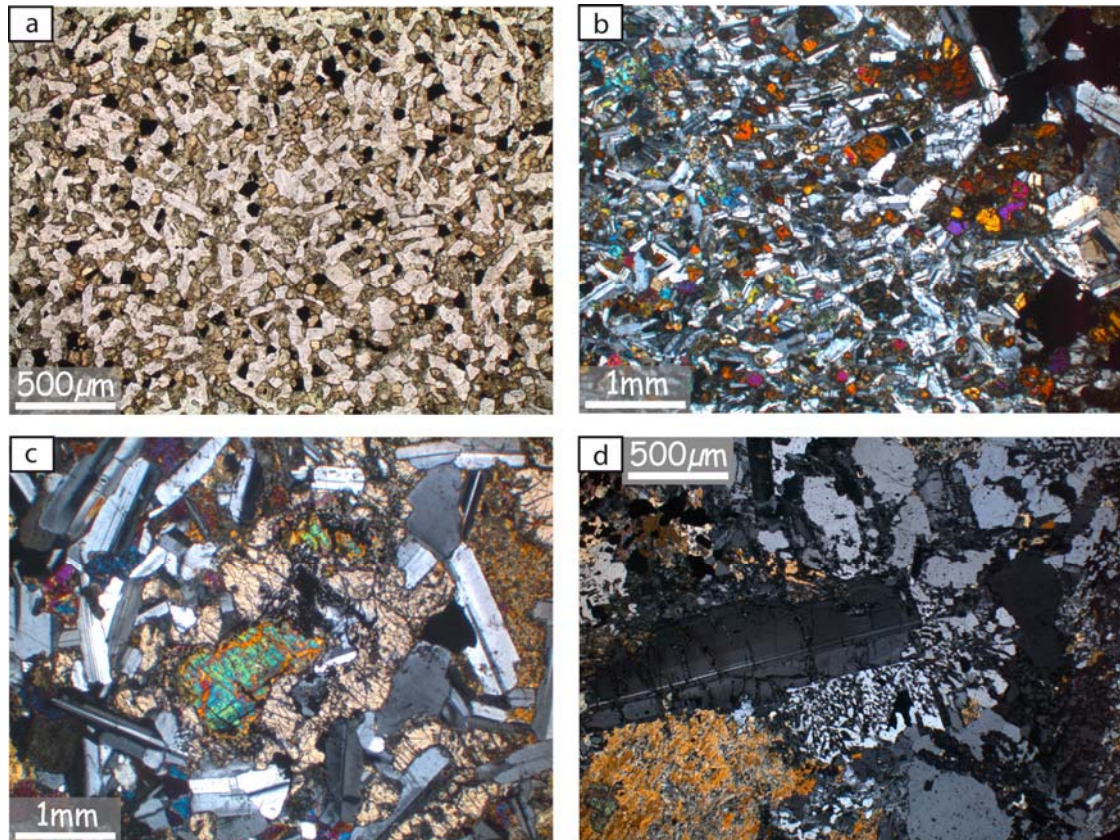


Figure II-14: Microphotographs of samples from the bottom of IODP Hole 1256D. a) Granoblastic texture in a microgabbro xenolith from a gabbro in zone 6 (plane-polarized light, sample 230R-1\_87-90); b) preferential orientation of plagioclases in a microgabbro xenolith from a gabbro in zone 6, the preferential orientation is nearly orthogonal to the contact with the host gabbro (cross-polarized light, sample 230R-1\_15-20); c) altered olivine rimmed by orthopyroxene in a gabbro in zone 6 (cross-polarized light, sample 232R-1\_82-85); d) lowermost sample in zone 6 displaying gabbroic assemblage with plagioclase and clinopyroxene associated to intergrowth of quartz-plagioclase (cross-polarized light, sample 232R-2\_98-100).

Zone 5 is composed of granoblastic microgabbronorites with grain size, similar to the coarser granoblastic microgabbronorite dikes in zone 2 (Figure II-12e). The main paragenesis is plagioclase, clinopyroxene, orthopyroxene, ilmenite, magnetite, secondary amphibole (actinolite, and magnesiohornblende), and rare quartz; inclusions of apatite in orthopyroxene have been observed in one sample. Several leucocratic intrusions of coarser grained material are observed (Figure II-13). The granoblastic microgabbronorite / leucocratic intrusion contact is either sharp (Figure II-13a) or diffuse but without any change in grain size (Figure II-13b). The recovery is very low (< 30%) in zone 5.

Zone 6 is composed of gabbro, which contains several xenoliths of granoblastic microgabbronorite that are similar to those in zone 5 (Figure II-14a). Some of the xenolith contain abundant orthopyroxene, one is noritic (plagioclase + orthopyroxene), and one displays a strong shape preferred orientation of plagioclases that forms a large angle with the gabbro contact (Figure II-14b). One xenolith contains olivine that is rimmed by orthopyroxene and inverse zoning in plagioclase (Figure II-15); this peculiar sample is discussed in section II.3. The gabbro (grain-size 1-4 mm) is composed of plagioclase, heterogranular to pseudo-poikilitic clinopyroxene, usually orthopyroxene and rare olivine that is mostly decomposed to a phyllosilicate assemblage (Figure II-14c); olivine or its alteration products is locally rimmed by orthopyroxene (Figure II-14c). The deepest sample in zone 6 (232R-2\_98-100) is composite, with gabbroic domains and domains of quartz-plagioclase intergrowths coexisting with primary amphibole mostly altered to actinolite (Figure II-14d).

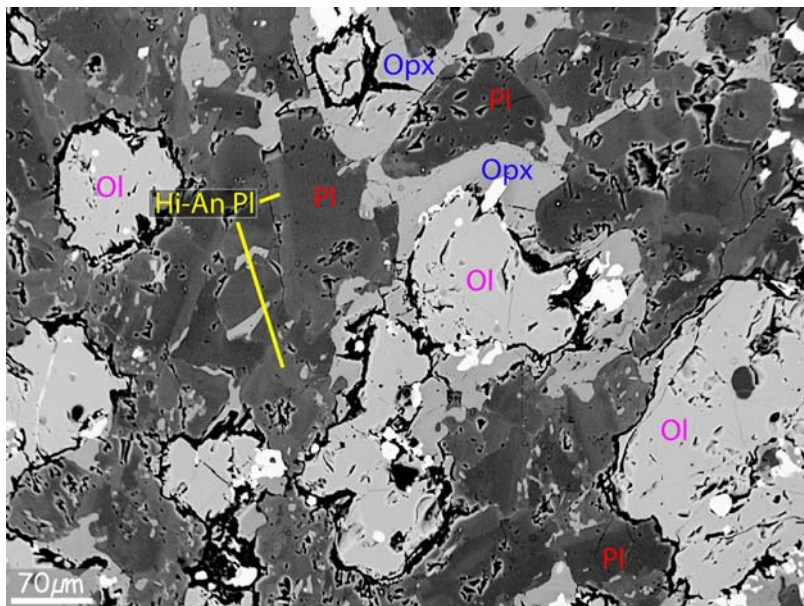


Figure II-15: Backscattered electron image of a xenolith of granoblastic olivine-microgabbronorite of zone 6 (sample 232R-1\_82-85). Ol: olivine; Opx: orthopyroxene; Pl: plagioclase; Hi-An Pl: plagioclase rims that are brighter on the BSE image and that correspond to An-rich plagioclase (see section II.3).



The contact between zone 6 and zone 7 is not recovered. Zone 7 is poorly recovered (< 15%) and is composed of granoblastic microgabbro that is similar to xenoliths of zone 6. It is composed of plagioclase, clinopyroxene, orthopyroxene, ilmenite and magnetite (Figure II-16a).

The contact between zone 7 and zone 8 is not recovered. Zone 8 is diabase with intergranular texture composed of plagioclase, pink-Ti-augite and some rare oxides (Figure II-16b) not affected by granoblastic overprint.

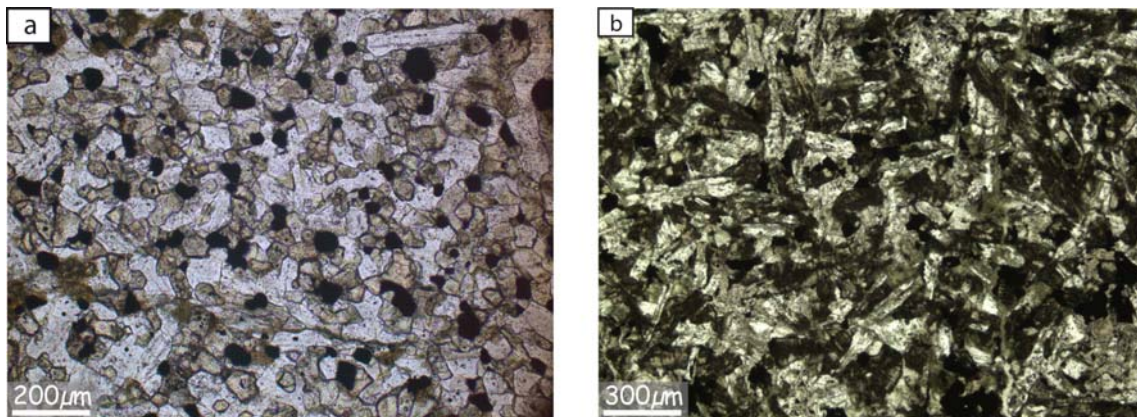


Figure II-16: Microphotographs of IODP Hole 1256D samples from zone 7 (a) and zone 8 (b). a) Granoblastic microgabbro composed of plagioclase, clinopyroxene, orthopyroxene and oxides assemblage (sample 234R-1\_7-9; plane-polarized light); b) late off-axis diabase composed of intergranular plagioclase, pink-Ti-augite and some rare oxides (sample 234R-1\_19-22; plane-polarized light).

### **II.3. Mineral major element compositions**

In-situ mineral major element compositions have been determined for minerals of all the described lithologies (Appendix B1; Figure II-17). Average mineral compositions of the lava pond, lava flows and sheeted dikes (Dziony et al., 2008) are given for comparison. Analyses have been performed at Géosciences Montpellier and at the Institut für Mineralogie, Hannover using a Cameca SX 100 electron microprobe equipped with 5 spectrometers and an operating system “Peak sight”. Data were acquired using a 15KV acceleration potential, a static (fixed) beam,  $K\alpha$  emission from all elements, and the “PAP” matrix correction (Pouchou and Pichoir, 1991) in Hannover or a modified matrix correction (Merlet, 1994) in Montpellier. Most element concentrations were obtained with a beam current of 15nA and a counting time of 10 to 120s on peak and background. In all samples, mineral cores have been analyzed, and except in the white patches areas of zone 3, mineral (cores) compositions are homogeneous and averages are used in the text below.

Plagioclase compositions range from An<sub>41</sub> in diorite (between zone 4 and zone 5) to An<sub>70</sub> in fine-grained olivine-gabbro (zone 4) (Figure II-17a). Plagioclase An contents in gabbros are in average higher than plagioclase An content in granoblastic microgabbro norites from zones 2, 5, 6, and 7. One gabbro sample from zone 6 has plagioclase An contents similar to the ones of granoblastic microgabbro norites, this gabbro is in contact with a xenolith (sample 230R-1\_118-121). In granoblastic microgabbro norite dikes, plagioclase An content is in average slightly lower than the one plagioclases of sheeted dike complex, lava flow and lava pond. No correlation is observed between the plagioclase An content and the plagioclase FeO<sub>t</sub> contents (Figure II-17a; and see Appendix A3 for a discussion on the iron content of plagioclases). The large heterogeneity in composition of plagioclases of the white patches areas (with An content ranging from 14 to 59) is attributed, first to initial plagioclases with lower An content than in the surrounding gabbro (cf. the “second magmatic episode” of Teagle et al., 2006), and second to various degrees of plagioclase albitisation during hydrothermal alteration.

Clinopyroxene is Ti-augite in the off-axis dolerite of zone 8 and augite in all other samples. Clinopyroxene Mg# ( $Mg\# = Mg/[Mg+Fe]$  in molar proportions) ranges from 61 in zone 8 to 83 in coarse-grained gabbros in zone 4, and correlates roughly with the An content of plagioclase (Figure II-17b). In Figure II-17b, dry and wet fractionation trends calculated with MELTS (Ghiorso and Sack, 1995) by Kvasnes et al. (2004) are shown; the studied samples are on average closer to the dry fractionation trends. Al<sub>2</sub>O<sub>3</sub> in clinopyroxene range from 0.46 wt% in a granoblastic microgabbro norite sample of zone 5 to 2.86 wt% in the lava flows and is roughly correlated to An content in plagioclase (Figure II-17c). On average, Al<sub>2</sub>O<sub>3</sub> in clinopyroxene from granoblastic microgabbro norites in zones 2, 5, 6, and 7 is lower than in clinopyroxene from gabbros in zone 3 and 4 and from basalt and diabase from lava pond, lava flows, sheeted dike, and zone 8 (Figure II-17c). The FeO<sub>t</sub> content of clinopyroxene is not correlated to the one of plagioclase (Figure II-17d), it may result from variations in the redox conditions during crystallization or subsequent reequilibration (Appendix A3). TiO<sub>2</sub> and Al<sub>2</sub>O<sub>3</sub> in clinopyroxene are correlated in granoblastic microgabbro norites from zones 2, 5, 6, and 7; most of the gabbro, lava pond, lava flow and sheeted dikes samples have clinopyroxenes slightly enriched in Al<sub>2</sub>O<sub>3</sub> (Figure II-17e). Clinopyroxene from one gabbro from zone 6 has low Al<sub>2</sub>O<sub>3</sub> content similar to the granoblastic microgabbro norites; it corresponds to the gabbro that is in contact with a xenolith (sample 230R-1\_118-121).

Orthopyroxene is enstatite in all samples; its Mg# range from 59 in zone 2 to 71 in coarse-grained gabbros in zone 4. It is correlated to the clinopyroxene Mg# (Figure II-17f).

Fo content of olivine present in fine-grained gabbro in zone 4 is 63-64.

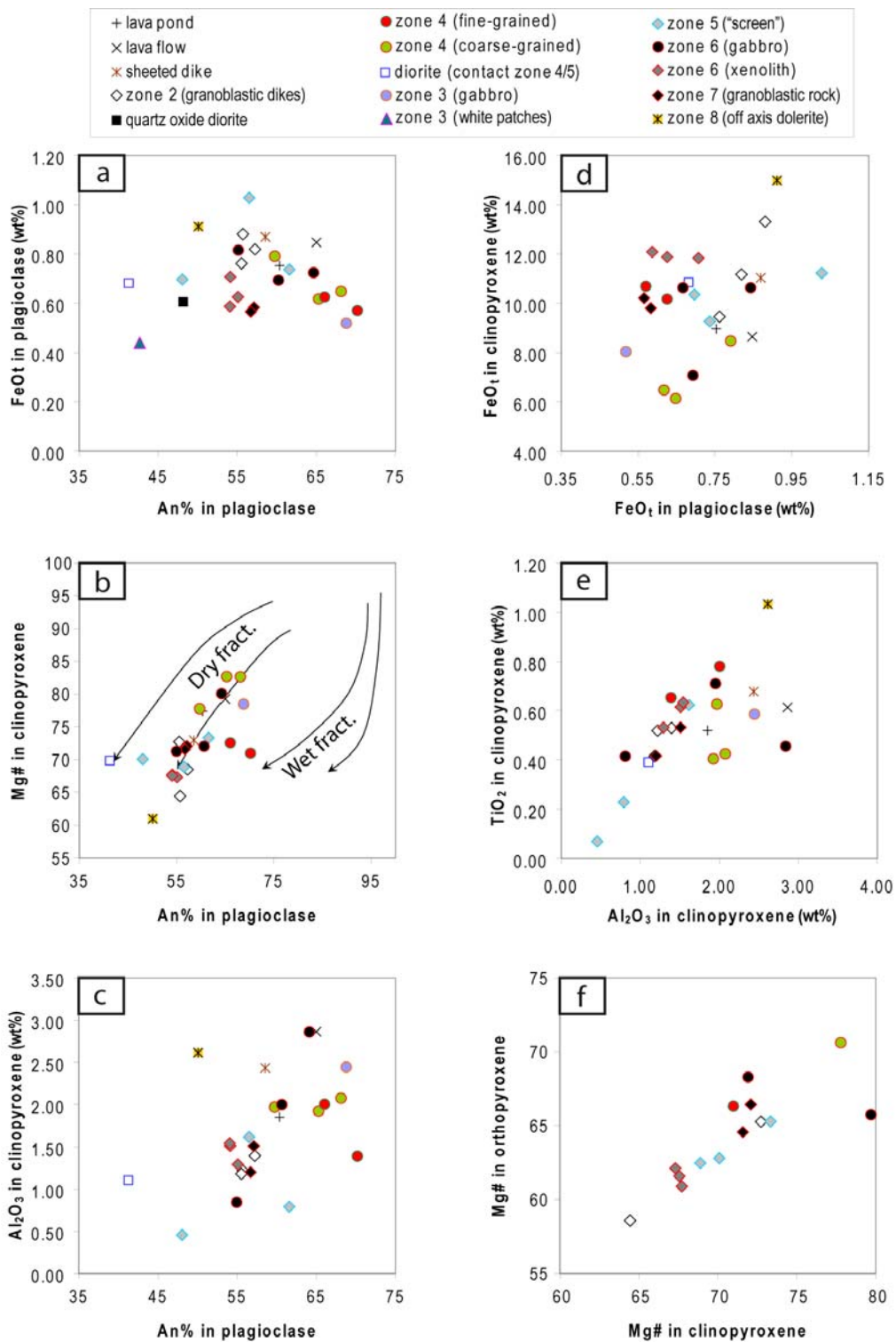


Figure II-17: Mineral compositions of samples from IODP Hole 1256D. a) FeO<sub>t</sub> (wt%) in plagioclase vs. An% in plagioclase; b) Mg# in clinopyroxene vs. An% in plagioclase; the dry and wet fractionation trends are from Kvassnes et al. (2004), and calculated using MELTS (Ghiorso and Sack, 1995); the two fractionation trends for the dry and wet case are calculated for two different starting compositions; c) Al<sub>2</sub>O<sub>3</sub> (wt%) in clinopyroxene vs. An% in plagioclase; d) FeO<sub>t</sub> (wt%) in clinopyroxene vs. FeO<sub>t</sub> (wt%) in plagioclase; e) TiO<sub>2</sub> (wt%) in clinopyroxene vs. Al<sub>2</sub>O<sub>3</sub> (wt%) in clinopyroxene; f) Mg# in orthopyroxene vs. Mg# in clinopyroxene.

In the xenolith of granoblastic olivine-microgabbro from zone 6 that contains olivine rimmed by orthopyroxene and plagioclase with inverse zonations in plagioclases (Figure II-15), olivine Fo content is 70. Plagioclase An content is lower in the grain cores (58) than in the grain margins (75). The association of orthopyroxene rims around olivine together with An-rich plagioclase margins may be interpreted as product of a hydrous partial melting event in this xenolith (Koepke et al., 2005a; 2005b).

Amphiboles are actinolites, and magnesiohornblendes (Figure II-18). Oxides are ilmenite, magnetite and titanomagnetite; the low TiO<sub>2</sub> content of magnetite in most of the samples attests to the low temperature equilibration and prevents the use of the 2-oxides thermo-oxybarometer (Sauerzapf et al., 2008). Calculations with magnetite and ilmenite are possible in the diorite sample close to the zone 4 / zone 5 transition (673°C;  $\Delta\text{NNO}=1.34$ ; where NNO is the Ni-NiO solid oxygen buffer equilibrium), in two xenoliths of zone 6 (612°C;  $\Delta\text{NNO}=2.66$  for sample 230R-1\_15-20, and 611°C;  $\Delta\text{NNO}=2.52$  for sample 230R-1\_87-90), and in one gabbro of zone 6 (620°C;  $\Delta\text{NNO}=2.46$  for sample 230R-2\_71-73). Titanomagnetite is present in the lava pond (904°C;  $\Delta\text{NNO}=-1.1$ ) and in granoblastic microgabbro dikes of zone 2 (851°C;  $\Delta\text{NNO}=0.75$ ). Obviously, the highly oxidizing conditions associated to temperatures that are characteristic of greenschist facies conditions constrain the conditions prevailing during the hydrothermal overprint of the samples. Redox conditions prevailing during the high temperature granoblastic overprint are probably closer to the value ( $\Delta\text{NNO}=0.75$ ) obtained at 851°C in the granoblastic microgabbro dikes from zone 2. Koepke et al. (2008) also show that highly oxidizing conditions ( $\Delta\text{NNO}$  varying from 2.6 to 3.3) are associated to low temperature equilibration (<650°C) in the granoblastic microgabbro dikes. In their study, only one granoblastic microgabbro is equilibrated at higher temperature (716°C) and as an intermediary redox value ( $\Delta\text{NNO}=1.7$ ); it is consistent with an increase of the redox conditions during the cooling.

Thermometry calculations are done using the amphibole-plagioclase thermometer (Holland and Blundy, 1994), the Ti in amphibole semiquantitative thermometer (Ernst and Liu, 1998) and the two-pyroxene thermometer (Andersen et al., 1993). The errors on these temperature estimates are  $\pm 35$ -40°C for the Holland and Blundy (1994) thermometer, are not estimated by Ernst and Liu (1998) for their semi-quantitative thermometer, and are indicated in the Table of Appendix B1 for the two-pyroxene thermometer. Temperature estimations performed with Ti in amphibole, and with the amphibole-plagioclase compositions are relatively coherent (Figure II-19a). They range between ~550°C and 890°C. Temperatures lower than 700°C are associated

to green magnesiohornblende and attest to the retrograde evolution of the rock. Temperatures obtained with the two-pyroxenes thermometer are significantly higher and ranges from ~950°C to ~1065°C (Figure II-19b).

The petrological and geochemical descriptions of IODP Hole 1256D presented herein, together with the article describing the root zone of the sheeted dike complex in the Oman ophiolite (Nicolas et al., 2008; Appendix A2), are used in the following chapters as a background for discussions.

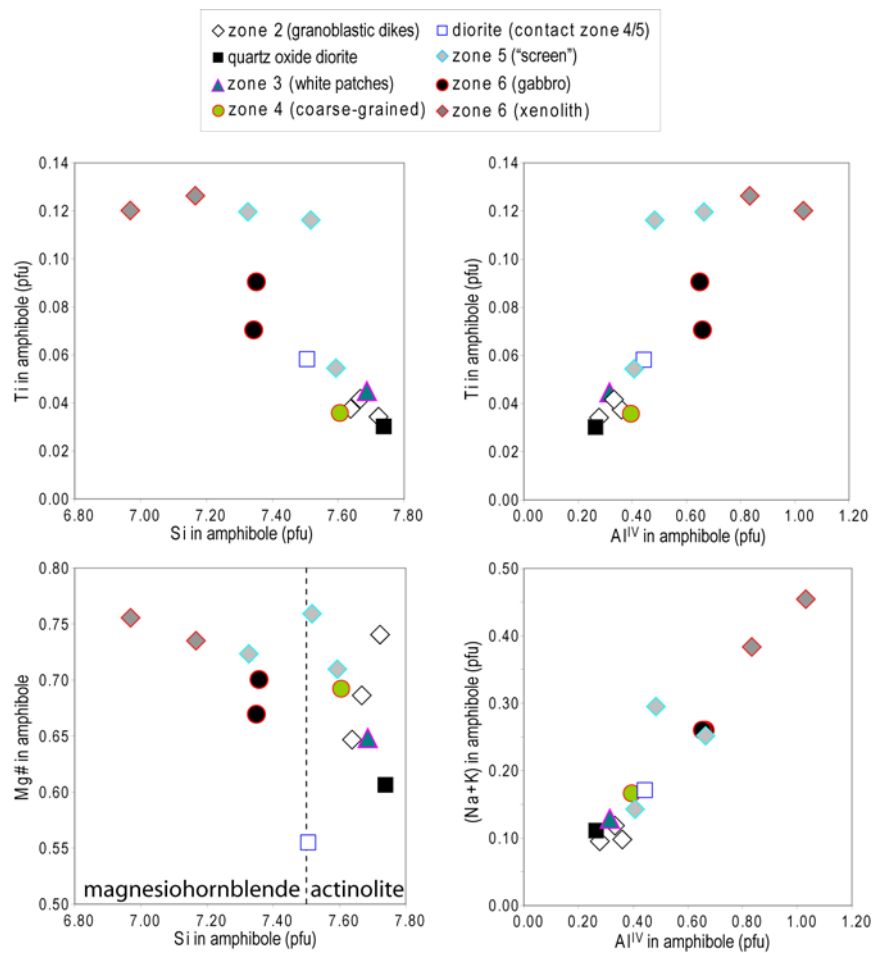


Figure II-18: Amphibole compositions in IODP Hole 1256D samples. pfu=per formula unit, Al<sup>IV</sup>=tetrahedral Al; same symbols as Figure II-17. No pargasite (amphiboles with [Na+K]>0.5) is observed.

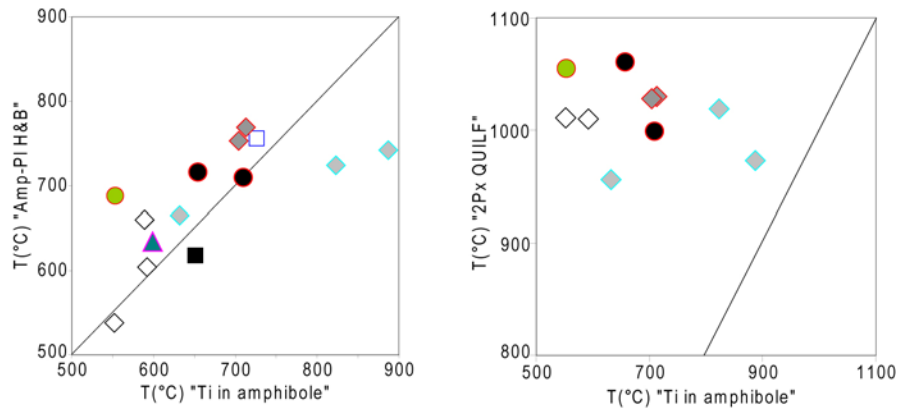


Figure II-19: Comparison of temperature estimations obtained with a) the amphibole-plagioclase thermometer (Holland and Blundy, 1994; "Amp-Pl H&B") and the Ti in amphibole semi-quantitative thermometer (Ernst and Liu, 1998; "Ti in amphibole"), and with b) the two-pyroxene thermometer (Andersen et al., 1993; "2Px QUILF") and the Ti in amphibole semi-quantitative thermometer (Ernst and Liu, 1998; "Ti in amphibole"). Black lines represent the 1:1 correlation.



## **Chapter III.**

# **“Magmatic / hydrothermal interactions in the Oman ophiolite”**





### **III.1. Visited areas**

The Cretaceous Oman ophiolite is regarded to present the best proxy of fast-spreading oceanic crust on land. Nevertheless controversial debates are on-going since decades, and questioned the mid-ocean ridge (MOR) versus supra-subduction zone (SSZ) initial setting (e.g., Warren et al., 2005; Boudier and Nicolas, 2007; Warren et al., 2007). Today, for most scientists at least part of the Oman ophiolite is regarded as subduction zone-related, but the nature of this subduction zone is still under controversial discussion. Many scientists believe that the subduction process is linked to the early stage of obduction (e.g., Boudier et al., 1988; Koepke et al., 2009), and is responsible for a second stage of magmatism (“V2” or “Lassai” lavas) following the major accretion of normal fast-spread crust (“V1” or “Geotimes” lavas). The main difference between lavas is that the "V2" lavas are interpreted as resulting of fluid-enhanced melting of previously depleted mantle, and contrast in composition with the "V1" lavas which resemble modern MORB (for details, and nomenclature of the lavas see Godard et al., 2003). The areas selected in this work are not notably affected by the late-stage magmatism (“V2”), thus the observed field record described here can be exclusively related to the primary magmatic processes of a “normal” fast-spreading ridge.

The Oman ophiolite represents an ideal complement to the detailed studies done on IODP cores related to fast-spread crust, as it provides spatial relationships in three dimensions that a single borehole does not offer. In order to relate the IODP Hole 1256D core in a 3D model, about ten areas along the 500 km long Oman ophiolite have been visited (Figure III-1). Among these, 3 areas where the outcrop continuity is best have been selected for detailed studies. These are located in the southern massifs (Gideah, Al Ahmadi Hills, and Aswad areas). Some peculiar samples from the isotropic gabbro horizon of the Rajmi area located in the northern massif will also be described in Chapter V (Figure III-1).

In all visited areas, the transition between the foliated gabbros and the sheeted dike complex has been examined. The main objective was to understand the structure and the organisation of the isotropic gabbro horizon, and its relations with the underlying foliated gabbros, and with the overlying sheeted dike complex. I present hereafter the different lithologies encountered and the relations observed in the visited areas. An evolutionary model is then presented using detailed mapping descriptions made in the Gideah area, in the Al Ahmadi Hills, and in the core recovered in IODP Hole 1256D; it is the topic of an article in press in *Geochemistry, Geophysics, and Geosystems* (France et al., 2009a). The outcome of this paper, a general model on the dynamics of the melt lens system and its key lithologies,

was applied to a third field target, the Aswad area, supporting the validity of the proposed model.

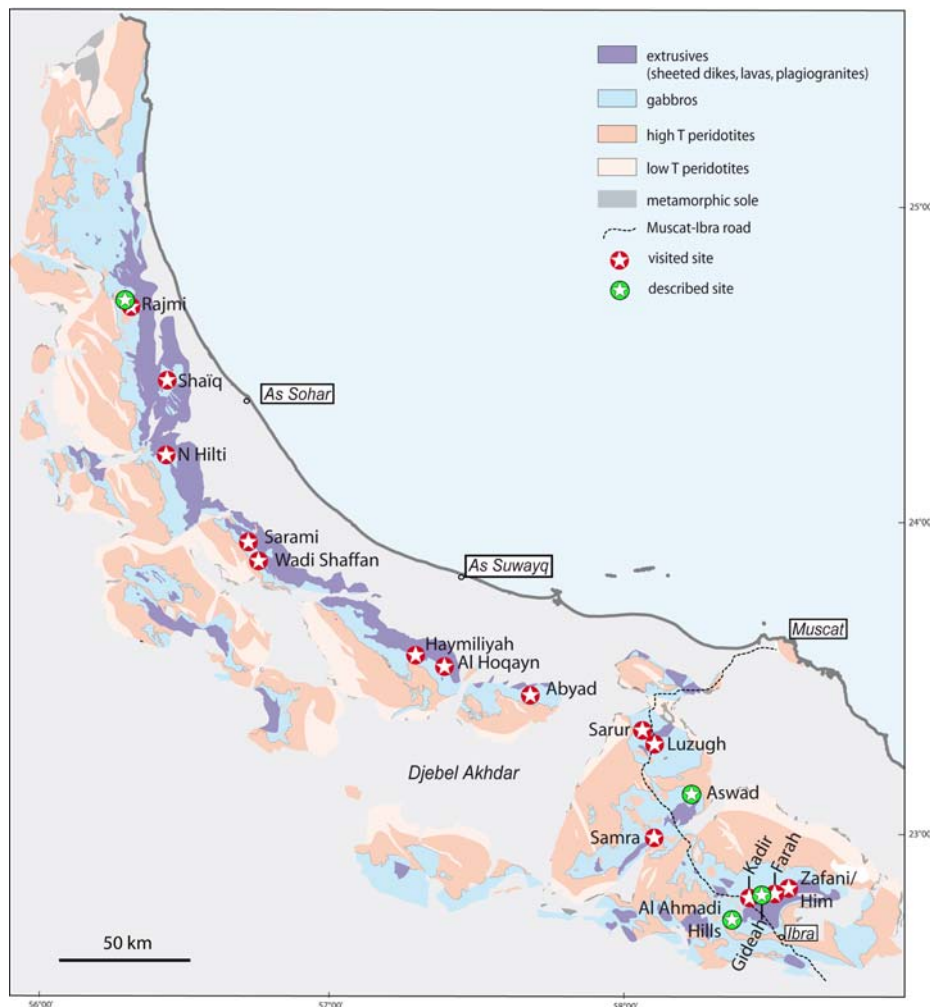


Figure III-1: Simplified geological map of the Oman ophiolite and location of the visited and described sites (after Nicolas et al., 2000).

### III.2. Lithostatigraphy

I describe hereafter the main lithologies encountered in various cross-sections, from the sheeted dike complex to the foliated gabbros.

The sheeted dike complex is typically composed of ~1 to 1.5 meters wide dikes intruding each others (Figure III-2), with chilled margins. From the chilled margins toward the dike interior, the texture progressively becomes intergranular, doleritic in the dike centers (Figure III-3). Samples are in general strongly hydrothermally altered, as attested by abundant actinolites and chlorites.



Figure III-2: Classical sheeted dike complex in the Oman ophiolite (Hilti massif).

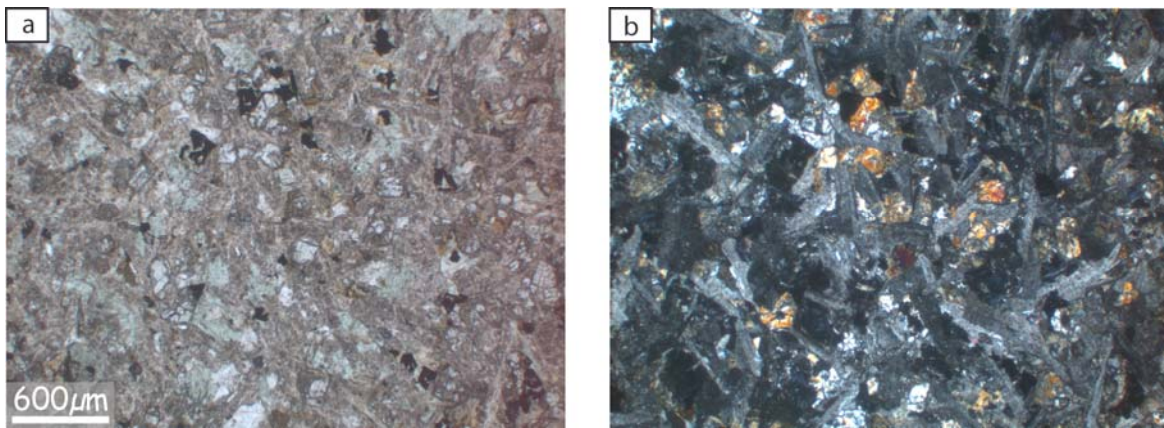
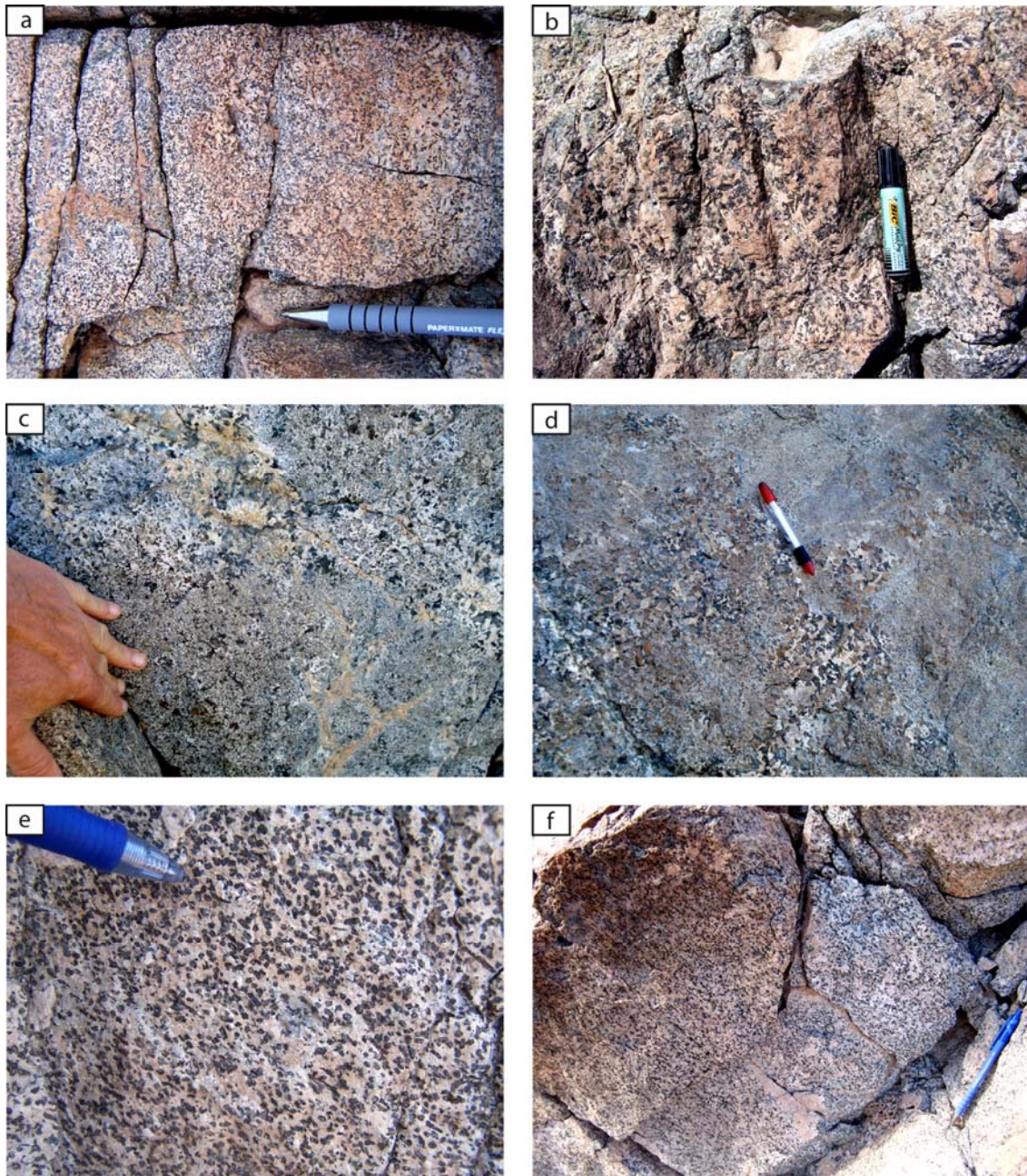


Figure III-3: Microphotographs of an Oman sheeted dike sample (Al Ahmadi Ridge area; sample 07OL01a) composed of plagioclase, clinopyroxene, actinolite, chlorite, and oxides. a) plane-polarized light; b) cross-polarized light.

Below the sheeted dike complex is the isotropic gabbro horizon, also named “varytextured gabbros” (e.g., MacLeod and Yaouancq, 2000). This horizon is approximately 100 meters thick and is mainly composed of isotropic fine-grained ophitic gabbros (Figure III-4a). These are composed of plagioclase, clinopyroxene, and locally amphibole (Figure III-5a-b). Coarser-grained isotropic gabbros are locally present in the varytextured gabbro horizon (Figure III-4b); they are 10 centimeters to a few meters large domains, and can be mingled with fine-grained gabbros (Figure III-4c-d). Coarse-grained gabbros are composed of plagioclase, clinopyroxene, amphibole, and locally orthopyroxene (Figure III-5c-d). They are commonly associated to xenoliths consisting of microgranular gabbros with well equilibrated textures that are frequently observed in the isotropic gabbro horizon (Figure III-6a; Figure III-7). These are composed of plagioclase, clinopyroxene, orthopyroxene, oxide, and secondary amphiboles; Figure III-7)



*Figure III-4: Various gabbro facies underlying the sheeted dike complex: a) fine-grained isotropic ophitic gabbro (Wadi Gideah area); b) coarse-grained isotropic ophitic gabbro (Al Ahmadi Hills area); c-d) heterogeneous, fine- and coarse-grained isotropic gabbro (Wadi Abyad); e-f) foliated granular gabbro (Aswad area).*

Microgabbro xenoliths with well equilibrated textures are observed at all levels in the isotropic gabbro horizon, but are commonly concentrated close to the transition with the sheeted dike complex and close to the transition with the foliated gabbros (Figure III-6). Magmatic breccias with a plagiogranitic, dioritic or gabbroic matrix and microgranular xenoliths of gabbro with well equilibrated textures are locally observed (Figure III-6), and are frequently located close to the sheeted dike complex base.

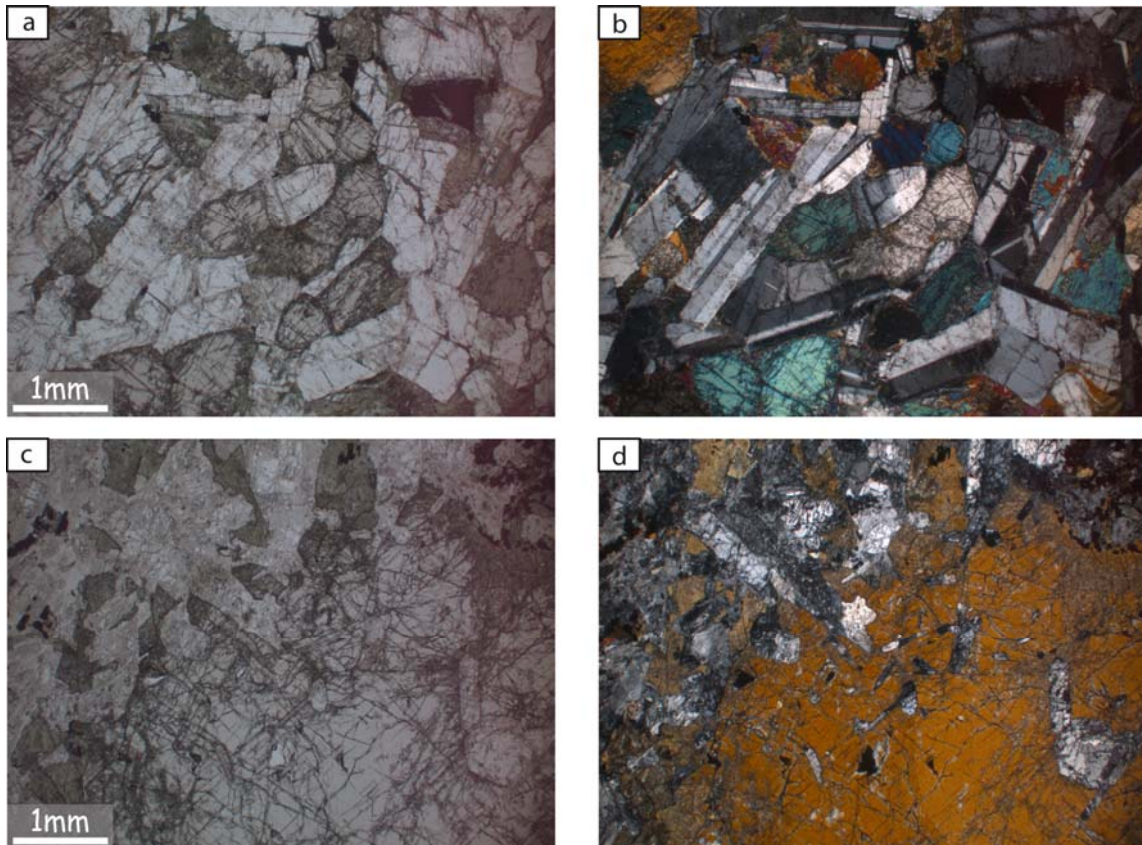


*Figure III-5: Microphotographs of Oman fine-grained (a-b), and coarse grained (c-d) isotropic gabbros. a-b) fine-grained isotropic gabbros are composed of plagioclase, clinopyroxene, oxides; this rock also contains locally amphibole and olivine which are not visible in the picture (Sarur area; sample 07OL15); c-d) coarse-grained isotropic gabbros are composed of plagioclase, clinopyroxene; this rock also contains amphibole, and locally orthopyroxene which are not visible in the picture (Sarami area; sample 07OL26a). a, c) plane-polarized light; b, d) cross-polarized light.*

About 100-200 meters below the base of the sheeted dike complex, gabbros grade to more granular textures and are foliated (Figure III-4e-f). This magmatic foliation is usually sub-parallel to the overlying sheeted dike and is interpreted as resulting from subsidence at the melt lens floor (Nicolas et al., 2009; see Appendix A1) or from the buoyant ascent of magma through the mush pile (MacLeod and Yaouancq, 2000). Foliated gabbros are composed of plagioclase, clinopyroxene, and locally amphibole, olivine, orthopyroxene (Figure III-8).

In most of the visited areas, the transition from the foliated gabbros to the isotropic gabbros and from the isotropic gabbros to the sheeted dike complex is not observed. These transitions, which occur over a few meters, only, are usually located in river beds (Wadi) that crosscut the outcrops and prevent detailed observation (e.g. Figure III-9, and Figure 1 in MacLeod and Yaouancq, 2000). Three selected zones where the transitions outcrop better are

described in details in sections III.3, III.4, and III.5. I rapidly present hereafter the complex intrusive relationships between isotropic gabbros and microgranular dikes that display well equilibrated textures.

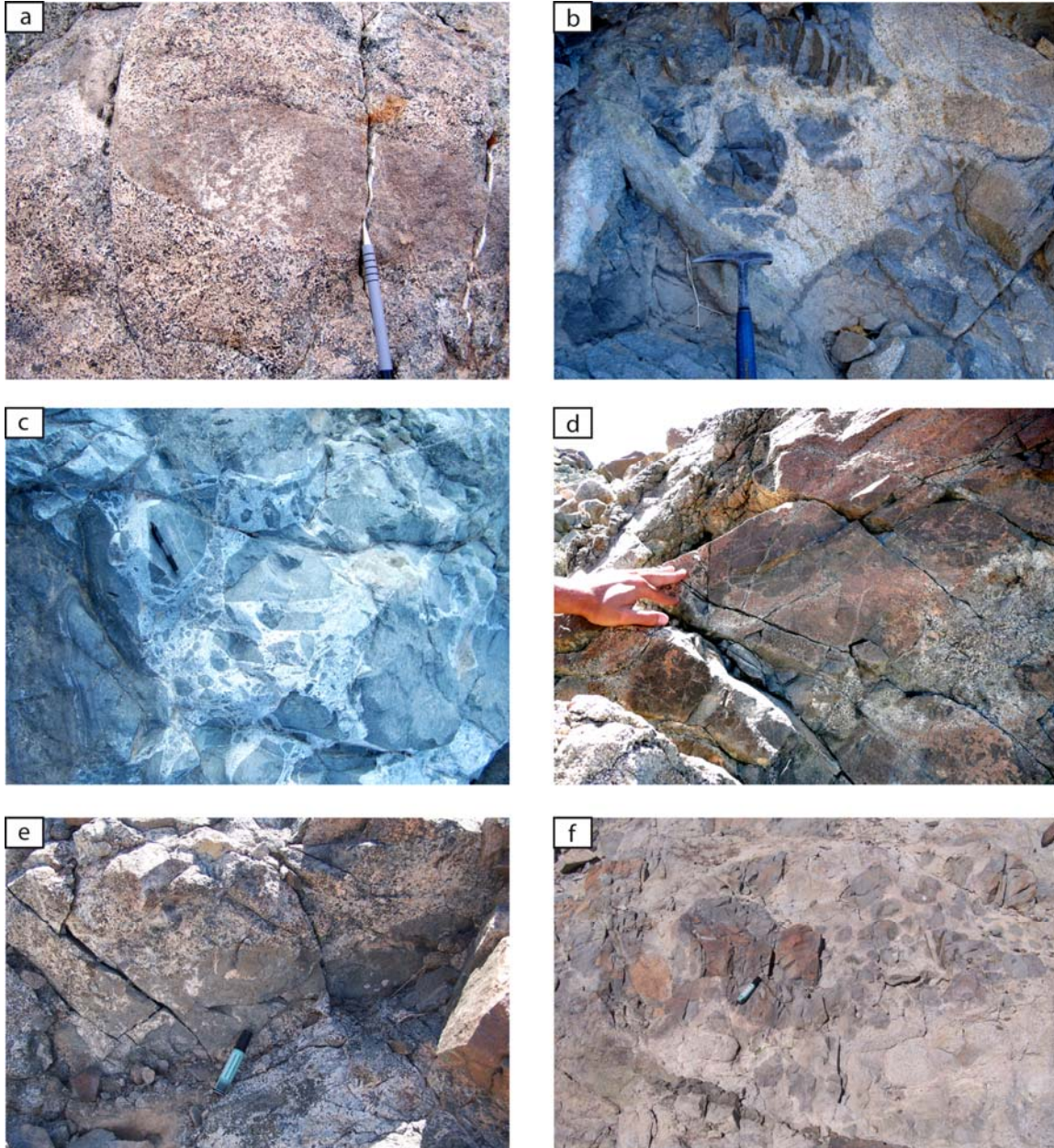


*Figure III-6: Magmatic breccias and xenoliths observed in the isotropic gabbro horizon. a) Microgabbro xenoliths with well equilibrated textures in isotropic gabbro (Gideah area); b-c) magmatic breccias observed close to the base of the sheeted dike (plagiogranitic matrix; b: Aswad area; c: Haymilyah area); d-f) xenolith accumulation in the isotropic gabbros horizon (d: Aswad area; e: Sarur area; f: Haymilyah area).*

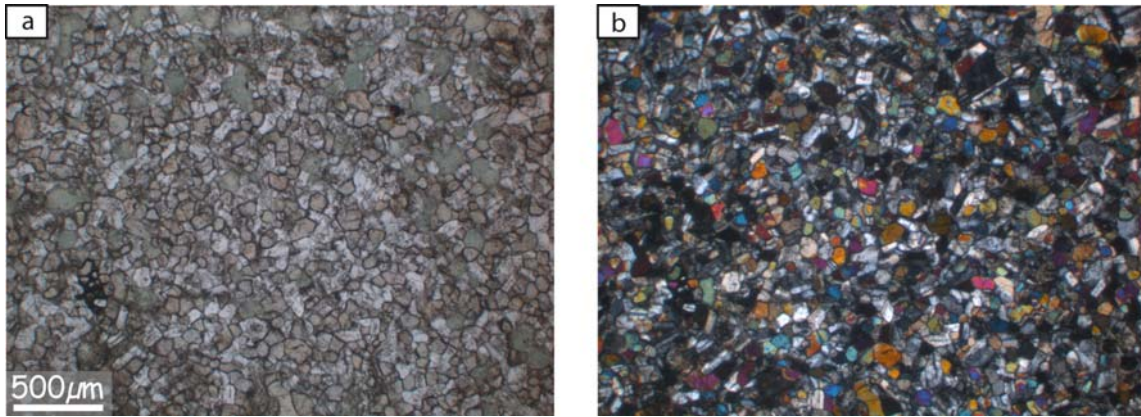


Figure III-7: Microphotographs of a microgranular xenolith with a well equilibrated texture present in the isotropic gabbros of the Aswad area consisting of plagioclase, clinopyroxene, orthopyroxene, and secondary amphibole (Oman ophiolite; sample 07OL54a). a) plane-polarized light; b) cross-polarized light.

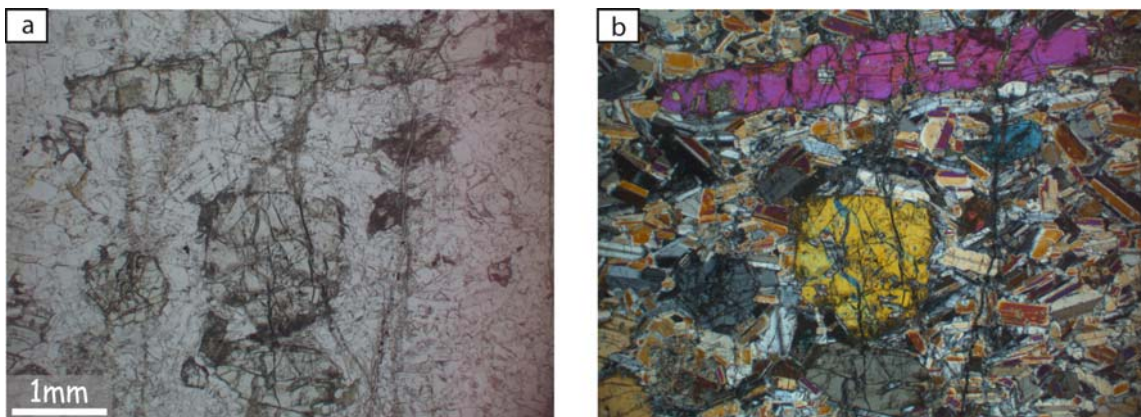


Figure III-8: Microphotographs of a foliated gabbro of the Al Ahmadi Hills area composed of plagioclase and clinopyroxene (Oman ophiolite; sample 08OL29b). a) plane-polarized light; b) cross-polarized light.

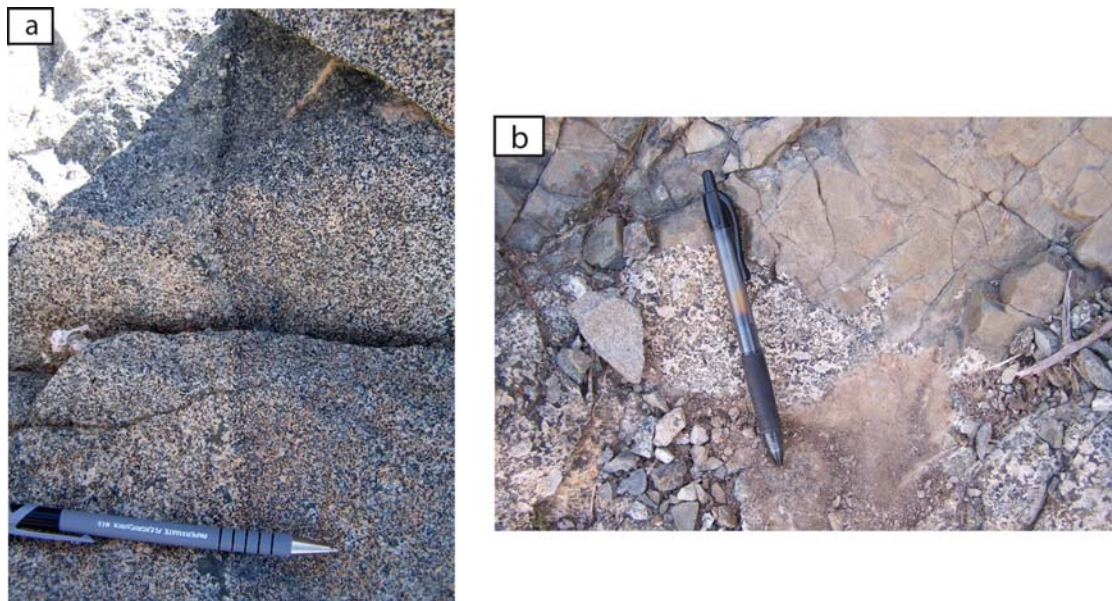


Figure III-9: SE-NW view of the area studied by Nicolas et al (2008) in the Aswad area. According Nicolas et al. (2008), the main hill (on the right hand of the picture) is composed of foliated gabbros and the small hills (on the left hand of the picture) are composed of sheeted dikes. The transition between foliated gabbros and the sheeted dike complex is located in the Wadi and outcrops poorly.

Understanding the chronology of intrusions at the base of the sheeted dike complex and in the isotropic gabbro horizon is particularly important to understand processes acting within and around the upper melt lens. Several intrusive relationships observed in this zone



are unclear, and it is difficult to determine which facies is intrusive and which one is intruded (Figure III-10a). The 3 main intrusion types encountered are: (i) gabbro intrusion in another gabbro; (ii) protodike intrusion in a gabbro; (iii) gabbro intrusion in dikes. This late situation is more complex due to the later intrusion of dikes into gabbro and the presence of xenoliths/enclaves in the gabbros. The cross-cutting relationships are sometimes relatively easy to interpret, for example when small intrusions of the intruding material are observed in the intruded one (Figure III-10b).



*Figure III-10: Igneous contacts observed in the isotropic gabbro horizon: a) intrusion of gabbro in another gabbro, the chronology of intrusion is unclear (Gideah area); b) coarse-grained gabbro intruding microgranular dikes (Aswad area).*

The gabbro intruding the base of the sheeted dike complex is either fine or coarse grained. It is composed of plagioclase, clinopyroxene, oxide, amphibole and when fine grained, locally containing olivine (Figure III-11).

In the Aswad area a peculiar outcrop allows discussing the intrusive relationships (Figure III-12). Several contacts between gabbro, diorite, and microgranular gabbro are observed. This outcrop is only ~4 x 5 meters large, and disconnected from neighbouring outcrops; relations with the underlying gabbros and with the overlying sheeted dikes are therefore very hard to identify. On this narrow outcrop, the relative timing of intrusions is locally very hard to identify (Figure III-12b-c). Locally, the gabbro appears clearly intrusive in microgranular gabbros (Figure III-12d). In order to replace these different intrusions in a general evolutionary model for the melt lens region, continuous outcrops are necessary.

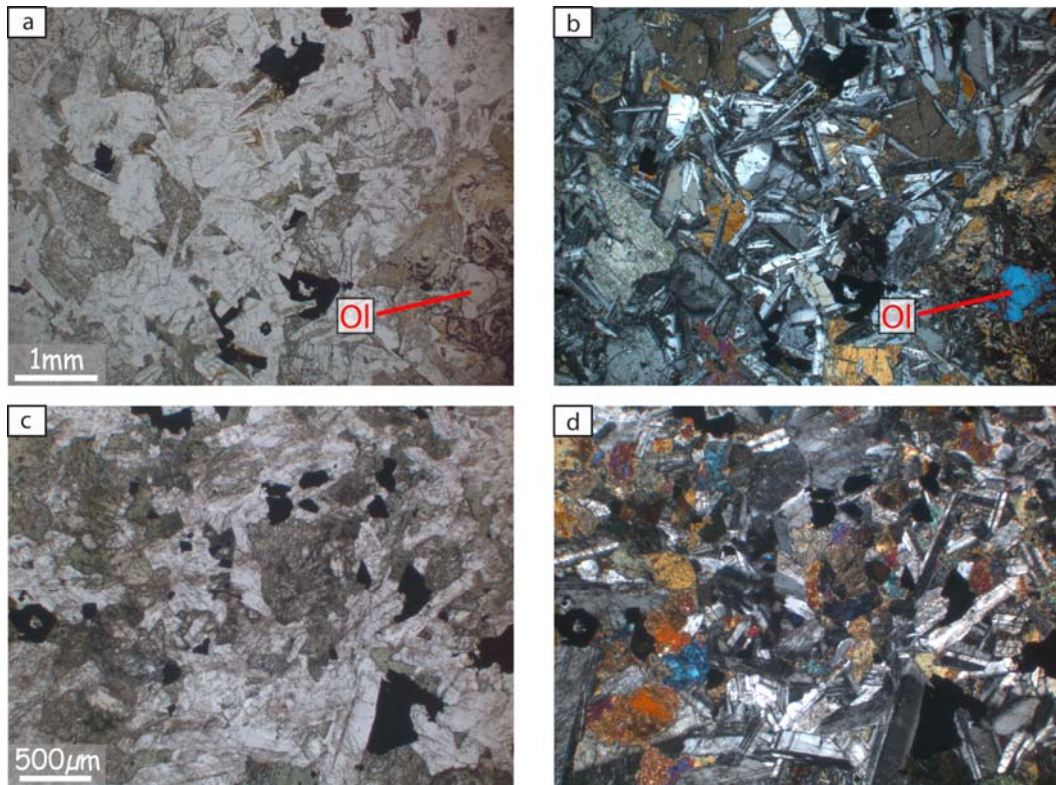


Figure III-11: Microphotographs of fine grained gabbros that intrude the sheeted dike complex. a-b) Al Ahmadi Hills area; sample 07OL01f1; c-d) wadi Gideah area; sample 08OL01c. Isotropic fine-grained gabbros are composed of plagioclase, clinopyroxene, amphibole, oxide, and locally olivine. a, c) plane-polarized light; b, d) cross-polarized light.

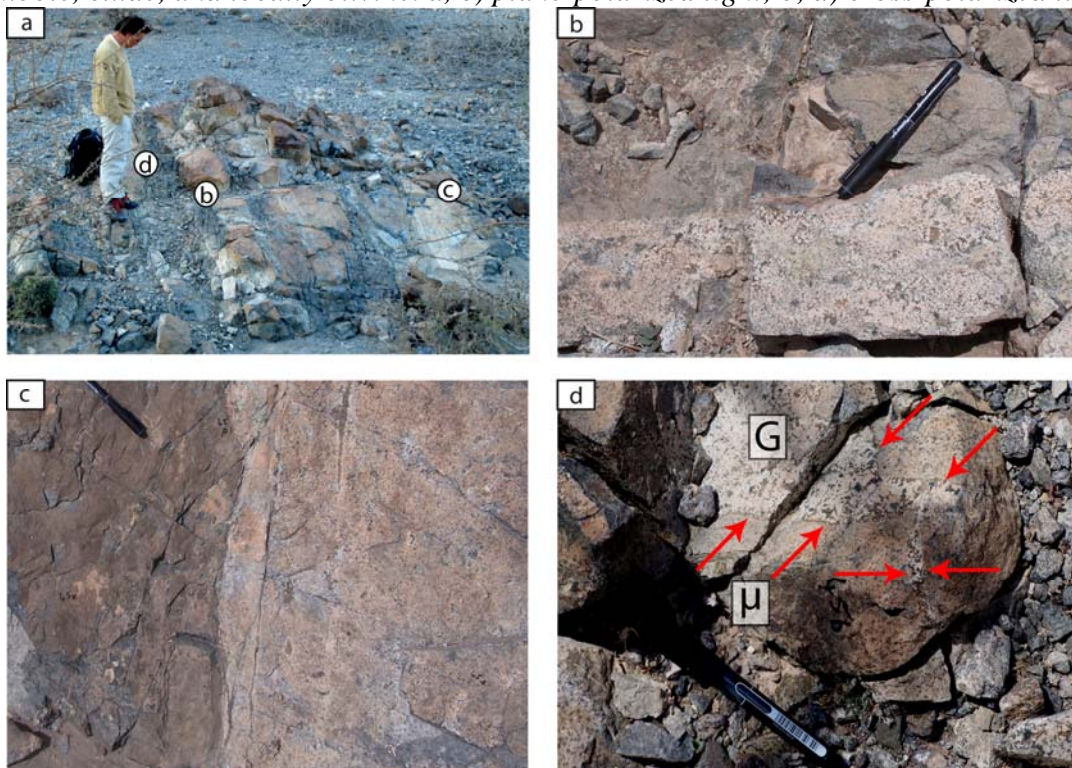


Figure III-12: a) Outcrop displaying multiple intrusive relationships (Aswad area); letters correspond to b), c), and d) pictures. b-c) Contacts between microgranular gabbro and diorite / gabbro, the chronology of intrusion is unclear. d) Microgranular gabbro ( $\mu$ ) intruded by a coarse-grained gabbro (G); contact is pointed by arrows.

### ***III.3. Interactions between magma and hydrothermal system in Oman ophiolite and in IODP Hole 1256D: fossilization of a dynamic melt lens at fast spreading ridges***

*France, L., Ildefonse, B., and Koepke, J., in press. Interactions between magma and hydrothermal system in Oman ophiolite and in IODP Hole 1256D: fossilization of a dynamic melt lens at fast spreading ridges. *Geochem. Geophys. Geosyst.* doi:10.1029/2009GC002652*

#### **III.3.a. Abstract**

The transition between the small melt lens observed on top of fast spreading ridge magma chambers and the overlying sheeted dike complex marks the interface between magma and the hydrothermal convective system. It is therefore critical to our understanding of fast spreading ridge accretion processes. We present maps of two areas of the Oman ophiolite where this transition zone is observed as continuous outcrops. Our observations, that include the base of the sheeted dike being cross-cut by gabbros, are consistent with episodic dike injections in a steady state model, but also suggest that the root of these dikes is commonly erased by vertical movements of the top of the melt lens. Dike assimilation is a possible mechanism for incorporating hydrated phases, which result from hydrothermal alteration, to the melt lens during upward migrations of its upper boundary. Upward migrations are also responsible for a granoblastic overprint of the root of the dikes that is also observed in the stopped diabase xenoliths. This granoblastic overprint attests to reheating of previously hydrothermally altered lithologies which can even trigger hydrous partial melting due to the lowering of the solidus of mafic lithologies by the presence of a water activity. Clinopyroxenes present in these granoblastic lithologies are typically low in Ti and Al content, thus strongly contrasting with corresponding magmatic clinopyroxene. This may attest to the recrystallization of clinopyroxenes after amphiboles under the peculiar conditions present at the root zone of the sheeted dike complex. Downward migrations of the top of the melt lens result in the crystallization of the isotropic gabbros at its roof, which represent the partly fossilised melt lens. Melt lens fossilization eventually occurs when magma supply is stopped or at the melt lens margins where the thermal conditions become cooler. Melt lens migration, recrystallization of hydrothermally altered sheeted dikes during reheating stages, and assimilation processes observed in the Oman ophiolite are consistent with the observations made in IODP Hole 1256D. We propose a general dynamic model in which the melt lens at fast-spreading ridges undergoes upward and downward movements as a result of either eruption / replenishment stages or variations in the hydrothermal / magmatic fluxes.

**Keywords:** fast spreading Mid-Ocean Ridges, Oman ophiolite, hydrothermal system, melt lens, axial magma chamber, ODP, IODP.

### III.3.b. Introduction

The structure of fast spreading ridges is inferred from geophysical studies (e.g., Morton and Sleep, 1985, Detrick et al., 1987; Harding et al., 1989; Kent et al., 1990) and from structural observations and mapping in ophiolites, in particular the Oman ophiolite (e.g., Hopson et al., 1981; Pallister and Hopson, 1981; Nicolas et al., 1988a, 2000; Umino et al., 2003). Geophysical studies have revealed the presence of a partly to totally molten melt lens (~30 to 100 meters thick) at the top of the mostly crystallized magma chamber (e.g., Sinton & Detrick, 1992; Hussenoeder et al., 1996; Collier and Singh, 1997; Singh et al., 1998; Dunn et al., 2000). The composition and evolution of this thin melt lens play a key role in oceanic crust genesis as it feeds, at least partly, the upper and lower crust (e.g., Sinton & Detrick, 1992; Boudier et al., 1996). This horizon is also a major exchange interface between sea water and the oceanic crust as it is located at the root of the sheeted dike complex, where the hydrothermal convective system and the melt lens can meet and interact. Several descriptions of the gabbro/sheeted dike transition zone in ophiolites have been published, to attempt understanding the complex structural and petrological relationships within this zone (Rothery, 1983; Nicolas & Boudier, 1991; MacLeod & Rothery, 1992; Gillis & Roberts, 1999; MacLeod & Yaouancq, 2000; Coogan et al., 2003; Gillis, 2008; Nicolas et al., 2008).

The IODP (Integrated Ocean Drilling Program) drilled Hole 1256D into a ~15 Ma crust that formed at the East-Pacific Rise at a superfast spreading rate (Teagle et al., 2006). It is to date the only place in present-day oceanic crust where the uppermost gabbros below the sheeted dike complex has been sampled *in-situ* below a continuous, intact section of upper oceanic crust (Teagle et al., 2006; Wilson et al., 2006; Alt et al., 2007). Studies in ophiolites or in present-day oceanic crust have led to the elaboration of a variety of models for the evolution of the complex magmatic / hydrothermal interface that constitutes the gabbro / sheeted dike transition zone. It is presented either as a steady state boundary layer (Rothery, 1983; Nicolas and Boudier, 1991; MacLeod and Yaouancq, 2000; Nicolas et al., 2008), or as a dynamic one (Gillis and Roberts, 1999; Coogan et al., 2003; Wilson et al., 2006; Gillis, 2008; Koepke et al., 2008). The processes occurring in this transition zone, and the relationships between observed present-day lithologies and the melt lens at the time of

accretion are still debated (e.g., MacLeod and Yaouancq, 2000; Gillis, 2008; Nicolas et al., 2008).

Nicolas et al. (2008) postulated that understanding the complex processes acting at the sheeted dike / gabbro transition requires studying undisturbed portions of the ridge, away from domains where accretion was under the influence of discontinuities due to ridge propagation or segmentation. In the present study, we have mapped in details the gabbro / sheeted dike transition zone in two localities of the Oman ophiolite that are, based on large scale structural mapping (Nicolas et al., 2000), away from major ridge axis tectonic activity. This study bears information on the evolution of the melt lens, and suggests a way to reconcile the apparently contrasting, previously published models.

### **III.3.c. Background**

At fast spreading ridges, the upper oceanic crust is composed of, from top to bottom, lavas, sheeted dikes, and isotropic ophitic gabbros (and associated coarse-grained gabbros and "oceanic plagiogranites"). The foliated gabbros, and layered gabbros form the lower crust. Many models, based on thermal modelling and/or ophiolite field data, have been proposed for the formation of the igneous lower crust (e.g., Sleep, 1975; Nicolas et al., 1988b; Nicolas, 1989; Henstock et al., 1993; Phipps Morgan & Chen, 1993; Quick & Denlinger, 1993; Nicolas & Boudier, 1995; Boudier et al., 1996; Kelemen et al., 1997; MacLeod & Yaouancq, 2000; Garrido et al., 2001). Most recent models predict that the lower crust is fed from the top, through subsidence of the crystallized material from the melt lens, and/or from the bottom through sill injections (Boudier et al., 1996; Kelemen et al., 1997; MacLeod & Yaouancq, 2000; Nicolas et al., 2009). The balance between these two processes, however, remains poorly constrained and is still debated (e.g., VanTongeren et al., 2008; Webb, 2008). MacLeod & Yaouancq (2000) proposed that the lower crust is not fed from the axial melt lens, and that the foliated gabbros in the upper part of the igneous section only preserve the last increment of strain during crystallization in an upwelling melt flow. They observed that plagioclase zoning tends to increase up-section from the layered gabbros to the foliated gabbro, possibly reflecting the evolution of the melt as it migrates toward the top of the crystal mush pile. In contrast, other detailed studies of the high level gabbros in the Oman ophiolite suggest that the melt lens does play a role in the genesis of the lower crust through subsidence processes (Coogan et al., 2002; Nicolas et al., 2009).

The upper crust (volcanics and sheeted dike) is considered to be injected from the melt lens (e.g., MacLeod and Yaouancq, 2000). However, it may not sample the whole melt lens. Based on observations made at Hess Deep (ODP Site 894), Natland & Dick (1996) proposed that the melt lens is partly filled with highly fractionated melts, too dense to erupt. These uneruptable melts are expelled from the underlying crystal mush column and seem to play a minor role in the upper crust accretion as they are expected to lie on the melt lens floor. The detailed structural, petrological, and geochemical study of the Wadi Abyad section, in the Oman ophiolite (MacLeod and Yaouancq, 2000) shows that, even if some highly fractionated pegmatitic gabbros may form up to 40% of the outcrops in some parts of the isotropic ophitic gabbro horizon, they are always subordinated to finer-grained and more magnesian gabbro. MacLeod and Yaouancq (2000) interpret the Fe-Ti pegmatitic gabbros as melts differentiated under reducing conditions and low water activities, at the border of the melt lens. They also propose that the average composition of the whole isotropic gabbro horizon represents the melt lens composition; their calculations lead to Mg# of 65 and a TiO<sub>2</sub> content of 1.1wt%, which is relatively similar to the associated sheeted dikes and to typical N-MORB erupted at intermediate to fast spreading ridges (e.g., Klein, 2003).

The evolution and stability of the melt lens, as well as its relationships with the overlying hydrothermally altered lithologies are also debated. These points are discussed through detailed studies of the root zone of the sheeted dike complex. This zone is composed of fine-grained isotropic ophitic gabbro, pegmatitic gabbro, some Fe-Ti gabbro and diorite, and oceanic plagiogranites. It has been described in the Oman ophiolite (Rothery, 1983; Nicolas and Boudier, 1991) and recently revisited in details (Nicolas et al., 2008). Based on petrological and structural observations, Nicolas et al. (2008) present a new steady-state model for the evolution of the melt lens. They propose that most of the isotropic gabbro horizon, called “root zone of the sheeted dike complex”, is generated by hydrous partial melting triggered by the intrusion of hydrothermal fluids in the recently crystallized, still hot, base of the sheeted dike complex. In this model, the root zone lithologies do not represent the crystallization of the melt lens, which is assumed to pinch out at its tips. MacLeod & Yaouancq (2000) also describe the root zone of the sheeted dike complex in the Oman ophiolite as a steady state horizon, but in contrast with Nicolas & Boudier (1991) and Nicolas et al. (2008), they interpret it as the crystallized melt lens under anhydrous and reducing conditions, implying little assimilation of hydrated doleritic roof material. However, they show some assimilation evidences (Figure 2d in MacLeod & Yaouancq, 2000). Reheating and

assimilation in the root zone are documented in the Oman ophiolite (Coogan et al., 2003; Gillis, 2008), in the Troodos ophiolite (Gillis & Roberts, 1999; Gillis, 2002; Gillis & Coogan, 2002; Gillis, 2008), and at Pito Deep and Hess Deep (Gillis, 2008). Wilson et al. (2006) and Koepke et al. (2008) recently described assimilation and reheating features within the root zone of the sheeted dike complex in the IODP Hole 1256D, the first and so far only borehole in present-day intact ocean crust that reaches the contact between sheeted dikes and gabbro. Nicolas et al. (2008) discuss these results by pointing out that reheating and assimilation features are well known in the Oman ophiolite in areas affected by ridge segmentation (Juteau et al., 1988; MacLeod and Rothery, 1992; Nicolas and Boudier, 1995; Boudier et al., 2000; Adachi and Miyashita, 2003; Miyashita et al., 2003; Umino et al., 2003), but have not been described in "undisturbed" zones, away from discontinuities, yet. They suggest that reheating and assimilation, in the Oman and Troodos ophiolite, and in the IODP borehole could be related to ridge segmentation.

To further constrain the characteristics of the transition from gabbros to the sheeted dike complex (i.e., the interface between the magmatic and the hydrothermal systems), we have mapped in details this transition in two "undisturbed" areas of the Oman ophiolite (Wadi Gideah area, in the Wadi Tayin Massif, and Al Ahmadi Hills area, in the Ibra plain at the southern end of the Wadi Tayin Massif). Because of its lithological heterogeneity, and of the presence of many igneous contacts and fractures, the root zone of the sheeted dike complex is a zone of preferential meteoric alteration and outcrops very poorly (see for example the Figure 1 in MacLeod and Yaouancq, 2000, which shows the outcrops discontinuity). Observations from these two regions are made over continuous outcrops and are consistent with many other visited sites where outcrops are not continuous.

#### **III.3.d. Field observations**

The two studied areas are located in the well exposed Wadi Tayin Massif, one of the southern Massifs in the Oman ophiolite where ridge segmentation effects are minor (Nicolas et al., 2000; Figure 1). The southern massifs are large and flat-bottomed synclines with the sheeted dike and sub-vertical gabbro foliation trending ~NW-SE. The NW-SE segments are opened in an older domain where the sheeted dike trends ~NE-SW. The Wadi Gideah area is situated in the Jebel Dimh, 10km to the north of Ibra and ~10km to the East of the main road between Muscat and Ibra. The Al Ahmadi Hills are located in the large Wadi Nam, 6km to the NW of the Al Ahmadi village and 10km to the NNW of the town of Ibra.

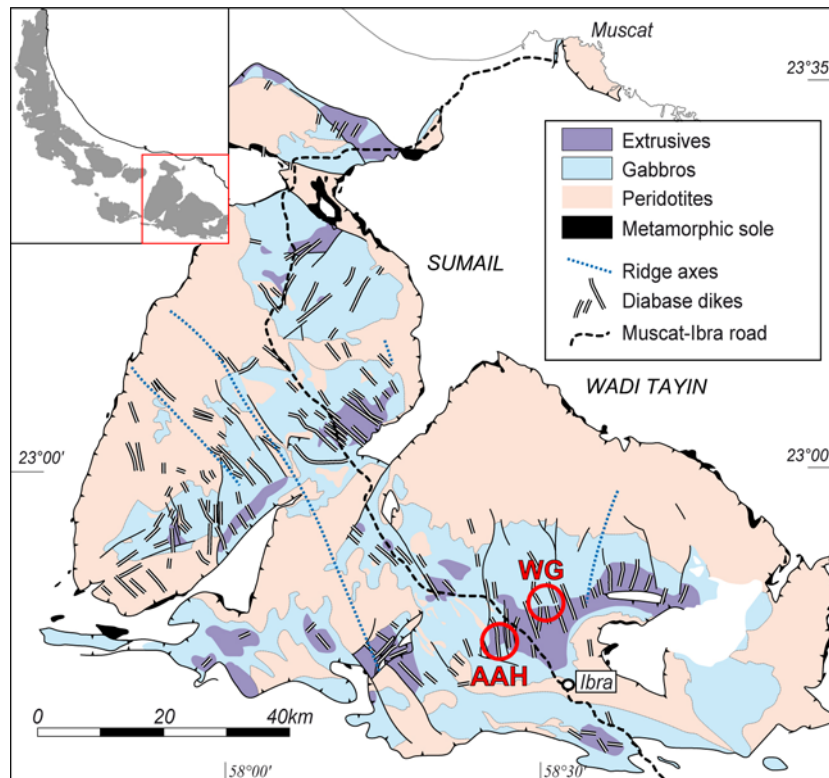


**Figure 1:** Simplified geological and structural map of the southern massifs and location (Red box) in the Oman ophiolite (after Nicolas et al., 2000). Red circles indicate the locations of the studied zones (WG= Wadi Gideah; AAH= Al Ahamadi Hills).

### III.3.d.1. The Wadi Gideah area

The mapped area in Wadi Gideah extends from the foliated gabbro in the North to the sheeted dikes in the South, and includes in between the heterogeneous, isotropic ophitic gabbro horizon (Figure 2a). The foliated gabbros present the same characteristics as anywhere else in the Oman ophiolite; they are granular, and display a sub-vertical foliation trending N-S (Figure 3). Close to the contact with the foliated gabbros, the isotropic ophitic gabbro horizon is very heterogeneous; it is composed of coarse-grained lithologies such as hornblende-olivine-gabbro or hornblende-gabbro, which contain some strongly altered xenoliths of predominantly fine-grained recrystallized diabase, but also gabbro and hornblende-diorite. The relationships between the different lithologies in this particular place are unclear because of the intense weathering. To the South, up-section, isotropic ophitic gabbros become more homogeneous. Some isolated narrow and elongated meter sized zones display a foliation (~N-S, sub-vertical) that seems to underline the contacts with gabbro injections. Rounded xenoliths of gabbro and diabase, about 10x10 cm on average, are accumulated at small hill summits in the whole isotropic gabbro horizon (Figures 2 and 4a). Magmatic breccias with a leucocratic matrix enclosing gabbro or dike xenoliths are also observed (Figure 2 and 4b).



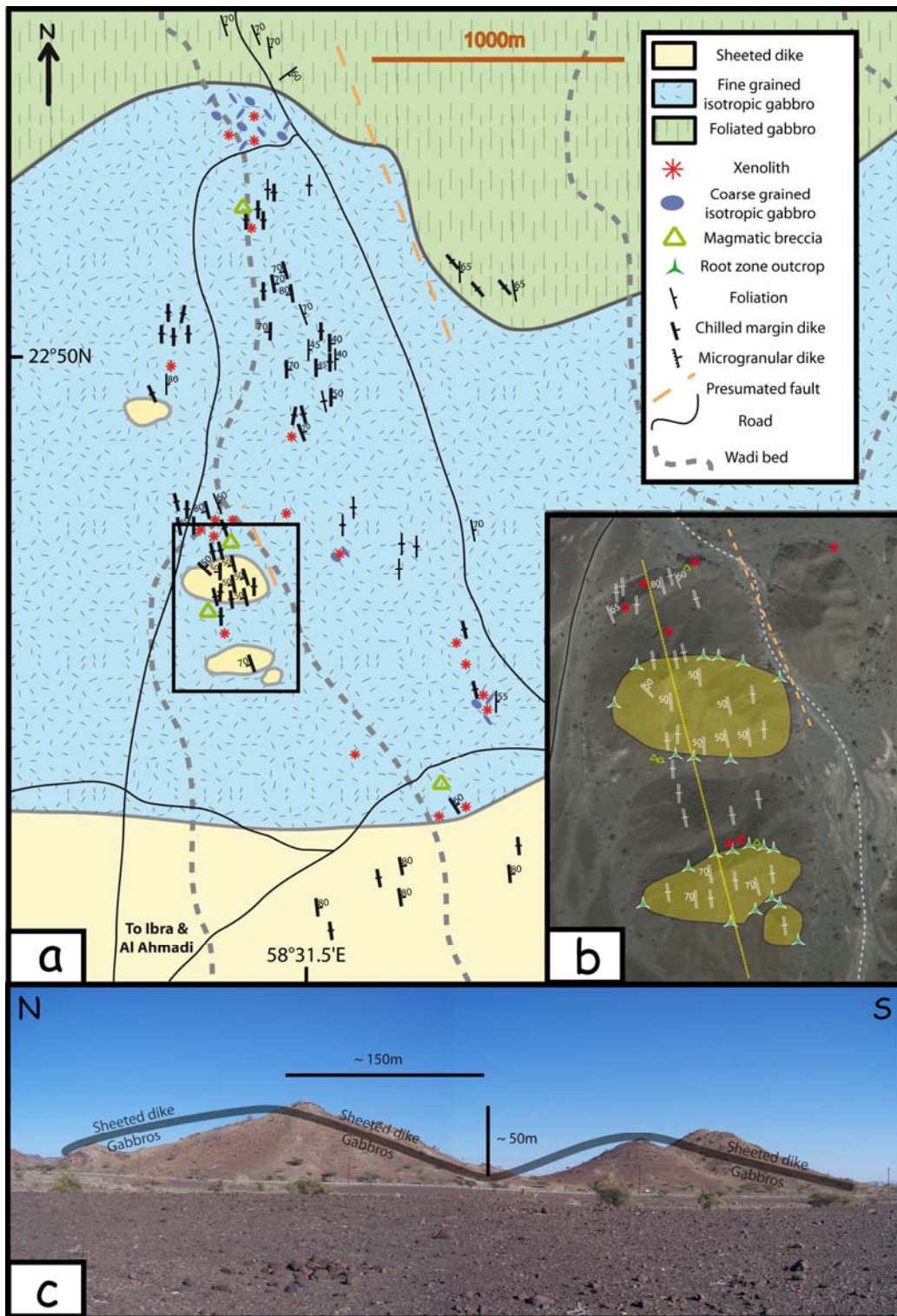


**Figure 2:** Wadi Gideah area; **a)** Geological and structural map; the black rectangle represents the location of **b)**. **b)** Zoom on the two hills that have their summits and southern flanks composed of sheeted dikes and their northern flanks composed of gabbros. The yellow line indicates the position of the cross section **c)**. **c)** Cross section showing the two hills from **b)**. The thick grey line indicates the gabbro / sheeted dike transition that is precisely mapped on **b)**. No fault has been observed.

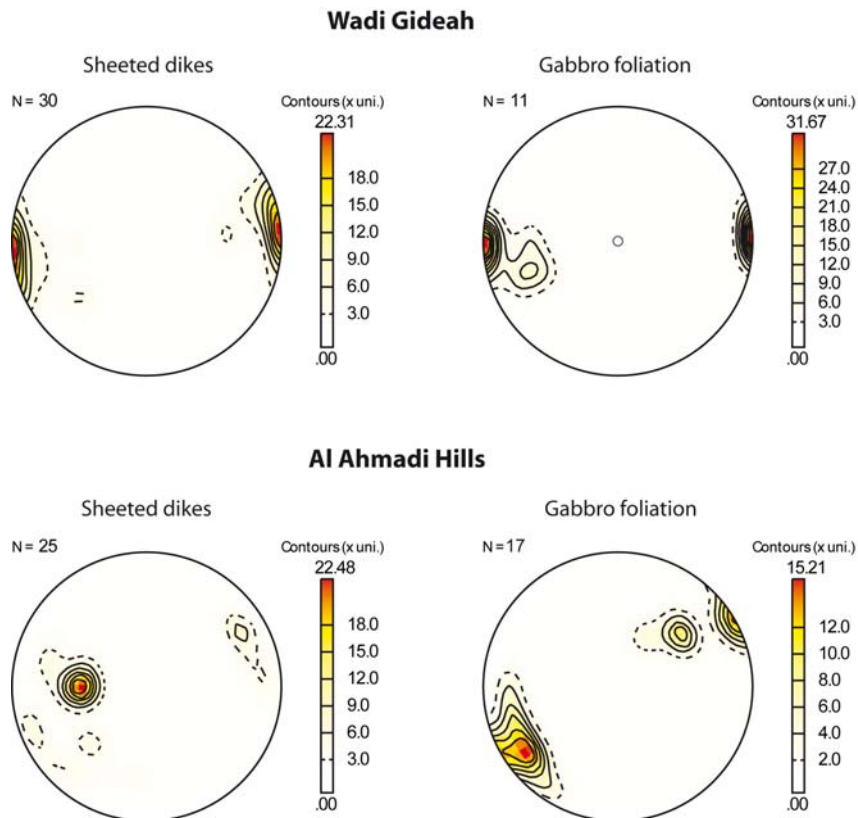


**Figure 3:** Stereonets (lower hemisphere; Non-polar data; geographical reference system) showing field structural measurements: sheeted dike (left) and magmatic foliations in foliated gabbros (right) in the Wadi Gideah area (top) and in the Al Ahmadi Hills area (bottom).



**Figure 4:** a) Xenoliths of granoblastic dikes in isotropic ophitic gabbro; b) magmatic breccia consisting of recrystallized sheeted-dike within a silicic (oceanic plagiogranite) matrix. Both outcrops are in the Wadi Gideah area.

Except for one occurrence close to the foliated gabbro (Figure 2), these breccias are located close to, or at the contact between the isotropic ophitic gabbro horizon and the sheeted dikes. Figures 2b and 2c show two hills in the ophitic gabbros topped by sheeted dike. No fault is observed between these two hills. The vertical offset of the contact between gabbros and sheeted dike is consequently assumed to represent initial depth variations of this contact along the ridge axis. To the South, the sheeted dikes present the same characteristics as

anywhere else in the Oman ophiolite, and trend N-S, sub-vertical (Figure 3). Each dike is about 1 to 1.5 meters wide and present chilled margins against other dikes. Some later dikes with chilled margins, also 1 to 1.5 meters wide, crosscut the isotropic gabbros and the previous sheeted dikes; they are sub-parallel to the sheeted dike complex (Figure 5).

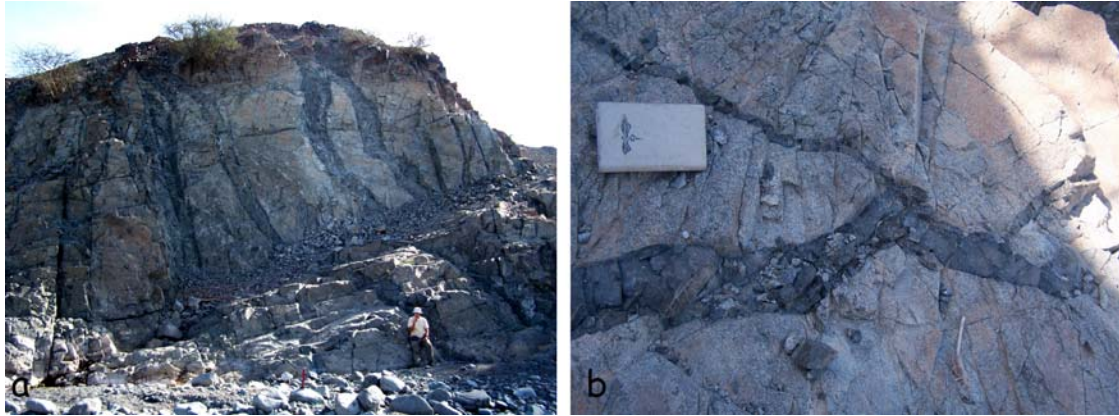


**Figure 5:** Late diabase dikes crosscutting isotropic ophitic gabbros in the Wadi Gideah area.

Isotropic ophitic gabbros intrude the base of the sheeted dikes, and locally assimilate dike fragments (Figure 6). Sparse diabase xenoliths are locally observed. Gabbros clearly crosscut former chilled margins (Figure 6), and locally intrude the sheeted dike base, but do not invade it further than about one meter above the main contact. Some contact outcrops show a gradation toward the contact from gabbroic rocks to more leucocratic ones (Figure 6c, e). Coarse-grained isotropic ophitic gabbros are also common in the root zone and at the contact with xenoliths (Figure 6f).

Dikes truncated by ophitic gabbro show well equilibrated (with  $\sim 120^\circ$  triple junctions), fine-grained granular textures, called hereafter “granoblastic textures” (Figure 7a). These textures are clearly distinct from the doleritic textures classically observed in Oman ophiolite sheeted dikes. Recrystallized texture is observed on both sides of dike margins, i.e., it overprints both last and former dikes (Figure 7a-b). The average grain size in the granoblastic margins overprinting the chilled margins is  $\sim 10\mu\text{m}$ . Ten centimeters away from the margins, the recrystallized textures display coarser granular grains ( $\sim 50\mu\text{m}$ ; Figure 7b); plagioclases are largely less recrystallized than pyroxenes. Patches with granoblastic texture (0.5 to 1mm wide) are also observed in the uppermost isotropic gabbros (Figure 7c). The paragenesis of granoblastic domains includes plagioclase, clinopyroxene, amphibole, magnetite, and ilmenite. Granoblastic texture lithologies are particularly rich in oxides (Figure 7a-b, e, g). The corresponding mineral assemblages are commonly complex with different

generations of clinopyroxenes and amphiboles (Figure 7f) and clinopyroxenes commonly contain numerous tiny oxide inclusions.

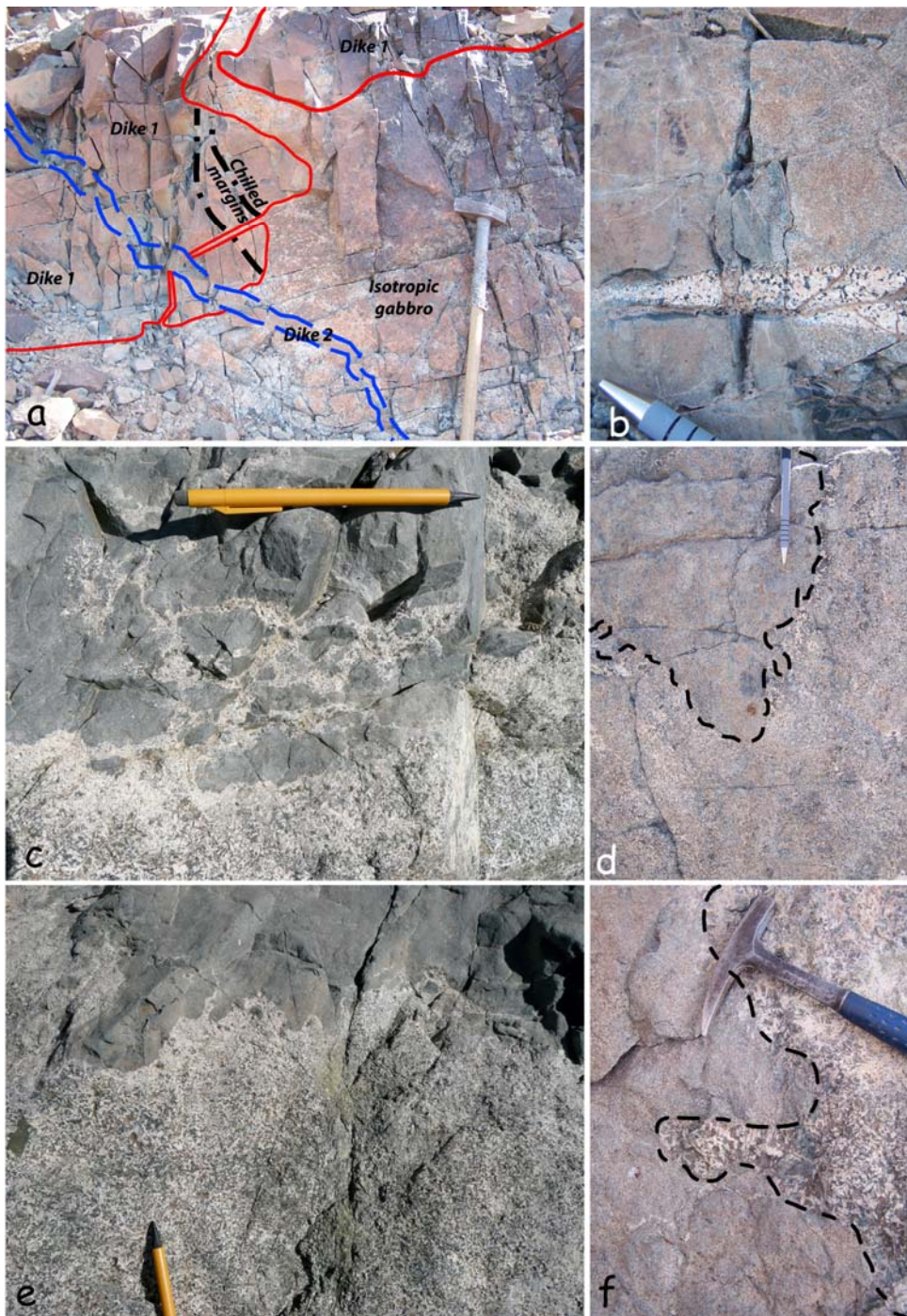


**Figure 6:** Outcrops in the root zone of the sheeted dikes; **a)** Recrystallized sheeted dike (granoblastic dike) intruded by gabbro. Recrystallized chilled margins are crosscut by the intrusive gabbro. A late dike (“dike 2”) crosscuts the gabbro and recrystallized dikes (“dike 1”). **b)** Dioritic intrusion that crosscuts a recrystallized dike margin with granoblastic texture. **c) and e)** Gabbro assimilating recrystallized sheeted dike. The gradation to more leucocratic lithology at the contact is visible. A small shear zone affecting the dikes and gabbro is visible on the right side of c). **d) and f)** Xenoliths of recrystallized dikes showing granoblastic texture in isotropic gabbro. Patches of coarser grained gabbro are observed around the xenolith in d), and all surrounding gabbro is pegmatitic in f).

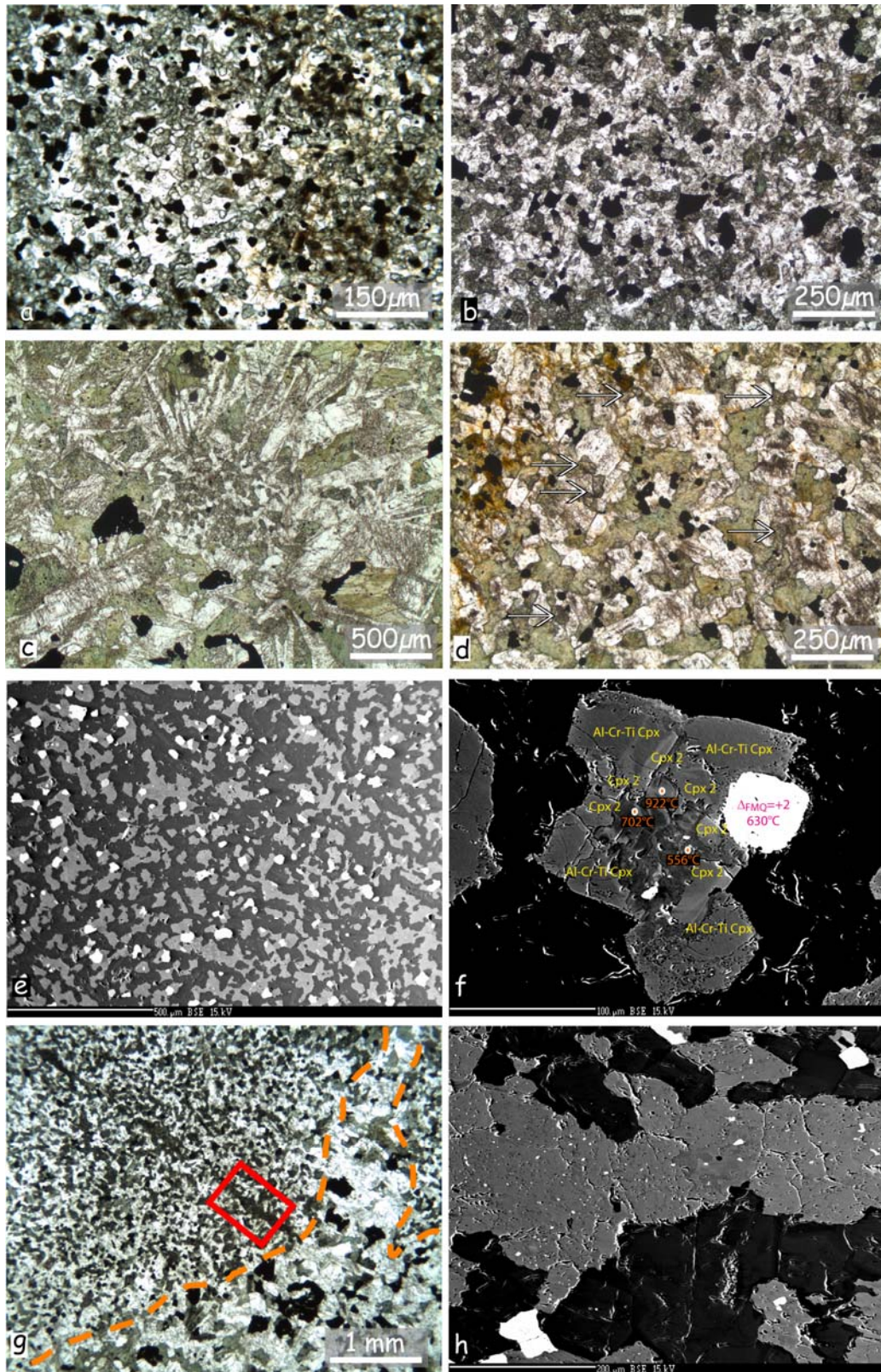


**Figure 7:** Photomicrographs and BSE images of samples from the Wadi Gideah area. **a)** Fine-grained granoblastic texture with a high oxide concentration in a recrystallized dike margin (plane-polarized light). **b)** Coarser-grained recrystallized texture in the center of a recrystallized dike (plane-polarized light). **c)** Granoblastic patch in isotropic gabbro in the center of the picture (plane-polarized light). **d)** Coarse-grained recrystallized texture partially erased by a strong greenschist facies alteration in a granoblastic dike (plane-polarized light). Arrows indicate granular grains. **e)** BSE image of the granoblastic texture in a recrystallized

*dike. Dark grey minerals are plagioclases, light grey minerals are clinopyroxene+amphibole, white minerals are oxides. f) BSE image focussing on Fe-Mg minerals present in the granoblastic dikes. Different generations of clinopyroxenes (Cpx) and amphiboles are present (orange numbers indicate temperatures estimated with Ernst and Liu, 1998). The white phase is a mixture of ilmenite and magnetite. Redox and temperature estimates are calculated using Sauerzapf et al. (2008). g) Isotropic gabbro crosscutting a recrystallized granoblastic dike. In the recrystallized dike, the truncated clinopyroxene vein is believed to derive from a former amphibole bearing hydrothermal vein (cross-polarized light). The red square indicates the position of the BSE image h). h) BSE image of the truncated clinopyroxene vein in g). Note the occurrence of numerous tiny oxide inclusions in the clinopyroxenes.*

Oxide inclusion-rich clinopyroxene veins (100 to 200µm wide) in the base of the sheeted dikes are crosscut by intrusive gabbros (Figure 7g-h). The leucocratic lithologies (oceanic plagiogranites) that are sometimes present at the base of the dikes contain tiny clinopyroxenes (20 to 50µm) associated with oxides, suggesting that these correspond to relics of parageneses from the granoblastic stage. These minerals have rounded shapes and appear to be relics of former larger grains. This observation is critical to constrain the origin (differentiation vs. hydrous partial melting) of these oceanic plagiogranites (see discussion below). All samples are moderately to strongly altered in the greenschist facies; actinolite and albitized plagioclases replace magmatic ones, clinopyroxenes and higher temperature amphibole (hornblende and pargasite). In some samples the granoblastic texture is so strongly altered that it is hardly recognizable (Figure 7d).

### **III.3.d.2. The Al Ahmadi Hills**

The Al Ahmadi Hills are aligned along a small, 3000 m long and ~50 m high ridge that trends NW-SE (Figure 8a). At the northern tip of this ridge, the first lithology encountered is olivine gabbro, with a steep, strong magmatic foliation oriented 160E75 on average (Figures 3 and 9a). In some rare, about 1 to 5 meters large domains, the foliation is hardly identifiable in the field. Microscopic observations show that the foliation is similar to what is observed in the other foliated samples, with olivine mantled by orthopyroxene and pargasite (Figure 9b). This assemblage is described in Koepke et al. (2005a, b) and Nicolas et al. (2003), and may trace late magmatic processes such as hydrous partial melting reactions or late crystallization in the presence of water.

The transition to the next horizon above, mostly composed of isotropic ophitic gabbros, is sharp. It occurs over less than 10 meters. This horizon is strongly altered in the

greenschist facies, as shown by the abundance of actinolite. Immediately above this contact, the ophitic gabbros contain numerous large xenoliths (up to 1.5m large; Figure 8a-b, d), which are composed either of oxide-rich granoblastic overprinted dikes (Figure 9c) or of gabbroic rocks. This area is composed of about 60% isotropic ophitic gabbros, 30% xenoliths, and nearly 10% pegmatitic gabbros very similar to those of Wadi Gideah (Figure 6d, f), forming the matrix around the xenoliths. In some localized (~10 m) zones, xenoliths represent up to 90% of the outcropping material. Xenolith accumulation appears more abundant in the lower third of the isotropic ophitic gabbro section (Figure 8a, d). Xenoliths and pegmatitic gabbros become less abundant, and nearly disappear upsection, to finally reappear close to the contact with the sheeted dikes.

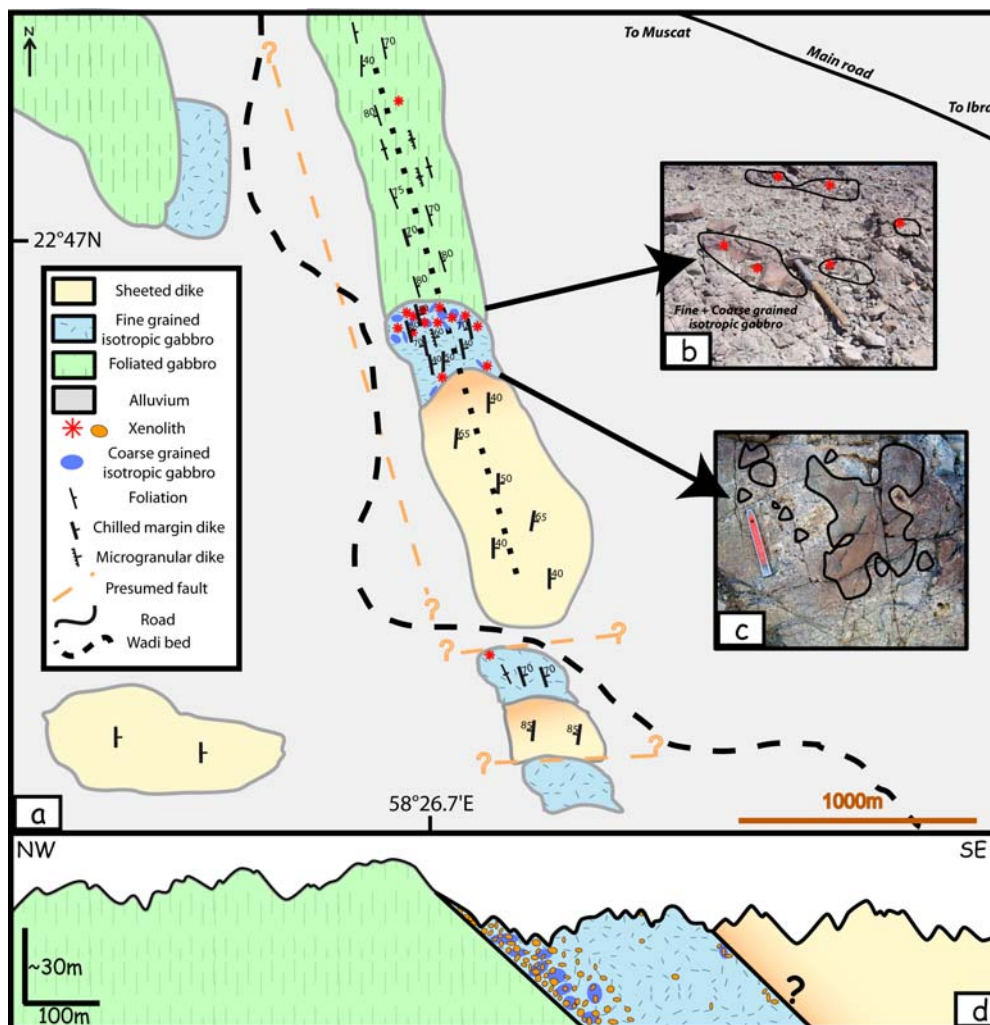


**Figure 8:** Al Ahmadi Hills area; **a)** Geological and structural map; the dotted line indicates the location of the cross section **d)**. **b)** Large xenoliths of recrystallized dike fragments close to the foliated gabbro / isotropic gabbro transition. **c)** Decimeter-sized xenoliths of recrystallized dikes close to the transition between isotropic gabbro and recrystallized sheeted dikes. **d)** NW-SE cross-section. Vertical exaggeration is x3; the isotropic gabbro horizon is ~100m thick. The base of the sheeted dike is reheated and recrystallized over a distance that is not constrained because of the strong weathering.

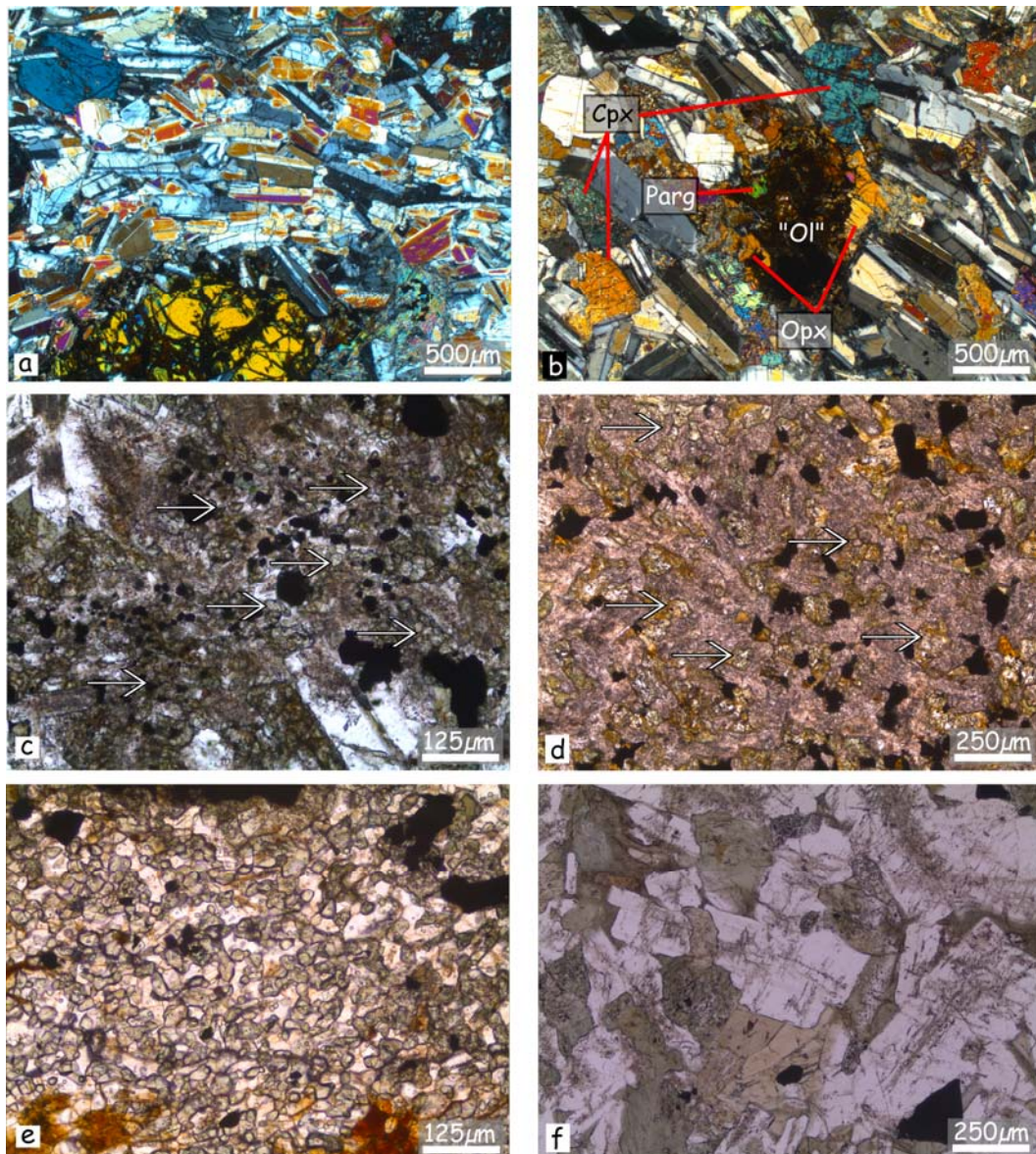


**Figure 9:** Photomicrographs of samples from the Al Ahmadi Hills area: **a)** Foliated olivine-gabbro (crossed-polarized light). **b)** Altered olivine (Ol) surrounded by orthopyroxene (Opx) and pargasite (Parg) in the foliated gabbro domains where the foliation is hardly identifiable in the field (cross-polarized light). **c)** Granoblastic overprint in a diabase xenolith; arrows indicate the small granoblastic grains (plane-polarized light). **d)** Strongly altered coarser-grained recrystallized texture from the base of the sheeted dike complex (centre of a recrystallized dike: plane-polarized light). Arrows indicate granular grains. **e)** Microgranular texture of a protodike margin (plane-polarized light). **f)** Protodike centre showing a texture similar to the isotropic ophitic gabbro (plane-polarized light).

As observed in Wadi Gideah (Figure 6), the contact between the isotropic ophitic gabbros and the overlying sheeted dike complex is very sharp. Gabbros are again intrusive in the sheeted dike and crosscut former dike margins. Close to this contact, dike xenoliths are locally accumulated, generally small (~10 cm, Figure 8c), and form ~one meter wide clusters (Figure 8c-d). These xenoliths have granoblastic textures; they are totally metamorphosed in



the greenschist facies and the granoblastic texture is commonly blurred. The base of the dikes is also very altered but the recrystallized granular texture, associated to an enrichment in granular oxides, is still recognizable in some samples (Figure 9d); these are interpreted as relics, after subsequent alteration, of the granoblastic overprint. Because of the strong greenschist facies overprint and of the strong weathering, it is not possible to estimate the vertical extent of the granoblastic overprint. These textures are identical to those observed in the same structural position in the Wadi Gideah area.

Upsection, the Al Ahmadi hills continue over ~1000 m with the sheeted dike complex, oriented 0E50 on average (Figure 3). The sheeted dikes are typical of what is observed elsewhere in the Oman ophiolite; it is made of parallel, about 1 to 1.5 meter wide, greenschist altered dikes, bounded by dark chilled margins against other dikes.

In the whole section, late dikes crosscut other lithologies. In the lower part of the section, late dikes display microgranular margins that are nearly free of oxides (Figure 9e), and ophitic coarser grained center (Figure 9f). They grade upsection, close to the contact with the sheeted dikes, to diabase dikes with chilled margins. Nicolas and Boudier (1991) and Nicolas et al. (2008) described in the root zone of the sheeted dike complex similar dikes with ophitic texture in the center and microgranular margins, which they name "protodikes", and ascribed to slow cooling in a hot and hydrous environment. The magmatic protodikes depart from the metamorphic granoblastic truncated dikes in that only their margins display microgranular textures (e.g., compare Figure 7a with Figure 9e for the margins, and Figure 7b with Figure 9f for the center of dikes). We interpret the late dikes observed in the mapped areas as protodikes that intrude the still hot, recently crystallized gabbros. Because a single protodike cannot be followed in the field over hundreds of meters, the textural transition from protodikes with microgranular margins to dikes with chilled margins up-section is not precisely located.

### **III.3.e. IODP Hole 1256D**

IODP Hole 1256D reached for the first time the sheeted dikes / gabbro transition in ultrafast-spread oceanic crust (Teagle et al., 2006; Wilson et al., 2006; Alt, 2007). The sheeted dikes / gabbro transition is sharp and represents an intrusive contact similar to those observed in Oman (Figure 4c in Wilson et al. (2006), and Figure 6 herein). The base of the sheeted dike complex comprises recrystallized, granoblastic texture domains (granulitic facies) over ~60 meters; this texture is identical to the granoblastic one described herein in samples from

Oman (see for example the concordance between Figure 7a and 10a for the fine granoblastic lithologies and 7b and 10b for coarser-grained recrystallized ones). The section below the sheeted dike / gabbro contact has been re-sampled for this study (Table A1).

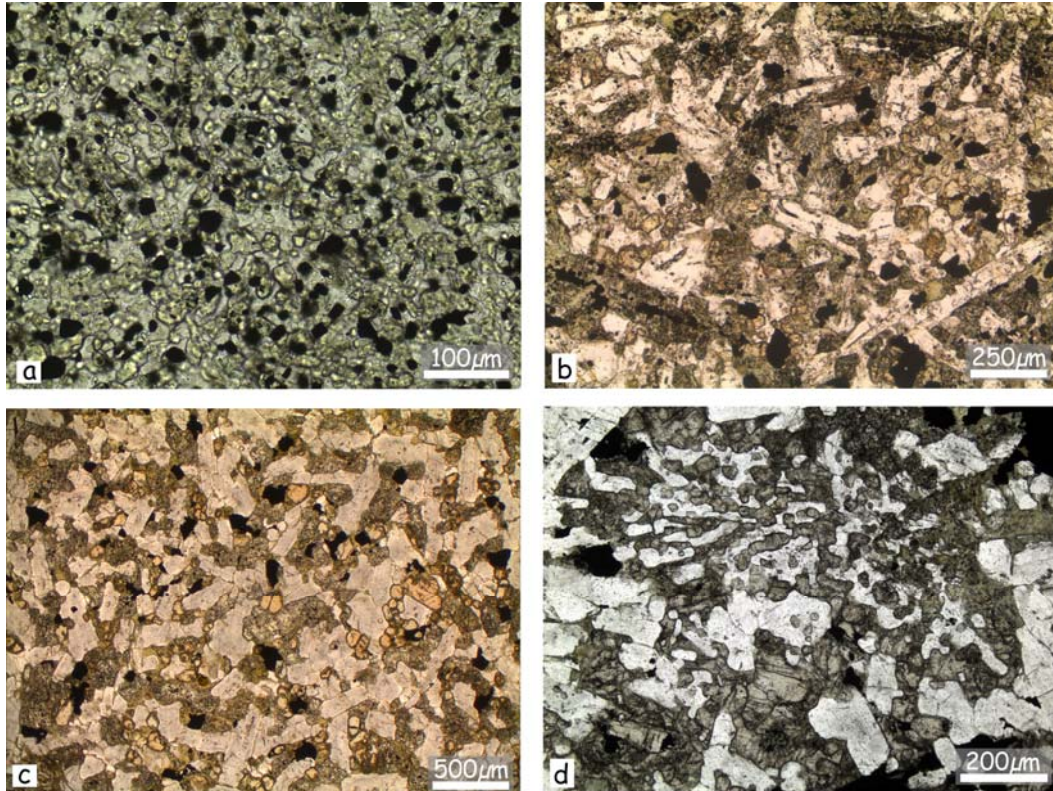


**Figure 10:** Photomicrographs of samples from IODP Hole 1256D (plane-polarized light). Photographs in a) and d) are from the IODP database (Expedition 312; <http://iodp.tamu.edu/janusweb/imaging/tsmicro.shtml>). a) High oxide concentration in a fine-grained granoblastic dike (recrystallized base of the sheeted dike complex; sample 312\_1256D\_205R1\_10-14). b) Coarser-grained, partially recrystallized texture (pyroxenes are granular and recrystallized) in diabase at the base of the granoblastic dike interval (sample 312\_1256D\_209R1\_17-19). c) Coarser-grained, partially recrystallized texture in the “granoblastic screen” located between gabbro 1 and gabbro 2 (interpreted as xenoliths of recrystallized dikes in the present study, see text for further discussion; sample 312\_1256D\_227R1\_30-34). Pyroxenes are granular and oxides-bearing clinopyroxenes are inferred to crystallize after former amphiboles. d) Patch with structure interpreted as a former granoblastic domain in isotropic gabbro (sample 312\_1256D\_223R3\_1-6).

Wilson et al. (2006) describe two granoblastic intervals that are interpreted as “screens of granoblastic dikes”, the first one (~15 to 25 m thick) is located between two gabbroic bodies (“gabbro 1” (~45m) and deeper “gabbro 2” (~15m)) and the second one (very poorly recovered) at the bottom of the “gabbro 2” interval, close to the bottom of Hole 1256D. The first thick “screen of granoblastic dikes” (Figure 10c) is poorly recovered (<30%; Figure 11). However, even in the most continuous cores of this interval, granoblastic lithologies are

crosscut by thin intrusions of gabbros and oceanic plagiogranites, with diffuse to sharp contacts (Figure 11).

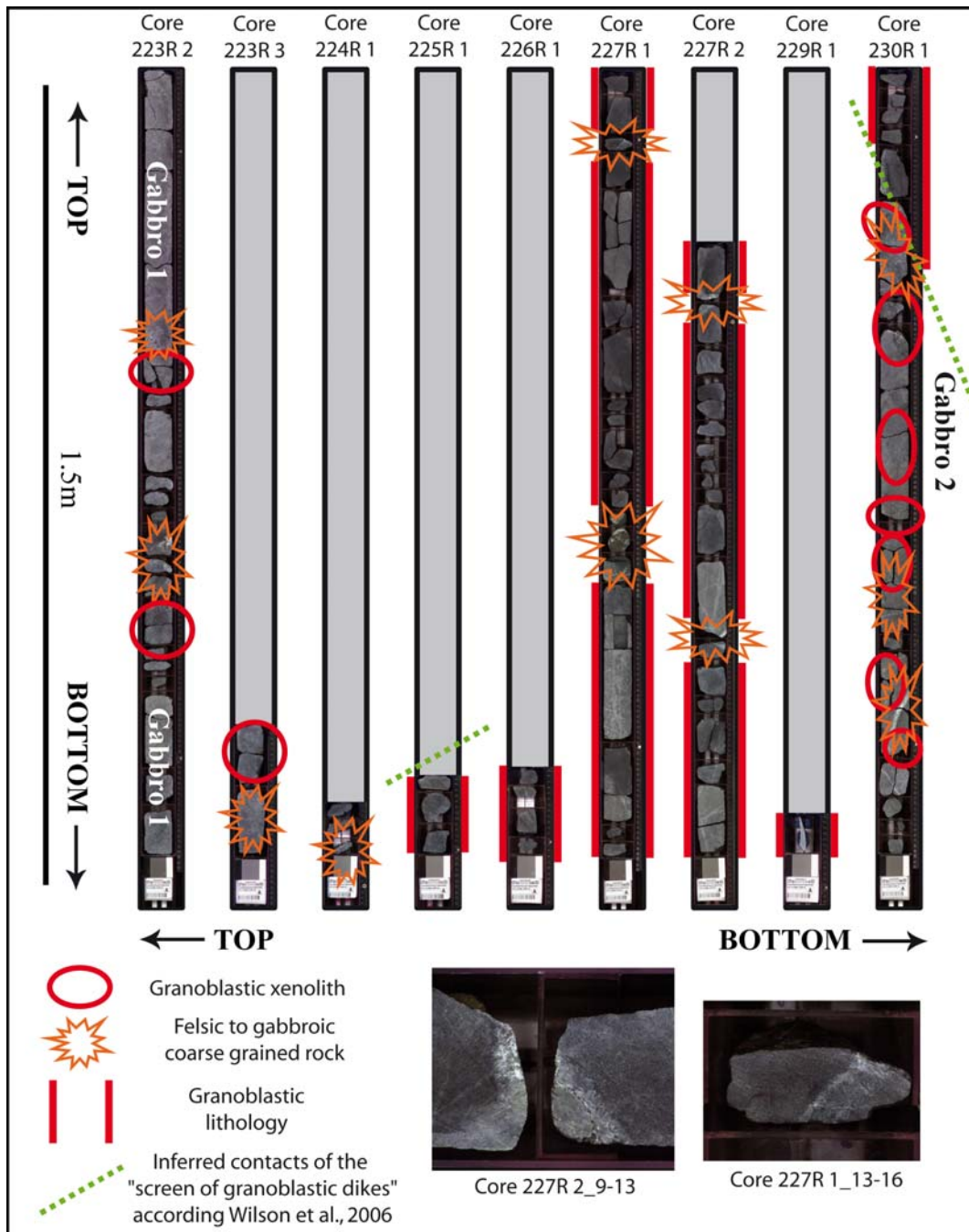


**Figure 11:** IODP 1256D drilled cores between 1450.8 and 1484.4 mbsf. From top to bottom, encountered lithologies are xenolith-bearing gabbro 1, granoblastic lithologies described as a “screen of granoblastic dikes” by Wilson et al. (2006), and xenolith-bearing gabbro 2. The two photographs show some of the felsic to mafic “melts” that crosscut the recrystallized granoblastic lithologies. Red circles highlight the xenoliths of granoblastic lithologies and orange stars highlight the occurrence of felsic to gabbroic coarse-grained material. Intervals with recrystallized granoblastic texture are highlighted by thick red lines along the core margins. The dotted green lines represent the upper and lower limits of the “screen of granoblastic dikes” described by Wilson et al. (2006). The continuous granoblastic domains are less than one meter thick.

We have also observed in the core the presence of sparse, small (cm to ~10cm) xenoliths in the upper part of the “gabbro 1” interval, at the contact with the base of the granoblastic dikes and, as described in Wilson et al. (2006), higher concentrations of xenoliths deeper in the “gabbro 2” interval, close to the bottom of the drilling hole. The sampled xenoliths show recrystallized textures similar to the ones of the base of the granoblastic dikes and to the ones of the thick “screen of granoblastic dikes” located between the “gabbro 1” and “gabbro 2” intervals. Granoblastic patches similar to those observed in Wadi Gideah (Figure 7c) are also observed in the “gabbro 1” and “gabbro 2” intervals (Figure 10d).

### **III.3.f. Mineral compositions and thermometry**

Mineral electron microprobe analyses were performed at Géosciences Montpellier and at the Institut für Mineralogie, Hannover using a Cameca SX 100 electron microprobe equipped with 5 spectrometers and an operating system “Peak sight”. Data were obtained using a 15KV acceleration potential, a static (fixed) beam,  $K\alpha$  emission from all elements, and the “PAP” matrix correction (Pouchou and Pichoir, 1991) in Hannover and its modification (Merlet, 1994) in Montpellier. Most element concentrations were obtained with a beam current of 15nA and a counting time of 10 to 120s on peak and background.

Analyses presented herein (Table A1) were acquired on samples from the base of the Oman sheeted dike (granoblastic domains), from diabase xenoliths that are present in the isotropic ophitic gabbros, from coarse grained gabbros that surround these xenoliths, from oceanic plagiogranites sampled at the base of the sheeted dikes, from a protodike, and from foliated gabbros. All Oman samples come from the Al Ahmadi Hills and Wadi Gideah areas. We also present for comparison analyses of IODP Hole 1256D samples. These samples come from the lowermost granoblastic dikes (just above the first recovered gabbro), from the “screen of granoblastic dikes” located between the “gabbro 1” and “gabbro 2” intervals, and from granoblastic xenoliths in gabbros.

#### ***III.3.f.1. Root zone lithologies and protodikes***

In Oman samples, plagioclase compositions are very variable; they range from  $An_{10}$  to  $An_{57}$  in granoblastic lithologies and xenoliths, and reach  $An_{74}$  in the protodike (Figure 12). Clinopyroxene Mg# ranges from 59 to 72 in granoblastic lithologies and reaches 75 in the protodike (Figure 12).  $Al_2O_3$  and  $TiO_2$  are significantly low compared to typically magmatic clinopyroxenes from oceanic mafic rocks and to those obtained experimentally in

corresponding tholeiitic systems (Figure 13).  $\text{TiO}_2$  is strongly correlated with  $\text{Al}_2\text{O}_3$  (with  $\text{Al}_2\text{O}_3/\text{TiO}_2 \approx 3$ ) and shows an apparent linear trend pronounced at low concentrations (Figure 13). CaO contents are high, and  $\text{Cr}_2\text{O}_3$  is nearly always under detection limits. Orthopyroxenes are present only in protodikes and have an Mg# of 68. Amphibole compositions are variables, including actinolite, hornblende, edenite, and pargasite. One granoblastic dike sample from the Wadi Gideah area contains zoned plagioclases, with  $\text{An}_{22}$  cores and  $\text{An}_{38}$  rims. Granoblastic patches observed in the isotropic ophitic gabbros (Figure 7c) are similar in compositions to other granoblastic lithologies, with  $\text{An}_{48}$  plagioclases and Mg# = 69 for clinopyroxenes. Oxide bearing clinopyroxene from the truncated veins observed at the sheeted dike / gabbro transition (Figure 7g-h) plot in the  $\text{TiO}_2$  vs.  $\text{Al}_2\text{O}_3$  linear trend (Figure 13).

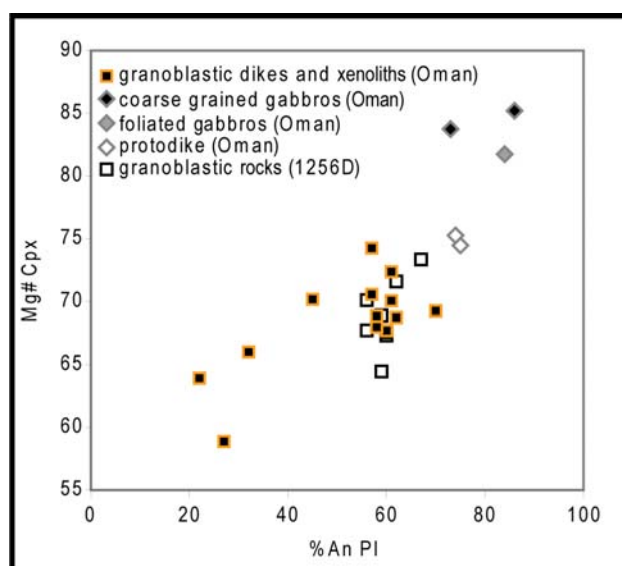


**Figure 12:** Mg# of clinopyroxene versus An content of plagioclases for recrystallized granoblastic dikes and xenoliths from Oman and from IODP Hole 1256D (average values for each sample). Protodike, foliated gabbro, and coarse-grained gabbro compositions are given for comparison. As low temperature alteration has led to a late albitisation of some samples, the maximum values of the An content are used.

In oceanic plagiogranites, plagioclases are albite to oligoclase with An ranging from 7 to 27. Small clinopyroxenes, which show petrographic features similar to those from granoblastic lithologies are characteristically low in Al, Ti, and Cr, and plot on the  $\text{TiO}_2$  vs.  $\text{Al}_2\text{O}_3$  linear trend (Figure 13).

Mineral compositions from the IODP Hole 1256D granoblastic lithologies are similar to those from the same lithologies in Oman (Table A1, Figure 12). Plagioclase composition ranges from andesine ( $\text{An}_{41}$ ) to labradorite ( $\text{An}_{67}$ ). Clinopyroxenes range from augite to

diopside, with Mg# between 63 and 74, low Al<sub>2</sub>O<sub>3</sub> and low TiO<sub>2</sub> contents, high CaO content, and Cr<sub>2</sub>O<sub>3</sub> always under the detection limit (Figure 13). These clinopyroxenes plot in the TiO<sub>2</sub> vs. Al<sub>2</sub>O<sub>3</sub> linear trend (Figure 13). Orthopyroxenes are enstatite, with Mg# between 58 and 66. Amphiboles are hornblende and pargasite with late actinolite.

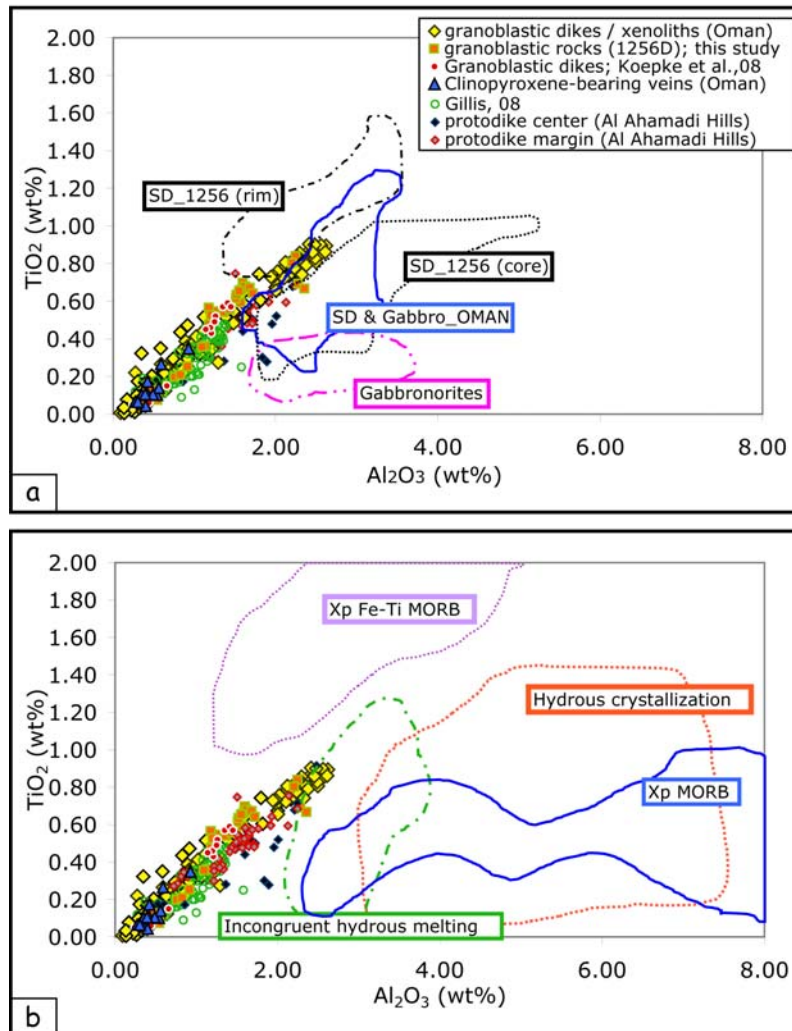


**Figure 13:** TiO<sub>2</sub> versus Al<sub>2</sub>O<sub>3</sub> in clinopyroxene for recrystallized granoblastic dikes and xenoliths from Oman and from IODP Hole 1256D. Fields represent data from literature for comparison (a: natural samples, b: experimental samples). Natural sample data are from Dziony et al. (2008) for the IODP Hole 1256D sheeted dikes not affected by granoblastic imprint (SD), from Miyashita et al. (2003) and Pallister and Hopson (1981) for the Oman ophiolite sheeted dikes and gabbros, and from Boudier et al. (2000) and Gerbert-Gaillard (2002) for the Oman gabbroonorites. Experimental data are from Snyder et al. (1993), Toplis and Carroll (1995), and Toplis et al. (1994) for Fe-Ti MORB crystallization experiments (Xp Fe-Ti MORB); from Berndt et al. (2005), and Feig et al. (2006) for hydrous crystallization experiments in primitive MORB-type system; from Grove and Bryan (1983), and Kinzler and Grove (1992) for MORB crystallization experiments (Xp MORB); and from Koepke et al. (2004) for clinopyroxenes formed during hydrous partial melting of gabbros. Note that the clinopyroxene in the granoblastic lithologies form a characteristic linear trend at low concentrations, which is not shown by data for typical MORB magmatic processes, neither from natural occurrences nor from experiments.

### ***III.3.f.2. Isotropic/foliated gabbros transition in Wadi Gideah***

Xenolith samples contain plagioclase ranging from An<sub>31</sub> to An<sub>57</sub>. Clinopyroxenes are either augite or diopside, and have Mg# between 61 and 77. They are depleted in Al<sub>2</sub>O<sub>3</sub> and TiO<sub>2</sub>, and enriched in CaO; Cr<sub>2</sub>O<sub>3</sub> is always under detection limits; they plot in the TiO<sub>2</sub> vs. Al<sub>2</sub>O<sub>3</sub> linear trend (Figure 13). Amphiboles are hornblende.

Gabbroic samples contain olivine with Mg# of 78; plagioclases range from An<sub>57</sub> to An<sub>86</sub> and clinopyroxenes are mostly diopside with Mg# of 86. Clinopyroxenes have high Al<sub>2</sub>O<sub>3</sub> contents and high Cr<sub>2</sub>O<sub>3</sub> contents (up to ~1%wt) and plot out of the TiO<sub>2</sub> vs. Al<sub>2</sub>O<sub>3</sub> linear trend defined by clinopyroxenes from granoblastic lithologies at the base of the sheeted dikes. Amphiboles are pargasite.

### ***III.3.f.3. Foliated gabbros***

In foliated gabbros olivine is Fo<sub>73</sub>, and plagioclase is bytownite with An<sub>84</sub>. Clinopyroxenes range from augite to diopside, with Mg# of 88 on average, and plot out of the TiO<sub>2</sub> vs. Al<sub>2</sub>O<sub>3</sub> linear trend defined by clinopyroxenes from the granoblastic samples. Cr<sub>2</sub>O<sub>3</sub> content is 0.55wt%, clearly above the detection limit. Amphiboles are hornblende, edenite and pargasite. In the domains of foliated gabbros that contain late orthopyroxene and pargasite rims around olivine, plagioclase is bytownite with An<sub>83</sub>, clinopyroxenes are augite to diopside with Mg# of 82 in average and also plot out of the TiO<sub>2</sub> vs. Al<sub>2</sub>O<sub>3</sub> linear trend defined by granoblastic clinopyroxenes. Cr<sub>2</sub>O<sub>3</sub> contents are also above the detection limit (0.17wt%). Orthopyroxene that rims olivine is enstatite with an average Mg# of 73.

### ***III.3.f.4. Thermometry***

Calculated temperatures obtained from amphibole compositions with the Ernst & Liu (1998) semi-quantitative thermometer, from coexisting amphibole and plagioclase with the Holland and Blundy (1994) thermometer, and from coexisting clino- and orthopyroxenes with the Andersen et al. (1993) thermometer, are summarized in Table 1. The errors on these temperature estimates are indicated in Table 1 for the two-pyroxene thermometer, are ±35-40°C for the Holland and Blundy (1994) thermometer, and are not estimated by Ernst and Liu (1998) for their semi-quantitative thermometer. Temperatures obtained from amphiboles compositions reach ~1020°C with the Ernst and Liu (1998) thermometer, ~820°C with the Holland and Blundy (1994) thermometer, and are consistent with granulite facies conditions.

Chapter III. Magmatic / hydrothermal interactions in the Oman ophiolite

Temperatures obtained with the Andersen et al. (1993) thermometer reach 1030°C in granoblastic lithologies (xenoliths and truncated dikes) and 950°C in protodikes.

<i>lithology</i>	<i>location</i>	<i>sample</i>	<i>%An Max</i>	<i>T<sub>max</sub> Amp (°C)</i>	<i>T Amp H&amp;B (°C)</i>	<i>T Opx-Cpx (°C)</i>
RZ_dike	Gideah	08OL15b-leuco	60	660	692	-
RZ_dike	Gideah	08OL15b	61	922	728	-
RZ_dike	Gideah	08OL01e	60	571	615	-
RZ_dike	Gideah	08OL04a	58	885	731	-
RZ_dike	Gideah	08OL05a	62	633	680	-
RZ_dike	Gideah	07OL51b	22	562	739	-
RZ_dike	Gideah	08OL06i	47	754	640	-
RZ_Cpx vein	Gideah	08OL15i1	70	853	711	-
RZ_dike	Al Ahmadi	08OL07b	32	650	820	-
RZ_Plagiogranite	Gideah	07OL48d	27	-	-	-
granoblastic patch in isotropic gabbro	Gideah	08OL01d	58	726	784	-
xenolith in isotropic gabbro	Gideah	08OL06f	61	998	727	-
xenolith close to isotropic/ foliated gabbro transition	Al Ahmadi	08OL29e	45	665	729	-
xenolith close to isotropic/ foliated gabbro transition	Gideah	07OL49c1	57	758	803	-
xenolith close to isotropic/ foliated gabbro transition	Gideah	07OL49b1	57	788	772	-
coarse grained gabbro	Gideah	07OL49d1	73	1023	811	-
coarse grained gabbro	Gideah	07OL49d2	86	953	683	-
protodike border	Al Ahmadi	08OL29c	75	831	672	949±40
protodike center	Al Ahmadi	08OL29d	74	868	676	-
foliated gabbro A	Al Ahmadi	08OL29b	87	750	701	-
foliated gabbro B	Al Ahmadi	08OL29a	84	999	731	773±18
granoblastic dikes	1256D	312_1256D_D202R1_8-10	59	592	604	1010±24
granoblastic screen	1256D	312_1256D_D225R1_4-8	67	887	699	965±77
granoblastic screen	1256D	312_1256D_D226-R1-4-6	59	823	724	1019±34
granoblastic screen	1256D	312_1256D_D227R1_30-34	56	632	665	956±77
granoblastic xenolith in isotropic gabbro	1256D	312_1256D_D230R1_15-20	56	-	-	1017±30
granoblastic xenolith in isotropic gabbro	1256D	312_1256D_D230R1_73-80	60	713	769	1030±35
granoblastic xenolith in isotropic gabbro	1256D	312_1256D_D230R1_87-90	60	704	753	1028±21
lower granoblastic interval	1256D	312_1256D_D233R1_14-18	62	-	-	1003±50

**Table 1:** Maximum An content of plagioclase, and, temperature estimates (amphibole thermometer, Ernst and Liu, 1998 [ $T_{max}$ ] and Holland and Blundy, 1994 [H&B]; two-pyroxene thermometer, Andersen et al., 1993).  $Pl_c$ =plagioclase core;  $Pl_b$ =plagioclase rim; Amp=amphibole; ilm=ilmenite; magt=magnetite; Cpx=clinopyroxene; Chlo=chlorite; Ol=olivine; Opx=orthopyroxene; Qz=quartz.



### III.3.g. Discussion

#### III.3.g.1. *A dynamic melt lens*

The occurrence of a sharp contact between sheeted dikes and underlying gabbro, with abruptly truncated sheeted dikes, and of gabbroic to oceanic plagiogranitic dikelets intruding the sheeted dike, together with the evidence that gabbroic and oceanic plagiogranitic bodies crosscut former dike margins, imply a magmatic contact that is not disturbed by tectonics (Figure 6). This magmatic contact could be the consequence of either the upwelling of a magma body which intrudes the dikes, or hydrous partial melting of the dikes. The latter could be induced either by an injection of hydrous fluids in a still hot (>850°C) environment (Nicolas et al., 2008), or by the upwelling of the magma body which reheats some previously hydrothermally altered lithologies above their hydrous solidus (e.g., Coogan et al., 2003; Wilson et al., 2006). Both hydrous melting processes lead to the generation of felsic to mafic melts, depending on temperature (Beard & Lofgren, 1991; Koepke et al., 2005b). Observations made in Oman and in IODP Hole 1256D allow the identification of active processes in the root zone of the sheeted dike complex.

The granoblastic textures at the base of the sheeted dikes could be ascribed to contact metamorphism, as proposed for IODP Hole 1256D (Wilson et al., 2006; Koepke et al., 2008), the Troodos ophiolite (Gillis & Roberts, 1999), or Wadi Him in Oman (Gillis, 2008). However, in contrast to what is postulated by Gillis (2008), contact metamorphism is not the only process producing well equilibrated fine grained textures. Alternatively, Rothery (1983), Nicolas & Boudier (1991) and Nicolas et al. (2008) argue that microgranular textures of “protodike” margins are magmatic and represent, in a steady state system, the roots of the sheeted dikes. We propose that the late dikes described herein correspond to such protodikes. However, several features described in the dikes truncated by gabbro and in granoblastic xenoliths depart from the protodike description:

- (1) The core of truncated dikes is also granoblastic (Figure 7b and 9d) while the core of protodikes is described as texturally close to isotropic ophitic gabbro (Nicolas et al., 2008; Figure 9f herein).
- (2) All granoblastic xenoliths and truncated dikes described in this study contain either high oxide concentrations (up to 10% of ilmenite+magnetite), or numerous oxide inclusions in pyroxenes, or both (Figures 7 and 9c, d). The observed oxide concentrations depart from

the published protodike descriptions (see for example Figure 6a in Nicolas et al. 2008), and the occurrence of numerous tiny oxides inclusions in the clinopyroxenes of granoblastic lithologies is interpreted as a consequence of the granulitic overprint of previously hydrothermally altered dike rocks. Koepke et al. (2008) described the evolution of the granoblastic metamorphism in the drilled core from site 1256D and show that similar clinopyroxenes with oxide inclusions, present in the granoblastic dikes from IODP Hole 1256D, recrystallized from former amphiboles. In Oman, the occurrence of veins composed of oxide-bearing clinopyroxenes at the base of the truncated granoblastic sheeted dikes (Figure 7g-h) also points to a metamorphic origin. Amphibole-bearing hydrothermal veins are common at the base of the sheeted dike complex, but magmatic clinopyroxenite veins have not been described. We postulate here that these peculiar veins result from the recrystallization of amphibole-bearing hydrothermal veins through dehydration reactions during a reheating episode.

(3) Clinopyroxenes from the prograde veins have compositions similar to those in the granoblastic dikes and xenoliths (Table A1, Figure 13). They are poor in  $\text{Al}_2\text{O}_3$ , rich in CaO and plot in the  $\text{TiO}_2$  vs.  $\text{Al}_2\text{O}_3$  linear trend defined by granoblastic clinopyroxenes (Figure 13). These compositions clearly differ from published ones for magmatic natural and experimental clinopyroxenes in oceanic lithologies (Figure 13). Such compositions with uncommon low  $\text{Al}_2\text{O}_3$  contents may indicate, as shown by Spear & Markussen (1997), infra-magmatic temperature equilibration ( $<1000^\circ\text{C}$ ), and are consistent with granulite facies conditions. The correlation of  $\text{Al}_2\text{O}_3$  with  $\text{TiO}_2$  could be explained by the fact that Ti stability in clinopyroxene is linked to its Al content (Lundstrom et al., 1998). The very low  $\text{Cr}_2\text{O}_3$  content (always under detection limits) also supports the metamorphic origin of these minerals, as magmatic oceanic pyroxenes contain higher amounts of Cr (Koepke et al., 2008). An incongruent origin linked to low degrees of hydrous partial melting of previously hydrothermally altered dikes may also be proposed as it would also result in the destabilization and dehydration of amphibole-bearing lithologies.

All granoblastic xenoliths and truncated dikes have similar petrological and geochemical characteristics, which are clearly different from protodikes. Their occurrence attests to a reheating stage that we relate to the upwelling of the top of the melt lens. The presence of granoblastic xenoliths and patches in the isotropic ophitic gabbros, which are believed to represent some reheated pieces of previously hydrothermally altered sheeted dike, attests to assimilation processes, and is consistent with an upwelling stage. Upward migration

of the melt lens summit can be triggered either by an upward migration of the whole melt lens, or by an inflation of its volume. Alternatively, the intrusive contact of gabbro with sheeted dikes, and associated reheating could be related to the off-axis injection of a new melt lens, as recently imaged at the East Pacific Rise by Canales et al. (2008).

The common occurrence of leucocratic rocks (oceanic plagiogranites) at the contact between the sheeted dikes and the underlying gabbros may be related either to differentiation at the top of the melt lens or to hydrous partial melting of the sheeted dikes (Pedersen & Malpas, 1984; Beard & Lofgren, 1991). In the present case, because reheating and magma upwelling are documented, and temperatures up to 920°C and 1000°C are calculated for the granoblastic dikes and the xenoliths, respectively, leucocratic rocks are likely generated by hydrous partial melting induced by reheating of hydrothermally altered dikes. This hypothesis is also supported by the occurrence, in the oceanic plagiogranites, of relic pyroxenes that are chemically identical to those of the reheated granoblastic dikes (Table A1). The reverse zoning observed in plagioclases at the base of one granoblastic dike in Wadi Gideah may result from an early hydrothermal alteration stage leading to the albitisation of plagioclases (An<sub>22</sub>), followed by hydrous partial melting that leads to the generation of wet dioritic melts percolating through the base of dikes and crystallizing An<sub>38</sub> plagioclase rims.

The late dikes (hereafter “dike 2”, Figure 5) that crosscut the isotropic ophitic gabbros postdate the contact between the gabbro and the sheeted dikes, and imply the crystallization of the isotropic ophitic gabbros subsequently to a downward migration of the melt lens. Dikes 2 could either be injected from the remaining melt lens, or be injected laterally along axis, or be related to an off-axis magmatic episode. Because dikes 2 grade downward to protodikes, they must be emplaced in a still hot environment (~950°C according the two-pyroxenes thermometer), hence not far off-axis. The low Al content of the clinopyroxenes present in protodikes also attests to a relatively low temperature equilibration that can correspond to subsolidus conditions. The equilibration of pyroxenes at these temperatures may result from slow cooling of the isotropic gabbro body. We interpret dikes 2 intrusion in ophitic gabbro as illustrating the downward migration of the top of the melt lens. This downward movement results in the crystallization of the isotropic ophitic gabbros, and allows injection of new dikes in this still hot environment from the underlying melt lens or laterally, along axis. The downward movement could be triggered either by downward migration of the whole melt lens or by a deflation of its volume.

In Wadi Gideah, the sheeted dikes / gabbro transition is a well defined contact that can be mapped in the field (Figure 2). We interpret the mapped contact (Figure 2c) as reflecting a ~50 m depth variation of the melt lens roof over a distance of ~150m. However, one cannot exclude that this offset is related to a thin fault or shear zone, which is not visible due to the poor outcropping conditions between the two hills. Larger amplitude (one to several kilometres) variations of the melt lens summit depth have been documented by seismic imaging at the East Pacific Rise (Cormier 1997; Hussenoeder et al. 1996; Solomon & Toomey 1992; Singh et al. 1998). An along-axis "fine-scale segmentation" of the melt lens reflector has been recently imaged in the 9°50'N region of the East Pacific Rise (Carbotte et al., 2008), and reveals comparable depth variations of tens of meters.

### ***III.3.g.2. Stopping, assimilation and coarse-grained gabbros***

In the context of magma upwelling at the root of the sheeted dikes, the occurrence of oxide-rich, granoblastic xenoliths in the isotropic ophitic gabbros is significant. Some xenoliths are located near the contact with sheeted dikes, but most of them appear to be accumulated at the base of the isotropic ophitic gabbro horizon, as seen in Al Ahmadi Hills, above the contact with foliated gabbros (Figure 8). The density of granoblastic xenoliths is ~3.02 g.cm<sup>-3</sup> (by considering the modal proportions from our petrological observations and crystal densities at 1000°C (Fei, 1995): ~60 % plagioclase,  $d \approx 2.6 \text{ g.cm}^{-3}$ ; ~30% clinopyroxene,  $d \approx 3.3 \text{ g.cm}^{-3}$ ; ~5% magnetite,  $d \approx 4.9 \text{ g.cm}^{-3}$  and ~5% ilmenite,  $d \approx 4.5 \text{ g.cm}^{-3}$ ). Because plagioclase is the only mineral of the granoblastic assemblage that has a density lower than the estimated whole rock, and samples with plagioclase contents > 60% are rare, this estimated density is a lower bound. It is significantly higher than the density of a dry basaltic melt that is thought to fill the melt lens, which is ~2.7 g.cm<sup>-3</sup>, (calculated with a pressure of 1 kbar and a temperature of 1100°C; e.g., Lange and Carmichael, 1990). The melt density can be slightly higher if more evolved, and slightly lower if hydrous, but such melts are not expected to be dominant in the melt lens. Stopping is also controlled by the rheology of the host magma. It requires that the crystal content in the melt lens is low enough that it does not change significantly the density and viscosity of the magma. Geophysical and petrophysical studies show that underneath the melt lens is the main magma chamber, which contains on average a minimum of 80% of crystals (e.g., Caress et al., 1992; Collier and Singh, 1997; Singh et al., 1998; Lamoureux et al., 1999; Dunn et al., 2000; Crawford and Webb, 2002). Xenoliths have therefore sunk through the mostly liquid melt lens to accumulate at its floor. These xenoliths are now observed in the lower part of the isotropic

ophitic gabbros, which we must then interpret as representing the melt lens fossilized once away from the axis. As the floor of the melt lens is believed to continuously subside (e.g., Nicolas et al., 2009), we speculate that the xenolith accumulation that we observe occurred close to the off-axis margin of the melt lens. Presumably, dike fragments are also stopped on axis, but they cannot be preserved as they are either fully assimilated or entrained and transposed downward within the foliated gabbros (Boudier et al., 1996; Nicolas et al., 2009) in which they are observed as recrystallized microgabbro centimeter to decimeter thick lenses (Boudier et al., 2000). Singh et al. (1998) have shown that the melt lens is not continuous along the ridge axis but that it ranges from pure melt to mush. The partly crystallized zones may represent the first step toward the fossilization of the melt lens occurring when a decrease in the magmatic activity happens in a given section of the ridge.

We also interpret the granoblastic patches (0.5 to 1mm wide) in the ophitic gabbros as relics resulting from the partial assimilation of sheeted dike fragments (Figure 7c). The oxide-rich granoblastic texture of xenoliths is consistent, as described above, with a granulitic overprint, and related dehydration of previously hydrothermally altered lithologies. Enclosing gabbros contain amphiboles that record temperatures ( $\sim 1020^{\circ}\text{C}$ ) higher than the hydrous solidus of gabbro, which points to the hydrated nature of the magma surrounding the xenoliths (Koepke et al., 2005b; Feig et al., 2006). The concentration of coarse-grained gabbro around xenoliths (Figure 6f) is also consistent with magma hydration, as water is known to enhance crystal growth. In natural settings, high water pressure generally leads to more oxidizing conditions (e.g., Botcharnikov et al., 2005). However, the hydrated nature of magmas that produced coarse-grained gabbros is not consistent with differentiation under reducing conditions as proposed by MacLeod & Yaouancq (2000). Nicolas et al. (2008) have proposed that coarse-grained gabbros could also be generated by the arrival of hydrothermal fluids in the root zone at high temperature ( $\sim 1100\text{-}1200^{\circ}\text{C}$ ), leading to local, nearly total melting of gabbroic rocks. The coarse-grained gabbros described herein are spatially associated to granoblastic xenoliths that come from the base of the sheeted dike ( $\sim 100\text{m}$  above in the section), and sunk through the melt lens. Therefore, we propose an alternative process for the genesis of coarse-grained gabbro present in the studied areas that involves fluids brought by the dehydration of stopped and assimilated hydrothermally altered diabases in the melt lens. A way to test the role of recycled water in the genesis of coarse-grained gabbro would be to analyse the fluorine and chlorine contents of amphiboles (Coogan et al., 2001). Amphiboles with high chlorine contents and low fluorine contents attest to a hydrothermal origin, and the

ones with low chlorine contents and high fluorine contents attest to a magmatic origin. We postulate that amphibole crystallizing from melts that are hydrated through recycling of previously hydrothermally altered dikes may have high fluorine and high chlorine contents. Coogan (2003) proposed that the fluids leading to the crystallization of many of the magmatic amphiboles that are present in the Oman ophiolite gabbros are brought by such recycling processes. A review of the amphibole compositions presented in Coogan (2003) shows that many of them are fluorine and chlorine rich (>1000ppm), which is consistent with our hypothesis. Gillis et al. (2003) show that magmatic amphiboles from fast spreading ridges are chlorine enriched regarding the ones from slow spreading ridges; it also argues for important recycling of hydrothermally altered lithologies at fast spreading centers.

Another consequence of stoping and assimilation of hydrothermally altered diabases is the geochemical contamination of the melt lens. Assimilation processes in the melt lens should have a significant effect on the composition of the melts, in particular for volatile elements (Gillis et al., 2003). Our results are consistent with the model (Coogan et al., 2003), which states, from the chlorine content of EPR basalts (e.g., Michael and Schilling, 1989; Michael and Cornell, 1998), that ~20% of the oceanic crust may go through a cycle of crystallization, alteration, and assimilation.

### ***III.3.g.3. Comparison with IODP Hole 1256D***

Many features in IODP Hole 1256D match the observations made in the Oman ophiolite. In particular, the root of the sheeted dike complex is recrystallized to granoblastic textures, oceanic plagiogranites are present close to the dike root zone, the isotropic ophitic gabbro horizon contains granoblastic xenoliths and patches, and the compositions of minerals that form the granoblastic textures are similar to Oman ones (Table A1, Figures 10-13). IODP Hole 1256D can therefore be included in the same general model for the melt lens dynamics and for the relationships between the hydrothermal and magmatic systems.

In the Al Ahmadi Hills section, large xenoliths (up to 1.5 meters) displaying granoblastic textures are observed close to the isotropic ophitic gabbros / foliated gabbros transition, and are highly concentrated in some areas. These xenoliths can be partly assimilated by enclosing gabbro, and be associated to felsic melts at their border. In IODP Hole 1256D, the ~20m thick "screen of granoblastic dikes" located ~50m below the sheeted dike / gabbro contact (Wilson et al., 2006) is poorly recovered (<30%), and several thin horizons of gabbros and oceanic plagiogranites isolate larger (<1 m) granoblastic zones

(Figure 11). In the light of the observations made in Oman, we propose that this zone may correspond to granoblastic xenoliths, surrounded by silicic to gabbroic melts, which are accumulated in the isotropic gabbro horizon about 50m below the sheeted dike / gabbro contact. It also suggests that the bottom of Hole 1256D is close to the transition with the foliated gabbros and so to the bottom of the fossilized melt lens that would be ~100m thick. This interpretation is in contrast with the model presented by Koepke et al. (2008) in their Figure 14c; they interpreted the two gabbro screens as two separate intrusions into the lowermost part of the granoblastic dikes, shortly above the top of the fossilized magma chamber, which was hence not yet reached in Hole 1256D.

#### ***III.3.g.4. A general model***

The model presented here elaborates on detailed mapping, sampling and descriptions made in the Wadi Gideah and Al Ahmadi Hills areas, and on subsequent petrological and geochemical study. We visited ~10 other areas in the Oman ophiolite, which are consistent with our model. As described above, observations and analyses made on samples from the sheeted dikes / gabbro transition zone in IODP Hole 1256D, are also consistent with what is observed in Oman, and with our model.

The evolution of a melt lens can be tracked through the observed geological and petrological features (Figure 14). We first assume an episodic, steady state melt lens that injects dikes in the upper crust (Figure 14b). The base of these dikes is made of protodikes with microgranular margins and grade upward to “normal” dikes with chilled margins (Rothery, 1983; Nicolas & Boudier, 1991; Nicolas et al., 2008). In this steady state system, the injection of hydrothermal fluids in the dike root zone may trigger, locally, hydrous partial melting (Nicolas et al., 2008). This steady state system can evolve as a dynamic one with upward and downward migrations of the top of the melt lens (Figures 14c-d) as proposed by Hooft et al. (1997); Gillis (2002; 2008); Gillis and Roberts (1999); Gillis and Coogan (2002); Coogan et al. (2003), and Koepke et al. (2008). These migrations can represent either vertical movements of the melt lens itself or inflation and deflation of its volume. Lateral migrations or injections may also be proposed as near-axis melt lenses have recently been observed at the East Pacific Rise (Canales et al., 2008).

Upward migrations or lateral intrusions can be for example triggered by magma replenishment and result in the assimilation of the hydrothermally altered dikes, with the formation of xenoliths (Figure 14c). The roof is reheated by magma upwelling, and

hydrothermally altered sheeted dikes recrystallize in a granulitic granoblastic assemblage; they may locally undergo hydrous melting. Granoblastic lithologies also develop in xenoliths, which are partly to totally assimilated while sinking through the melt lens. If not totally assimilated, xenoliths sink down to the melt lens floor where they accumulate. They can then either be entrained downward in the igneous lower crust and be transposed in foliated gabbros, or be fossilized with the isotropic ophitic gabbros.

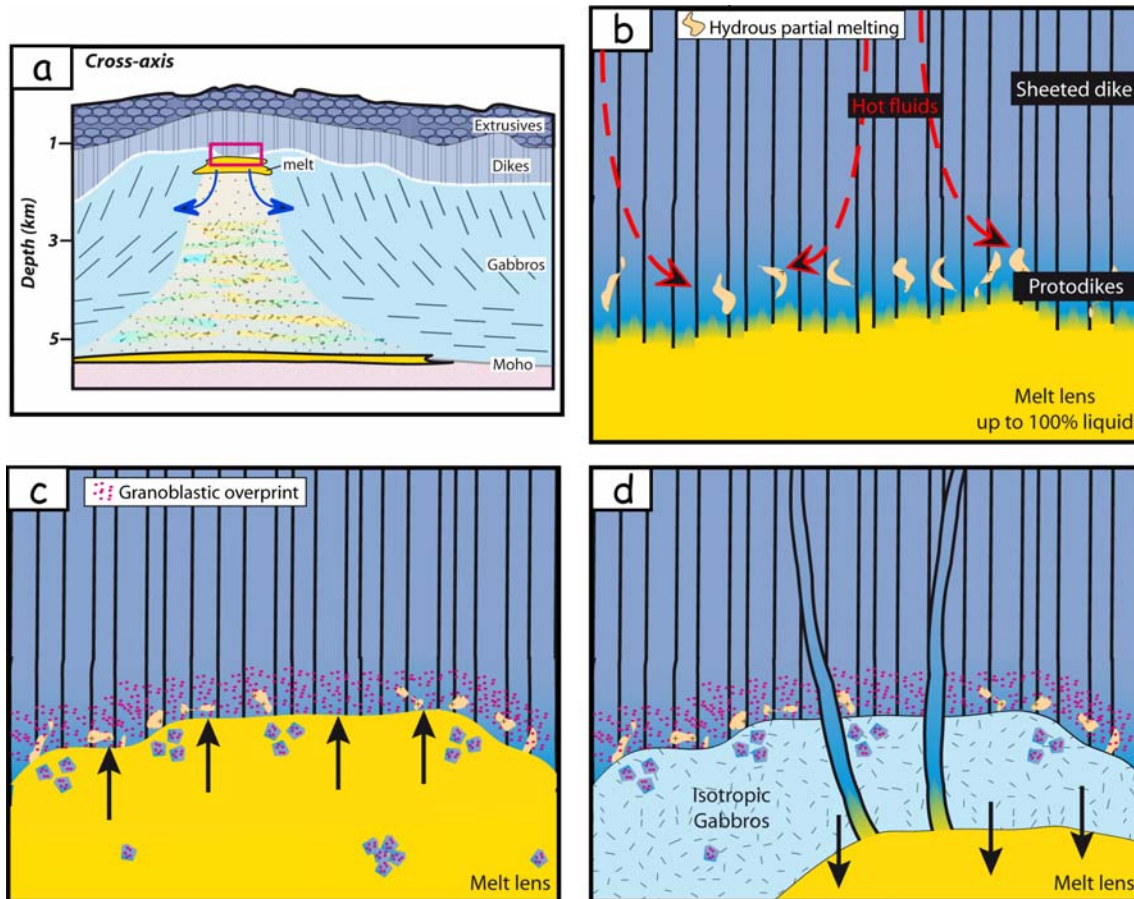


**Figure 14:** General schematic model for the dynamics of the melt lens; **a)** Schematic cross section at the axis of a fast spreading ridge (modified after Sinton and Detrick, 1992). The red rectangle indicates the location of the axial melt lens. **b)** Steady state stage with injection of dikes that have at their base microgranular margins (protodikes); hydrous partial melting is proposed to occur in the root zone of the sheeted dike complex as a result of hydrothermal fluid intrusion (Nicolas et al., 2008), **c)** Upward migration of the top of the melt lens resulting in reheating, and recrystallization of the base of the dikes (red dots) to granoblastic dikes, and in assimilation of xenoliths in the melt lens. Hydrous partial melting of the hydrothermally altered base of the dikes can also occur. **d)** Downward migration of the top of the melt lens resulting in the crystallization of the isotropic ophitic gabbros. New dikes can be injected laterally or from below; their root is typical of protodikes, with microgranular margins, and they grade upward to “classical” dikes with chilled margins (See text for further discussion).



Downward or lateral migrations can be triggered by a waning magmatic activity of the melt lens and/or by an eruption-related draining stage, and result in the crystallization of the isotropic gabbros at the roof and/or at the sides of the melt lens (Figure 14d). This crystallization corresponds to a partial fossilization of the melt lens which would become complete if melt supply to the melt lens was stopped.

Numerous scenarios can be elaborated combining the three stages described above: steady state, upward migration of the top of the melt lens, and downward migration of the top of the melt lens. Several episodes of upward and downward migrations may alternate, and only the highest level reached by the top of the melt lens will be eventually recorded at the contact with the sheeted dike. In the case of an upward migration following a downward one, the melt lens would assimilate the recently crystallized gabbros, and the overlying recrystallized sheeted dike if the upward migration is large enough. The presence of gabbroic xenoliths in the isotropic ophitic gabbro horizon attests to this process.

### ***III.3.g.5. Time scale constraints***

At fast spreading ridges, the time scales associated with magma migration, its residence within the main magma chamber and within the melt lens, and depth variations of the melt lens represent major parameters of the dynamics of oceanic crust formation. Unfortunately these time scales remain poorly constrained. We compile here published data dealing with these different time scales in order to replace our model on the evolution of a dynamic melt lens into a possible time frame.

Seismic reflection profiles of the East Pacific Rise (EPR) at 19°S (spreading rate: ~15 cm/y; Hooft et al., 1997) suggest variations in the magma supply on a time scale of ~100 000 years. Hooft et al. (1997) also propose that spreading events like dike intrusions and eruptions occur on much shorter time scales (tens to hundred years). Lagabrielle and Cormier (1999) propose that elongated summit troughs present at the EPR (17-18°S, spreading rate: ~15 cm/y) represent elongated collapsed calderas that form every ~100 000 years when a given ridge section deflates as a result of waning magma supply. Pollock et al. (2009) propose, based on spatial and temporal variations of basalt MgO contents at the EPR (Pito Deep, spreading rate: ~14 cm/y), that the magmatic temperatures, hence the magma supply, remain constant over time scales of tens of thousands of years, suggesting a nearly continuous magma recharge of the system at that time-scale. It is in agreement with the observations of Sinton et al. (2002) on the South EPR that suggest, based on the MgO content of successive units, that magmatic temperatures can remain constant over hundreds to tens of thousands of years.

Rannou et al. (2006) use a mathematic model based on geochemical data to infer that the magmatic system of the EPR at 17-19°S has a replenishment period of ~750 years for a magma residence time of ~300 years. This residence time is in good agreement with the estimate of Rubin et al. (2005) who propose, based on  $^{210}\text{Pb}$ - $^{226}\text{Ra}$ - $^{230}\text{Th}$  radioactive disequilibria on samples from the EPR at 9°N (spreading rate: ~11 cm/y) and 17°S, and from the Juan de Fuca Ridge (spreading rate: ~5.6 cm/y), that melt can be transferred within decades from the mantle to melt lens where it mixes and resides during ~200-400 years. Rubin and Sinton (2007) also propose a magma replenishment time <1 000 years at fast spreading ridges. Using the chemical zonations of olivine crystals present in four samples from the EPR (9°30'N and 10°30'N), Pan and Batiza (2002) have proposed that magma mixing events and eruptions may be in some cases separated by times as short as a few months.

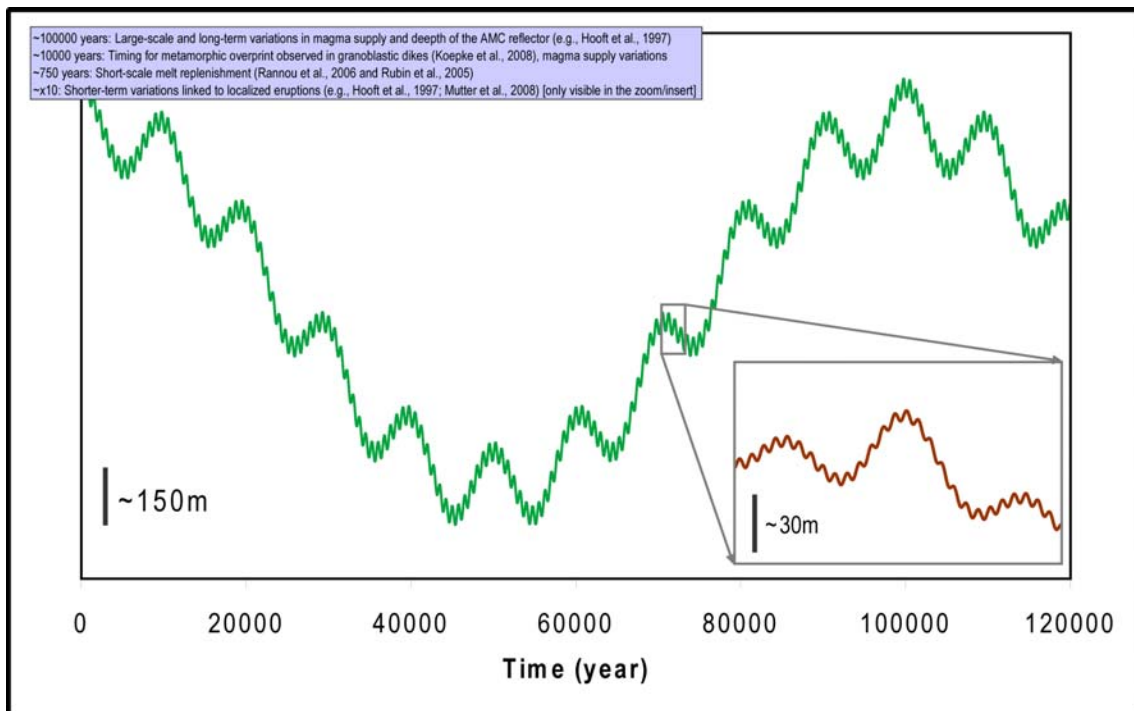


**Figure 15:** Compilation of estimated time scales for the dynamics of the melt lens, in a depth vs. time schematic graph. Four periods of depth variation are displayed (100 000, 10 000, 750, x10 years). The insert on a portion of the curve allows the visualization of the shortest time period (x10 years). See text for further discussion.

Preliminary results of the recent multi-streamer reflection imaging experiment in the 9°50'N region of the EPR (Mutter et al., 2008) show significant variation in the depth of the melt lens reflector between 1985 and 2008 at 9°50'N, possibly as a result of the 1991 and/or 2005-2006 eruptions in that area, while there is no significant variation observed at 9°30'N and 9°40'N. Carton et al. (2008) report a variation in the reflectivity strength of the melt lens

that they interpret as indicating a lower melt percentage between 9°45.2'N and 9°51.9'N, consistent with melt drainage during 1991 and 2005-2006 eruptions. These observations suggest that if replenishment has occurred or started since the last eruption, it is either incomplete or reduced (compared to the erupted melt volume). The timing between these events is in agreement with the time scale of ten to tens of years proposed for spreading events by Hooft et al. (1997). Sinton et al. (2002) and Bergmanis et al. (2007) also propose that eruptions along intermediate to superfast spreading centers are highly episodic and have repose times of ten years to a few hundred years.

Gillis (2008) and Koepke et al. (2008) have tried to estimate the duration of the thermal overprint, which we link to upward movements of the melt lens summit, by studying plagioclase zoning in granoblastic domains. Gillis (2008) estimates a minimum duration of 50 years for Hess Deep sample (spreading rate: ~13.5 cm/year). Koepke et al. (2008) propose an overprint duration of ~10 000 years for a sample from IODP Hole 1256D.

In summary, multi-disciplinary results provide indirect constraints on time scales for the vertical fluctuations of the melt lens ranging from a few tens of years to ~ 100 000 years. In figure 15, we propose a way to take into account these apparently contrasting results and to interpret them in a single schematic model. Four different time scales, consistent with published estimates, are used to describe the evolution of the summit of the melt lens: 100 000, 10 000, 750 and tens of years (Figure 15). These different time scales correspond to different processes and/or to different spatial scales. The long period (~ 100 000 years) proposed by Hooft et al. (1997) may represent variations in the magma supply from the mantle and correspond to variations of the depth of the melt lens in the scale of several hundreds of meters. The higher the spreading rate (hence the magma supply), the shallower the depth of the melt lens (Purdy et al., 1992; Phipps Morgan and Chen, 1993; Wilson et al., 2006). The ~10 000 years period is identified by Koepke et al. (2008) and Pollock et al. (2009) and may correspond to temporary high positions of the melt lens related to shorter term variations in the magma supply. The ~750 years period is the one identified by Rannou et al (2006), Rubin et al. (2005) and Rubin and Sinton (2007) for the melt lens replenishment. The shortest period corresponds to local, individual eruptions (e.g., Hooft et al., 1997; Mutter et al., 2008). The oscillatory evolution proposed in Figure 15 is an attempt to integrate published time scales constraints that are currently available. However, it remains schematic and probably too simplistic to illustrate natural processes. The regular oscillatory evolution is probably too simple and irregularities are likely to occur at each time scale. The very short time between magma mixing and eruptions documented by Pan and Batiza (2002) may be an

example of such episodic irregularities. The insert in Figure 15 proposes, as an example, an irregular evolution of the 750 years period for a portion of the curve. The depth variations of the summit of the melt lens identified in the present study range from meters to several tens of meters and match the short and middle time-scales ( $\leq 10\,000$  years).

### **III.3.h. Conclusions**

New detailed mapping and petrological studies of the gabbro / sheeted dikes transition zone performed in “undisturbed” zones of the Oman ophiolite provide information about the evolution of the melt lens at fast spreading ridges. It further constrains the interactions between the magmatic system and the convective hydrothermal system at the ridge axis. The comparison of the Oman ophiolite with IODP Hole 1256D results in a global coherent model, which reconciles the apparently contrasting previous published ones (Figure 14).

We assume that sheeted dikes can be injected from an episodically steady state melt lens as described by Nicolas et al. (2008). However, this steady-state behaviour is overprinted by upward migrations of the melt lens that are documented in the Oman ophiolite and at the East-Pacific Rise. These upward migrations induce reheating, dehydration, and hydrous partial melting at the roof of the melt lens, leading to the occurrence of oceanic plagiogranites and assimilation of hydrothermally altered rocks in the melt lens. These processes imply a contamination of the melt lens by silicic melts formed during hydrous partial melting and by hydrothermal fluids recycled through assimilation. Downward migrations of the top of the melt lens can also occur and result in the crystallization of the isotropic ophitic gabbros that represent a fossilized melt lens. Melt lens crystallization eventually occurs at the melt lens margins where the thermal regime is cooler.

We also show that the well equilibrated, fine grained diabase textures observed in numerous oceanic or ophiolitic sites can have either a magmatic origin (protodikes) or a metamorphic origin (granoblastic dikes). Composition (e.g., Ti, Al, Cr in clinopyroxene), mineralogy (abundance of oxides), detailed petrographic observations (e.g., presence of clinopyroxenes with characteristic oxide inclusions), and description of associated lithologies (e.g., texture in the dike cores) are required to distinguish these two origins.

At fast spreading ridges, the top of the melt lens, which corresponds to the magmatic / hydrothermal interface, should be considered as a dynamic interface. On the first order, the

melt supply from the underlying main magma chamber, the occurrence of eruptions, and the vigor of the hydrothermal convecting system regulate its position. Short wave-length variations of the depth of the summit of the melt lens are observed (50m of variation for distance of 150m along axis).

TABLE A1 is available as a supplementary material on the G-cubed web-site.

### III.4. Aswad area: further constrains on the model

In order to test and constrain further the model proposed in France et al. (2009a), I have done detailed mapping in the Aswad area (Sumail massif, Oman ophiolite; Figure III-13). The studied area includes the zone mapped and described by Nicolas et al. (2008) (Figure III-14).

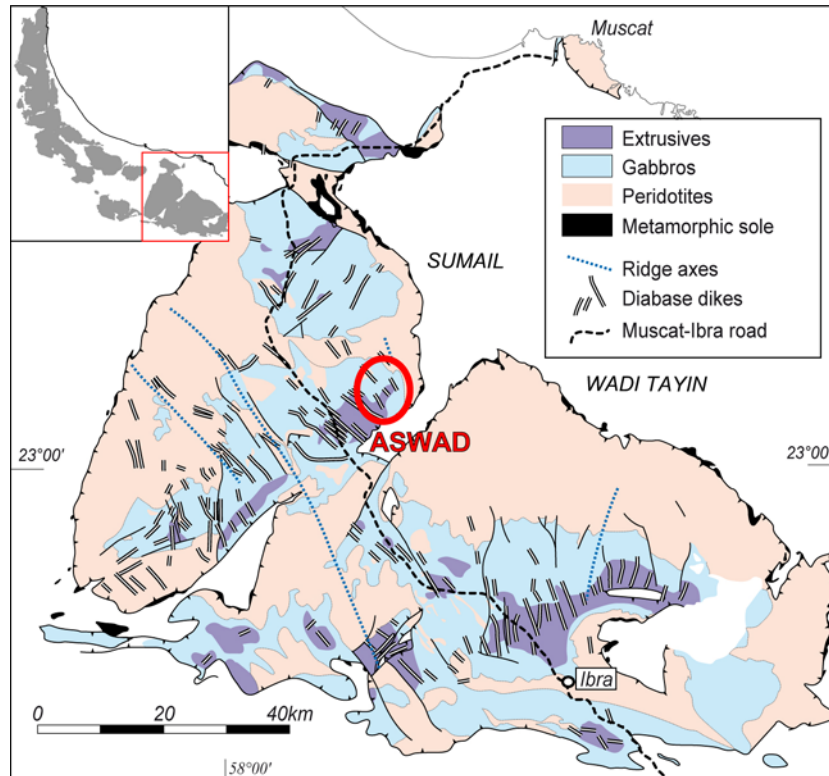


Figure III-13: Simplified geological and structural map of the southern massifs and location (Red box) in the Oman ophiolite (after Nicolas et al., 2000). The red circle indicates the location of the Aswad area.

The studied area is ~2.5 x 2.5 km large, and extends from the foliated gabbros to the sheeted dike complex. A preliminary petrological study of the collected samples has been done and is presented in section III.5. The mapping work consisted in precisely located field observations (lithology identification, structure measurements, and sampling) that are reported on the geological map (Figure III-14; Figure III-15). The foliation in the foliated gabbros is generally parallel to the sub-vertical sheeted dike orientation (trending ~140°N). As in the sections studied in France et al. (2009a), isolated foliated gabbro domains (a few meters large) are observed within the isotropic gabbro horizon; the foliation is parallel to the general direction defined by the foliated gabbros and by the sheeted dike complex. The contact between the isotropic gabbros and the sheeted dike complex is observed in several places (“SD/gabbro contact” in Figure III-15), and is always sharp (Figure III-16) and intrusive

(Figure III-17; Figure III-11). Coarse-grained isotropic gabbros are abundant along the contact (Figure III-15). Consistent with observations of France et al. (2009a), coarse-grained gabbros are commonly concentrated around the microgranular gabbro xenoliths (Figure III-18). Microgranular xenoliths are present at nearly all the SD/gabbro contact outcrops (Figure III-15), but are also observed sparsely in the isotropic gabbros (Figure III-15). The sharp contact between the microgranular base of the sheeted dike complex and the isotropic gabbros, together with the abundance of microgranular xenoliths (Figure III-15), attest to upward migrations of the top of the melt lens associated to important assimilation processes (France et al., 2009a). The microgranular base of the sheeted dike complex, and the microgranular gabbro xenoliths are therefore recrystallized after a reheating event and can be called granoblastic.

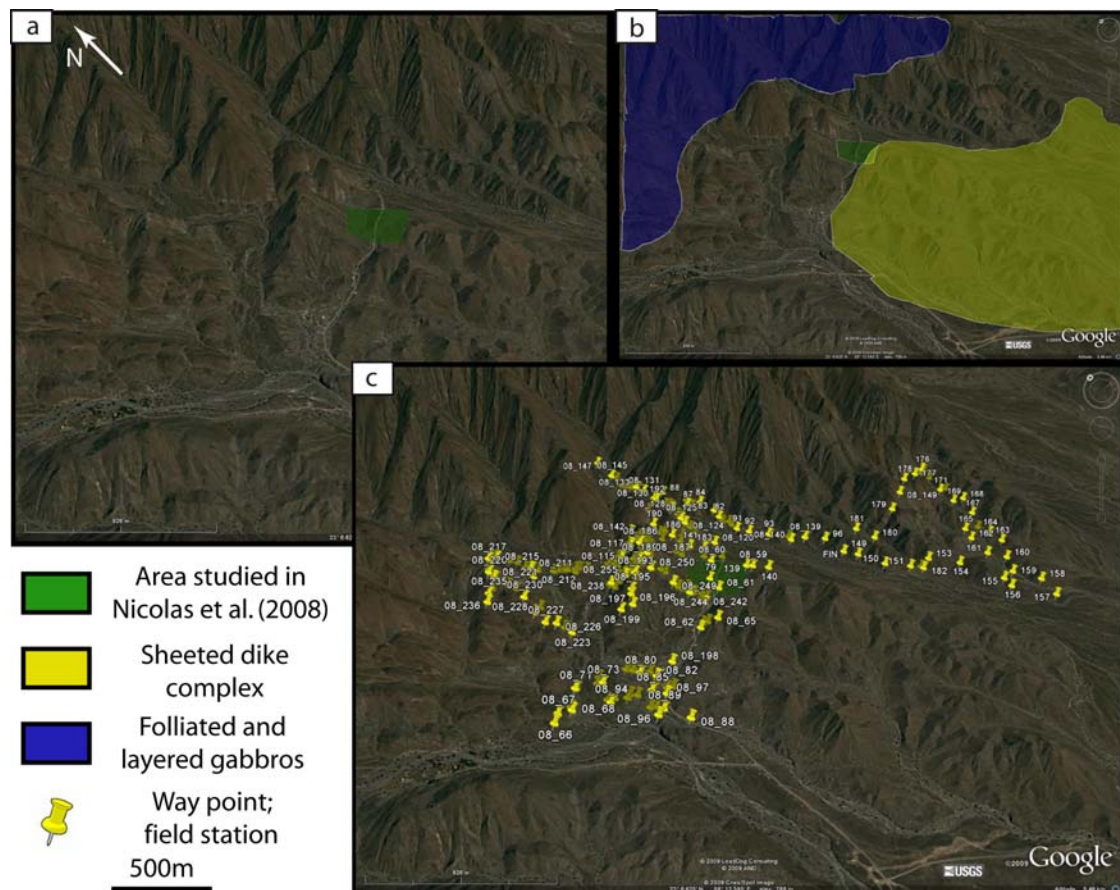


Figure III-14: Google Earth ® view of the Aswad area. a) studied area; the green box indicates the area mapped and described in Nicolas et al. (2008). b) The studied area is located between the sheeted dike complex (yellow) and the foliated gabbros (blue). c) Measurement and sampling stations (~250 stations).

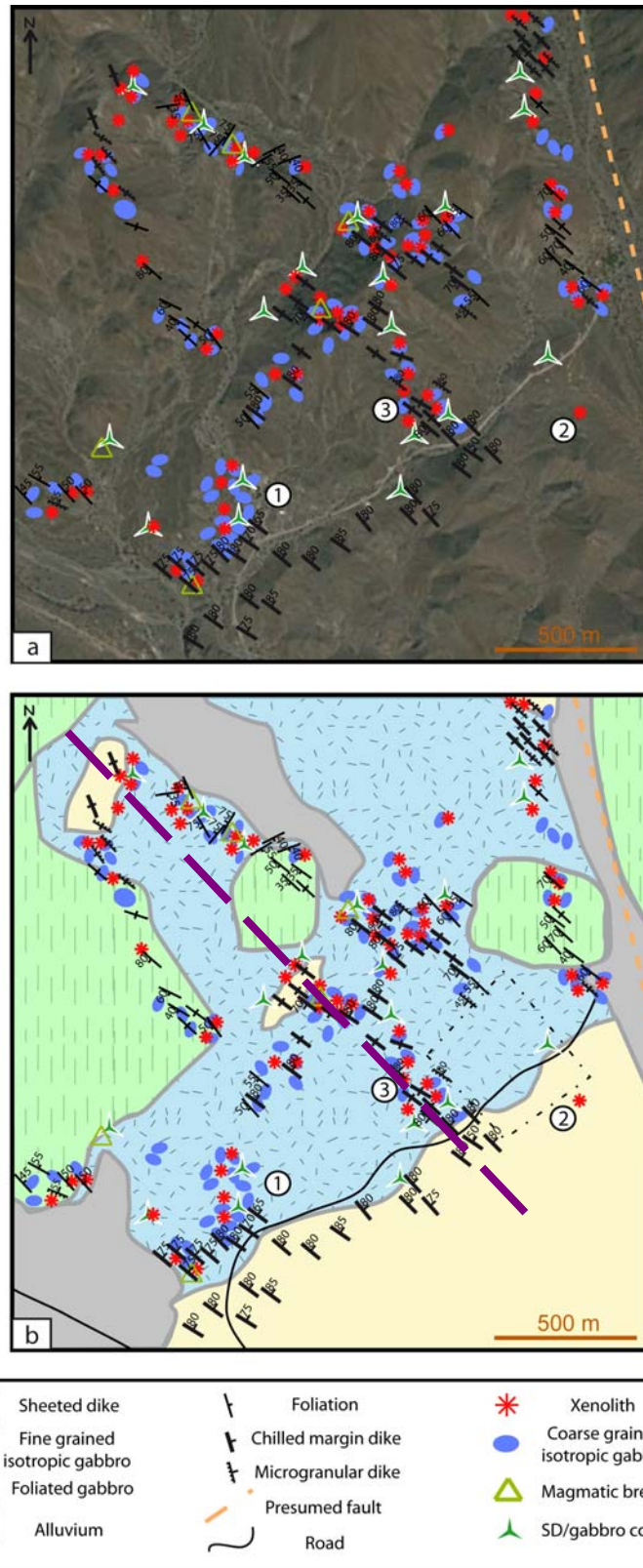


Figure III-15: Aswad area structural and lithological information on a Google Earth® view (a) and on a geological map (b). The root zone outcrops represent zones of contact between the sheeted dike complex base and the isotropic gabbros. Purple dashed line: cross-section of Figure III-19. 1: location of photographs in Figure III-16; 2 is discussed in text at the end of this section and indicates the location of the outcrop presented in Figure III-20; 3: location of samples presented in section III.5. The dashed box indicates the area mapped and described in Nicolas et al. (2008).



The main difference with the areas studied in France et al. (2009a) is that several sheeted dike complex bodies (some meters wide) are observed within the isotropic gabbros (see “SD/gabbro contact” in Figure III-15). These bodies correspond to outcrops where gabbros intrude the base of the sheeted dike complex (recrystallized to granoblastic microgabbro), and represent the fossilized roof of the melt lens. The widespread occurrence of these “SD/gabbro contact” outcrops lead to propose the schematic and interpretative cross section of Figure III-19. As no fault has been identified in these areas, the depth variation of the sheeted dike / gabbro contact is interpreted as initial depth variations of the melt lens roof.

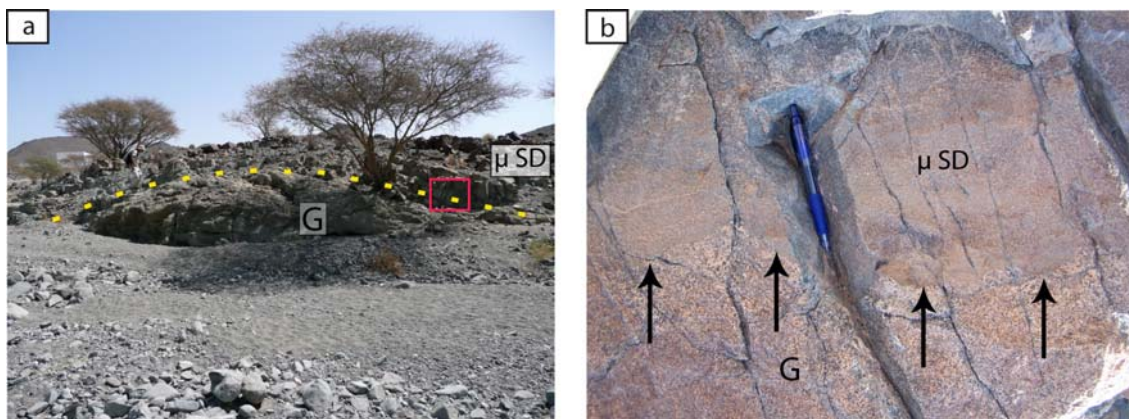


Figure III-16: Sharp contact between intrusive isotropic gabbro (G) and the recrystallized sheeted dike complex / granoblastic microgabbro dikes ( $\mu$  SD). This outcrop corresponds to station 1 on Figure III-15. The red box indicates the location of the photograph in b) and arrows point the contact.

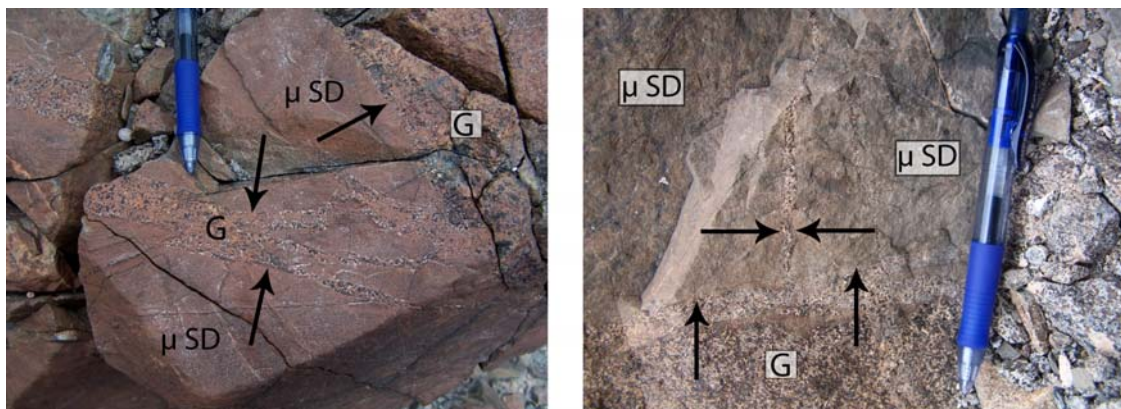


Figure III-17: Recrystallized sheeted dike complex ( $\mu$  SD) / isotropic gabbro (G) contact. The contact (pointed by arrows) is sharp and fine-grained isotropic gabbro intrudes the granoblastic microgabbro dikes.

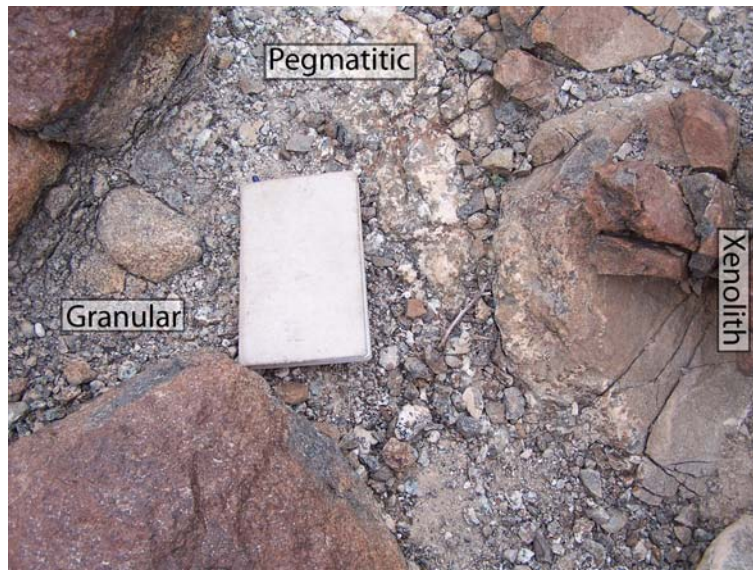


Figure III-18: Coarse-grained (pegmatitic) gabbros are preferentially located at the margins of a granoblastic microgabbro xenolith within granular gabbros. The occurrence of coarse-grained gabbro around xenoliths representing previously hydrothermally altered sheeted dikes is attributed to dehydration of xenoliths (France et al., 2009a).

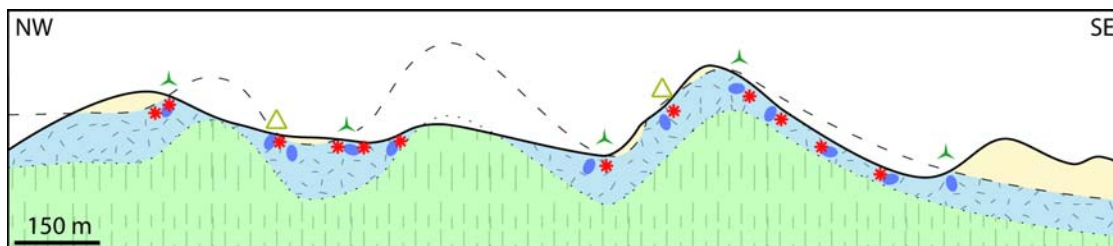


Figure III-19: Schematic and interpretative NW-SE cross-section from the Aswad area (see location in Figure III-15). The dashed line represents the contact between the sheeted dike complex and the isotropic gabbro horizon (inferred melt lens roof), and the dotted line represents the foliated gabbros / isotropic gabbros transition (inferred melt lens bottom). Symbols are the same as in Figure III-15.

Upward migrations are supported by the truncated base of the sheeted dike complex that are recrystallized to granoblastic microgabbro, and by granoblastic microgabbro xenoliths present in the isotropic gabbro horizon, but large downward migrations are also suggested by precise inspection of the sheeted dike complex. Within the sheeted dike complex, ~50-100m above the contact with the isotropic gabbros, some rare isotropic gabbro screens,  $\leq 1$  meter large, are observed (e.g., station 2 on Figure III-15; Figure III-20). These may be relicts of a former higher level of the melt lens that has migrated downward and crystallized these isotropic gabbros. Following this downward migration, new dikes have been injected and compose the new sheeted dike complex. One of these gabbro screens contains a granoblastic microgabbro xenolith (Figure III-20). The presence of xenoliths in these gabbro screens highlights former upward migrations of the melt lens that have resulted in assimilation.

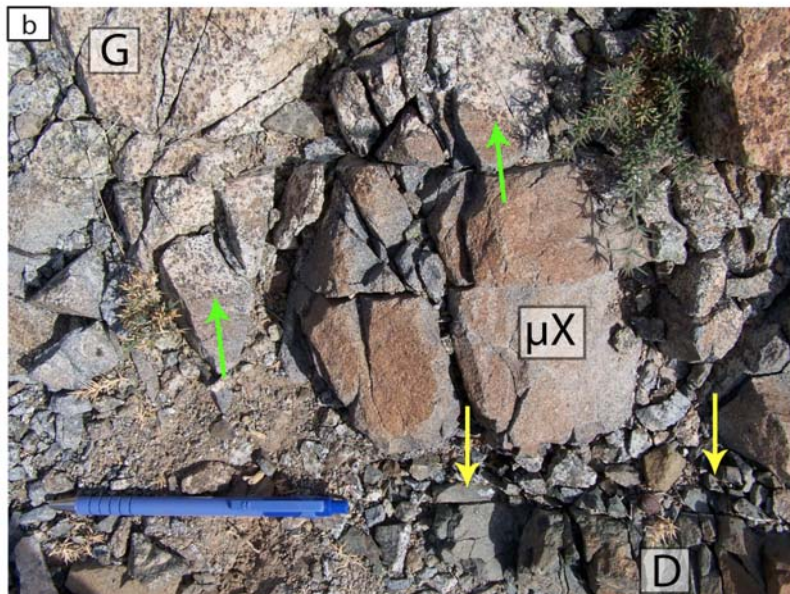
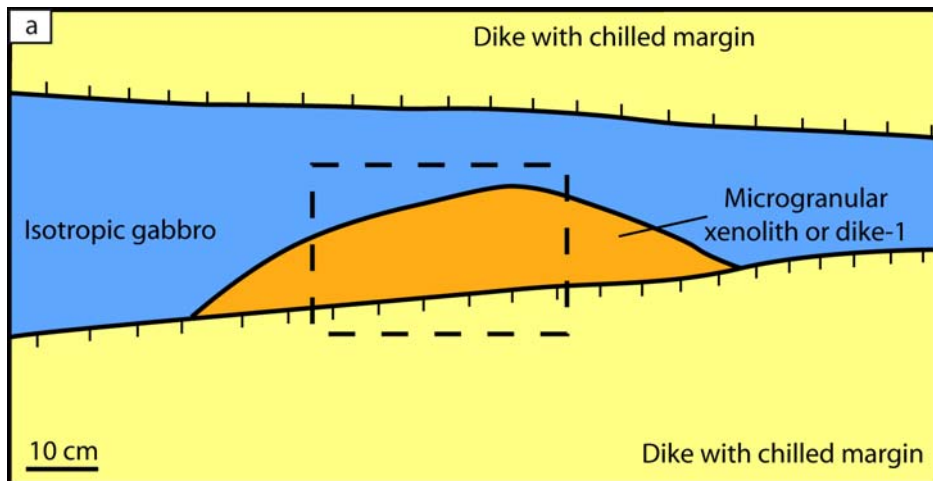


Figure III-20: Zone 2 on map of Figure III-15; gabbro screen containing a microgranular xenolith (or former granoblastic microgabbro dike ["dike-1]) within the sheeted dike complex. The dashed box in a) corresponds to the photograph in b). In b) green arrows point the isotropic gabbro (G) / microgranular xenolith ( $\mu X$ ) contact, and yellow arrows point the dike chilled margin (D).

Observations made in the Aswad area support upward and downward migrations of the melt lens, its fossilization, and assimilation processes, as proposed in France et al. (2009a). However in the Aswad area xenoliths are more abundant and assimilation of hydrothermally altered dikes and therefore upward migrations of the melt lens seems to be more abundant.

### **III.5. Reheating of the Aswad sheeted dikes**

Samples from the Aswad area have been studied in collaboration with Christian Nicollet during the research practice of Baptiste Debret (first Master year) at the Laboratory “Magmas & Volcans” of Clermont-Ferrand (France). An article that will be submitted to *Lithos* is in preparation. I present hereafter the purpose of this study and the main results that are relevant to my PhD work.

The objective of this study was to determine the metamorphic evolution of Oman samples that have been exposed to high temperature after their crystallization. Samples from different depths of the ophiolitic complex are used (the sheeted dike base; the upper isotropic gabbros; the lower layered gabbros; meta-gabbro dikes from the Moho transition zone). Samples are studied through petrographic observations, in-situ microanalyses, and thermometry. Results highlight two different metamorphic evolutions, corresponding to the upper and lower gabbroic complex, that are mainly controlled by temperature, presence and quantity of fluids, cooling rate, deformation, and initial texture and mineralogy.

I present here petrological descriptions and mineral in-situ analyses of a sample (08OLC6) from the center of a dike close to the sheeted dike / gabbro transition; the sample location is station 3 in Figure III-15. In this area and similarly to other visited areas, the isotropic gabbros intrude the base of the sheeted dike complex base (Figure III-12d; Figure III-16; Figure III-17) and contain several microgranular enclaves (Figure III-15).

The studied sample is composed of plagioclase, clinopyroxene, different generations of amphibole, magnetite, and ilmenite. Microprobe in-situ analyses are given in Table III.1.

Isotropic gabbros and dikes show a similar retrograde evolution from the magmatic stage (plagioclase + clinopyroxene), through amphibolite facies conditions (brown amphibole crystallization [edenite and pargasite]), to green schist / low amphibolite facies conditions (green amphibole crystallization [edenite and hornblende]). Under green schist facies conditions, amphibole can also recrystallize as actinolites. The retrograde evolution can be observed in single amphibole grains that display zonations (Figure III-21).

mineral	SiO <sub>2</sub>	Al <sub>2</sub> O <sub>3</sub>	TiO <sub>2</sub>	CaO	Na <sub>2</sub> O	K <sub>2</sub> O	MnO	MgO	FeO	Cr <sub>2</sub> O <sub>3</sub>	NiO	Total	X	Pl/Hb (°C)	Ti in Amp (°C)
Hbb	44.94	8.96	3.36	10.66	2.18	0.23	0.24	13.74	13.33	0.01	0.02	97.66	64.76	812	973
Hbb	44.24	8.77	3.40	10.90	2.16	0.25	0.17	13.39	13.71	0.05	0.00	97.04	63.50	820	976
Hbb	44.88	9.02	3.11	11.32	1.89	0.29	0.17	13.19	12.87	0.00	0.04	96.78	64.62	843	953
Hbb	43.76	9.44	3.76	10.81	2.21	0.22	0.21	13.36	12.89	0.03	0.00	96.70	64.87	885	998
Hbb	43.91	9.57	3.45	11.44	2.12	0.27	0.15	12.01	14.12	0.03	0.02	97.11	60.26	828	979
Hbb	44.28	8.95	3.51	10.71	2.09	0.21	0.25	13.25	13.56	0.00	0.03	96.85	63.54	819	983
Hbb-g	46.11	9.07	0.61	11.78	1.75	0.34	0.15	14.44	13.06	0.03	0.03	97.39	66.34	808	608
Hbg	46.47	8.35	0.48	11.37	1.59	0.18	0.18	14.37	12.78	0.00	0.02	95.80	66.71	771	582
Hbg	46.22	8.80	0.71	11.65	1.69	0.42	0.23	13.48	13.89	0.02	0.05	97.16	63.37	792	627
Hbg	44.23	11.05	0.45	11.50	1.98	0.38	0.19	13.27	13.17	0.07	0.04	96.32	64.24	860	576
Hbg	49.94	5.28	1.29	11.56	0.91	0.18	0.15	14.68	12.33	0.05	0.05	96.41	67.97	647	729
Hbg	51.54	4.81	1.05	11.50	0.80	0.21	0.13	15.50	12.30	0.17	0.02	98.04	69.21	624	687
Hbb (2)	51.16	4.66	0.59	11.65	0.80	0.20	0.20	15.06	12.23	0.05	0.04	96.64	68.70	608	604
Hbb (2)	47.15	7.26	1.89	11.60	1.45	0.41	0.22	13.41	14.50	0.00	0.00	97.89	59.38	470	818
Hbb (2)	45.87	7.91	2.16	11.37	1.54	0.45	0.20	12.76	14.30	0.08	0.04	96.68	61.39	761	855
Hbg (2)	48.48	4.26	0.76	11.52	1.54	0.27	0.21	15.93	13.61	0.02	0.02	96.63	67.59	678	636
Hbg (2)	43.03	10.19	0.33	11.42	1.62	0.37	0.19	13.60	12.59	0.00	0.06	93.41	65.80	857	551
Actinolite (2)	52.95	2.99	0.46	11.45	0.54	0.08	0.26	16.34	11.57	0.08	0.01	96.73	71.57	544	577
Pl	58.82	25.49	0.05	8.14	6.92	0.27	0.00	0.03	0.41	0.00	0.00	100.13	38.8		
Pl	58.52	25.67	0.08	8.20	6.94	0.22	0.04	0.02	0.46	0.00	0.00	100.14	39.0		
Pl	49.31	32.33	0.10	15.59	2.89	0.06	0.00	0.03	0.64	0.00	0.00	100.94	74.6		
Pl	48.59	32.02	0.05	15.49	2.73	0.11	0.04	0.01	0.65	0.00	0.00	99.69	75.3		
Pl	51.44	28.73	0.01	13.93	3.18	0.15	0.00	0.32	2.64	0.00	0.00	100.39	70.1		
Cpx	53.76	0.39	0.07	24.03	0.12	0.04	0.19	14.34	7.25	0.00	0.01	100.22	77.9		
magnetite	3.22	0.49	3.62	2.99	0.00	0.03	0.00	0.10	81.89	1.91	0.00	94.27			
Ilmenite	0.03	0.04	47.48	0.06	0.00	0.01	1.30	0.07	53.19	0.04	0.00	102.22			

*Table III.1: Microprobe data for sample 08OLC6 from the Aswad area of the Oman ophiolite. X: compositional parameter (mol %): plagioclase- An %; clinopyroxene and amphibole-Mg# (where  $Mg\# = Mg/[Mg+Fe_1]$ ); Pl/Hb: temperature calculated with the plagioclase-amphibole thermometer (Holland and Blundy, 1994); Ti in Amp: temperature calculated with the Ti in amphibole semiquantitative thermometer (Ernst and Liu, 1998), which is valid if Ti-oxides (e.g., ilmenite or titanomagnetite) coexist with amphibole; Hbb: brown hornblende; Hbg: green hornblende; (2): second generation (granoblastic); Pl: plagioclase; Cpx: clinopyroxene.*

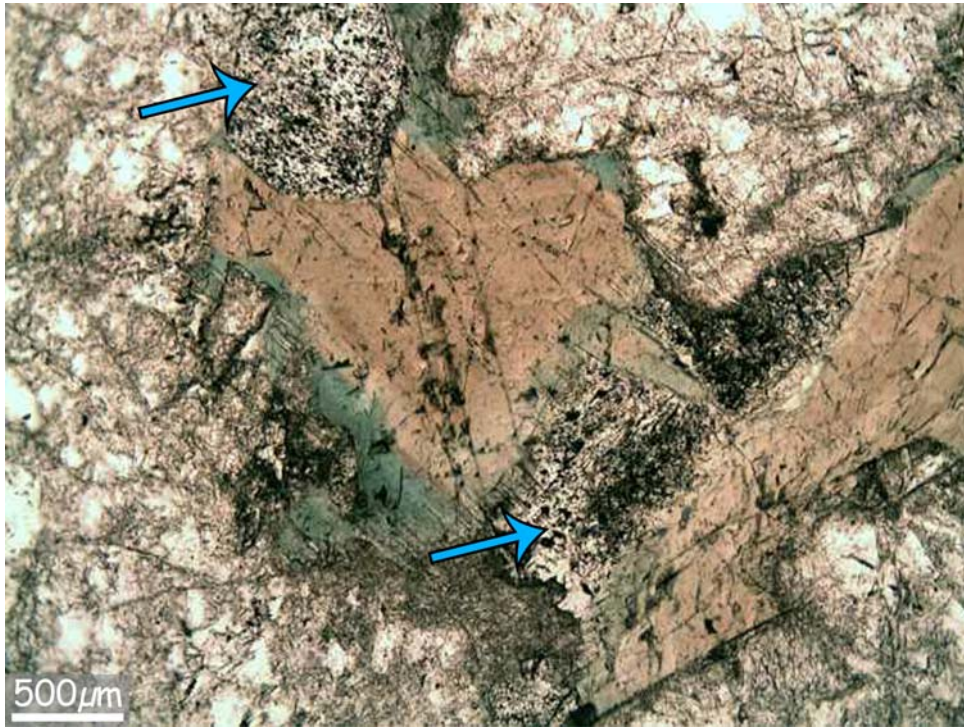
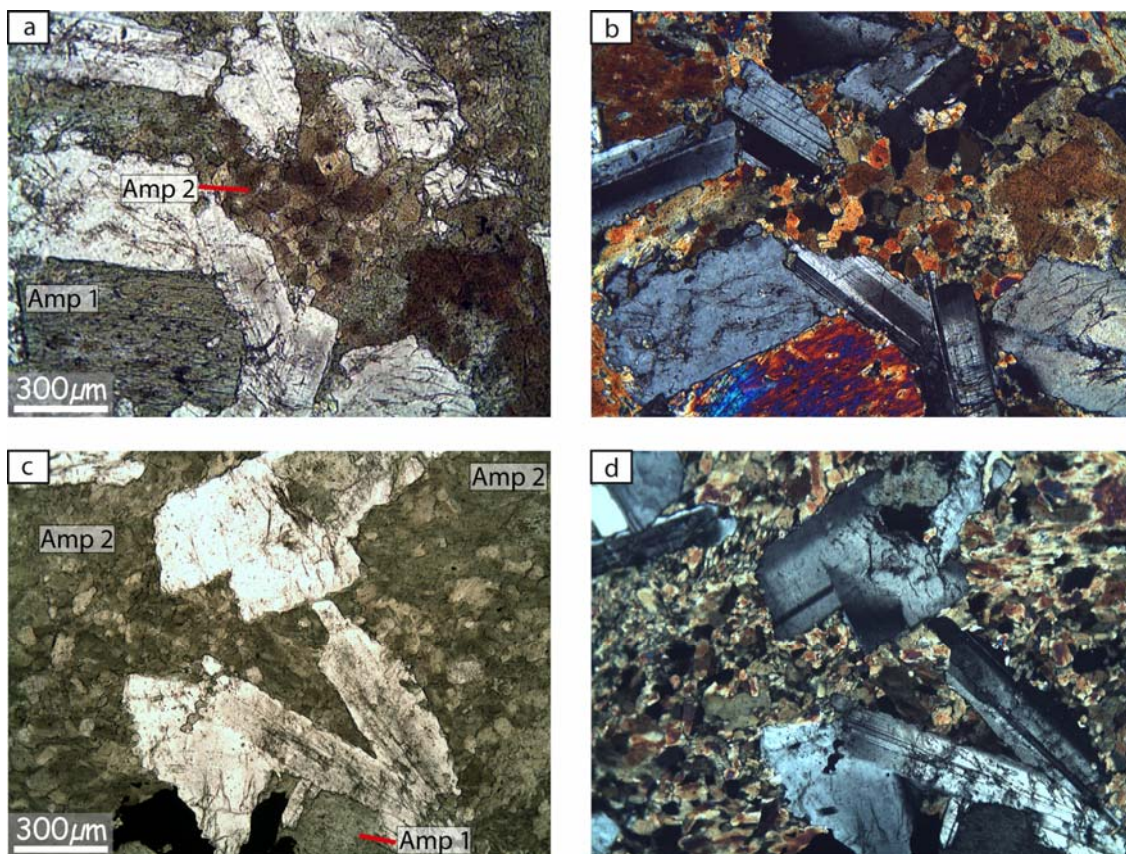


Figure III-21: Microphotograph of an isotropic gabbro sample (sample 08OLC3b) showing the retrograde evolution from the magmatic stage to the green schist facies conditions (plane-polarized light). Altered clinopyroxenes (blue arrows) attest to the magmatic conditions, brown amphibole attests to the amphibolite facies conditions and green amphibole attests to the green schist / amphibolite facies conditions.

Temperature estimations have been performed for retrograde amphiboles using the amphibole-plagioclase thermometer (Holland and Blundy, 1994) and the Ti in amphibole semiquantitative thermometer as Ti-bearing oxides are present (Ernst and Liu, 1998), and range from 885°C to 624°C and from 998°C to 582°C, respectively. For both thermometers, the higher estimated temperatures correspond to brown amphiboles, and the lower to green amphiboles. Another amphibole generation (brown/green amphiboles [hornblende and edenite] and actinolites) is observed in granoblastic assemblages (Figure III-22). Some areas are totally recrystallized to granoblastic assemblages and mimic the magmatic ophitic texture (Figure III-22c-d). These assemblages are present in the whole sample and can develop after former large amphibole grains (Figure III-23).



*Figure III-22: Microphotographs of granoblastic amphibole assemblages (Amp 2) (a, c: plane-polarized light; b, d: cross-polarized light). Former large amphibole grains are also observed (Amp 1). Amp 1 seems to mimic former clinopyroxenes, and granoblastic assemblages of Amp 2 overprint former Amp 1 grains. The granoblastic assemblages of Amp 2 mimic the magmatic ophitic texture. Sample 08OLC6.*

Temperature estimations for the granoblastic assemblages range from 857°C to 470°C using the amphibole-plagioclase thermometer (Holland and Blundy, 1994), and from 855°C to 551°C using the Ti in amphibole semiquantitative thermometer (Ernst and Liu, 1998). In contrast with the large amphibole grains, the granoblastic domains do not crystallize after clinopyroxenes in a purely retrograde system. It should either overprint the larger grains during a deformation stage or under increasing temperatures (prograde evolution). In the present case, no deformation is evidenced (e.g., plagioclase grains display magmatic textures; Figure III-21; Figure III-22; Figure III-23), and the overgrowths relations show that brown-amphibole granoblastic assemblages recrystallize after large green-amphibole grains (Figure III-23). The green-amphibole granoblastic assemblages are equilibrated at lower temperatures than the brown-amphibole granoblastic assemblages. It shows that the green-amphibole granoblastic assemblages overprint the brown-amphibole granoblastic assemblage during a second retrograde evolution.



Figure III-23: Microphotograph of sample 08OLC6 from the base of the sheeted dike complex (plane-polarized light). The large green amphibole is overgrown by aggregates of granoblastic brown amphibole. The granoblastic brown amphibole assemblage has crystallized at higher temperature than the large green amphibole grain.

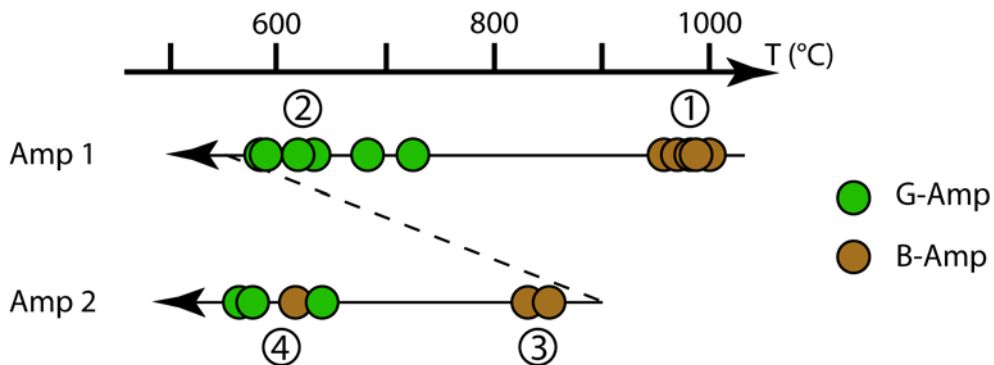


Figure III-24: Temperature evolution for different generations of amphiboles in sample 08OLC6: 1) large brown amphibole grains (B-Amp) crystallize, 2) following a retrograde evolution (Amp 1), large green amphibole (G-Amp) grains form. 3) Following a prograde event (reheating), granoblastic brown amphibole assemblages crystallize before 4) a second retrograde evolution (Amp 2) that leads to the crystallization of the granoblastic green assemblages (replacing the brown ones).

The succession of different amphibole types is: 1) large brown-amphibole grains, 2) large green-amphibole grains, 3) small granoblastic assemblages of brown-amphibole, 4) small granoblastic assemblages of green-amphibole, and 5) the lower temperature alteration to



actinolites. This evolution is summarized in Figure III-24 and is characterized by a reheating event (between stages 2 and 3).

Similar brown-amphibole granoblastic domains (as in stage 3) are observed in isotropic gabbro samples, and also attest to prograde metamorphism of these rocks (Figure III-25).

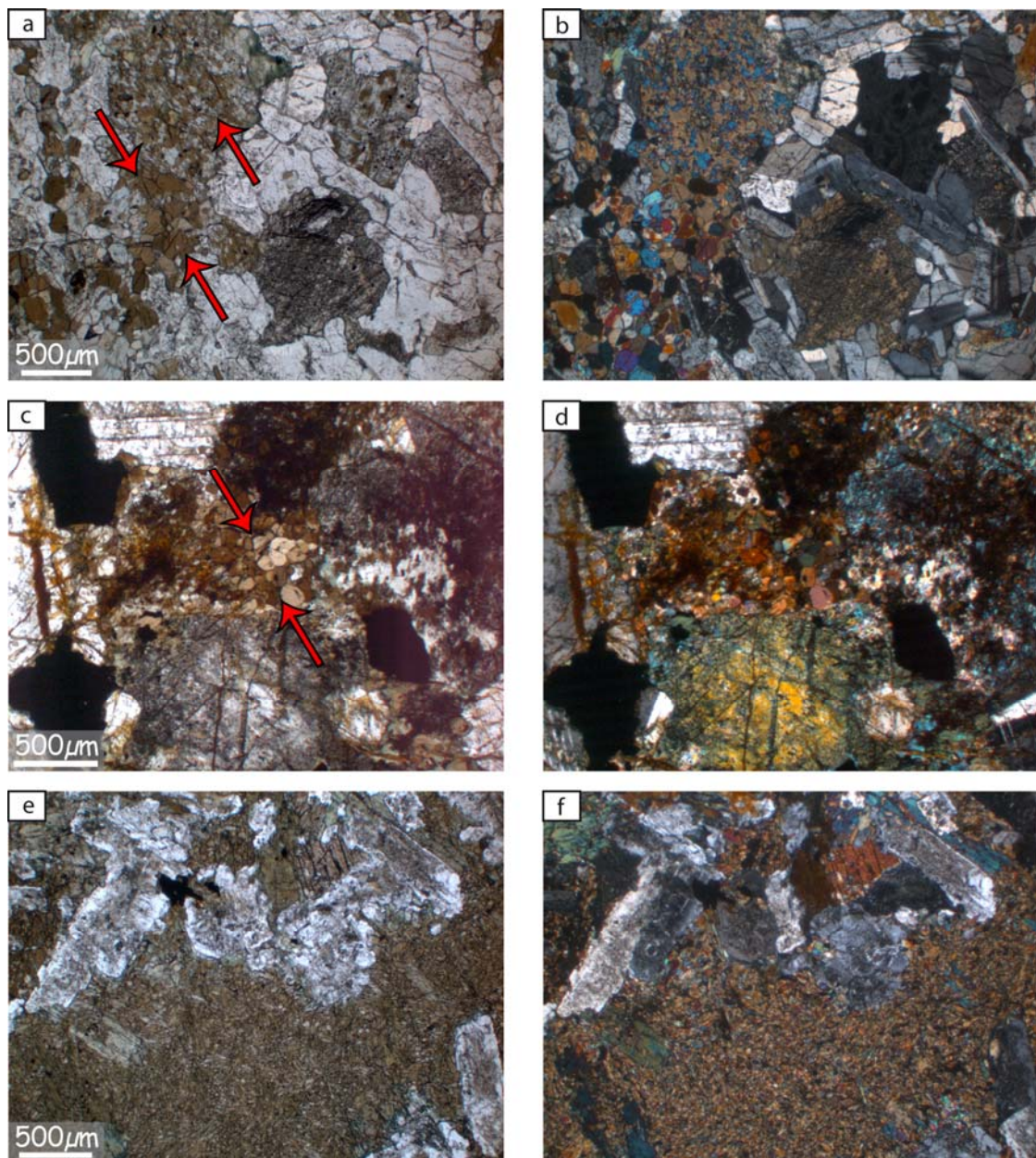


*Figure III-25: Microphotographs of amphibole granoblastic assemblages in fine-grained isotropic gabbros (a-b: sample 07OL47b; c-d: sample 07OL57a; e-f: sample 07OL53a). a, c, e) plane-polarized light; b, d, f) cross-polarized light. In a-d amphibole granoblastic assemblages are pointed by arrows; in e-f the large brown-amphibole assemblage is overprinted and recrystallized to a brown-amphibole granoblastic assemblage.*

The petrographic and micro-analytical characteristics observed in lithologies at the base of the sheeted dike complex from the Aswad area show that it has been reheated, which is consistent with the field observations (gabbro intrusion in the base of the sheeted dike complex, and occurrence of granoblastic microgabbro xenoliths in gabbros). The petrological characteristics observed in the Aswad area are consistent with the general model proposed in France et al. (2009a), in which the top of the melt lens is a dynamic horizon that can move up and down with the potential to reheat the previously hydrothermally altered lithologies.

### ***III.6. Conclusion***

Coupled structural, petrological, and geochemical studies of different areas of the Oman ophiolite, and a comparison with the IODP Hole 1256D support a common general model (France et al., 2009a) reconciling previous, apparently contrasting models for the interactions between the base of the sheeted dike complex and the upper melt lens present at fast spreading ridges. The results of this study are consistent with the hypothesis that the melt lens is a dynamic horizon that can migrate upward and downward, and that becomes fossilized off axis. Upward migrations results in prograde metamorphic reactions in the base of the sheeted dikes, which recrystallize to granoblastic dikes. Depending on the temperature increase occurring during upward migrations and on the extent of previous hydrothermal alteration, the granoblastic dikes represent either dehydrated previously altered dike rocks or hydrous partial melting residues. Assimilation is evidenced by the occurrence of granoblastic xenoliths in the isotropic gabbro horizon, and by the microgranular lenses observed in the foliated gabbros. The assimilation process can be responsible for the high chlorine content measured in the MORB melts of fast spreading ridges. Downward migrations of the melt lens result in the crystallization of isotropic gabbros at its roof and margins. Some gabbro screens present within the sheeted dike complex (50-100 m above their truncated base) attest to former higher levels of the melt lens.

The precise recrystallization processes, and the detailed evolution of the mineral assemblages in the granoblastic dikes have been described by Koepke et al. (2008). However the origin of the peculiar composition of the granoblastic dikes minerals remain poorly constrained. The melt formed during the hydrous partial melting of the base of the sheeted dike complex can mix with the melt lens magma and contaminate it. Constraining the composition of the formed melt is therefore of major importance to discuss the composition of MORB present at fast spreading ridges. In order to test the evolution of the mineral assemblages, to precise the recrystallization processes, and to better understand the melting

processes occurring at the base of the sheeted dike complex, we present in Chapter IV an experimental study reproducing the melting of hydrothermally altered dikes at the base of the sheeted dike complex.

## **Chapter IV.**

# **“Melting the hydrothermally altered sheeted dike complex: experimental study”**

#### ***IV.1. Introduction***

In Chapter III, I have shown, through a study of the root zone of the sheeted dike complex in the Oman ophiolite and a comparison with rocks recovered in IODP Hole 1256D, that the upper melt lens present at fast spreading ridges is a dynamic system, which can migrate vertically (Gillis, 2008; France et al., 2009a). Upward migrations are associated to reheating of the previously hydrothermally altered roof (sheeted dikes and isotropic gabbros), and hydrous partial melting can proceed as a result of lowering the solidus temperature in the presence of water (Gillis and Coogan, 2002; Coogan et al., 2003; France et al., 2009a). The granoblastic dikes present at the base of the sheeted dike complex, and the granoblastic xenoliths that are observed in isotropic gabbros in association with plagiogranitic rocks result from recrystallization under amphibolite to granulite facies conditions, and may have undergone hydrous partial melting (France et al., 2009a). The melt formed during partial melting of hydrothermally altered dikes is believed to be compositionally close to typical oceanic plagiogranites (for low degrees of partial melting; Beard and Lofgren, 1991); for definition of the term "ocean plagiogranites" see Koepke et al., (2008). The associated residue may be similar to granulites, and may contain amphiboles depending on the temperature, and on the water activity. The hydrous solidus temperature is around 900°C (Beard and Lofgren, 1991). Redox conditions have a strong influence on the composition of the newly formed melt, on the composition of the residual phases, and on their liquidus temperatures (e.g., Appendix A3). Gillis and Coogan (2002), Coogan et al. (2003), and France et al. (2009a) have shown that hydrous partial melting of altered dikes at the base of the sheeted dike complex, has the potential of mixing the newly generated melt with primitive MORB in the melt lens, thus playing a significant role in MORB contamination at fast spreading ridges. This is potentially an effective crustal contamination process, as attested by the chlorine content of MORBs (Michael and Schilling, 1989; Michael and Cornell, 1998). Determining the precise composition (major, trace and volatile elements) of the melt formed during partial melting of previously hydrothermally altered dikes is therefore of major importance to evaluate the MORB components (primary melt, assimilated melt, and fractionated melt), and to constrain the composition of anatectic plagiogranites and discuss the origin of oceanic plagiogranites. Determining the mode and the mineral compositions of the residual assemblage and comparing these with the granoblastic rocks will help to test the dynamic model proposed by France et al. (2009a).

## *Chapter IV. Melting the hydrothermally altered sheeted dike complex: experimental study*

I have performed partial melting experiments using a hydrothermally altered sheeted dike sample as starting material. The starting material sample comes from the Oman ophiolite, and matches the average sheeted dike complex composition; it is highly hydrothermally altered, and no relics of magmatic phases are present. Experimental conditions have been selected to match the ones present at the base of the sheeted dike complex: a pressure of 100MPa, a temperature ranging from 750°C to 1030°C, water saturated conditions, and precisely constrained redox conditions (~NNO where NNO is the Ni-NiO solid buffer equilibrium). Experiments have been performed at the Institut für Mineralogie of the Leibniz University Hannover (Germany) using a cold-seal pressure vessel (CSPV; below 850°C), and at higher temperature, an internally heated pressure vessel (IHPV) equipped with a Shaw membrane (for details see below). Details on starting material, experimental conditions and results are presented in a paper submitted to *Contributions to Mineralogy and Petrology* (section IV.3); I present hereafter details on the experimental procedure.

### ***IV.2. Detailed experimental techniques***

#### **IV.2.a. Sample preparation**

The starting material (sample 08OL30) has been crushed to a powder, and then sieved in order to obtain a powder homogeneous in grain size. Precious metal tubes were used as capsule containers; in the present case I have used gold that prevent iron loss toward the capsule wall. 15-20 mm long tubes (diameter=2.8 mm) were used (N°1 in Figure IV-1). First, tubes were cleaned using an acetone bath plunged in an ultrasonic cleaner (~15 min); then gold tubes were placed at 800°C in a one atmosphere oven for ~20 min. Then, one tube end was pinched (N°2 in Figure IV-1) and welded (N°3 in Figure IV-1). Subsequently the capsule was filled; for water added experiments (see details in section IV.3), ~5 mg of distilled water was first added into the capsule, then ~50 mg of rock powder was added, and the whole assemblage was compressed in the capsule. The other tube end was then pinched and welded (N°4 in Figure IV-1). Because the welding heat could trigger water loss, a special cooling procedure using liquid nitrogen was required. After the welding, the capsule was weighed and placed in a 110°C furnace for 5 min, and then weighed again to verify that no water loss occurred during the welding process. Capsule is weighed after each preparation step, and if the weight remains stable during the different stages, the capsule is considered closed and can be used for experiments.

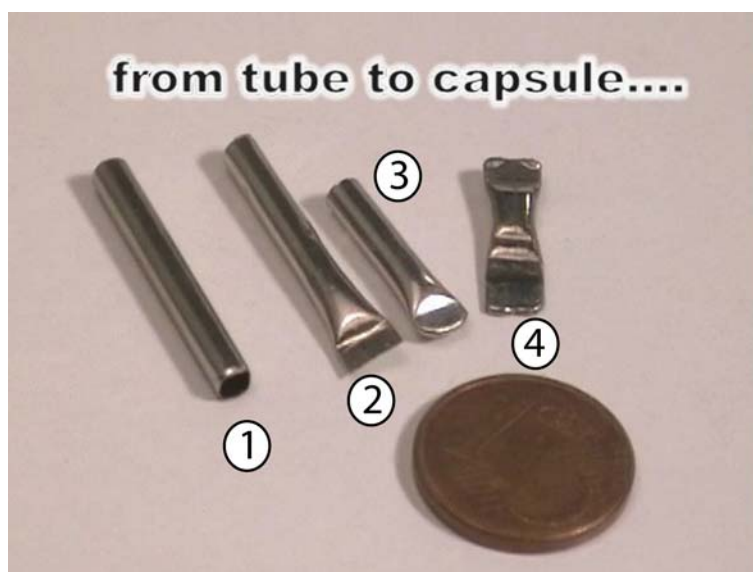


Figure IV-1: Steps in the capsule making (1 cent coin for scale). 1) 1.5 cm long tube; 2) one tube end has been pinched, and 3) welded; 4) after the filling, the second capsule end has been pinched and welded.

#### IV.2.b. Cold-seal pressure vessel

The used CSPV are horizontal externally heated vessels (Figure IV-2) that are pressurized with water. Pressure was controlled with a pressure transducer calibrated against a strain gauge manometer, and temperature was controlled using an external Ni-CrNi thermocouple. Before this study, ovens were calibrated to identify the hottest zone. The capsules were centered in this zone. In CSPV, the redox conditions were controlled using a solid buffer (a Ni-NiO assemblage in the present case). However, Scaillet et al. (1992) have shown that the maximum buffer lifetime is in the order of a few days, which is much less than the time spanned by our experiments. The redox conditions are nevertheless considered to be close to the NNO buffer because of the vessel composition (Ni), and of the use of water for pressurization (Klimm et al., 2003).

To run an experiment, the oven was first pre-heated to the desired temperature in order to shorten the heating time for samples. The vessel that contains the sample was then pressurized to the desired pressure (~100 MPa) before being introduced in the oven. The heating results in a pressure increase; pressure was therefore decreased during the heating stage to maintain ~100 MPa. When pressure and temperature were stable (after 30-60 min), the experiment was started, and pressure and temperature were controlled twice a day. At the end of the experiment, the vessel was removed from the oven and immediately exposed to a

*Chapter IV. Melting the hydrothermally altered sheeted dike complex: experimental study*

flux of compressed air (initial cooling rate  $\sim 200^\circ/\text{min}$ ). In order to ensure isobaric quenching, pressure was increased during the cooling.

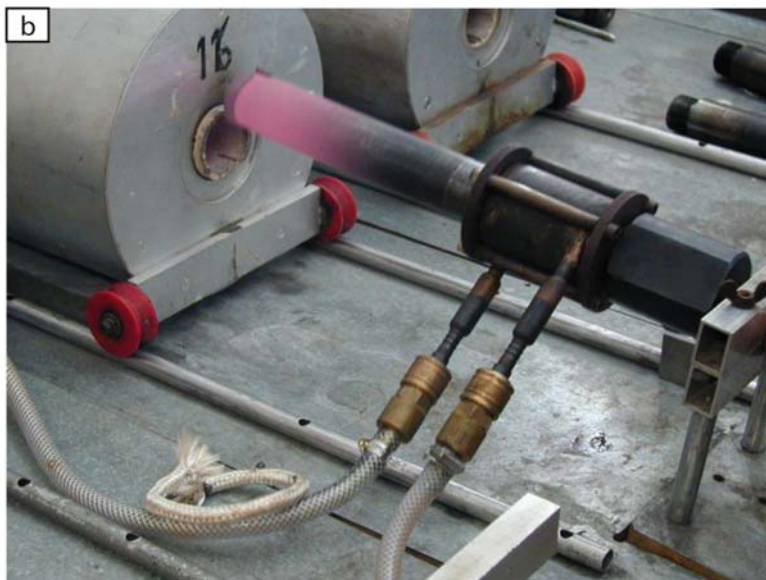
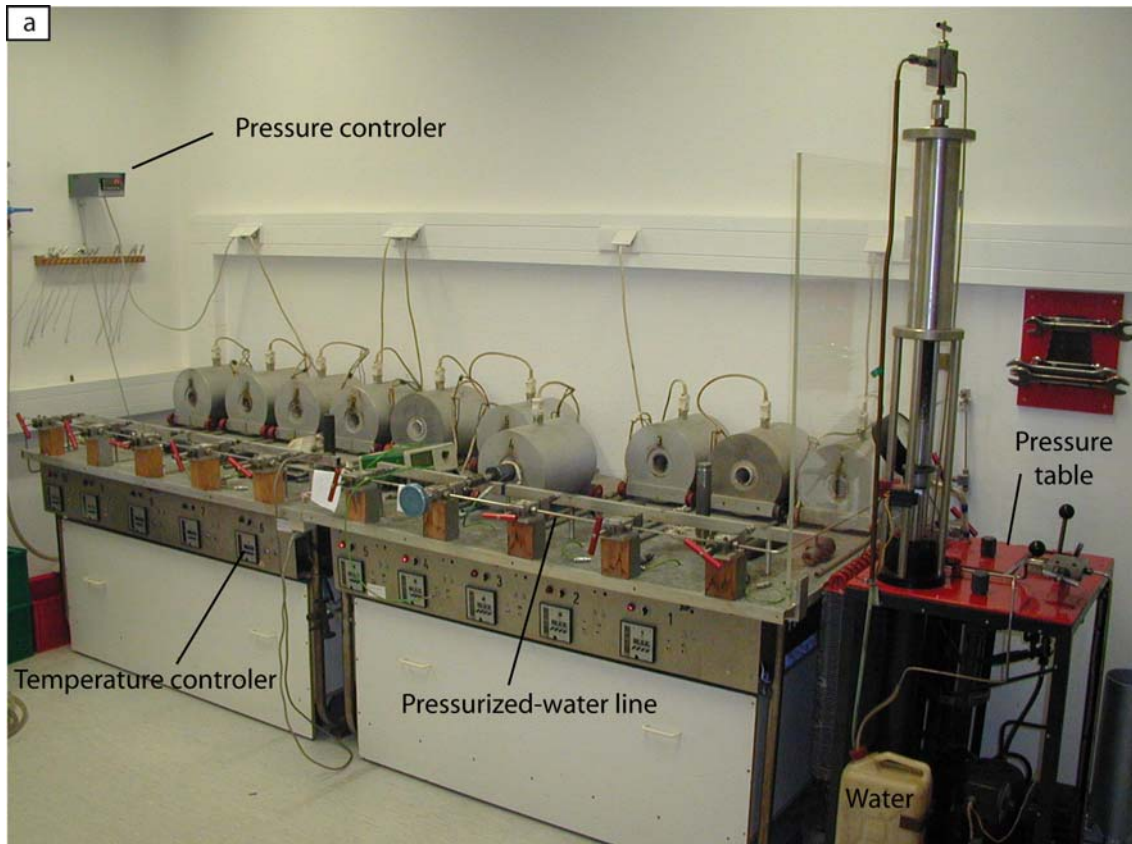


*Figure IV-2: Water pressurized CSPV ramp of the experimental lab of the Institut für Mineralogie of the Leibniz Univeristy Hannover. a) ovens, and b) hot vessel just removed from the oven.*



### IV.2.c. Internally heated pressure vessel

The used IHPV are vertical internally heated vessels (Figure IV-3) that are pressurized with argon. Pressure was controlled with a strain gauge manometer, and temperature was controlled using four S-type thermocouples. Details are given in Berndt et al. (2002).

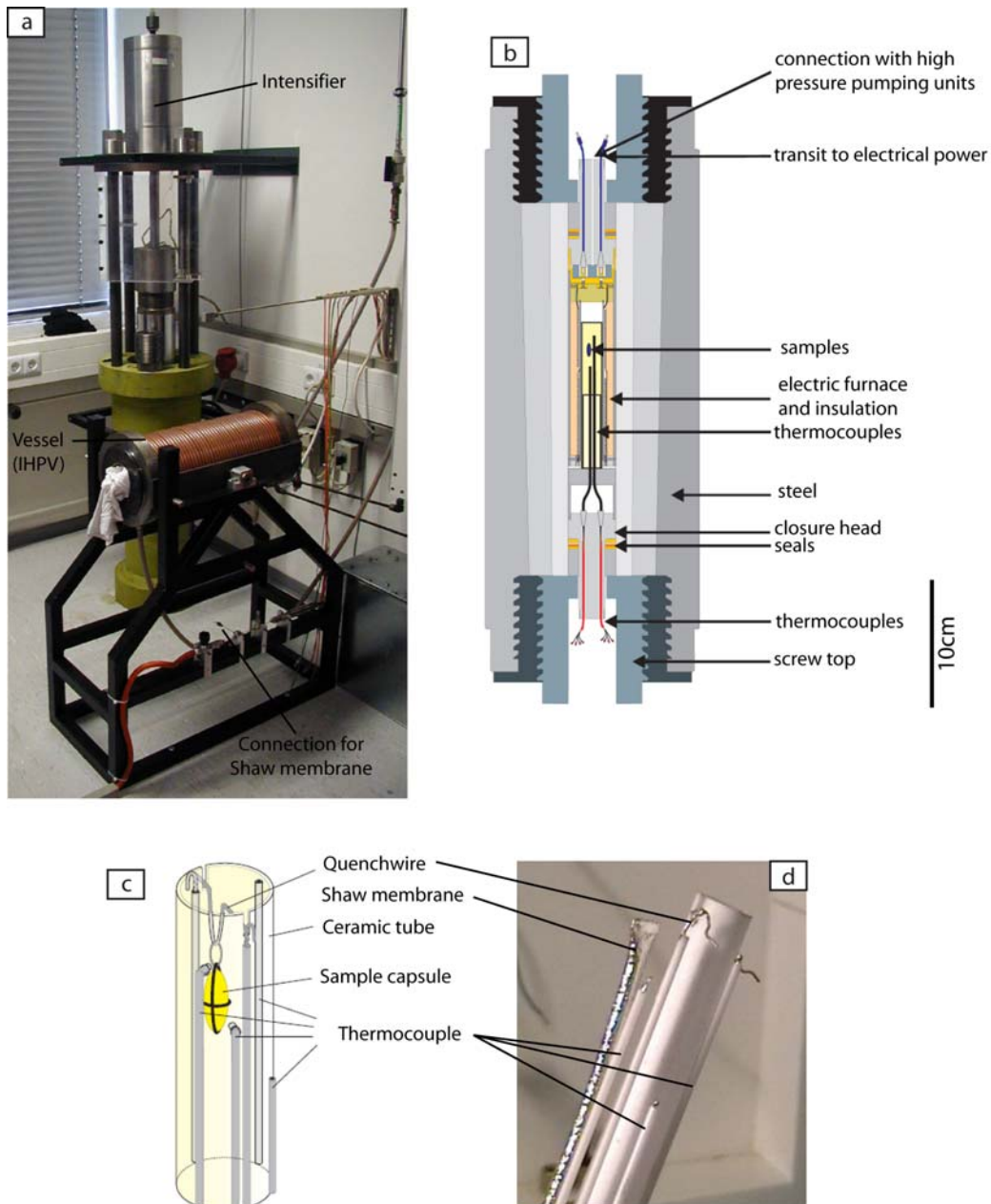
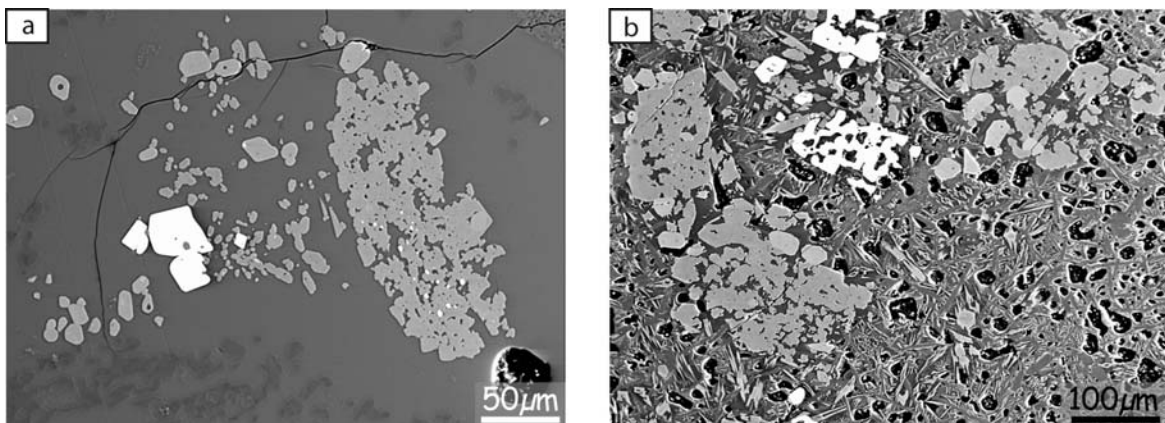


Figure IV-3: Argon pressurized IHPV equipped with a Shaw membrane as used in the experimental lab of the Institut für Mineralogie of the Leibniz Univeristy Hannover. a) IHPV before the sample loading; b) vessel internal structure; c-d) focus on the sample area, capsules are hanged using a thin platinum wire, which is fused electrically at the end of the experiment to allow rapid quenching (see text for further description); 4 S-type thermocouples are used to control the temperature gradient present around the sample, and a Shaw membrane is present to control the redox conditions.

*Chapter IV. Melting the hydrothermally altered sheeted dike complex: experimental study*

In the IHPV, redox conditions were fixed by the given H<sub>2</sub> pressure which was measured using a Shaw membrane (e.g., Scaillet et al., 1992; Berndt et al., 2002; Figure IV-3d). Berndt et al. (2002) have shown that H<sub>2</sub> pressure in the used pressure vessel is constant during experiment duration, after an initial phase of equilibration. They have also shown that osmotic hydrogen equilibrium between membrane and vessel is obtained in less than 48 hours at 1000°C and 207 MPa. As the experiments presented herein were longer, it is expected that the final H<sub>2</sub> pressure measured within the membrane corresponds to the vessel one.

Capsules were hanged into the sample holder using a thin platinum wire (the "quench" wire; Figure IV-3c-d) and introduced horizontally in the vessel (Figure IV-3a). The whole IHPV was then toppled over vertically and thermocouples, Shaw membrane, and high pressure tubes were connected. Then, the vessel was first evacuated and then flushed with hydrogen. Then, the initial H<sub>2</sub> pressure of the run was applied, and the vessel was isolated from the H<sub>2</sub>-reservoir. Afterwards, about 50% of the final Argon pressure was applied from the intensifier (Figure IV-3a) and the vessel was isolated from the Argon-pressure line. Temperature was then continuously rose (~30°/min), up to the desired temperature reached after ~30 min. Temperature, pressure and H<sub>2</sub> pressure were continuously recorded, and controlled after experiment to check the experiment conditions stability. At the end of the experiment, the quench wire was fused electrically and the capsules dropped isobarically into the cold quench area (~20°C); the cooling rate was ~150°/s. Effective quenching is evidenced by the absence of "quench minerals" (Figure IV-4).



*Figure IV-4: The quenching quality is evidenced by the absence of "quench minerals" (a). When quenching fails, melt is partially to totally recrystallized to "quench minerals" (b) (experiments at 1000°C).*

### ***IV.3. Hydrous partial melting in the sheeted dike complex at fast spreading ridges: Experiments and nature***

Article submitted to *Contributions to Mineralogy and Petrology* (August 6, 2009).

**Lydéric France<sup>1,2,\*</sup>, Juergen Koepke<sup>2</sup>, Benoit Ildefonse<sup>1</sup>, Sarah B. Cichy<sup>2</sup>, Fabien Deschamps<sup>3</sup>**

1: Géosciences Montpellier, CNRS, Université Montpellier 2, CC60, F-34095 Montpellier Cedex 05, France

2: Institut für Mineralogie, Leibniz Universität Hannover, Callinstrasse 3, D-30167 Hannover, Germany

3: LGCA UMR CNRS 5025, université Joseph-Fourier, BP 53, 38041 Grenoble cedex, France

#### **IV.3.a. Abstract**

In ophiolites and in present day oceanic crust formed at fast spreading ridges, oceanic plagiogranites are commonly observed at, or close to the base of the sheeted dike complex. They can be produced either by differentiation of mafic melts, or by hydrous partial melting of the hydrothermalized sheeted dikes. In addition, the hydrothermalized base of the sheeted dike complex, which is often infiltrated by plagiogranitic veins, is locally recrystallized into granoblastic dikes that are commonly interpreted as a result of prograde granulitic metamorphism. To test the anatectic origin of oceanic plagiogranites, we performed melting experiments on a natural hydrothermalized dike, under conditions that match those prevailing at the base of the sheeted dike complex.

All generated melts are water saturated, transitional between tholeiitic and calc-alkaline, and match the compositions of oceanic plagiogranites observed close to the base of the sheeted dike complex. Newly crystallized clinopyroxene and plagioclase have compositions that are characteristic of the same minerals in granoblastic dikes. Published silicic melt compositions obtained in classical MORB fractionation experiments also broadly match the compositions of oceanic plagiogranites; however, the compositions of the coexisting experimental minerals significantly deviate from those of the granoblastic dikes.

Our results demonstrate that hydrous partial melting is a likely common process in the root zone of the sheeted dike complex, starting at temperatures exceeding 850°C. The newly formed melt can either crystallize to form oceanic plagiogranites, or may be recycled within the melt lens resulting in hybridized and contaminated MORB melts. The residue after the partial melting event is represented by the granoblastic dikes. Our results support a model with a dynamic melt lens that has the potential to trigger hydrous partial melting reactions in the previously hydrothermalized sheeted dikes.

## *Chapter IV. Melting the hydrothermally altered sheeted dike complex: experimental study*

**Keywords:** mid-ocean ridge, axial magma chamber, hydrothermal system, sheeted dike complex, partial melting, experimental petrology, oceanic plagiogranite, granoblastic dikes

### **IV.3.b. Introduction**

At fast spreading ridges, the root zone of the sheeted dike complex is a peculiar geological horizon where the thermal gradient can be as high as  $7^{\circ}\text{C}/\text{m}$ , one of the highest, nearly stable gradient observed on earth (Nicolas et al., 2008). Moreover, the contact of the sheeted dike with the underlying melt lens can be regarded as an interface between two convecting systems, the magmatic and the hydrothermal one. Highly hydrothermalized basaltic rocks from the base of the sheeted dike complex are therefore in the vicinity of a relatively constant heat source, which has the potential to trigger dehydration and/or melting reactions. Nicolas et al. (2008) have studied in the Oman ophiolite the varytextured gabbro horizon located directly below the sheeted dike complex, and have interpreted most of the observed lithologies as hydrous partial melting products. Gillis and Coogan (2002), Wilson et al. (2006), Gillis (2008) and Koepke et al. (2008) investigated the base of the sheeted dike complex in the Troodos ophiolite, in the Oman ophiolite, and in IODP (Integrated Ocean Drilling Program) Hole 1256D. They described typical granoblastic, hornfelsic lithologies in amphibolite- to granulite-facies, and relate them to reheated, dehydrated sheeted dike ("granoblastic dikes"). To further understand the active processes at the sheeted dike / gabbro transition, France et al. (2009a) have compared this zone in the Oman ophiolite with the recent IODP Hole 1256D, and propose a dynamic model with up- and downward migrations of the gabbro/sheeted dike interface that is consistent with published models and descriptions of Gillis and Coogan (2002), Wilson et al. (2006), Gillis (2008) and Koepke et al. (2008). The mobility of the melt lens is supported by the observed reheating of the base of the sheeted dike, and recycling of the previously hydrothermalized sheeted dike in the underlying varytextured gabbros. The occurrence of partly assimilated sheeted dike fragments within the uppermost gabbros suggests that the lowermost sheeted dikes underwent hydrous partial melting.

Oceanic plagiogranites, as defined in Koepke et al. (2007), are common in the oceanic crust, in particular at the base of the sheeted dike complex (e.g., Pallister and Hopson, 1981), where they are generally found as relatively small bodies (Koepke et al., 2004; 2007). These oceanic plagiogranites are believed to represent products of either differentiated MORB, liquid immiscibility between a mafic and a felsic melt, or hydrous partial melting of gabbros

or sheeted dikes. Formation from MORB differentiation has been proposed in natural settings (e.g., Beccaluva et al., 1977; Coleman and Donato, 1979; Dubois, 1983; Lippard et al., 1986; Amri et al., 1996; Floyd et al., 1998; Selbekk et al., 1998; Beccaluva et al., 1999; Niu et al., 2002; Rao et al., 2004; Bonev and Stampfli, 2009; Rollinson, 2009) and has also been verified in experimental studies (Dixon-Spulber and Rutherford, 1983; Berndt et al., 2005; Feig et al., 2006). Liquid immiscibility has been observed in rapidly quenched basaltic flows from the upper oceanic crust (e.g., Sato, 1978; Philpotts, 1982), inferred from ophiolites (Ménot, 1987; Ulrich and Borsien, 1996; Shastry et al., 2001) and described experimentally (Dixon and Rutherford, 1979).

#### **IV.3.c. Natural occurrences and previous experiments on hydrous partial melting of mafic rocks**

Hydrous partial melting of mafic rocks has been proposed or described in several studies (e.g., Malpas 1979; Gerlach et al., 1981; Pedersen and Malpas, 1984; Flagler and Spray, 1991; Spray and Dunning, 1991; Twinning, 1996; Floyd et al., 1998; Selbekk et al., 1998; Gillis and Coogan, 2002; Coogan et al., 2003; Stakes and Taylor, 2003; Koepke et al., 2004, 2005a; Luchitskaya et al., 2005; Koepke et al., 2007; Nicolas et al., 2008; Rollinson, 2009). Most of these studies deal with ophiolites and attempt to determine the origin of plagiogranitic rocks. The interpretation of an anatectic origin is based on structural evidences, and/or on trace element geochemical modeling. Evidences of hydrous partial melting of mafic lithologies have also been reported from young oceanic crust at both slow spreading (e.g., Mével, 1988) and fast spreading (e.g., Koepke et al., 2005b; 2008) centers. The partial to complete assimilation of previously hydrothermalized sheeted dike, in magma chambers at fast spreading ridges, implies that the assimilated hydrothermalized rocks undergo hydrous partial melting. This recycling process is described in ophiolites (Coogan et al., 2003; Gillis, 2008; France et al., 2009a), and in present day oceanic crust (Wilson et al., 2006; Koepke et al., 2008; France et al., 2009a), or inferred from chlorine contents in amphiboles (Coogan, 2003; Coogan et al., 2003) and MORB (e.g., Michael & Schilling, 1989).

Experimental work that precisely matches the conditions (low pressure, high temperature, hydrous and highly oxidizing conditions, basaltic composition, hydrothermal alteration) prevailing at the base of the sheeted dike is lacking. Several experimental studies (e.g., Beard and Lofgren, 1989; Hacker 1990; Beard and Lofgren, 1991; Rapp et al., 1991; Rushmer 1991, 1993; Sen and Dunn, 1994; Wolf and Wyllie, 1994; Rapp and Watson, 1995;

#### *Chapter IV. Melting the hydrothermally altered sheeted dike complex: experimental study*

Patino Douce and Beard, 1995; Prouteau et al., 1999; Johannes and Koepke, 2001) have focused on the melting of mafic lithologies to investigate the origin of Archean tonalites, trondhjemites and granodiorites (TTG rocks; Barker 1979), which are believed to result from dehydration melting of amphibolites. Other authors have studied the melting of basalts in hydrous environment (Holloway and Burnham, 1972; Helz 1973; Beard and Lofgren, 1991; Kawamoto, 1996). Although some of these works approach the appropriate natural conditions (e.g., Beard and Lofgren, 1991), they are not fully relevant to the study of hydrous melting at the base of the sheeted dikes. These studies deal with subduction processes and most of them are conducted at pressures (in general  $\geq 500$  MPa) that are much higher than those ( $\sim 100$  MPa) prevailing at the base of the upper, basaltic oceanic crust. Moreover, most of these studies use dehydration melting experiments which are valid for the subduction environment but not for the base of the sheeted dikes where a lot of water is available at low pressure, resulting in water saturated conditions. The study of Beard and Lofgren (1991) approaches those conditions relevant to partial melting/assimilation of hydrothermalized sheeted dike at the gabbro/dike transition. Unfortunately, they don't provide the mineral compositions, and the redox conditions are not fixed but roughly estimated. The redox conditions, which are influenced by the presence of a high temperature hydrothermal system at the base of the sheeted dike (Nicolas et al., 2008), must be precisely controlled to understand and follow the evolution of melt and minerals with temperature. Koepke et al. (2004) have performed hydrous partial melting experiments on gabbroic lithologies from the lower oceanic crust with controlled redox conditions, but these experiments are not applicable to hydrous partial melting at the base of the sheeted dike complex. Hydrous partial melting of sheeted dike and gabbro may produce different melts and different residual phases because of different composition and mineralogy of the used starting material. While typical oceanic gabbros show a marked refractory character (e.g., extremely depleted in incompatible elements like Ti and K; mostly high in Mg#, with  $Mg\# = Mg/[Mg+Fe]$ ), most sheeted dikes are more evolved with compositions of evolved MORB. Another characteristic feature of the dikes at the gabbro/dike transition is related to significant hydrothermal alteration responsible for the formation of considerable amounts of hydrous minerals, which affects the melting behavior of a rock, in particular at lower temperatures, where the completion of a global equilibrium is often hampered.

#### IV.3.d. Experimental and analytical techniques

##### IV.3.d.1. Starting material

In order to closely match natural processes, we have selected a representative sample (08OL30) of typically altered sheeted dikes from the Oman ophiolite. It has been sampled in the Aswad area located in the southern Sumail massif, which is inferred to correspond to typical oceanic crust away from ridge discontinuities, and not affected by ridge tectonics or obduction-related deformation (Nicolas et al., 2000; Nicolas et al., 2008). Its whole rock composition is representative of typical sheeted dike from the Oman ophiolite (Fig. 1; Table 1). Compared to the average sheeted dike rocks sampled at ODP/IODP Hole 1256D and ODP Hole 504B, at Hess Deep, and at the Blanco Depression (Table 1), the chosen starting material is slightly more evolved. It is strongly altered due to a static hydrothermal overprint, which is a common feature of the sheeted dike complex in the studied area. The selected sample is composed of albitized plagioclase ( $An_{03}$ ), actinolite, prehnite, pumpellyite, titanite, and some magnetite (Fig. 2), an assemblage typical of greenschist-facies conditions (see section “phase compositions in the partly molten system” for mineral compositions). Primary magmatic phases are not observed.

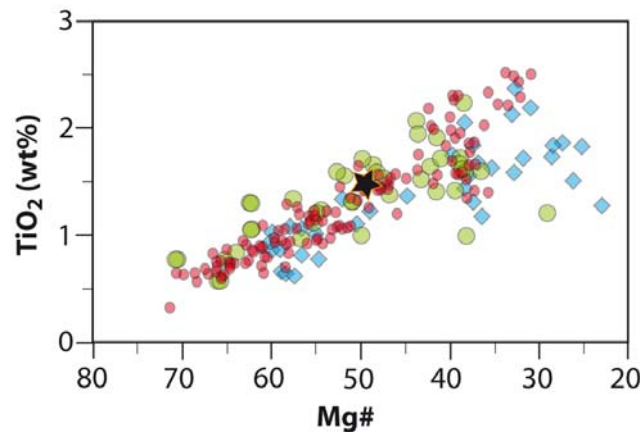


**Figure 1:** Comparison of the bulk rock composition of the starting material (08OL30) with those of sheeted dike complex and extrusives of the Oman ophiolite in a  $TiO_2$  vs  $Mg\#$  diagram (with  $Mg\# = Mg/[Mg + Fe_{total}]$ ); after Miyashita et al. (2003). Symbols are black star: starting material, red small circle: sheeted dike complex by Miyashita et al. (2003), green large circle: sheeted dike complex by Lippard et al. (1986), and Type 1 dikes by Rochette et al. (1991), blue diamonds: Geotimes volcanics by Lippard et al. (1986) and V1 lava by Einaudi et al. (2000).

After crushing the starting rock, three grain size fractions were obtained by sieving (30-100  $\mu m$ , 100-150  $\mu m$ , and 150-250  $\mu m$ ) and were used for preliminary experiments. These experiments were performed at a temperature of 1000°C to study the effect of grain

*Chapter IV. Melting the hydrothermally altered sheeted dike complex: experimental study*

size of the starting material on the kinetics of the melting reaction (Table 2). In the three experimental products, minerals and melts have identical compositions within the analytical errors. Moreover, the phases are homogeneous, crystals display no zonation, and compositions are identical within the whole capsule volume, independent of the grain size of the starting material (Fig. 3a). No relict phases of the starting material were observed. As experiments performed with coarser grain size produce larger experimental crystals and melt pools, which are more suitable for electron microprobe measurements, we chose the 150-250  $\mu\text{m}$  fraction as starting material (Table 1).

	SiO <sub>2</sub>	TiO <sub>2</sub>	Al <sub>2</sub> O <sub>3</sub>	Fe <sub>2</sub> O <sub>3</sub> (t)	MnO	MgO	CaO	Na <sub>2</sub> O	K <sub>2</sub> O	P <sub>2</sub> O <sub>5</sub>	LOI	total	Mg #
<b>08OL30</b>	50.38	1.40	15.04	10.29	0.06	4.99	7.19	4.44	0.19	0.11	4.74	98.8	-
<b>08OL30 recalculated</b>	53.55	1.48	15.98	10.94	0.07	5.30	7.64	4.72	0.20	0.12	-	100	49.0
<b>Oman, Umino et al., 2003</b>	52.51 ± 2.09	1.17 ± 0.45	16.06 ± 0.92	10.41 ± 1.83	0.15 ± 0.05	6.68 ± 1.28	8.51 ± 2.81	4.21 ± 1.34	0.18 ± 0.15	0.11 ± 0.03	-	100	56.0
<b>Oman, Miyashita et al., 2003</b>	52.59 ± 1.72	1.33 ± 0.50	15.64 ± 0.76	10.89 ± 2.16	0.16 ± 0.05	6.03 ± 1.55	8.86 ± 2.68	4.24 ± 1.39	0.16 ± 0.12	0.11 ± 0.05	-	100	52.3
<b>1256D, Teagle et al., 2006</b>	50.56	1.55	13.75	13.57	0.23	6.88	10.75	2.53	0.05	0.13	-	100	50.1
<b>Hess Deep, Pollock et al., 2009</b>	50.57	1.37	14.31	11.58	0.20	8.02	10.82	2.78	0.05	0.31	-	100	57.8
<b>504B, Bach et al., 1996</b>	49.36	0.80	16.12	9.60	0.15	8.93	13.11	1.86	0.01	0.06	-	100	64.8
<b>Blanco Depression, Cordier et al., 2007; Juteau et al., 1995</b>	50.08	1.99	13.97	13.15	0.21	6.79	10.60	2.82	0.22	0.16	-	100	50.5

*Table 1: Whole rock compositions of the starting material and of sheeted dike complex from different oceanic localities. Composition of the sheeted dike complex from Oman (Umino et al., 2003; Miyashita et al., 2003), from IODP Hole 1256D in the Cocos plate (Teagle et al., 2006), from Hess Deep (East Pacific Rise [EPR]; Pollock et al., 2009), from ODP Hole 504B (Bach et al., 1996), and from the Blanco Fracture Zone on the Juan de Fuca ridge (average of data from Juteau et al., 1995 and Cordier et al., 2007). For comparison, compositions of sample 08OL30 (starting material) are recalculated at 100%. Standard deviations are given for the Oman sheeted dike. Mg# = Mg/(Mg + Fe<sub>total</sub>); LOI = loss on ignition.*

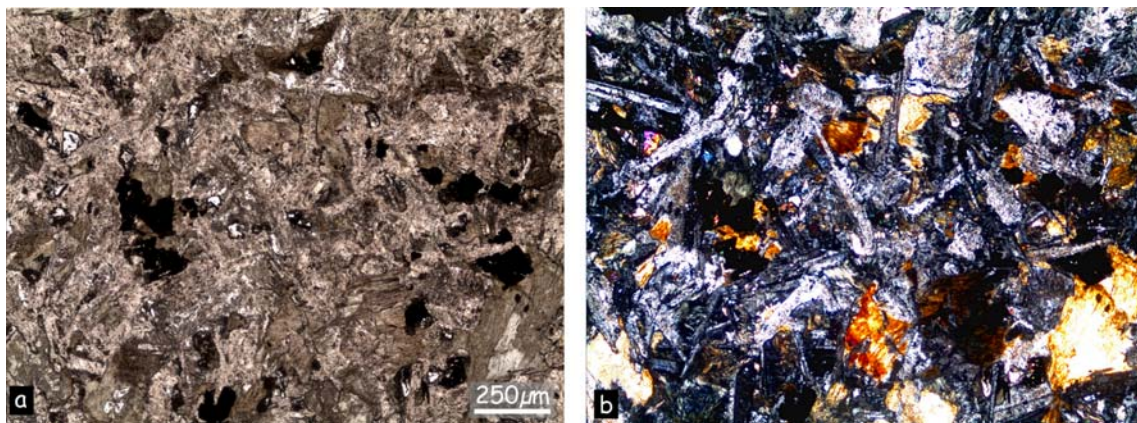


**Figure 2:** Microphotographs of the starting material (08OL30). **a)** plane-polarized light; **b)** cross-polarized light.



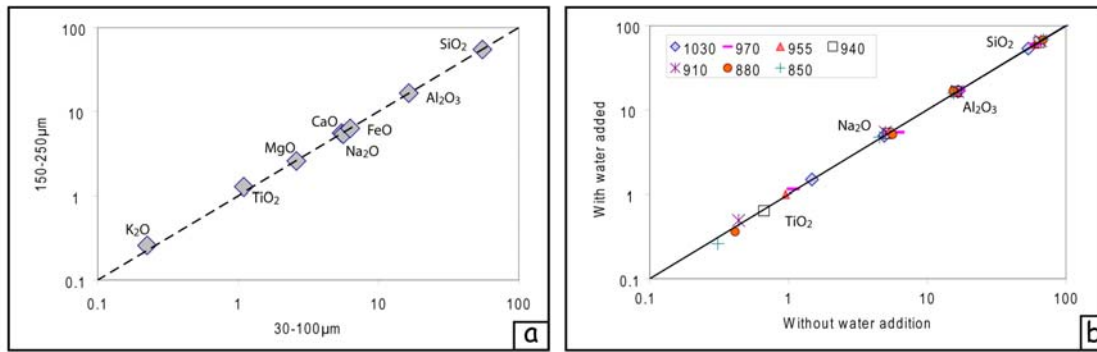


**Figure 3:** Comparison of melt compositions from experiments performed with identical starting compositions (wt%) for different grain sizes of the starting material (a). Each data point represents the average for one oxide (as indicated). The corresponding experiments were performed at 1000°C. b) Comparison of melt compositions from experiments performed with identical starting compositions (wt%) for experiments with and without water added shown for the TiO<sub>2</sub>, Na<sub>2</sub>O, Al<sub>2</sub>O<sub>3</sub> and SiO<sub>2</sub> at different temperatures. In both logarithmic plots, the line represents the 1:1 correlation. Grain size (a), and the addition of water to the starting material (b) have no influence on the melt composition.

#### IV.3.d.2. Experimental method

Melting experiments ( $\geq 850^\circ\text{C}$ ) have been performed in an internally heated pressure vessel (IHPV) at the experimental lab of the Institut für Mineralogie (Hannover, Germany), equipped with a Shaw membrane and a rapid quench device. Details of the IHPV are presented in Berndt et al. (2002). The vessel was pressurized with argon at 100 MPa, a pressure relevant to the level of the axial melt lens within the ocean crust. The pressure was controlled with a strain gauge manometer (uncertainty of  $\pm 5$  MPa). Previous calibrations on the vessel show that temperature is homogeneous over the sample with less than  $10^\circ$  of variation and a measurement accuracy better than  $\pm 10^\circ$ . This is also indicated by the regular evolution of the melt and mineral compositions with temperature (see below). Experimental conditions are summarized in Table 2. In all experiments, the prevailing  $f\text{O}_2$  corresponds to FMQ+1 – FMQ+2, where FMQ is the fayalite-magnetite-quartz oxygen buffer equilibrium (for values see Table 2). At the beginning of the experiment, the temperature rises continuously ( $30^\circ\text{C}/\text{min}$ ) to reach the final experimental temperature after  $\sim 30$  min. At the end of experiments, the samples were quenched isobarically using a rapid quench facility to prevent crystallization during cooling ( $\sim 150^\circ/\text{s}$ ). Effective quenching is evidenced by the absence of “quench minerals” in melts in spite of the presence of low viscous basaltic melts with high water content.

Chapter IV. Melting the hydrothermally altered sheeted dike complex: experimental study

RUN N°	Capsule	Temp. (°C)	f(H <sub>2</sub> )	Δ <sub>FMQ</sub>	Phases	duration	grain size
#3	#10[D] #12[W]	1030	2.18	1.38	melt, Ol, Cpx	72h	150-250μm
#1	#2c[W] #3b[W] #4a[W]	1000	2.77	1.56	melt, Ol, Cpx, Pl, TiMagt, Pl <sub>m</sub>	72h	150-250μm 100-150μm 30-100μm
#4	#13[D] #14[W]	970	1.89	1.51	melt, Ol, Cpx, Pl, TiMagt, Pl <sub>m</sub>	96h	150-250μm
#7	#23 [D] #25[W]	955	2.63	1.24	melt, Ol, Cpx, Pl, TiMagt, Ilm, Pl <sub>m</sub>	96h	150-250μm
#6	#17[D] #18[W]	940	2.02	1.45	melt, Ol, Cpx, Pl, Amp, Opx, TiMagt, Ilm, Pl <sub>m</sub> , Titanite, Apatite	96h	150-250μm
#2	#5[D] #8[W]	910	2.24	1.36	melt, Cpx, Pl, Amp, Opx, TiMagt, Ilm, Pl <sub>m</sub> , Titanite	120h	150-250μm
#5	#15[D] #16[W]	880	0.97	2.09	melt, Cpx, Pl, Amp, Opx, TiMagt, Ilm, Pl <sub>m</sub> , Titanite, Act	120h	150-250μm
#8	#24[D] #26[W]	850	2.53	1.13	melt, Cpx, Pl, Amp, Opx, TiMagt, Ilm, Pl <sub>m</sub> , Titanite, Act	144h	150-250μm
#metam 1	#9[D] #11[W]	800	-	0.79	Pl, Amp, Opx, TiMagt, Ilm, Titanite, Act, Ab (+Pl <sub>m</sub> +Cpx)	504h	150-250μm
#metam 2	#21[D] #22[W]	750	-	0.80	Pl, Amp, Opx, TiMagt, Ilm, Titanite, Act, Ab (+Pl <sub>m</sub> +Cpx)	624h	150-250μm

Table 2: Experimental conditions. Temp.=temperature; D = experiment without water addition, W = experiment with water addition. The oxygen fugacity is given in log units relative to the FMQ oxygen buffer. Minerals in parentheses (+Pl<sub>m</sub>+Cpx) are localized in the prehnite reaction zones (see “prehnite break-down reaction” part for further details). Ol=olivine, Cpx=clinopyroxene, Pl=plagioclase, TiMagt=titanomagnetite, Pl<sub>m</sub>=metastable plagioclase, Ilm= ilmenite, Amp=amphibole, Opx=orthopyroxene, Act=actinolite, Ab=albite, Magt=magnetite.

In addition to the high temperature runs in the partially molten regime, subsolidus experiments (750°C and 800°C) have been performed in an externally heated cold-seal pressure vessel (CSPV). This vessel was pressurized with water at 100 MPa and controlled with a pressure transducer calibrated against a strain gauge manometer. The accuracy of pressure measurements was 1 MPa and pressure variations during the experiments were less than ±5 MPa. The temperature was controlled with an external Ni-CrNi thermocouple (vessels were calibrated for temperature). The temperature variations were less than 5°C, while the accuracy was estimated to be ±10°C. Experiment conditions are summarized in Table 2. In all experimental runs, fO<sub>2</sub> corresponds to the NNO oxygen buffer (≈FMQ+1), established by adding a solid buffer composed of a Ni-NiO assemblage around the gold capsule. After experiments, samples were quenched isobarically by using a flux of compressed air (initial

cooling rate  $\sim 200^\circ/\text{min}$ ). For all the experiments gold was used as capsule material. Thus, iron diffusion into the capsule material can be neglected.

Since the natural samples from the root zone of the sheeted dike complex contain high amounts of hydroxyl-bearing minerals (actinolite, prehnite, pumpellyite), it was expected that water would be released in the partial melting experiments (dehydration melting). Due to the relatively low water solubility in basaltic melts at the given shallow pressure of 100 MPa ( $\sim 3\%$ ; Berndt et al., 2002), water-saturating in the experiments was expected. We performed one experimental series under water-saturated conditions by adding distilled water (5 mg) to the starting material (50 mg) and another series without adding water, corresponding to typical dehydration experiments. The two capsules (with and without water addition) were run simultaneously at each temperature. For each temperature, results from both capsules are identical for the phase relations and phase compositions (Fig. 3b), suggesting that in both experimental series, water saturation was reached, and that the dehydration melting produces enough water for reaching water-saturated condition. In all experiments bubbles are present, attesting fluid (mainly composed of water) saturation (Fig. 4). The similarity between the two series show that experiments are reproducible.

#### ***IV.3.d.3. Analytical method***

Experimental results were analyzed using a Cameca SX100 electron microprobe (Institut für Mineralogie, Hannover, Germany) equipped with 5 spectrometers, “Peak sight” software is used. All analyses were performed using a 15 kV acceleration potential, a static (fixed) beam,  $K\alpha$  emission from all elements. The matrix correction is based on Pouchou and Pichoir (1991). Analyses of crystals were performed with a beam current of 15 nA using a focused beam and a counting time of 10 to 30 s on peak and background. Analyses of glass were performed with a beam current, which was set to 6 nA to minimize migration and volatilization of the alkali elements. Counting time was from 2 to 5 s for Na and K and from 5 to 10 for other elements (Si, Ti, Al, Mg, Fe, Ca, Mn, Cr). In the experiments where melt pools are large enough, the beam was defocused to a spot size of 5 to 20  $\mu\text{m}$ . Backscattered electron (BSE) images were also obtained on the Cameca SX100 electron microprobe.

#### **IV.3.e. Experimental results**

##### ***IV.3.e.1. Attainment of equilibrium***

The use of fine grained starting material ( $\leq 1 \mu\text{m}$ ) in partial melting experiments enhances the achievement of global equilibrium. Unfortunately, it prevents suitable

#### *Chapter IV. Melting the hydrothermally altered sheeted dike complex: experimental study*

microprobe analyses due to very small newly formed experimental phases. The advantage of using coarser grained starting material is the formation of relatively large crystals in the experimental products, which enables easy microprobe analyses of the experimental phases. However, too coarse-grained starting material may prevent the achievement of global equilibrium, since cores of unreacted starting material may be still present after the experiment, as observed in many typical dehydration melting experiments of mafic protoliths (e.g., Hacker, 1990; Beard and Lofgren, 1991; Patino Douce and Beard, 1995; Johannes and Koepke, 2001). This effect is most pronounced concerning plagioclase, which is the rate-controlling phase in many basaltic systems (Johannes and Koepke, 2001). These authors show that reaction kinetics can be significantly enhanced in water-saturated systems, as it was the case in our experiments. Moreover, the starting material in our experiments shows a pervasive alteration overprint (plagioclase with  $An < 03$ , actinolite, titanite, prehnite, pumpellyite, magnetite), and no typical primary magmatic phases (e.g., olivine, pyroxene, An-rich plagioclase, or magmatic amphibole) were present. Hence, the phase assemblage had to change completely during the melting reaction, thus minimizing the risk of formation of typical core/rim complexes of the reacting minerals. Due to the favorable conditions in our melting experiments, no relics of the starting material are present in most of the melting experiments, in particular those experiments performed at temperatures  $> 910^{\circ}\text{C}$ .

Several lines of evidence are listed below, which suggest that a state close to equilibrium has been attained in our "magmatic" experiments (i.e., temperatures  $> 910^{\circ}\text{C}$ ): (1) No zonations in newly formed crystals are observed (Fig. 4) and crystal compositions are homogeneous within each experiment and between the two series (with and without addition of water). (2) Newly formed crystals are euhedral (e.g., Ol) or mimic previous minerals that are not present anymore (e.g., Cpx and Pl; Fig. 4). (3) No relictic phases from the starting materials are observed (for temperature  $> 910^{\circ}\text{C}$ ). (4) All phase compositions vary systematically with temperature, and compositional trends are consistent with the ones expected from literature (e.g., rise of the plagioclase An content; see "phase compositions in the partly molten system" section). (5) Glass compositions also vary systematically with temperature (see "phase compositions in the partly molten system" section), and are homogeneous within each experiment and between the two series (with and without addition of water).

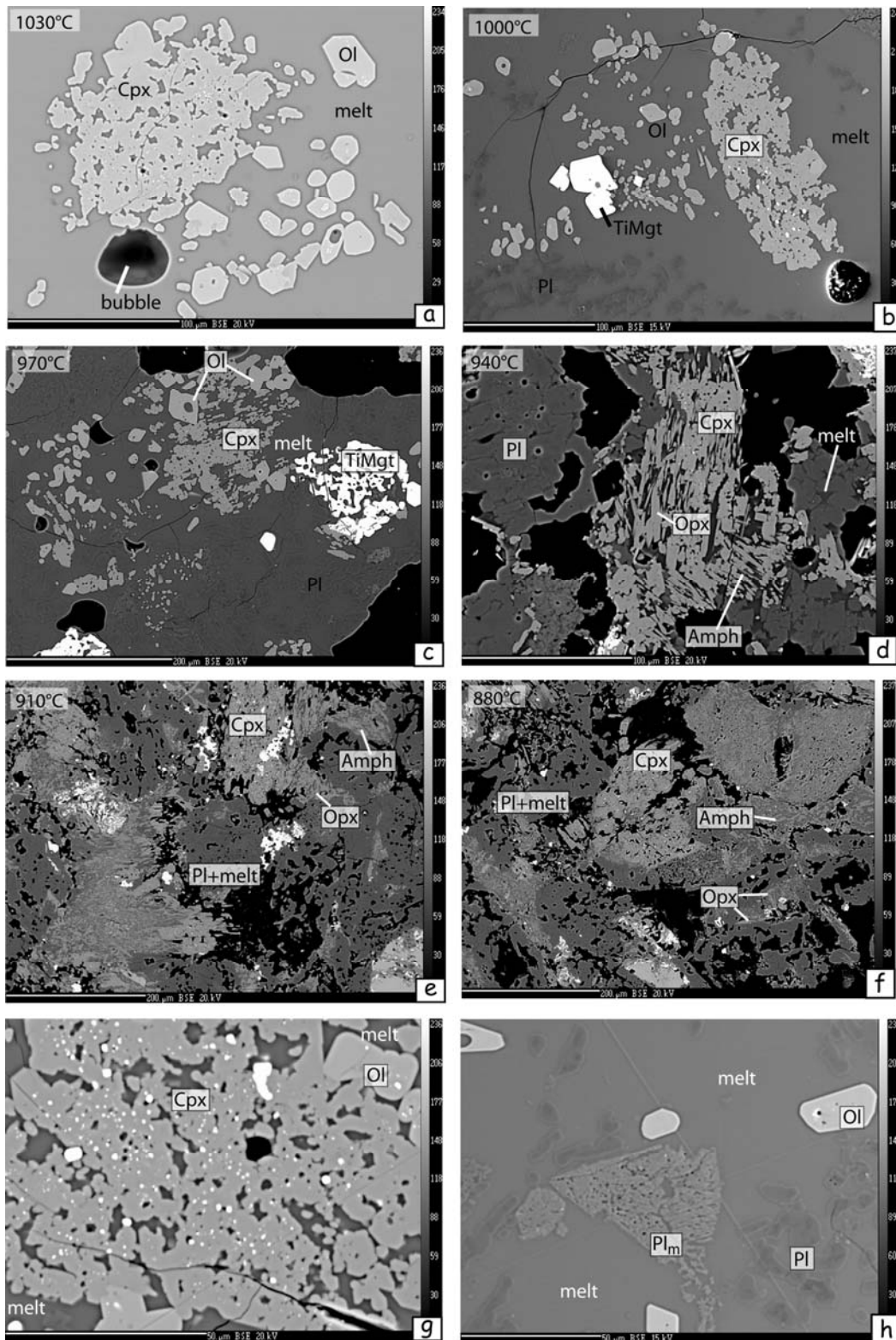


**Figure 4:** Backscattered electron images of the experimental results in the partly molten system for different temperatures **a)** 1030°C with water added (melt proportion is not representative for the whole sample which shows >90% melt); **b)** 1000°C with water added; **c)** 970°C with water added; **d)** 940°C without water addition; **e)** 910°C without water addition; **f)** 880°C without water addition; **g)** numerous tiny oxide-inclusions in clinopyroxene and olivine in the experiment performed at 970°C without water addition; **h)** “metastable plagioclase” in the experiment performed at 1000°C with water added. Minerals abbreviations are the same as in Table 2.

Nevertheless, a second type of plagioclase was observed in all experiments at temperatures  $\leq 1000^{\circ}\text{C}$ . Compared to the equilibrium plagioclase which shows an idiomorphic habit, these are spongy with very irregular grain boundaries (Fig. 4h) and highly enriched in An component (Table in Appendix B2). These crystals are interpreted to represent metastable phases which were recrystallized after prehnite (for further details see section “Prehnite break-down reaction”). Since these crystals occur only very rarely, we consider that the approaching of global equilibrium in these experiments is not hampered.

In subsolidus experiments, reactions are not complete and new phases are only observed as coronitic assemblages. Therefore, these experiments will only be used to understand the metastable assemblages present in the partly molten system (see section “prehnite break-down reaction”).

#### IV.3.e.2. Phase relations in the partial molten system

The evolution of the phase relations (Fig. 5) was established with the help of backscattered electron images (BSE) images (e.g., Fig. 4).

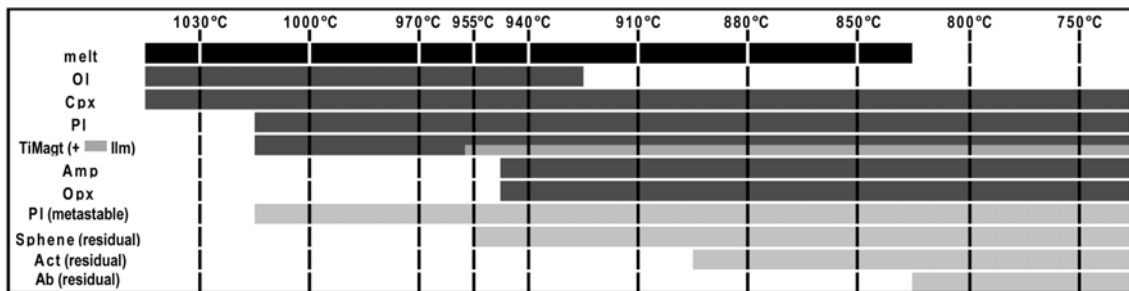


**Figure 5:** Phases present in the products of partial melting and subsolidus experiments as a function of temperature. Minerals abbreviations are the same as in Table 2.

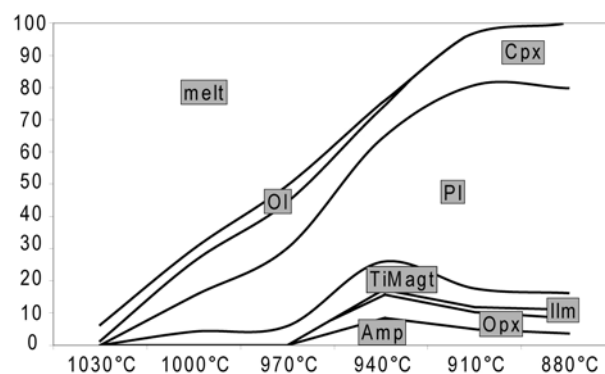


**Figure 6:** Phase proportions in the partly molten system calculated with a least square model according Albarède and Provost (1977). Standard deviation  $< 1$  for all values. Values obtained for experiments at temperatures  $< 950^{\circ}\text{C}$  are less accurate. Incoherent values are obtained at  $850^{\circ}\text{C}$ . Minerals abbreviations are the same as in Table 2.

Figure 6 gives a rough estimate of the phase proportions which were obtained via least square calculations (Albarède and Provost, 1977). The first melt was observed at temperatures as low as 850°C, and the liquidus temperature is slightly higher than 1030°C. While in the low-temperature experiment performed at 850°C melt pools seem to remain isolated, at temperatures > 910°C the melt phase forms a connected framework. Melt proportion is low (<10%) for temperatures < 910°C, and a large increase is observed between 940°C and 970°C (Fig. 4); above 970°C the melt proportion continues to increase linearly until the liquidus is reached. The liquidus phases are olivine and clinopyroxene; plagioclase and titanomagnetite are present below 1000°C. The saturation of olivine and clinopyroxene at near liquidus condition in tholeiitic systems is somewhat uncommon, but can be ascribed to the high water activities as experiments are water saturated (e.g., Gaetani et al. 1993, Feig et al., 2006). First olivine appears at 940°C. Amphibole is stable in experiments up to 940°C. At this temperature, when applying the TiO<sub>2</sub> contents of amphibole to the semi-quantitative TiO<sub>2</sub>-in-amphibole thermometer of Ernst and Liu (1998), the estimated temperature is 950°C and matches very well the run temperature, implying the achievement of equilibrium condition. The application of this thermometer is justified, since the amphibole in our experiments is coexisting with a Ti-rich oxide phase (Ernst and Liu, 1998).

Orthopyroxene is stable up to 940°C. Application of the 2-pyroxene thermometer (Andersen et al., 1993) reveals equilibrium temperatures which are largely overestimated: 1092±31°C for the 940°C run; 1039±30°C for the 910°C run; 1041±36°C for the 880°C run, and 1056±14°C for the 850°C run (data of Table in Appendix B2 are used, these are averages of experiments with and without water addition). This large discrepancy can be explained by the presence of a high water activity, as the presence of water shifts the Mg# of clinopyroxene and orthopyroxene to higher values and consequently to higher calculated temperatures (Feig et al., 2006). Ilmenite is present up to temperatures of 955°C; at higher temperatures, only titanomagnetite is stable. Application of the 2-oxide thermo-oxybarometer (Sauerzapf et al., 2008) reveals an equilibrium temperature of 929°C and  $\Delta\text{NNO}=+0.58$  for the 955°C experiment, 901°C and  $\Delta\text{NNO}=+1.01$  for the 940°C experiment, 872°C and  $\Delta\text{NNO}=+0.83$  for the 910°C experiment, 814°C and  $\Delta\text{NNO}=1.35$  for the 880°C experiment, 779°C and  $\Delta\text{NNO}=+0.82$  for the 850°C experiment, and 719°C and  $\Delta\text{NNO}=+0.89$  for the 750°C subsolidus experiment (data of Table in Appendix B2 are used, these are averages of experiments with and without water addition). The accuracy of the 2-oxide thermo-oxybarometer is  $\pm 70^\circ$  for the temperature and  $\pm 0.4$  log units for the oxygen fugacity (Sauerzapf et al., 2008). Hence, these estimations are consistent with the conditions of the

experiments (Table 2). Numerous tiny oxides with grain sizes  $< 5 \mu\text{m}$  were observed as inclusions in nearly all olivine and clinopyroxene grains (Fig. 4g). This observation is of significance, since similar features are observed in clinopyroxenes from the granulite-facies granoblastic dikes in natural settings (e.g., Koepke et al., 2008; France et al., 2009a), providing a tool for identifying such clinopyroxenes as residual phases after hydrous partial melting. Titanite is stable from low temperature experiments to  $940^\circ\text{C}$ . In experiments from  $910^\circ\text{C}$  to  $1000^\circ\text{C}$ , some rare grains of a metastable plagioclase ( $\text{Pl}_m$ ) are observed (Fig. 4h).

#### **IV.3.e.3. Prehnite break-down reaction**

In the subsolidus experiments, some sparse, complex mineral assemblages with an apparent coronitic structure are locally present (Fig. 7).

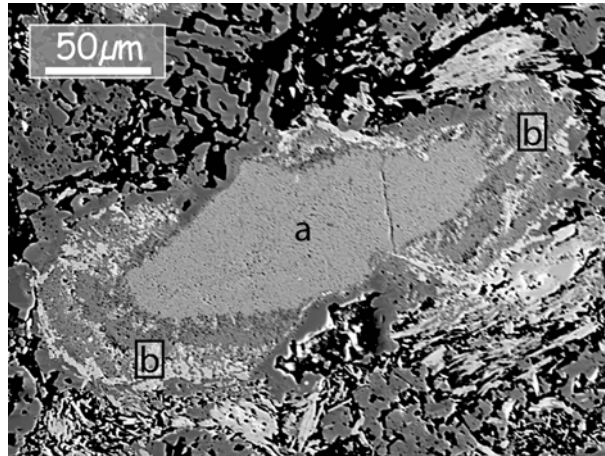


**Figure 7:** Backscattered electron image of a coronitic assemblage ( $750^\circ\text{C}$  with water added experiment) that displays in the center (a) a mineral assemblage compositionally similar to “dry prehnite”; it is interpreted as an anorthite+wollastonite assemblage. At the rim (b) of this assemblage, an assemblage of metastable plagioclase ( $\text{Pl}_m$ ) and Ca-Al-rich clinopyroxene is observed (brighter). This assemblage is interpreted to be derived from the prehnite break-down reaction (see the part “Prehnite break-down reaction” for more details).

In the center of these assemblages, the composition is similar to that of a “dry prehnite”. The margins consist of a close intergrowth of plagioclase, which is slightly enriched in An compared to the equilibrium plagioclase, and clinopyroxene. Clinopyroxene is not present elsewhere in the subsolidus experiments, but these ones present in the coronitic assemblages are enriched in CaO and  $\text{Al}_2\text{O}_3$  compared to the ones of partial melting experiments. According to Liou (1971), prehnite, which is present in our starting material, should react to an assemblage of anorthite + wollastonite when temperature increases ( $1 \text{ prehnite} \Leftrightarrow 2 \text{ anorthite} + 1 \text{ wollastonite} + \text{H}_2\text{O}$ ). The composition of the assemblage “2 anorthite + 1 wollastonite” corresponds exactly to that of the “dry prehnite” which was analyzed in the corresponding run (Table in Appendix B2). Since the compositions of the phases forming the



close intergrowth network of the rim also deviate slightly from the corresponding equilibrium compositions of plagioclase and clinopyroxene, we interpret the whole coronitic assemblage as a metastable product of the prehnite breakdown reaction. We speculate that the sparse plagioclases with an apparent spongy structure as presented in Figure 4h, which are much richer in An compared to the equilibrium plagioclases, correspond to metastable relics of such prehnite breakdown reactions. It should be noted that in experimental dehydration melting of mafic systems relics of An-rich plagioclases may persist metastably for a very long time, even at high water activities (more than 36 days in experiments of Johannes and Koepke, 2001).

#### **IV.3.e.4. Phase compositions in the partial molten system**

The phase compositions of the starting material and of the experimental products are listed in Table in Appendix B2; indicated compositions are averages of mineral compositions in experiments with and without water addition (Fig. 3b). Detailed compositions for each series (with and without water addition) are provided as supplementary material. The dependence of olivine composition on temperature is shown in Figure 8a. The forsterite content (Fo) is nearly identical between the 1000°C and the 1030°C experiments; it may reflect the identical Mg# of the melt in these two runs. The partitioning of Fe and Mg between olivine and melt ( $K_{D_{Fe-Mg}}^{Ol-melt} = \frac{X_{Liq}^{Mg} / X_{Ol}^{Mg}}{X_{Liq}^{Fe^{2+}} / X_{Ol}^{Fe^{2+}}}$ ) is classically considered to be 0.30±0.02 (Roeder and Emslie, 1970). Toplis (2005) has reviewed this partitioning coefficient, and has proposed a new equation to calculate  $K_{D_{Fe-Mg}}^{Ol-melt}$  that can vary as a function of temperature, alkalis, and water. Using this equation for the conditions of our experiments leads to a predicted value of 0.30±0.02.  $K_{D_{Fe-Mg}}^{Ol-melt}$  measured in our experiments is ~0.25 by using the FeO<sup>tot</sup> of the melt, which is not in the accepted error range. However, as the oxygen fugacity is known in our experiments, the real FeO value (including only the Fe<sup>2+</sup>) in the melt can be calculated using the Kress and Carmichael (1991) model; the resulting average  $K_{D_{Fe-Mg}}^{Ol-melt}$  is 0.28 which is in the accepted range of error according to Toplis (2005), which support the assumption that equilibrium is nearly attained in our experiments.

In the melting experiments, typical clinopyroxene is augite. As expected, its composition varies systematically with temperature. With rising temperature, the wollastonite component and the Mg# increase (from 38 to 44, and from 66 to 78, respectively), as well as the concentration of TiO<sub>2</sub> and Al<sub>2</sub>O<sub>3</sub>. Clinopyroxene Al<sub>2</sub>O<sub>3</sub> content decreases with temperature from 3 to 1.26 wt% (Fig. 8b) whereas the melt Al<sub>2</sub>O<sub>3</sub> content is nearly stable.

In the melting experiments, typical clinopyroxene is augite. As expected, its composition varies systematically with temperature. With rising temperature, the wollastonite component and the Mg# increase (from 38 to 44, and from 66 to 78, respectively), as well as the concentration of TiO<sub>2</sub> and Al<sub>2</sub>O<sub>3</sub>. Clinopyroxene Al<sub>2</sub>O<sub>3</sub> content decreases with temperature from 3 to 1.26 wt% (Fig. 8b) whereas the melt Al<sub>2</sub>O<sub>3</sub> content is nearly stable.

Chapter IV. Melting the hydrothermally altered sheeted dike complex: experimental study

This demonstrates the dependence of the partition coefficient  $D_{Al_2O_3}^{Cpx-melt}$  on temperature. It decreases by a factor of  $\sim 2$  (from  $\sim 0.2$  to  $\sim 0.1$ ) with temperature. Orthopyroxene is clinoenstatite; the wollastonite component and Mg# are, for all temperatures, between 3 and 4, and between 63 and 72, respectively.

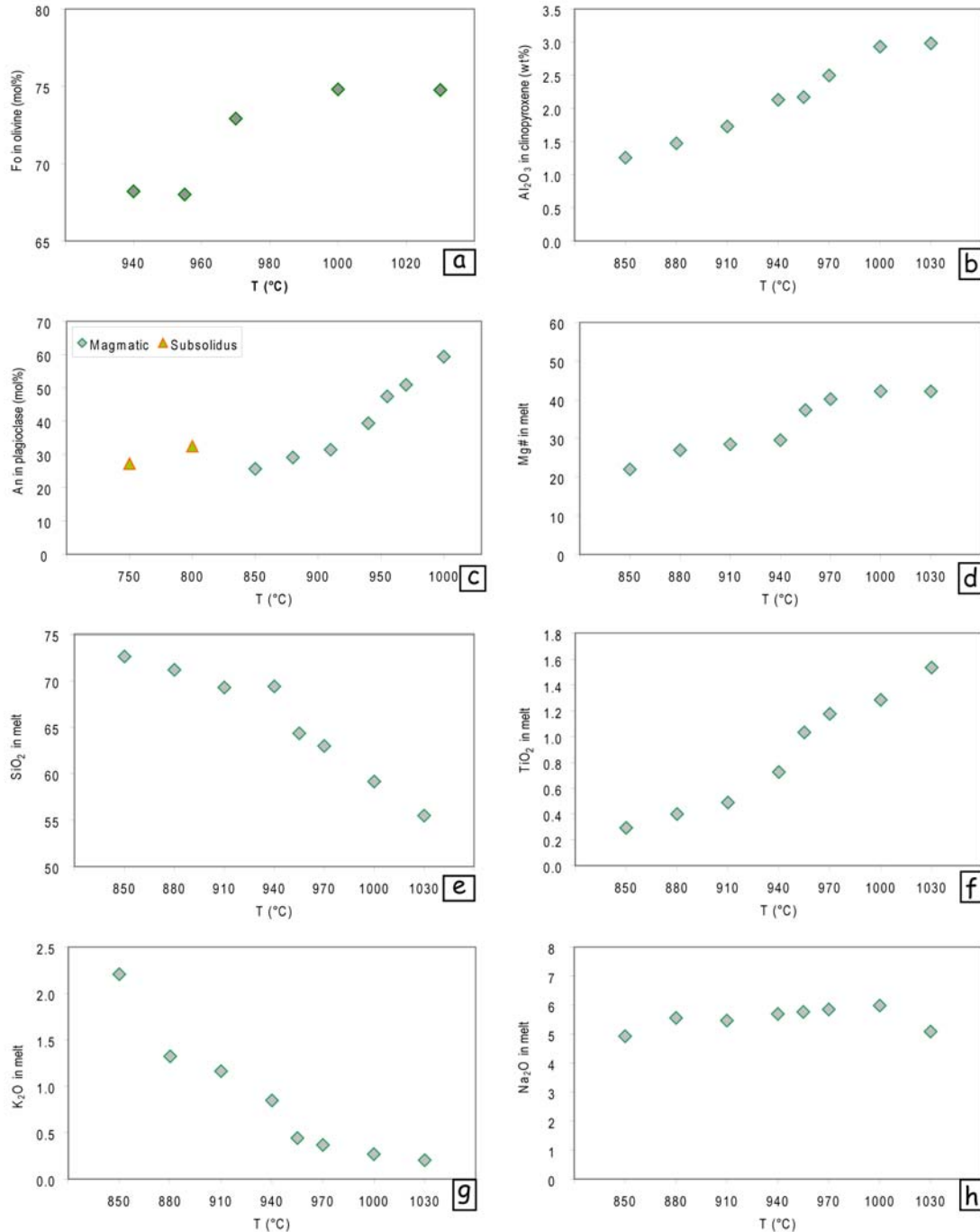


**Figure 8:** Compositional features of the experimental phases as a function of temperature. **a)** Forsterite content in olivine; **b)** Al<sub>2</sub>O<sub>3</sub> content of clinopyroxene in the partly molten system; **c)** Anorthite content of plagioclase in the partly molten and subsolidus systems; **d)** Mg# in melt; **e)** SiO<sub>2</sub> in melt; **f)** TiO<sub>2</sub> in melt; **g)** K<sub>2</sub>O in melt; **h)** Na<sub>2</sub>O in melt.

The anorthite (An) content of plagioclase increases with temperature from 26 to 59. For comparison, subsolidus plagioclase compositions are indicated in Figure 8c; the An content increases with temperature from 27 to 31.5. In the partly molten system the  $\text{FeO}_t$  content of plagioclase increases with temperature, reaching 0.94 wt% in the 1000°C run. This increase is correlated with increasing  $\text{FeO}_t$  content in the melt. In contrast, the partition coefficient  $D_{\text{FeO}_t}^{\text{Pl-melt}}$  increases with decreasing temperature. Lundgaard and Tegner (2004) have shown that  $D_{\text{FeO}_t}^{\text{Pl-melt}}$  depends on the redox conditions and on the silica content of the melt ( $D_{\text{FeO}_t}^{\text{Pl-melt}}$  is higher for more oxidizing conditions and for higher silica contents). As our experiments are performed at very similar redox conditions, we attribute this increase of  $D_{\text{FeO}_t}^{\text{Pl-melt}}$  to the increase in silica content of the melt with decreasing temperature.

Titanomagnetite is present from 850°C to 1000°C; it contains between 8 and 14 wt% of  $\text{TiO}_2$  while the  $\text{Al}_2\text{O}_3$  and  $\text{MgO}$  contents increase with temperature (from 1.55% to 4.21%, and from 1.26% to 4.39%, respectively). Ilmenite is present from 850°C to 955°C; minor components as  $\text{SiO}_2$ ,  $\text{Al}_2\text{O}_3$ , and  $\text{MgO}$  globally increase with temperature. The amount of  $\text{Cr}_2\text{O}_3$  in both oxides is below detection limit.

Amphiboles in the experiments with melt present are edenite and pargasite. As expected, their  $\text{TiO}_2$ ,  $\text{Al}_2\text{O}_3$ , and  $\text{Na}_2\text{O}$  contents increase with temperature. For comparison, they vary from actinolite to hornblende in subsolidus experiments.

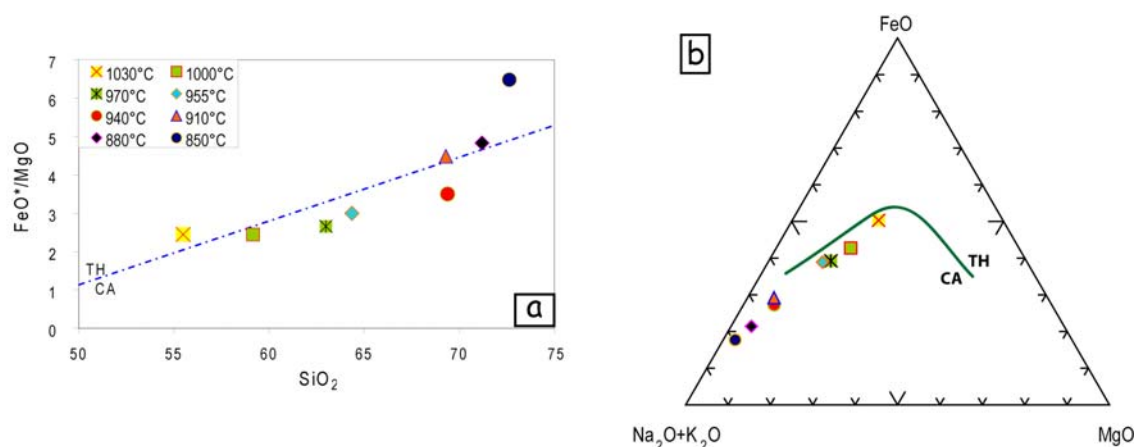


**Figure 9:** a)  $\text{FeO}^*/\text{MgO}$  versus  $\text{SiO}_2$  diagram from Miyashiro (1974).  $\text{FeO}^* = \text{FeO}_{\text{total}}$ ; TH=tholeiitic field, CA=Calc-alkaline field b) Alkaline ( $\text{Na}_2\text{O}+\text{K}_2\text{O}$ )- $\text{FeO}_{\text{total}}$ - $\text{MgO}$  discriminating diagram from Irvine and Baragar (1971).

Melt is saturated with water in all experiments (presence of bubbles). In the experimental melt obtained with the highest temperature (1030°C), which displays the largest

melt pools, a water content of 4.8 wt% has been determined by FTIR (Fourier Transformed InfraRed spectroscopy). The Mg# of the melt increases with temperature from 22 to 42.2 (Fig. 8d). The SiO<sub>2</sub> and K<sub>2</sub>O contents decrease with increasing temperature, whereas the TiO<sub>2</sub>, MgO, FeO and CaO contents increase (Fig. 8). Those melts formed at the lowermost temperature (~850°C) reach SiO<sub>2</sub> contents of 72.6 wt%. In a FeO<sub>total</sub>/MgO versus SiO<sub>2</sub> discriminating diagram (Miyashiro, 1974), and in an Alkaline (Na<sub>2</sub>O+K<sub>2</sub>O)-FeO<sub>total</sub>-MgO discriminating diagram (Irvine and Baragar, 1971), the experimental melts plot close to the transition between the calc-alkaline and tholeiitic series (Fig. 9).

### **IV.3.f. Discussion**

#### ***IV.3.f.1. Melt evolution: Origin of oceanic plagiogranites at the base of the Sheeted Dikes***

Our experimental melts are compared with other experimental results and with natural data in Figure 10. For comparison with experimental data, we used MORB fractionation experiments (Dixon-Spulber and Rutherford, 1983; Berndt et al., 2005), Fe-Ti MORB fractionation experiments (Juster et al., 1989; Toplis and Carroll, 1995), immiscible melt compositions (Dixon and Rutherford, 1979), and gabbro, amphibolite and basalt anatexis experiments (Koepke et al., 2004, Beard and Lofgren, 1991, and Thy et al., 1999, respectively). Our experiments are relatively similar to those of Beard and Lofgren (1991), and the melt compositions are therefore similar. Nevertheless, our experiments reach lower silica contents despite lower temperature equilibration (850°C in our experiments and 900°C in the Beard and Lofgren ones). The K<sub>2</sub>O contents of our experimental melts are similar to most of the Beard and Lofgren (1991) experiments, except for one of their series that display lower contents, and which corresponds to a highly K<sub>2</sub>O depleted starting composition. Fe-Ti MORB fractionation melts and immiscible liquids are depleted in Al<sub>2</sub>O<sub>3</sub> and enriched in TiO<sub>2</sub> regarding other experiments. Interestingly, in our lower temperature experiments, the composition of the melt is below the line of saturation for TiO<sub>2</sub> in basaltic melts defined by Koepke et al. (2007) (Fig. 10). This allows us to discriminate between gabbro melting (Koepke et al., 2004) and hydrothermalized dikes melting (Beard and Lofgren, 1991, and this study) as only hydrothermalized dikes melts reach silica contents higher than 68 wt% for TiO<sub>2</sub> concentrations <0.5wt% (Fig. 10). Our experimental melts are relatively similar with those formed in MORB fractionation experiments, except for the lower temperatures (i.e., with the higher silica content), which are slightly depleted in MgO and CaO and slightly enriched in K<sub>2</sub>O (Fig. 10).

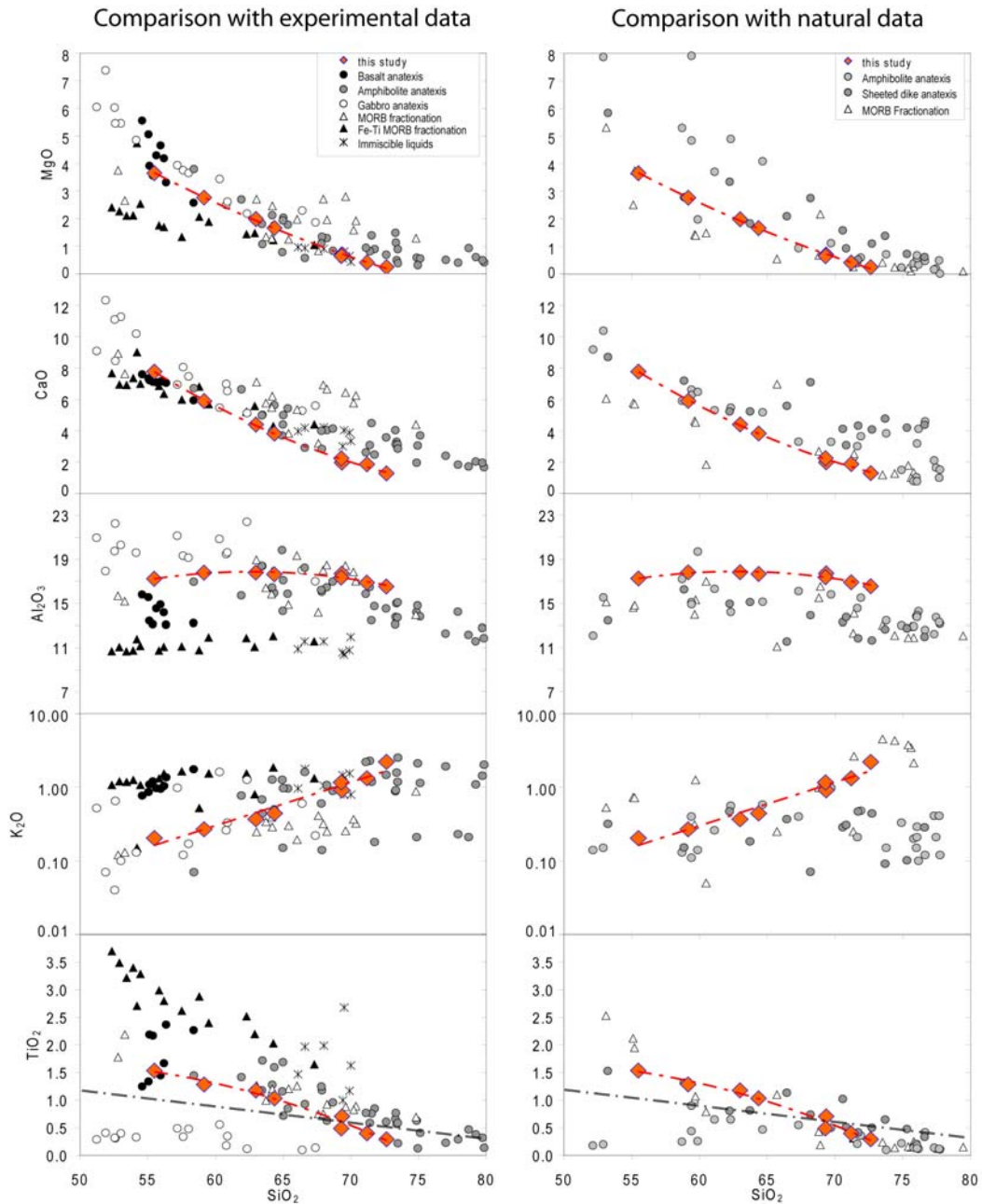


**Figure 10:** Harker diagrams (Oxide versus  $\text{SiO}_2$ ). Comparison of melts from this study with other experimental melts (left column) and with natural rocks (right column). Experimental data are from Dixon-Spulber and Rutherford (1983) and Berndt et al. (2005) for MORB fractionation experiments, from Juster et al. (1989) and Toplis and Carroll (1995) for Fe-Ti MORB fractionation experiments, from Dixon and Rutherford (1979) for immiscible liquid compositions and from Koepke et al. (2004), Beard and Lofgren (1991), and Thy et al. (1999) for gabbro, amphibolite and basalt anatexis, respectively. Natural data are from Gillis and Coogan (2002) for rocks interpreted as sheeted dikes partial melts, from Gerlach et al. (1981), Pedersen and Malpas (1984) and Flagler and Spray (1991) for rocks interpreted as amphibolite partial melts and from Beccaluva et al. (1977), Beccaluva et al. (1999) and Ghazi et al. (2004) for rocks interpreted as MORB fractionation. The dashed line corresponds to the regression line for the experimental melt compositions of this study. The dashed-dotted line in  $\text{TiO}_2$  vs.  $\text{SiO}_2$  diagrams represent the saturation of  $\text{TiO}_2$  in basaltic melts defined by Koepke et al. (2007).

#### *Chapter IV. Melting the hydrothermally altered sheeted dike complex: experimental study*

To compare our experimental results with natural data, we used published analyses of oceanic plagiogranites interpreted as sheeted dikes partial melts (Gillis & Coogan, 2002), as amphibolite partial melts (Gerlach et al., 1981; Pedersen and Malpas, 1984; Flagler and Spray, 1991), and as differentiated MORB (Beccaluva et al., 1977; Beccaluva et al., 1999; Ghazi et al., 2004). In these studies, the oceanic plagiogranite origin has been inferred from trace element concentrations and structural relationships. These natural rocks have relatively homogeneous compositions, and globally match our experimental melts. Nevertheless, the melts formed in our lower temperature experiments and oceanic plagiogranites interpreted as differentiated MORB are slightly enriched in  $K_2O$  compared to other natural oceanic plagiogranites (Fig. 10). Our experimental melts are also slightly enriched in  $Al_2O_3$  compared to all natural plagiogranites (Fig. 10).

To summarize, despite small differences, the melts produced during the experimental hydrous partial melting of hydrothermalized sheeted dike have major element compositions that are similar to other experimental works testing the partial melting of oceanic lithologies, and to natural plagiogranites interpreted as products of oceanic lithologies anatexis (Fig. 10). However, the observed major element trends are also very similar to those obtained by experiments simulating MORB fractionation and to oceanic plagiogranites interpreted as resulting from MORB fractionation (Fig. 10). Thus, whole rock major element compositions of our experimental melts cannot be used as a tool for discriminating different processes of oceanic plagiogranite genesis. Field studies and major element compositions have been combined with trace element compositions (especially rare earth elements) to better constrain their origin (e.g., Gerlach et al., 1981; Flagler and Spray, 1991; Floyd et al., 1998; Luchitskaya et al., 2005; Bonev and Stampfli, 2009; Brophy, 2008, 2009; Rollinson, 2009). At fast spreading ridges, the granoblastic dikes that are spatially associated to oceanic plagiogranites present at or close to the base of the sheeted dike complex, and as xenoliths in plagiogranites, may help to further constrain the plagiogranites origin. If these granoblastic dikes represent the residue after a hydrous partial melting event (Coogan et al., 2003; Gillis, 2008; France et al., 2009a), then their forming mineral compositions should match the ones of our experimental residual minerals.

##### ***IV.3.f.2. Evolution of the residual minerals: formation of "granoblastic dikes"***

Detailed petrological descriptions of the granoblastic dike horizon from the Oman ophiolite and from IODP Hole 1256D are given in France et al. (2009a), and Koepke et al. (2008). Gillis (2008) also describe granoblastic dikes (called hornfelsic lithologies) from Pito

Deep, Hess Deep, and the Troodos ophiolite. A typical granoblastic assemblage is composed of clinopyroxene, plagioclase and two oxides (ilmenite and magnetite to titanomagnetite). In IODP Hole 1256D, orthopyroxene is also present. This paragenesis matches well the residual mineral assemblage observed in our partial melting experiments coexisting with a plagiogranitic melt. Olivine, which is a stable residual phase in experiments performed at temperatures  $> 940^{\circ}\text{C}$ , is absent from the described natural granoblastic dikes. This implies relatively low temperatures associated to their formation.

In natural granoblastic dikes, plagioclase compositions range from  $\text{An}_{20}$  to  $\text{An}_{60}$ , and clinopyroxene is augite with  $\text{Mg\#}$  varying from 60 to 75. These compositions are similar to our experimental results, in which plagioclases vary from  $\text{An}_{26}$  to  $\text{An}_{59}$  (Fig. 8c) and clinopyroxene showing  $\text{Mg\#}$  varying from 66 to 78. Magnetite from granoblastic dikes have lower  $\text{TiO}_2$  contents than residual magnetite in our experiments, but as shown by Koepke et al., (2008), they were probably re-equilibrated at lower temperature ( $\sim 600^{\circ}\text{C}$ ) during a later, retrograde step ("second" hydrothermal alteration; see Koepke et al., 2008). In contrast, the composition of plagioclase and pyroxene obtained in MORB differentiation experiments (Berndt et al., 2005) does not match the composition of those from granoblastic assemblages. In differentiation experiments, plagioclase compositions range from  $\text{An}_{55}$  to  $\text{An}_{88}$  and clinopyroxene is mostly augites with  $\text{Mg\#}$  varying from 72 to 86.

Gillis (2008), Koepke et al. (2008), and France et al. (2009a) have shown that clinopyroxene from granoblastic dikes are particularly low in  $\text{Al}_2\text{O}_3$  and  $\text{TiO}_2$  (Fig. 11). France et al. (2009a) propose that such compositions are characteristic of granoblastic lithologies (Fig. 11a). Residual clinopyroxene in the present study displays also very low, correlated  $\text{Al}_2\text{O}_3$  and  $\text{TiO}_2$  contents that follow a trend similar to that for granoblastic dike clinopyroxene (Fig. 11b). For comparison, clinopyroxene in MORB differentiation experiments from Berndt et al. (2005) has higher  $\text{Al}_2\text{O}_3$  contents (between 3.3 and 6.8 wt% instead of 1.2 to 3 wt% in the present study). This difference may be related to the much higher temperature in differentiation experiments. The peculiar  $\text{TiO}_2$  vs.  $\text{Al}_2\text{O}_3$  trend obtained for clinopyroxene in the present study seems to be characteristic of hydrous partial melting of previously hydrothermalized basaltic lithologies, and may be linked to the low temperature conditions coupled to water saturated conditions at high oxygen fugacities in our experiments. These peculiar conditions prevail in the root zone of the sheeted dike complex. A critical parameter controlling this trend is the oxygen fugacity, which controls the stability of Fe-Ti oxides; the latter in turn controls the Ti budget for Ti partitioning between clinopyroxene and melt.

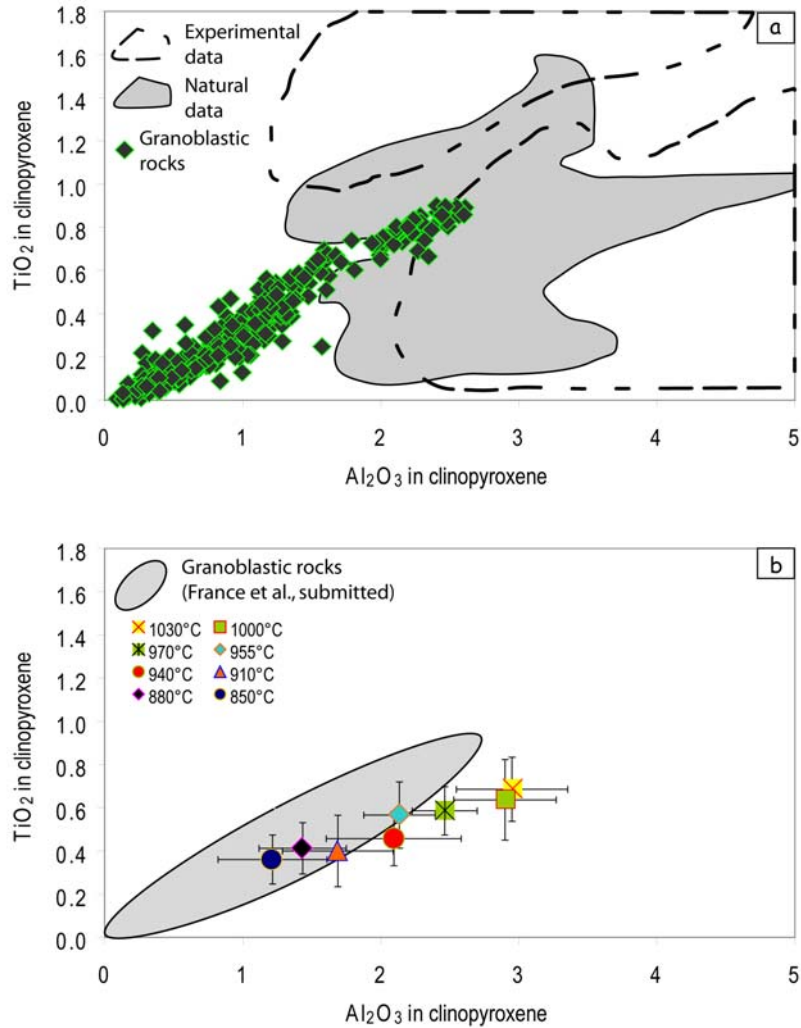


**Figure 11:** Correlation between  $\text{TiO}_2$  and  $\text{Al}_2\text{O}_3$  in clinopyroxene. **a)** Comparison between clinopyroxenes in granoblastic dikes (diamonds; compositions from France et al., 2009a) and experimental and natural data from oceanic crust lithologies; after France et al. (2009a). Experimental data (dashed field) are from Snyder et al. (1993), Toplis and Carroll (1995) and Toplis et al. (1994) for Fe-Ti MORB crystallization experiments, from Berndt et al. (2005) and Feig et al. (2006) for hydrous crystallization experiments in primitive MORB-type system; from Grove and Bryan (1983) and Kinzler and Grove (1992) for MORB crystallization experiments, and from Koepke et al. (2004) for clinopyroxenes formed during hydrous partial melting of gabbros. Natural data (grey field) for oceanic crust lithologies are from Dziony et al. (2008) for IODP Hole 1256D sheeted dikes not affected by granoblastic imprint, from Miyashita et al. (2003) and Pallister and Hopson (1981) for Oman ophiolite sheeted dikes and gabbros, and from Boudier et al. (2000) and Gerbert-Gaillard (2002) for Oman gabbro-norites. **b)** Comparison between clinopyroxenes of granoblastic rocks (dikes and xenoliths; grey field) and clinopyroxenes in the partly molten system of the present study equilibrated at different temperatures. Note that the grey field corresponds to the diamonds of a).

The experimental trend in the present study has a slightly lower slope than in natural granoblastic dikes; the correspondence between the two trends is best at low  $\text{TiO}_2$  and  $\text{Al}_2\text{O}_3$  contents of clinopyroxene (Fig. 11b). For the strongly oxidizing conditions of our



experiments, the stability field of Fe-Ti oxides is larger, and  $\text{TiO}_2$  is consequently incorporated in lesser amount into silicates, resulting in a lower  $\text{TiO}_2/\text{Al}_2\text{O}_3$  ratio for clinopyroxene. The observed difference suggests that dehydration and melting reactions at the base of the sheeted dike complex in natural settings proceed at slightly less oxidizing conditions than in our experiments, which were performed at redox conditions corresponding to an oxygen fugacity between QFM+1 and QFM+2.

Figures 11 and 12 show that  $\text{TiO}_2$  and  $\text{Al}_2\text{O}_3$  contents in clinopyroxene strongly depend on temperature. The relation between  $\text{Al}_2\text{O}_3$  and temperature can be fitted by a regression curve ( $R^2=0.98$ ) with:

$$T = 93.145 \text{ Al}_2\text{O}_3 + 742$$

Where  $T$  is temperature in  $^\circ\text{C}$  and  $\text{Al}_2\text{O}_3$  the  $\text{Al}_2\text{O}_3$  content in clinopyroxene in wt%. The result can be considered accurate with an uncertainty of  $\pm 40^\circ\text{C}$ . This thermometer seems appropriate for estimating equilibration temperatures of the granoblastic dikes and related lithologies at the base of the sheeted dike complex in the oceanic crust. Since pressure and composition also strongly influence the  $\text{Al}_2\text{O}_3$  content in clinopyroxene, the use of this thermometer is restricted to shallow pressure (100 MPa in this study).

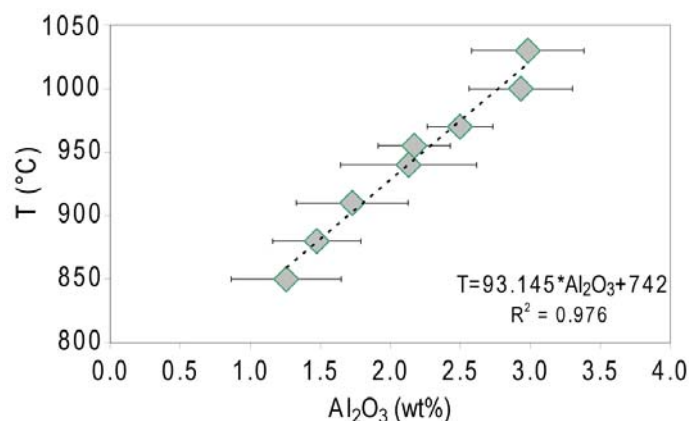


**Figure 12:**  $\text{Al}_2\text{O}_3$  content (wt%) in clinopyroxene from our experiments as a function of temperature. Standard deviations of analyses are shown. The dashed line is the linear regression with the equation  $y=93.145x+742$  ( $R^2=0.976$ ).

One interesting feature of typical granoblastic dikes is reproduced by our experiments. Granoblastic dikes usually contain clinopyroxenes with countless inclusions of tiny oxide with grain sizes from  $<1 \mu\text{m}$  to some tens of  $\mu\text{m}$  (Koepke et al., 2008; France et al., 2009a). Oxides associated to clinopyroxene have also been observed in hydrothermalized altered gabbros but in close association with amphibole (Manning and MacLeod, 1996). In granoblastic dikes, oxide represents inclusions in pure clinopyroxene, and amphibole is not

#### *Chapter IV. Melting the hydrothermally altered sheeted dike complex: experimental study*

associated to the inclusions. The oxide inclusions present in granoblastic dikes have been ascribed to the prograde evolution of secondary clinopyroxenes developing from complex alteration assemblages originating from primary clinopyroxenes which include fibrous actinolitic amphibole and extremely fine-grained (<5  $\mu\text{m}$ ) coexisting ilmenite and magnetite oxide phases (for details see Koepke et al., 2008, and France et al., 2009a). In our experiments, primary material does not contain clinopyroxene and new clinopyroxene crystallizes mostly after amphibole. However, we observe similar features, i.e., newly crystallized clinopyroxenes that contain numerous tiny oxide inclusions (Fig. 4g). The presence of these oxide inclusions can be explained by the Mg/Fe budget of the minerals involved in the reaction. Amphibole from the starting material has a lower Mg# (~61) than that of the newly crystallized clinopyroxene (e.g., 78 at 1000°C). An iron excess is therefore available during clinopyroxene crystallisation, resulting in the concentration of iron in the tiny oxides. Since our experiments were performed under highly oxidizing conditions, the stability of Fe-Ti oxides is possible.

The results of our experiments (phase relations, mineral and melt compositions, and other petrographic characteristics such as tiny oxide inclusion in clinopyroxene) support the working models in which granoblastic dikes and associated oceanic plagiogranites at the base of the sheeted dike complex at fast-spreading ridges are formed by dehydration and partial melting of previously hydrothermalized sheeted dikes. Temperatures as high as 1000°C has been recorded in the granoblastic dikes from several natural settings (Gillis, 2008; Koepke et al., 2008; France et al., 2009a), this is clearly above the hydrous solidus temperature determined in this study (~850°C), and implies that hydrous partial melting locally proceeded. Koepke et al. (2008) observed in the granoblastic dikes from IODP Hole 1256D the presence of domains of both "dry" and "hydrous" parageneses. Such "dry" domains, for which significantly higher equilibration temperatures were recorded, probably represent zones which were not, or less hydrothermalized, preventing the triggering of hydrous partial melting, since the temperature did not exceed the corresponding dry solidus. These similarities between our experimental results and the corresponding natural settings strongly support an anatectic origin of those plagiogranites that are commonly observed at the base of the sheeted dike complex and that are associated with granoblastic lithologies.

#### ***IV.3.f.3. MORB contamination at the base of the sheeted dikes***

Our experimental study supports models in which, at fast-spreading ridges, the magmatic / hydrothermal interface is a dynamic horizon with magma that can reheat

previously hydrothermalized sheeted dikes during upward migrations of the top of the melt lens. The absence of olivine in granoblastic dikes of all studied natural settings implies that the temperatures for the partial melting process did not exceed 940 °C (Figs. 5, 6), corresponding to a melt fraction  $\leq 30$  %. In our experiments, such melts are highly silicic ( $\text{SiO}_2$  of  $\geq 68.5$  %; Fig. 8). Hence, they are expected to be highly viscous (for the 850°C experimental melt, and using a theoretical water content of 5wt%,  $\eta=10^{4.4}$  Pa.s, when calculated using Giordano et al., 2008). Due to the very strong thermal gradient at the interface between the melt lens and the sheeted dikes, melt formation is restricted to a relatively narrow zone at the base of the sheeted dikes, and the amount of such silicic melts is probably relatively low. As the formed melts are of relative low temperature and highly viscous, they probably do not have the potential to erupt, and can therefore get trapped as small intrusive veins near the location of generation. Such a scenario is described in the core recovered in IODP Hole 1256D; a 20 mm-wide vein of trondhjemitic composition intrudes the granoblastic dikes at 1404 meters below sea-floor (mbsf),  $\sim$  two meters above the first appearance of gabbro marking the top of the fossil melt lens (Teagle et al., 2006). Felsic igneous rocks are also relatively abundant in the coarse-grained material recovered in junk baskets during hole clearing operations at 1373 mbsf (Teagle et al., 2006). These leucocratic rock fragments, which consist of plagioclase, quartz, and altered green hornblende, are probably derived from leucocratic intrusions that were not recovered in the core. These felsic lithologies most likely represent products of hydrous partial melting of previously hydrothermalized sheeted dikes. As hydrous partial melting is believed to occur during upward migrations of the melt lens, the newly formed, highly viscous, silica-rich melt can also be assimilated into the MORB melt within the melt lens. This melt is transitional between tholeiitic and calc-alkaline (Fig. 9) and represents a source of contamination for primary tholeiitic MORB. It will in particular increase the  $\text{SiO}_2$  content of the MORB melt, but also the amount of  $\text{K}_2\text{O}$ , rare earth elements and chlorine. This assimilation process may be responsible for the formation of andesitic extrusives which are locally observed in recent oceanic crust (e.g., Haase et al., 2005) and for the chlorine contamination of MORB (e.g., Michael and Schilling, 1989). On the other hand, the residual phases of the hydrous partial melting reaction behave rather refractory, resulting in the occurrence of residual enclaves in the corresponding melts, which display granulite facies granoblastic parageneses consisting of clinopyroxene + plagioclase + Fe-Ti oxides  $\pm$  orthopyroxene. These enclaves are described in IODP Hole 1256D (Teagle et al., 2006; Koepke et al., 2008; France et al., 2009a), at Pito Deep and Hess Deep (Gillis, 2008), and in the Troodos and Oman ophiolites (Gillis, 2008;

## *Chapter IV. Melting the hydrothermally altered sheeted dike complex: experimental study*

Nicolas et al., 2009; France et al., 2009a). All of these geological settings are portions of present-day or fossil mid-ocean ridges where a dynamic dike / gabbro transition has been proposed.

### **IV.3.g. Conclusion**

Partial melting experiments of a sample of the hydrothermalized sheeted dike complex from the Oman ophiolite have been performed to test the origin of oceanic plagiogranites present at the base of the sheeted dike complex at fast spreading centers. These oceanic plagiogranites are associated to granoblastic lithologies that form the base of the sheeted dike complex and xenoliths in plagiogranites and gabbros. Our experimental results show that:

- Melts produced during partial melting of hydrothermalized sheeted dikes are highly silicic (up to 72.6 wt%) and match the composition of oceanic plagiogranites.
- The residue of the partial melting experiments matches the modal and peculiar chemical compositions of granoblastic lithologies. Granoblastic lithologies are therefore interpreted to represent the residue after the partial melting event that produce the oceanic plagiogranites.
- The heat source necessary to trigger the partial melting event is believed to be provided by the underlying melt lens. This study therefore supports a model in which the sheeted dike complex / gabbro transition is a dynamic horizon that migrates vertically, with the potential to locally reheat the base of the sheeted dike complex during upward movements.
- Partial melting of hydrothermalized sheeted dikes, and partial assimilation of newly formed melts in the axial melt lens are potential candidates for the contamination (e.g., the chlorine enrichment) observed in some MORB.

### ***IV.4. Mineral recrystallization during experiments: a preliminary study***

In France et al. (2010a), we have studied the evolution of mineral mode, and mineral and melt compositions with increasing temperature. The evolution of mineral shapes, fabrics and associations can also bring information on the recrystallization processes, and on incongruent reactions. Using the electron back-scattered diffraction (EBSD) technique, I present hereafter a preliminary study of the mineral orientations in the experimental results, and compare these results to natural samples.

EBSD measurements are performed using a CamScan X500FE “crystal probe” at the Geosciences Montpellier laboratory. For each measurement point, EBSD result is a diffraction diagram displaying Kikuchi bands that are characteristic of one crystal orientation for one given mineral. A software (Channel 5, HKL technology) is then used to convert Kikuchi bands to crystallographic orientation maps (e.g., Figure IV-5) and pole figures. EBSD results can be used to build modal maps (Figure IV-5a) and crystal orientation maps (Figure IV-5b-d).

France et al. (2010a) show that in experimental results, assemblages (100-250  $\mu\text{m}$  large) of several small grains ( $\sim 10 \mu\text{m}$ ) mimic starting material mineral shapes. For example, clinopyroxene assemblages mimic previous large actinolite assemblages (e.g., Figure 4b-d in section IV.3.e.1, and Figure IV-5a herein), and newly formed plagioclase assemblages mimic previous large albite grains. Nevertheless, clinopyroxenes crystallized after actinolite aggregates formed of millions of fine needles that are either parallel or randomly oriented, and it is therefore expected that in a single clinopyroxene assemblage, the small apparently individual newly formed grains have different crystal orientations.

For this preliminary study, I have mapped the crystallographic orientations of a portion of the 970°C experimental product (with water added). At this temperature all minerals are newly formed and no relic of starting material is observed. Crystal orientation maps show that clinopyroxene assemblages are composed of small grains that have uniform crystal orientation in a single assemblage (Figure IV-5). This suggests that each “assemblage” represent one single, sponge-like grain with coherent orientation, rather than an aggregate of small, individual, randomly orientated grains. In plagioclase assemblages, small grains mostly show uniform crystal orientation, and some are organized along narrow sub-parallel bands with coherent crystal orientation in an individual band (Figure IV-5b). The observed structures imply that crystallization was not a random process starting from individually orientated nuclei in the melt, as it would be expected for typical crystallization experiments using a homogeneous glass as starting material. Here, it is indicated that the characteristic properties of the starting material (hydrothermally altered dolerite) with its characteristic textural and structural mineral features represent special precursor leading to the observed crystal orientation in plagioclase and clinopyroxene aggregates. Olivine grains have grown from the melt through the melting reactions, and display random crystallographic orientations.

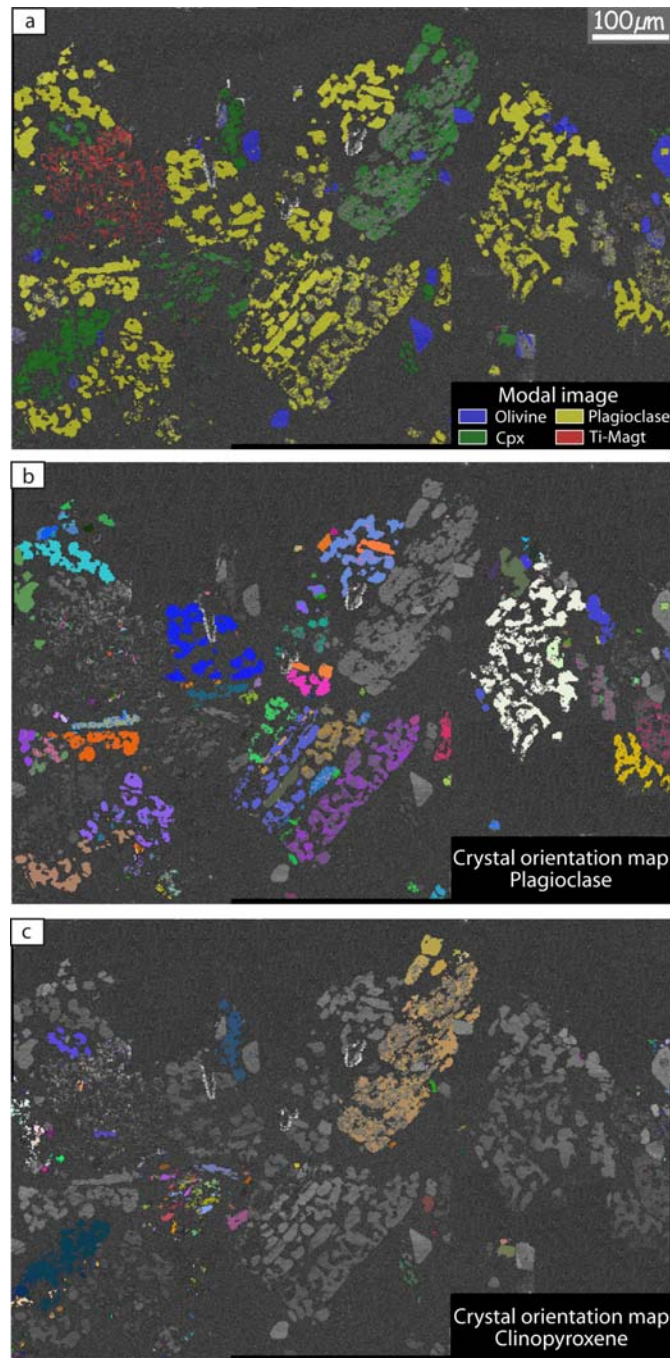
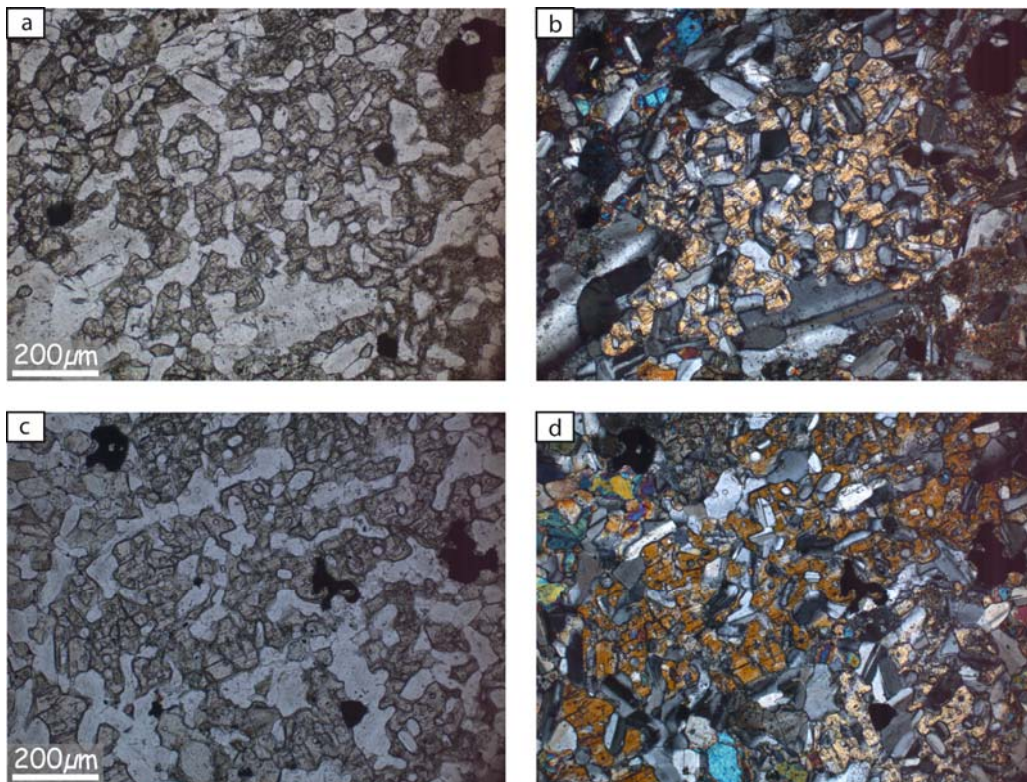


Figure IV-5: EBSD maps; in b) and c) the color is a function of crystal orientation generated using the “all euler” function in HKL software. a) modal map; b) plagioclase crystals orientations, the grain in the central bottom part is composed of narrow sub-parallel bands that display uniform crystal orientation in a single band, other grain assemblages as the white one, have uniform crystal orientation; c) clinopyroxene crystals orientations, the grain assemblages have uniform crystal orientations.

The observed orientation effect in the experiments can be related to the drilled natural rocks from the EPR: In strongly recrystallized microgabbro xenoliths present in the isotropic gabbro horizon of IODP Hole 1256D, and described by France et al. (2009a), clinopyroxenes showing a characteristic poikilitic to poikiloblastic feature, are locally

observed (Figure IV-6), suggesting that recrystallization processes are similar in nature and experiments. In natural recrystallized samples similar poikiloblastic plagioclases are not observed. However, clinopyroxene and orthopyroxene inclusions are observed in some plagioclase grains (Figure IV-7). These inclusions are localized in a given plagioclase grain, along domains that display different optical properties and different chemical compositions (lower An content) than the main plagioclase grain, attesting to distinct plagioclase generations (Figure IV-7). The occurrence of such inclusions is not well understood but may attest to former poikilitic plagioclases similar to the ones observed in experimental results. These poikilitic plagioclases would have then recrystallized in the presence of melt. This process would result in the occurrence of the second generation of plagioclase associated to pyroxenes inclusions.



*Figure IV-6: Sponge-like clinopyroxenes in xenolith with granoblastic features in zone 6 gabbros from the bottom of IODP Hole 1256D (see Chapter II, sample 232R-2\_37-41). The two domains (a-b and c-d) display sponge-like poikiloblastic clinopyroxene grains containing plagioclase inclusions. These textures are similar to those observed in experimental results (Figure IV-5). Note that both clinopyroxenes show homogeneous interference colors implying that these represent single crystals with a sponge-like structure. a and c: plane-polarized light microphotographs, b and d: cross-polarized light microphotographs.*

To summarize, EBSD measurements in the experimental products can help to explain specific structures observed in the natural rocks from the dike / gabbro transition, as steps of

*Chapter IV. Melting the hydrothermally altered sheeted dike complex: experimental study*

complex crystallization events using specific components of granoblastic lithologies as precursors (e.g., clinopyroxenes with poikiloblastic features). They also show that, despite a randomly orientated starting material, newly formed minerals in a given assemblage can show a unique crystallographic orientation, suggesting that they form one single grain. The detailed processes occurring during recrystallization and their evolution with temperature are not well understood and further studies are needed. A systematic EBSD survey using products of experiments performed at different temperatures (from 750°C to 1030°C in a subsolidus and partly molten regime) by France et al. (2010a) would help to shed light on the details and mechanisms of the recrystallization processes occurring during the melting of hydrothermally altered dikes.

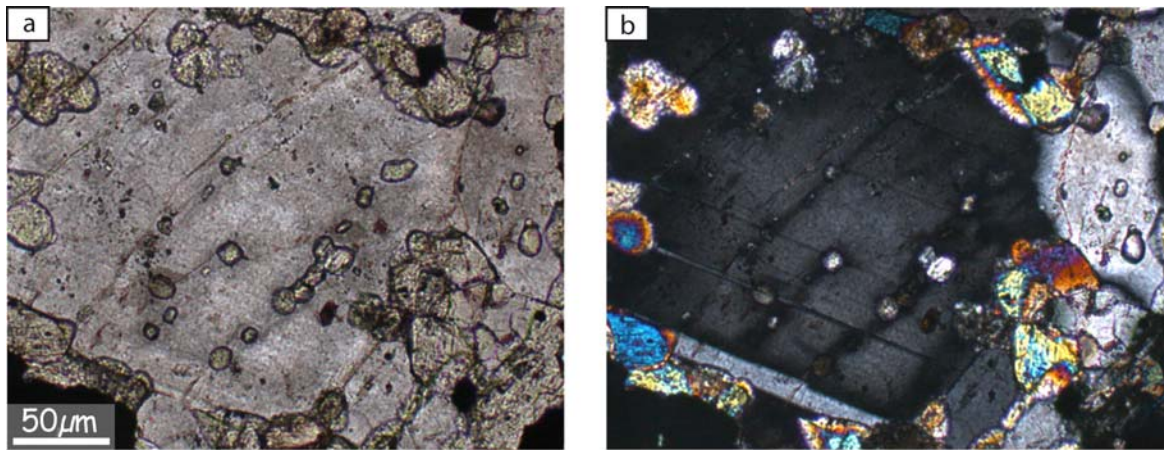


*Figure IV-7: Plane- (a) and cross- (b) polarized light microphotographs of a plagioclase grain containing clinopyroxene and orthopyroxene inclusions (IODP Hole 1256D, sample 233R-1\_8-12).*



#### ***IV.5. Melting the hydrothermally altered sheeted dike complex: an experimental / trace elements study***

Preliminary version of an article that will be submitted to *Geology*.

**Lydéric France<sup>1,2</sup>, Benoit Ildefonse<sup>1</sup>, Juergen Koepke<sup>2</sup>, Chris J. MacLeod<sup>3</sup>, Marguerite Godard<sup>1</sup>**

1: Géosciences Montpellier, CNRS, Université Montpellier 2, CC60, F-34095 Montpellier Cedex 05, France

2: Institut für Mineralogie, Leibniz Universität Hannover, Callinstrasse 3, D-30167 Hannover, Germany

3: School of Earth, Ocean and Planetary Sciences, Cardiff University, Main Building, Park Place, Cardiff CF10 3YE, UK

##### **IV.5.a. Abstract**

Oceanic plagiogranites are ubiquitously sampled in oceanic crust. At fast spreading ridges, they are preferentially located close to the gabbro / sheeted dike transition. The origin of oceanic plagiogranites is still debated; the favored formation processes are late-stage fractionation of tholeiitic melt, and hydrous partial melting of mafic rocks. Experimental studies have shown that major element compositions alone are not sufficient to discriminate between these two processes. Geochemical modeling is needed, but because melting and crystallization are complex processes, models need experimental verifications. Here we present the first in-situ trace element measurements of partial melts generated in partial melting experiments of hydrothermally altered sheeted dikes. The experiments were performed at those conditions prevailing at the base of the sheeted dike complex overlying active axial magma chambers. We also present for comparison trace element analyses of natural samples from the Oman ophiolite. An anatectic origin for the oceanic plagiogranites that are observed close to the root of the sheeted dike complex is supported by similar trace element patterns of experimental and natural melts. Experiment residue have the same composition as the so-called "granoblastic microgabbro dikes" sampled at the base of the sheeted dike complex, which is consistent with their interpretation as reheated and partially molten hydrothermally altered dikes. These results finally support a model in which the top of the melt lens representing the interface between magmatic and hydrothermal system is a dynamic horizon that can migrates vertically and interact with the overlying sheeted dikes. Our results imply that anatectic plagiogranitic melt formed during upward melt lens migrations represent the main crustal contaminant for the MORB-type melts filling the melt lens. The trace element compositions of anatectic silicic melts presented in this study is therefore of major importance to understand and simulate real MORB compositions under fast-spreading ridges.

**Key words:** *oceanic plagiogranites, fast spreading mid-ocean ridge, hydrous partial melting, trace element, experimental petrology, granoblastic dikes.*

#### **IV.5.b. Introduction**

Oceanic crust commonly contains relatively small intrusions of leucocratic, evolved material generally called oceanic plagiogranites (e.g., Koepke et al., 2004, 2007). These are most commonly believed to be generated either by differentiation of MORB melts (e.g., Coleman and Peterman, 1975; Pallister and Knight, 1981; Bonev and Stampfli, 2009), or by hydrous partial melting of mafic rocks (e.g., Pedersen and Malpas, 1984; Amri et al., 1996; Koepke et al., 2004). At slow spreading ridges, hydrous partial melting of mafic rocks is commonly described associated to shear zones that allow hydrothermal influx (e.g., Flagler and Spray, 1991; Koepke et al., 2007). In oceanic crust formed at fast spreading centers away from ridge segmentation and tectonic discontinuities, the origin of oceanic plagiogranites, commonly present at the base of the sheeted dike complex (SDC; Fig. 1a) remains debated. In these zones, the thermal regime and the magma supply are believed to remain stable over periods of tens of thousand of years (Pollock et al., 2009) preventing differentiation; only gaps in the magma supply would result in strongly differentiated igneous rocks. Large shear-zones in fast-spread crust are spatially associated to ridge segmentation zones (Nicolas et al., 2000; Nicolas and Boudier, 2008), and cannot provide hydrous fluids, with the potential to trigger hydrous partial melting, away from these zones. In segment centers, away from discontinuities, only the hydrothermal convecting system has the potential to bring fluids close to the magma chamber (Manning et al., 1996). Nicolas et al. (2008) propose that the intrusion of hydrothermal fluids in the recently crystallized, still hot, root zone of the SDC can trigger hydrous partial melting without any reheating event. Gillis and Coogan (2002), Coogan et al. (2003) and France et al. (2009a) propose that the melt lens underneath the SDC is a dynamic horizon that migrates vertically, with the potential of locally triggering hydrous partial melting in the reheated base of the hydrothermally altered SDC. In this dynamic model, the new melts formed during upward migrations of the melt lens can subsequently be incorporated into the melt lens, thus providing a source of contamination of MORB melts (e.g., Haase et al. 2005).



*Figure 1: a) Outcrop in the Aswad area of the Oman ophiolite (coordinates: 23°07'23N 58°12'06E) showing oceanic plagiogranites (felsic rocks) at the base of the sheeted dike complex (dark rocks). The microgabbro xenoliths and the sheeted dike complex base are recrystallized to granoblastic textures.*

Discriminating between fractionation and hydrous partial melting is not trivial and both processes may operate jointly in modern ocean crust (e.g., Brophy, 2008, 2009). Experimental studies have shown that major element compositions of oceanic plagiogranites are similar for the two processes (e.g., Koepke et al., 2004; France et al., 2010a). Several authors have proposed to model the trace element evolution of melts during both MORB fractionation and hydrous partial melting in order to reproduce natural trace element trends (e.g., Gerlach et al., 1981; Pedersen and Malpas, 1984; Flagler and Spray, 1995; Floyd et al., 1995; Luchitskaya et al., 2005; Bonev and Stampfli, 2009). One weakness of these models is that hydrous partial melting of hydrothermally altered lithologies results in the simultaneous destabilization and stabilization of different mineral phases (incongruent melting), which complicate the models. However, the modal evolution is known from some relevant experimental studies (e.g., Beard and Lofgren; 1991, Berndt et al., 2005; France et al., 2010a) and can be used to improve the models (e.g., Haase et al., 2005; Brophy, 2008). Direct measurement of trace elements in experimental products matching the base of the SDC conditions is lacking for crystallization experiments simulating crystal fractionation, and only Fisk et al. (1995) have analyzed trace element contents of melt formed during partial melting experiments. However, these experiments were performed at one atmosphere and under dry conditions, thus, at conditions which are not relevant to those anatexis processes ongoing at the base of the hydrothermally altered SDC. In order to shed light on the origin of oceanic plagiogranites at the base of the SDC, to provide new constraints for the associated modeling, and to constrain the composition of the main crustal MORB contaminant, we have analyzed

for the first time the trace element contents of melts formed by the experimental melting of hydrothermally altered sheeted dikes from experiments performed by France et al. (2010a). These results are compared to natural samples from the Oman ophiolite, which is the best analogue for a fast-spreading ridge on land.

#### **IV.5.c. Experimental and analytical techniques**

Hydrous partial melting experiments have been performed using a representative sample of hydrothermally altered SDC from the Oman ophiolite as starting material (08OL30, details on experiments and starting material in France et al., 2010a). After crushing, two fractions (100-150 $\mu$ m and 150-250 $\mu$ m) have been used in a preliminary experiment to control the effect of grain size on the experimental results; the 150-250 $\mu$ m fraction has been used as it allowed us to obtain larger melt pools. Conditions were selected to match those prevailing at the base of the SDC; pressure was 100MPa, oxygen fugacity corresponded to FMQ+1.2 to +1.6 (where FMQ is the fayalite-magnetite-quartz oxygen buffer equilibrium) and temperature ranged from 850 to 1030°C. Two capsules containing 50mg of rock powder were run simultaneously at each temperature, one of them containing 5mg of additional distilled water.

Major elements were measured using a Cameca SX 100 electron microprobe (Institut für Mineralogie, Hannover, Germany) and trace elements in experimental melts using a Cameca IMS4f ion probe (Géosciences Montpellier, France). Natural sample trace element contents have been measured using an ICP-MS (Department of Earth Sciences, Cardiff, UK). Details on analytical methods can be found in the Data Repository DR1. Analytical results can be found in the Data Repository DR2 and DR3.

#### **IV.5.d. Trace element contents**

The chondrite normalized rare earth element (REE) concentrations of the starting material show convex shape from the light REE to the middle REE, a slight Eu positive anomaly and slightly decreasing values from the middle REE to the heavy REE (Fig. 2a).

Trace element contents of the experimental melts have been measured for experimental runs from 1030°C to 955°C (Figs. 2a and 2d). At lower temperatures (i.e., higher silica content and lower degree of partial melting) melt-pools are too small (<20 $\mu$ m) to be analyzed. REE and other trace elements continuously evolve with temperature. For

example, light REE continuously increase, to more than 30 times the chondrite, by progressively decreasing the temperature to 955°C (Fig. 2a).

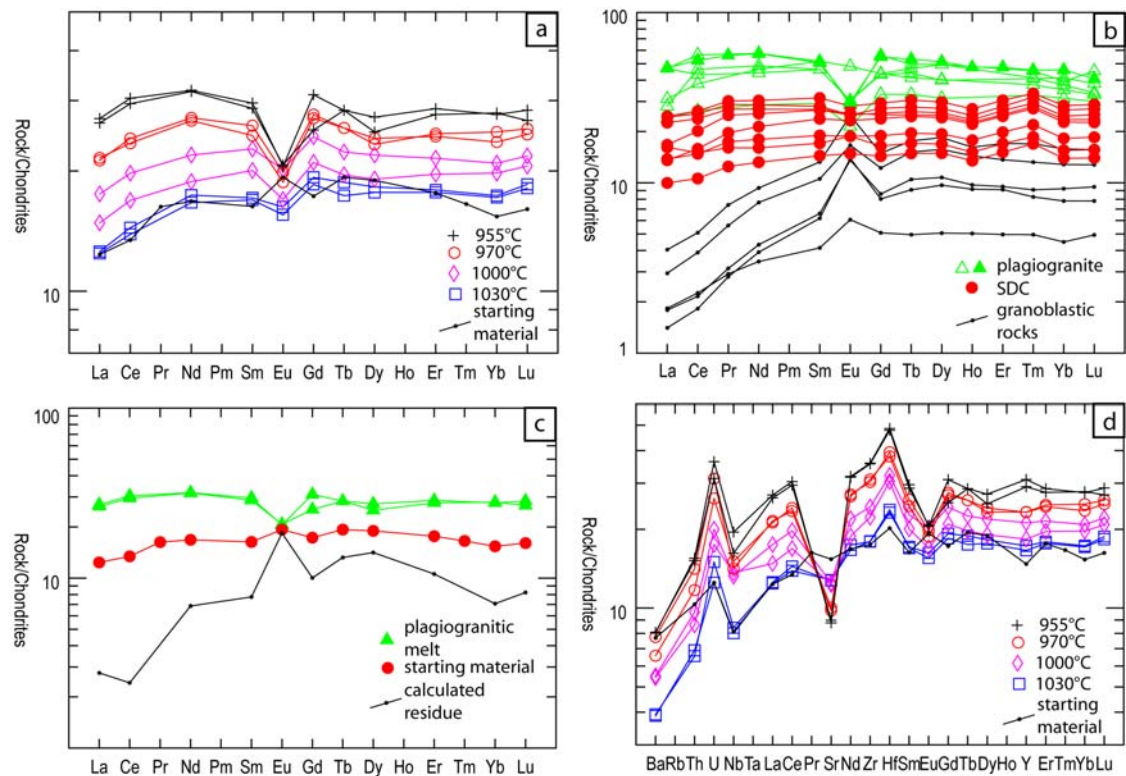


**Figure 2:** Chondrite normalized REE and trace elements contents (normalization after Anders and Grevesse, 1989). a) Experimental melts: black crosses: 955°C (40% of melt); red circles: 970°C (50% of melt); pink diamonds: 1000°C (70% of melt); blue boxes: 1030°C (93% of melt), and starting material (08OL30): black dots. b): Oman samples: green triangles: oceanic plagiogranites (this study + Pallister and Knight, 1981); red circles: sheeted dike complex; black dots: granoblastic microgabbro dikes and xenoliths. c) Green triangles: newly formed plagiogranitic melt (955°C); red circles: starting material (highly hydrothermally altered sheeted dike); black dots: calculated residue (with a melt proportion of 40% estimated by France et al., 2010a from experiments). d) Trace element concentrations of experimental melts and starting material (08OL30); same symbols as a).

Experiments performed to test the grain size effect (France et al., 2010a) show that concentrations are slightly higher when using the coarser grain size. Nevertheless, trace element concentrations are similar and fractionations of REE are of the same order (e.g.,  $(La/Sm)_N=1.18$  in the finer grained experiment and 1.23 in the coarser one). The small differences in concentration may be linked to a slight difference in the mode of the starting material probably related to a sieving artifact. For each temperature, experiments containing only the starting material and those containing additional water have similar REE and other trace element contents. Light REE normalized concentrations (Fig. 2a) show convex shapes from La to Sm with a depletion of the lighter elements. A negative europium anomaly is

observed, which increases with decreasing temperature. From Gd to Lu, spectrums are mostly flat or slightly decrease (Fig. 2a). Normalized trace element contents (Fig. 2d) show U, and Zr-Hf positive anomalies, low Ba and Th values and a Sr negative anomaly; these anomalies are more pronounced when temperature decreases. V also strongly decreases with temperature. Ti/V ratio increases from ~20 at 1030°C to more than 50 at 955°C.

Natural samples from the SDC / gabbro transition of the Oman ophiolite (Wadi Abyad; for map and details on the locality see MacLeod and Yaouancq, 2000) show interesting similarities with our experimental results (Fig. 2b). Sheeted dike complex samples display nearly flat REE spectrums with normalized concentrations ranging from 10 to 30 times the chondrite. Plagiogranites are enriched in REE compared to the SDC; chondrite normalized spectrums show a convex shape from La to Sm and a negative Eu anomaly. Normalized contents slightly decrease from Gd to Lu. Enrichments reach 50 times the chondrite. The granoblastic microgabbro dikes, intruded by gabbros at the base of the SDC and the associated granoblastic microgabbro xenoliths present in the isotropic gabbros are largely depleted in light REE, display a positive Eu anomaly, and show slightly decreasing contents from middle REE to heavy REE (Fig. 2b).

#### **IV.5.e. Discussion**

France et al. (2010a) have shown that in the corresponding sheeted dike melting experiments, that the modal content of plagioclase increases with decreasing temperature. This is the rationale for the low  $Ba_N$  contents and the negative Eu, and Sr anomalies present in the partial melts, since these elements are strongly incorporated in plagioclase. In experimental melts Sr shows a compatible behavior, whereas Eu is slightly incompatible. The incompatible behavior of Eu probably reflects the highly oxidizing conditions prevailing during the experimental runs, as the oxidized species ( $Eu^{3+}$ ) is more incompatible in a plagioclase / melt system, than the reduced one ( $Eu^{2+}$ ; Wilke and Behrens, 1999). The evolution of Ti/V ratio in natural compositions is classically used to determine the tectonic settings of ophiolitic rocks (Shervais, 1982). However, the presence of titanomagnetite in experimental results (France et al., 2010a) and the large increase of the Ti/V ratio in the experimental melts (from 20 to more than 50) with decreasing temperature clearly attests to the incorporation of V in titanomagnetite ( $D_V^{TiMgt-melt} \gg 1$ ), and prevents the use of the Ti/V ratio as a discrimination tool. As experimental conditions (pressure, temperature, redox

conditions and composition) closely match those external parameter controlling the natural process, the discriminating use of such a ratio should be carefully evaluated.

Experimental melts formed during partial melting of hydrothermally altered dikes reproduce the REE contents of most of the analyzed Oman plagiogranites samples (Fig. 2a-b). However, some natural plagiogranites show REE concentrations which are notably higher than those of the experimental runs (Fig. 2b). Figure 2a shows that the REE content of experimental melts increase by decreasing the temperature (from 1030 to 955°C). It is therefore to expect that in those runs performed at lower temperature, where the melt pools are too small to be analyzed by SIMS, the REE contents continuously increase, probably matching values of those natural plagiogranites with higher REE contents. Pallister and Knight (1981) have shown that the REE contents of Oman plagiogranites (Fig. 2c) can also be reproduced by MORB fractionation modeling. Thus, the mineral associations left back after melt extraction for both processes (incongruent mineral assemblage or residue for partial melting and fractionated cumulate minerals for fractional crystallization) may have similar REE compositions, but correspond to distinct lithologies. The residue of partial melting of the base of the SDC would be represented by the recrystallized base of the SDC, and by the associated granoblastic microgabbro xenoliths observed in underlying gabbros. The cumulate after the fractionation of a basaltic melt within the melt lens would be represented by plutonic rocks as gabbros, troctolites or werhlites. France et al. (2009a, 2010a) have shown that the granoblastic microgabbro dikes and xenoliths represent reheated parts of the SDC that may have suffered hydrous partial melting. To test this hypothesis, we have calculated the trace element composition of the residue present in our experiments, using the relation:

$$[concentration]_{starting\ material} = x [concentration]_{melt} + (1-x) [concentration]_{residue},$$

with  $x$  the melt fraction. The melt fraction present in our experiments has been determined by France et al. (2010a) via least square calculations using major element compositions of the starting material (corresponding to the composition of the system), the melt, and the residual minerals (93% of melt at 1030°C; 70% at 1000°C; 50% at 970°C and 40% at 955°C). Since the starting material and the melt compositions are known, the composition of the residue in equilibrium with the plagiogranitic melt can be calculated (Fig. 2c). Experimental melts have been analyzed in experiments performed between 1030°C and 955°C; as the melt formed at the lower temperature is the closest of plagiogranitic compositions, this experiment is used to calculate the residue composition. The calculated residue REE pattern is largely depleted in light REE, displays a positive Eu anomaly and has a convex shape from the middle REE to

the heavy REE, thus matching the corresponding patterns of natural granoblastic dikes and xenoliths from the Oman ophiolite (Fig. 2b), implying a residual origin for these rocks.

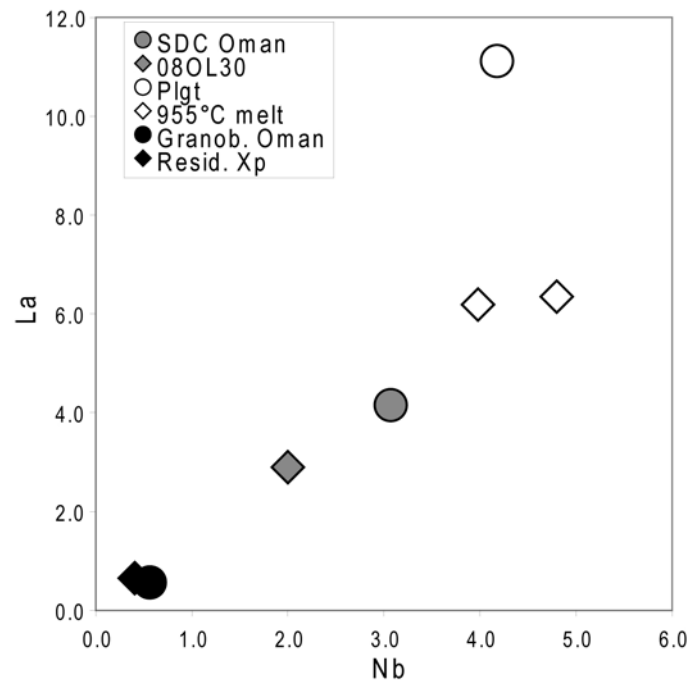


Figure 3: *La vs. Nb* plot ruling out a pure dehydration origin for granoblastic dikes and xenoliths: average of Oman ophiolite sheeted dike (SDC Oman); starting material from the Oman ophiolite (08OL30); Oman ophiolite plagiogranites (Plgt); experimental melts formed at 955°C (955°C melt); average of Oman ophiolite granoblastic microgabbro dikes and xenoliths (Granob. Oman); calculated residue in equilibrium with the experimental plagiogranitic melt formed at 955°C (Resid. Xp). During pure dehydration, Nb is not mobilized by fluids and its concentration in the dehydrated rock should be similar to the concentration in the altered SDC. La can be mobilized by fluids and would be depleted in the dehydrated rock. During partial melting, both La and Th are incompatible elements and are enriched in the newly formed melt and depleted in the residue.

Alternatively, the granoblastic lithologies may represent previously hydrothermally altered lithologies that have been reheated very slowly allowing dehydration without any partial melting. Figure 3 compares the evolution of incompatible elements that have different behavior during hydrous fluid percolation; La has a mobile behavior when Nb is an immobile element. In comparison to the sheeted dike average composition, the granoblastic microgabbro dikes and xenoliths are depleted in both La and Nb, whereas oceanic plagiogranites are enriched (Fig. 3). Similar observation can be done with experimental results (Fig. 3). In the case of an origin through SDC dehydration, the granoblastic microgabbro dikes would have Nb contents similar to the SDC ones. Figure 3 clearly attests of the incompatible behavior of La and Nb during partial melting process and rules out a pure dehydration origin. The composition similarities between experimental melts and oceanic



plagiogranites, between the experimental residue and granoblastic microgabbros and the close association of plagiogranitic rocks with granoblastic microgabbros in natural settings clearly attest of the anatectic origin of oceanic plagiogranites present at the sheeted dike gabbro transition. Granoblastic microgabbro dikes and xenoliths are therefore interpreted as residue of partial melting of previously hydrothermally altered dikes.

The anatectic origin of oceanic plagiogranites present at the base of the SDC, and the prograde origin of granoblastic microgabbros support recent models proposing that the upper melt lens imaged at the base of the SDC of fast spreading centers is a dynamic horizon (e.g., Gillis and Coogan, 2002; Coogan et al., 2003; Koepke et al., 2008; France et al., 2009a). Upward migrations of this melt lens should therefore be responsible for the reheating stage triggering partial melting of the previously hydrothermally altered SDC base. During the melt lens upward migrations, the formed plagiogranitic liquid can be mixed into the melt lens and contribute to MORB composition. Melt lens migrations are inferred from several oceanic settings as the EPR (e.g., Hooft et al., 1997; Koepke et al., 2008; France et al., 2009a), the Troodos ophiolite (e.g., Gillis and Coogan, 2002), and the Oman ophiolite (e.g., Gillis, 2008; France et al., 2009a), and 20% of the oceanic crust are considered to go through a cycle of crystallization, alteration, and then assimilation (Coogan et al., 2003). The melt formed during melting of hydrothermally altered dikes is hence the main contaminant component at the melt lens level, and the knowledge of its composition determined herein is therefore of major interest.

#### **IV.5.f. DR 1: Analytical methods:**

Experimental results were analyzed using a Cameca SX100 electron microprobe (Institut für Mineralogie, Hannover) equipped with 5 spectrometers, “Peak sight” software is used. All analyses were performed using a 15kV acceleration potential, a static (fixed) beam,  $K\alpha$  emission from all elements. The matrix correction is based on Pouchou and Pichoir (1991). Analyses of glass were performed with a beam current which was set to 6nA to minimize migration and volatilization of the alkali elements. Counting time was from 2 to 5 s for Na and K and from 5 to 10 for other elements (Si, Ti, Al, Mg, Fe, Ca, Mn, Cr). In the experiments where melt pools are large enough, the beam was defocused to a spot size of 5 to 20 $\mu$ m. Backscattered electron (BSE) images were also obtained on the Cameca SX100 electron microprobe.

Trace element analyses on experimental results were carried out at the Géosciences Montpellier lab (Montpellier, France) using a Cameca IMS4f ion probe. Polished sections of the experimental results were carbon-coated. We used a 15 kV accelerating voltage of  $O^-$  primary beam with a 10 nA intensity. To reduce mass interference by molecular ion species, the energy filtering method was used where secondary ions were subjected a 4500 V accelerating voltage with a -80 V offset with  $\pm 30$  eV energy window (Shimizu and Hart, 1982). A mass resolving power of 500, and a projected beam size between 20 and 30  $\mu$ m were used. Each analysis consists of 10 cycles starting from 25.7 mass (used as background and for magnet adjustment), then  $^{30}\text{Si}$  (2 s),  $^{45}\text{Sc}$  (2 s),  $^{47}\text{Ti}$  (2 s),  $^{51}\text{V}$  (2 s),  $^{88}\text{Sr}$  (2 s),  $^{89}\text{Y}$  (2 s),  $^{90}\text{Zr}$  (2 s),  $^{93}\text{Nb}$  (10 s),  $^{137}\text{Ba}$  (10 s),  $^{180}\text{Hf}$  (20 s),  $^{232}\text{Th}$  (30 s),  $^{238}\text{U}$  (30 s) and almost all the rare earth isotopes (10 s) (counting time in bracket). The counting time is 30 s for Eu and 20 s for Lu. The data were corrected for oxide interferences (e.g., Fahey et al., 1987). Concentrations recalculated using  $^{30}\text{Si}$  as the reference mass showed no systematic offset induced by the choice of the reference element. The calibration factor was determined from the measurement of NIST 610 (Reed, 1992; Pearce et al., 1997) at the beginning and the end of each analytical session. Typical error on the samples (1 sigma error of mean:  $s/pn$ ,  $n$  = number of cycles) is less than 15% for all trace elements, except for Tb, Er, Lu, Hf (<17.5%), Th (23%) and U (32%). Signal stability was also carefully monitored for every analysis.

Trace element contents of Oman samples have been performed at the Department of Earth Sciences at the Cardiff University by using an ICP-MS.

#### IV.5.g. DR 2: Major element compositions

Sample	Phase	SiO <sub>2</sub>	Al <sub>2</sub> O <sub>3</sub>	TiO <sub>2</sub>	CaO	Na <sub>2</sub> O	K <sub>2</sub> O	MnO	MgO	FeO	Cr <sub>2</sub> O <sub>3</sub>	NiO	P <sub>2</sub> O <sub>5</sub>	Total	n	Mg#
08OL30	whole rock	53.55	15.98	1.48	7.64	4.72	0.20	0.07	5.30	9.84	-	-	0.12	98.90	1	49.0
1030	melt_recalc.	55.48	17.25	1.54	7.77	5.09	0.20	0.05	3.66	8.94	0.00	0.00	0.00	100.00	58	42.2
1000	melt_recalc.	59.16	17.80	1.29	5.90	5.98	0.27	0.07	2.77	6.76	0.00	0.00	0.00	100.00	33	42.2
970	melt_recalc.	62.99	17.81	1.18	4.40	5.85	0.37	0.05	1.99	5.29	0.00	0.00	0.09	100.00	38	40.2
955	melt_recalc.	64.36	17.66	1.03	3.83	5.76	0.44	0.04	1.67	4.99	0.02	0.00	0.11	100.00	22	37.3
940	melt_recalc.	69.34	17.72	0.71	1.98	5.66	0.91	0.02	0.71	2.70	0.08	-	0.13	100.00	35	28.0
910	melt_recalc.	69.29	17.35	0.49	2.25	5.46	1.16	0.02	0.65	2.93	0.13	0.00	0.06	100.00	27	28.5
880	melt_recalc.	71.19	16.90	0.40	1.88	5.56	1.32	0.02	0.42	2.01	0.06	0.00	0.04	100.00	27	27.0
850	melt_recalc.	72.63	16.54	0.29	1.30	4.92	2.21	0.00	0.25	1.62	0.08	0.00	0.02	100.00	12	22.0

The sample name is 08OL30 for the starting material; for experiments, it corresponds to the experimental temperature (in °C); “melt\_recalc.”: melt composition recalculated at 100%; n: number of analyses; Mg#=Mg/[Mg+Fe] in molar proportions.

#### IV.5.h. DR 3: Trace element compositions

These are presented in Appendix B3.

### IV.6. Conclusion

The experimental study and associated geochemical investigations presented in this chapter, coupled with the field and petrological studies presented in Chapter III, support the interpretation of oceanic plagiogranites that are present close to the base of the sheeted dike complex at fast spreading ridges, as anatectic rocks formed during the reheating of altered sheeted dikes. Such a reheating stage is consistent with the models presented by Gillis (2008), Koepke et al. (2008), and France et al. (2009a), which describe the melt lens present at fast spreading ridges as a dynamic system that can migrate vertically. The chemical composition (major and trace elements) of the experimentally formed melt, which can mix within the melt lens, is also determined for the first time, well-suited for the quantification of MORB contamination at fast-spreading ridges.

The performed experiments also provide new constraints on the origin of granoblastic microgabbros occurring at the base of the SDC, and as xenoliths in the isotropic gabbro horizon below the SDC. The granoblastic microgabbro dikes and xenoliths have lower incompatible element contents (e.g., light REE) than the regular diabases from the sheeted dike complex, resulting from dehydration and / or partial melting. Granoblastic microgabbro dikes and xenoliths therefore should be distinguished from those

#### *Chapter IV. Melting the hydrothermally altered sheeted dike complex: experimental study*

microgabbros which are regarded as the roots of late basaltic dikes emplaced in the very hot environment at base of the SDC and slowly cooled to typical protodikes (e.g., Nicolas et al., 2008). A partial melting event, locally triggered by a fluid ingression in recently crystallized rocks as proposed by Nicolas et al. (2008) is also ruled out. In that model, the fluids migrate downward along localized pathways (cracks and/or faults); hence one should expect to see gradients of recrystallization from fully recrystallized rocks close to fluid pathways to doleritic rocks away of these pathways. This is in contrast with the base of the sheeted dike complex that is pervasively recrystallized to granoblastic microgabbroites.

The occurrence of numerous tiny oxide inclusions in newly formed clinopyroxenes, interpreted as results from prograde metamorphism (Chapter II), is reproduced experimentally, and results from recrystallization after amphibole. Manning and MacLeod (1996) have described metamorphic retrograde clinopyroxenes that are associated to oxides. However, these oxides occur in association with granular clinopyroxene grains at the contact with amphibole, close to amphibole bearing veins, and not as inclusions in clinopyroxenes as in granoblastic microgabbro dikes. These retrograde oxide-clinopyroxene assemblages may recall the petrology of granoblastic microgabbro dikes that contain several granular oxides; nevertheless in the case of retrograde evolution, it only occurs in normal gabbros close to late hydrothermal veins in contrast with granoblastic microgabbro dikes where the oxides occurs pervasively and associated to fully recrystallized textures.

The peculiar characteristics of granoblastic microgabbro dikes presented herein (mineral major element compositions, whole-rock trace element composition, occurrence of oxide inclusions in clinopyroxenes, and occurrence of granoblastic microgabbro xenoliths in the isotropic gabbro and foliated gabbro) clearly show that their formation is related to prograde metamorphism, i.e. reheating. Trace elements also support a residual origin after partial melting rather than a metamorphic one in the sub-solidus regime (where rocks are reheated and dehydrated without any partial melting). Nevertheless, both processes may co-exist. Samples with the lowest  $\text{TiO}_2$  and  $\text{Al}_2\text{O}_3$  contents in clinopyroxenes are expected to be equilibrated under temperatures that are below the hydrous solidus, and may represent dehydrated rocks that have not undergone any hydrous partial melting. Koepke et al. (2008) have shown that in a single sample, “dry” and “wet” domains coexist. Hence, it is expected that both pure dehydration and anatexis can occur in a single sample, depending on the previous hydrothermal alteration extent and heterogeneity.

The experimental results also provide the basis for a new thermometer, which can be applied to tholeiitic to calc-alkaline rocks crystallized at shallow pressure (~100 MPa) at the

transition between magmatic and metamorphic processes, under water-saturated conditions and relatively oxidizing conditions (slightly higher than the FMQ equilibrium). It is based on the temperature dependence of Al incorporation in clinopyroxene under these conditions.

# **Conclusion**



## Conclusion

At least part of the upper and lower oceanic crust formed at fast spreading ridges is fed by the upper melt lens that is imaged at the base of the sheeted dike complex. Hence the role of the melt lens in oceanic crust genesis is critical. Interactions between the melt lens and the overlying, hydrothermally altered sheeted dike complex may have first-order consequences on the melt composition, and therefore on the whole oceanic crust composition. The objective of this study was to identify the different processes occurring within the melt lens and at the interface between this melt lens and the overlying sheeted dikes. To study these processes, I carried out comparison between the Oman ophiolite and IODP Hole 1256D, the first drilling hole that has reached the sheeted dikes / gabbro transition. Detailed field studies have been performed in the Oman ophiolite, and the Oman samples have been petrologically and geochemically studied, and compared to samples from IODP Hole 1256D. An experimental study that reproduces partial melting of hydrothermally altered dikes at the top of the melt lens has also been carried out.

The main results are:

- ✘ In the Oman ophiolite and at IODP Site 1256, the base of the sheeted dike complex is truncated by isotropic gabbros. These gabbros locally contain olivine and can be either fine or coarse grained.
- ✘ The base of the truncated dikes is recrystallized to a well equilibrated (granoblastic texture) granulitic assemblage. The granoblastic dikes are composed of plagioclase, clinopyroxene, oxides, and orthopyroxene. The clinopyroxenes contain numerous tiny oxide inclusions.
- ✘ Numerous xenoliths of either gabbro or granoblastic microgabbro and granoblastic microgabbro norite are observed within the isotropic gabbro horizon. A xenolith accumulation is also observed close to the isotropic / foliated gabbro transition.
- ✘ Numerous granoblastic patches and other evidences of assimilation are observed within the isotropic gabbro horizon.
- ✘ Experimental melts formed during partial melting of hydrothermally altered dikes are highly silicic and similar to the oceanic plagiogranites observed close to the sheeted dikes / gabbro transition.
- ✘ Patterns of trace element analysed with SIMS in the experimental melts are similar to those of typical oceanic plagiogranites observed close to the sheeted dikes / gabbro transition.



- ✘ The residual assemblage after the experimental partial melting of hydrothermally altered sheeted dikes is petrographically and geochemically similar to the granoblastic dikes and xenoliths.

These different observations support the following conclusions:

- ✘ The sheeted dikes / gabbro transition (hydrothermal / magma transition) in the Oman ophiolite and at IODP Site 1256 can be described in a single coherent model, which reconciles apparently contrasting previous models. This model proposes that the melt lens underlying the sheeted dike complex is a dynamic horizon that can inflate and deflate and / or migrate upward and downward. A review of the associated time-scales is presented Chapter III.3; it shows that the identified melt lens migrations are associated to time scales  $\leq 10,000$  years.
- ✘ Upward migrations of the top of the melt lens result in the reheating of the base of the sheeted dike complex, and in the assimilation of hydrothermally altered diabases (Chapter III.3; Koepke et al., submitted\_Appendix A4).
- ✘ The origin of microgranular dikes and xenoliths present at the base of the sheeted dike complex is bimodal. Some have crystallized in a still hot, hydrous environment and have a pure magmatic origin (protodikes; Nicolas et al., 1991, 2008), and some are recrystallized in the amphibolite to granulite facies during the reheating event associated to upward migrations, and can therefore be regarded as metamorphic products (granoblastic dikes). Both processes result in very similar textures, and a multi-disciplinary study (field observations, petrological characterization, and geochemical characterization) is necessary to decipher the origin of a given sample.
- ✘ The partial melting of hydrothermally altered diabase start at temperatures as low as 850°C.
- ✘ The chemical composition (major and trace elements) of the melt formed experimentally during hydrous partial melting of the base of the sheeted dikes, and the associated phase relations have been determined (Chapter IV). The obtained trace element composition is a useful reference for future detailed geochemical MORB investigations.

## Conclusion

- ✘ Hydrous partial melting of the base of the hydrothermally altered sheeted dike complex produces a plagiogranitic hydrous melt, and a residue that is compositionally similar to granoblastic dikes (Chapter IV).
- ✘ Assimilation of hydrothermally altered diabases in the melt lens is a common process and results in contamination processes in the melt lens (Chapter IV).
- ✘ Downward migrations of the top of the melt lens result in the crystallization of isotropic gabbros. The isotropic gabbro horizon represents the fossilized melt lens (Chapter III).
- ✘ At IODP Site 1256, the bottom of the hole is expected to be very close to the melt lens / magma chamber transition, which is assumed to be the isotropic / foliated gabbro transition (Chapter III.3).
- ✘ A new thermometer relevant for rocks crystallized at the melt lens level has been elaborated (Chapter IV). It is based on the Al content of clinopyroxenes:

$$T = 93.145 Al_2O_3 + 742$$

The proposed model could be further tested by complementary studies, which include the following:

- ✘ As proposed in France et al. (2009a), analyzing the Cl and F content of amphiboles present in the isotropic gabbros should attest of the recycled origin of the fluid crystallizing the magmatic amphiboles.
- ✘ A detailed petrological and geochemical study of the isotropic gabbro horizon in the Oman ophiolite, compared with the precise study of this horizon at IODP Site 1256 (Koepke et al., submitted; Appendix A4), and an in-situ trace element study of the different minerals from the isotropic gabbro horizon, in both the Oman ophiolite and IODP Hole 1256D, should bring further constraints to our understanding of the processes occurring within the melt lens, and of the processes that result in the melt lens fossilization.
- ✘ An experimental study of the melting of partially hydrothermally altered sheeted dikes containing magmatic minerals relics may precise the melting reactions occurring during the upward migrations of the top of the melt lens. Results presented in Chapter IV are obtained using a fully altered starting material which may be too simplistic to reproduce natural processes.

✘ An in-situ measurement of the  $Fe^{3+}/Fe^{2+}$  ratio in minerals of the different oceanic lithologies will help to further constrain the available models for the accretion of ocean crust, of lower crustal rocks, down to the base of the crust. It will also help to constrain the influence of water during the crystallization of the different oceanic lithologies. Such analyses should be performed with the help of synchrotron radiation tools. A corresponding proposal was submitted to ESRF (European Synchrotron Radiation Facility) in September 2009 (L. France: “A Redox log of the oceanic crust from plagioclases  $Fe^{3+}/Fe^{2+}$  micro-XANES in-situ measurements”). The results are expected to provide the first redox log of an oceanic crust section and will also help to further constrain the new oxybarometer proposed in France et al. (2009b; Appendix A3). This oxybarometer is based on microprobe analyses of two of the most common minerals present in basaltic series (clinopyroxene + plagioclase). It will be useful for all petrological and geochemical studies of oxidizing magmatic systems.

# **References**



## References

- Adachi Y, Miyashita S (2003) Geology and petrology of the plutonic complexes in the Wadi Fizh area: Multiple magmatic events and segment structure in the northern Oman ophiolite. *Geochemistry Geophysics Geosystems* **4-9**: 8,619. doi:10.1029/2001GC000272
- Albarède F, Provost A (1977) Petrological and geochemical mass balance equations: an algorithm for least-square fitting and general error analysis. *Computers and Geosciences* **3**:309-326. doi:10.1016/0098-3004(77)90007-3
- Allen CR (1975) The petrology of a portion of the Troodos Plutonic Complex, Cyprus. *Thesis, PhD, Univ. of Cambridge (unpubl.)*
- Alt JC, Honnorez J, Laverne C, Emmermann R (1986) Hydrothermal alteration of a 1km section through the upper oceanic crust, deep sea drilling project Hole 504b\_Mineralogy, chemistry, and evolution of seawater-basalt interactions. *J. Geophys. Research* **91-B10**: 10,309-10,335
- Alt JC, Laverne C, Vanko DA, Tartarotti P, Teagle DAH, Bach W, Zuleger E, Erzinger J, Honnorez J, Pezard PA, Becker K, Salisbury MH, Wilkens RH (1996) Hydrothermal alteration of a section of upper oceanic crust in the eastern equatorial Pacific: a synthesis of results from Site 504 (DSDP Legs 69, 70, and 83, and ODP Legs 111, 137, 140, and 148.). In Alt, J.C., Kinoshita, H., Stokking, L.B., and Michael, P.J. (Eds.), *Proc. ODP, Sci. Results, College Station, TX (Ocean Drilling Program)* **148**: 417-434
- Alt JC, Teagle DAH, Umino S, Miyashita S, Banerjee NR, Wilson DS, the IODP Expeditions 309 and 312 Scientists, and the ODP Leg 206 Scientific Party (2007) IODP Expeditions 309 and 312 drill an Intact Upper Oceanic Basement into Gabbros. *Scientific Drilling* **4**: 4-10. doi:10.2204/iodp.sd.4.01.2007
- Amri I, Benoit M, Ceuleneer G (1996) Tectonic setting for the genesis of oceanic plagiogranites: evidence from a paleospreading structure in the Oman ophiolite. *Earth and Planetary Science Letters* **139**: 177-194
- Anders E, Grevesse N (1989) Abundances of the elements: meteoritic and solar. *Geochimica et Cosmochimica Acta* **53**: 197-214.
- Andersen DJ, Lindsley DH, Davidson PM (1993) QUILF: A Pascal program to assess equilibria among Fe-Mg-Mn-Ti oxides, pyroxenes, olivine, and quartz. *Computers and Geosciences* **19**: 1,333-1,350. doi:10.1016/0098-3004(93)90033-2
- Asimow PD, Stolper EM (1999) Steady-state mantle-melt interactions in one dimension: equilibrium, transport and melt focusing. *Journal of Petrology* **40-3**: 475-494. doi:10.1093/petrology/40.3.475
- Bach W, Erzinger J, Alt JC, Teagle DAH (1996) Chemistry of the lower sheeted dike complex, Hole 504B (Leg 148): influence of magmatic differentiation and hydrothermal alteration. In Alt JC, Kinoshita H, Stokking LB, Michael PJ (Eds.), *Proc. ODP, Sci. Results, College Station, TX (Ocean Drilling Program)* **148**: 39-55. doi:10.2973/odp.proc.sr.148.114.1996
- Barker F (1979) Trondhjemites, dacites and related rocks. *Elsevier, Amsterdam* 659 pp.
- Backer ET, Urabe T (1996) Extensive distribution of hydrothermal plumes along the superfast spreading East Pacific Rise, 13°30'-18°40'S. *Journal of Geophysical Research* **101-B4**:8,685-8,695
- Bascom WN (1961) A Hole in the Bottom of the Sea: The Story of the Mohole Project. *Doubleday and Company, Inc., Garden City, New York*, 352 pp.
- Batiza R, Niu Y (1992) Petrology and magma chamber processes at the East Pacific Rise. *Journal of Geophysical Research* **97**:6,779-6,797
- Beard JS, Lofgren GE (1989) Effect of Water on the Composition of Partial Melts of Greenstone and Amphibolite. *Science* **244**: 195-197
- Beard JS, Lofgren GE (1991) Dehydration melting and water saturated melting of basaltic and andesitic greenstones and amphibolites at 1, 3, and 6.9 kb. *Journal of Petrology* **32**: 365-401
- Beccaluva L, Ohnenstetter D, Ohnenstetter M, Venturelli G (1977) The trace element geochemistry of Corsican ophiolites. *Contributions to Mineralogy and Petrology* **64**: 11-31
- Beccaluva L, Chinchilla-Chaves AL, Coltorti M, Giunta G, Siena F, Vaccaro C (1999) Petrological and structural significance of the Santa Elena-Nicoya ophiolitic complex in Costa Rica and geodynamic implications. *European Journal of Mineralogy* **11**: 1,091-1,107
- Bedard JH, Sparks RSJ, Renner R, Cheadle MJ, Hallworth MA (1988) Peridotite sills and metasomatic gabbros in the eastern layered series of the Rhum complex. *J. Geol. Soc. London* **145**: 207-224

- Bergmanis EC, Sinton J, Rubin KH (2007) Recent eruptive history and magma reservoir dynamics on the southern East Pacific Rise at 17°30'S. *Geochemistry Geophysics Geosystems* **8-12**: Q12O06. doi:10.1029/2007GC001742
- Berndt J, Liebske C, Holtz F, Freise M, Nowak M, Ziegenbein D, Hurkuck D, Koepke J (2002) A combined rapid-quench and H<sub>2</sub>-membrane setup for internally heated pressure vessels: Description and application for water solubility in basaltic melts. *American Mineralogist* **87**: 1,717-1,726
- Berndt J, Koepke J, Holtz F (2005) An experimental investigation of the influence of water and oxygen fugacity on differentiation of MORB at 200 MPa. *Journal of Petrology* **46**: 135-167
- Bloomer SH, Natland JH, Fisher RL (1989) Mineral relationships in gabbroic rocks from fracture zones of Indian Ocean ridges: evidence for extensive fractionation, parental diversity and boundary-layer recrystallization. In *Magmatism in the Ocean Basins*, edited by Saunders AD and Norry MJ, Geol. Soc. London Spec. Publ. **42**: 107-124
- Bonev N, Stampfli G (2009) Gabbro, plagiogranite and associated dykes in the supra-subduction zone Evros Ophiolites, NE Greece. *Geological Magazine* **146-1**: 72-91. doi:10.1017/S0016756808005396
- Bosch D, Jamais M, Boudier F, Nicolas A, Dautria JM, Agrinier P (2004) Deep and high temperature hydrothermal circulation in the Oman ophiolite: Petrological and isotopic evidence. *Journal of Petrology* **45(6)**: 1,181-1,208. doi:10.1093/petrology/egh010
- Botcharnikov RE, Koepke J, Holtz F, McCammon C, Wilke M. (2005) The effect of water activity on the oxidation and structural state of Fe in a ferro-basaltic melt. *Geochimica et Cosmochimica Acta* **69**: 5,071-5,085. doi:10.1016/j.gca.2005.04.023
- Boudier F, Nicolas A (2007) Comment on “dating the geologic history of Oman’s Semail ophiolite: insights from U-Pb geochronology” by C.J. Warren, R.R. Parrish, D.J. Waters and M.P. Searle. *Contributions to Mineralogy and Petrology* **154**: 111-113
- Boudier F, Ceuleneer G, Nicolas A (1988) Shear zones, thrusts and related magmatism in the Oman ophiolite: initiation of thrusting at an ocean ridge. *Tectonophysics* **151**: 275-296
- Boudier F, Nicolas A, Ildefonse B (1996) Magma chambers in the Oman ophiolite: fed from the top and the bottom. *Earth and Planetary Science Letters* **144**: 239-250. doi:10.1016/0012-821X(96)00167-7
- Boudier F, Godard M, Armbruster C (2000) Significance of gabbro occurrence in the crustal section of the Semail ophiolite. *Marine Geophysical Research* **21**: 307-326. doi:10.1023/A:1026726232402
- Brophy JG (2008) A study of rare earth element (REE)-SiO<sub>2</sub> variations in felsic liquids generated by basalt fractionation and amphibolite melting: a potential test for discriminating. *Contributions to Mineralogy and Petrology* **156**: 337-357. doi: 10.1007/s00410-008-0289-x
- Brophy JG (2009) La-SiO<sub>2</sub> and Yb-SiO<sub>2</sub> systematics in mid-ocean ridge magmas: implications for the origin of oceanic plagiogranite. *Contributions to Mineralogy and Petrology* **158**: 99-111. doi: 10.1007/s00410-008-0372-3
- Browning P (1982) The petrology, geochemistry and structure of the plutonic rocks of the Oman Ophiolite. *PhD Thesis, The Open University, Milton Keynes* 405 pp.
- Browning P (1984) Cryptic variation within the cumulate sequence of the Oman ophiolite: magma chamber depth and petrological implications. In: *Gass I, Lippard SJ, Shelton AW (Eds.), Ophiolites and Oceanic Lithosphere. Special Publication-Geological Society of London*, **13**: 71-82
- Bryan W, Frey BFA, Dickey JS (1976) Inferred geologic settings and differentiation in basalts from the Deep Sea Drilling Project. *Journal of Geophysical Research* **81**: 4,285-4,304
- Canales JP, Detrick RS, Carbotte SM, Kent GM, Diebold JB, Harding A, Babcock J, Nedimovic MR, Van Ark E (2005) Upper crustal structure and axial topography at intermediate spreading ridges: Seismic constraints from the southern Juan de Fuca Ridge. *Journal of Geophysical Research* **110**: B12,104. doi: 10.1029/2005JB003630
- Canales JP, Carbotte SM, Mutter JC, Nedimovic MR, Carton H, Xu M, Newman K, Aghaei O, Marjanovic M, Stowe LC (2008) Discovery of off-axis melt lenses at the RIDGE-2000 East Pacific Rise integrated studies site. *Eos Trans. AGU, Fall Meet. Suppl.* **89-53**: B21A-0319
- Canales JP, Nedimovic MR, Kent GM, Carbotte SM, Detrick RS (2009) Seismic reflection images of a near-axis melt sill within the lower crust at the Juan de Fuca ridge. *Nature* **460**: 89-94. doi:10.1038/nature08095

## References

- Cande SC, Kent DV (1995) Revised calibration of the geomagnetic polarity timescale for the Late Cretaceous and Cenozoic. *Journal of Geophysical Research* **100**: 6,093–6,095. doi:10.1029/94JB03098
- Cann JR (1974) A model for oceanic crustal structure developed. *Geophysical Journal of the Royal Astronomical Society* **39**: 169-187
- Carbotte SM (2008) Focusing in on Mid-Ocean Ridge Segmentation. *Eos Trans. AGU Fall Meet. Suppl.* **89-53**: T34B-01
- Carbotte SM, Mutter C, Mutter J, Ponce-Correa G (1998) Influence of magma supply and spreading rate on crustal magma bodies and emplacement of the extrusive layer: Insights from the East Pacific Rise at lat 16°N. *Geology* **26-5**: 455-458
- Carbotte SM, Mutter JC, Canales JP, Nedimovic MR, Carton H, Xu M, Newman K, Marjanovic M, Aghaei O, Stowe L (2008) New observations of the magmatic segmentation of the East Pacific Rise from Siquieros to Clipperton from a multi-streamer seismic reflection imaging study. *Eos Trans. AGU Fall Meet. Suppl.* **89-53**: B21A-0320
- Caress DW, Burnett MS, Orcutt JA (1992) Tomographic image of the axial low velocity zone at 12°50'N on the East Pacific Rise. *Journal of Geophysical Research* **97-B6**: 9,243-9,263
- Caroff M, Lagabrielle Y, Spadea P, Auzende JM (1997) Geochemical modeling of nonsteady-state magma chambers: A case study from an ultrafast spreading ridge, East Pacific Rise, 17-19°S. *Geochimica et Cosmochimica Acta* **61-20**: 4,367-4,374
- Carton H, Carbotte SM, Mutter JC, Canales JP, Nedimovic MR, Newman K, Marjanovic M, Xu M, Aghaei O, Stowe L (2008) Characteristics of the crustal magma body in the 2005-06 eruption area at 9°50'N on the East Pacific Rise from a 3D multi-channel seismic investigation. *Eos Trans. AGU Fall Meet. Suppl.* **89-53**: B23F-03
- Casey JF, Karson JA (1981) Magma chamber profiles from the Bay of Islands ophiolite complex. *Nature* **298**: 295-301
- Coleman RG, Donato MM (1979) Oceanic plagiogranite revisited. In: *Barker F (eds) Trondhjemites, dacites, and related rocks. Elsevier, Amsterdam* 149-167
- Coleman RG, Peterman ZE (1975) Oceanic plagiogranite. *Journal of Geophysical Research* **80-8**: 1,099-1,108
- Collier JS, Singh SC (1997) Detailed structure of the top of the melt body beneath the East Pacific Rise at 9°40'N from waveform inversion of seismic reflection data. *Journal of Geophysical Research* **102-B9**: 20,287-20,304. doi: 10.1029/97JB01514
- Conference Participants (1972) Penrose field conference on ophiolites. *Geotimes* **17**: 24-25
- Coogan LA (2003) Contaminating the lower crust in the Oman ophiolite. *Geology* **31-12**: 1,065-1,068. doi: 10.1130/G20129.1
- Coogan LA, Wilson RN, Gillis KM, MacLeod CJ (2001) Near-solidus evolution of oceanic gabbros: Insights from amphibole geochemistry. *Geochimica et Cosmochimica Acta* **65-23**: 4,339-4,357. doi: 10.1016/S0016-7037(01)00714-1
- Coogan LA, Thompson G, MacLeod CJ (2002) A textural and geochemical investigation of high level gabbros from the Oman ophiolite: implications for the role of the axial magma chamber at fast-spreading ridges. *Lithos* **63**: 67-82. doi: 10.1016/S0024-4937(02)00114-7
- Coogan LA, Mitchell NC, O'Hara MJ (2003) Roof assimilation at fast spreading ridges: An investigation combining geophysical, geochemical, and field evidence. *Journal of Geophysical Research* **108-B1**: 2002 doi: 10.1029/2001JB001171
- Cordier C, Caroff M, Juteau T, Fleutelot C, Hémond C, Drouin M, Cotton J, Bollinger C (2007) Bulk-rock geochemistry and plagioclase zoning in lavas exposed along the northern flank of the Western Blanco Depression (Northeast Pacific): Insight into open-system magma chamber processes. *Lithos* **99**: 289-311
- Cormier MH (1997) The ultrafast East Pacific Rise: instability of the plate boundary and implications for accretionary processes. In: *Cann JR, Elderfield H, Laughton A (Editors), Mid-Ocean Ridges. Dynamics of processes associated with creation of new ocean crust, Phil. Trans. R. Soc. Lond. A*, **355-1,723**: 341-367. doi: 10.1098/rsta.1997.0012



- Crawford WC, Webb SC (2002) Variations in the distribution of magma in the lower crust and the Moho beneath the East Pacific Rise at 9°-10° N. *Earth and Planetary Science Letters* **203**: 117-130
- Detrick RS, Buhl P, Vera E, Mutter J, Orcutt J, Madsen J, Brocher T (1987) Multi-channel seismic imaging of a crustal magma chamber along the East Pacific Rise. *Nature* **326**: 35-41
- Detrick R, Collins J, Stephen R, Swift S (1994) In situ evidence for the nature of the seismic Layer 2/3 boundary in oceanic crust. *Nature* **370**: 288-290. doi: 10.1038/370288a0
- Dewey JF, Kidd SF (1977) Geometry of plate accretion. *Geological Society of America Bulletin* **88**: 960-968
- Dixon S, Rutherford MJ (1979) Plagiogranites as late-stage immiscible liquids in ophiolite and mid-oceanic ridge suites: an experimental study. *Earth and Planetary Science Letters* **45**: 45-60
- Dixon-Spulber S, Rutherford MJ (1983) The origin of rhyolite and plagiogranite in oceanic crust: an experimental study. *Journal of Petrology* **24**: 1-25
- Dubois M (1983) Plagiogranite and hydrothermalism: an approach from Cyprus and Oman ophiolitic complexes. *PhD dissertation, University of Nancy I, France*
- Dunn RA, Toomey DR, Solomon SC (2000) Three-dimensional seismic structure and physical properties of the crust and shallow mantle beneath the East Pacific Rise at 9°30'N. *Journal of Geophysical Research* **105-B10**: 23,537-23,555
- Dunn RA, Toomey DR, Detrick RS, Wilcock WSD (2001) Continuous mantle melt supply beneath an overlapping spreading centre on the East Pacific Rise. *Science* **291**: 1,955-1,958
- Dziony W, Koepke J, Holtz F (2008) Data report: Petrography and phase analyses in lavas and dikes from the hole 1256D (ODP Leg 206 and IODP Expedition 309, East Pacific Rise). In *Teagle DAH, Alt JC, Umino S, Miyashita S, Banerjee NR, Wilson DS, and the Expedition 309/312 Scientists. Proc. IODP, 309/312: Washington, DC (Integrated Ocean Drilling Program Management International, Inc.)*. doi: 10.2204/iodp.proc.309312.201.2008
- Einaudi F, Pezard P, Cocheme JJ, Coulon C, Laverne C, Godard M (2000) Petrography, geochemistry and physical properties of continuous extrusive section from the Sarami Massif, Semail ophiolite. *Marine Geophysical Research* **21**: 387-407
- Ernst WG, Liu J (1998) Experimental phase-equilibrium study of Al- and Ti-contents of calcic amphibole in MORB - A semiquantitative thermobarometer. *American Mineralogist* **83**: 952-969
- Fahey AJ, Zinner EK, Crozaz G, Kornacki AS (1987) Microdistributions of Mg isotopes and REE abundances in a Type A calcium-aluminum-rich inclusion from Efremovka. *Geochimica et Cosmochimica Acta* **51**: 3,215-3,229. doi: 10.1016/0016-7037(87)90130-X
- Fei Y (1995) Thermal expansion. In: *Mineral Physics & Crystallography. A Handbook of Physical Constants*. Eds. Thomas J. Ahrens 354 pp. **2**: 29-44
- Feig ST, Koepke J, Snow JE (2006) Effect of water on tholeiitic basalt phase equilibria: An experimental study under oxidizing conditions. *Contributions to Mineralogy and Petrology* **152-5**: 611-638. doi:10.1007/s00410-006-0123-2
- Fisher AT (2003) Geophysical constraints on hydrothermal circulation: Observations and models. In *Energy and Mass Transfer in Marine Hydrothermal Systems (eds. Halbach PE, Tunncliffe V, Hein JR)*, Dahlem Univ. Press, Berlin **Vol. 3**: 29-52
- Fisk MR, Johnson KTM, Alt JC (1995) Effect of assimilation of altered oceanic crust on magma chemistry: an experimental study. In *Erzinger J, Becker K, Dick HJB, Stokking LB, Proceedings of the Ocean Drilling Program, Scientific Results* **137-140**: 43-51
- Flagler PA, Spray JG (1991) Generation of plagiogranite by amphibolite anatexis in oceanic shear zones. *Geology* **19**: 70-73
- Floyd PA, Yaliniz MK, Goncuoglu MC (1998) Geochemistry and petrogenesis of intrusive and extrusive ophiolitic plagiogranites, central Anatolian Crystalline Complex, Turkey. *Lithos* **42**: 225-241
- France L, Ildefonse B, Koepke J (2009) Dynamics of the axial melt lens / dike transition at fast spreading ridges: assimilation and hydrous partial melting. *Geophysical Research Abstracts* **11**: 10,159-1

## References

- France L, Ildefonse B, Koepke J (2009a) Interactions between magma and hydrothermal system in Oman ophiolite and in IODP Hole 1256D: fossilization of a dynamic melt lens at fast spreading ridges. *Geochemistry Geophysics Geosystems* **in press** doi: 10.1029/2009GC002652 (Chapter III)
- France L, Koepke J, Ildefonse B, Bech F (2009b) A new method to estimate the oxidation state of basaltic series from microprobe analyses. *Journal of Volcanology and Geothermal Research* Accepted for publication after moderate revision (Appendix A3)
- France L, Koepke J, Ildefonse B, Cichy S, Deschamps F (2010a) Hydrous partial melting in the sheeted dike complex at fast spreading ridges: Experiments and nature. *Submitted to Contributions to Mineralogy and Petrology* (Chapter IV)
- France L, Ildefonse B, Koepke J, MacLeod CJ, Godard M (2010b) Melting the hydrothermally altered sheeted dike complex: an experimental / trace element study. *In prep. for Geology* (Chapter IV)
- Gaetani GA, Grove TL, Bryan WB (1993) The influence of water on the petrogenesis of subduction-related igneous rocks. *Nature* **365**: 332-334
- Garel E, Dauteuil O, Lagabrielle Y (2002) Deformation processes at fast to ultra-fast oceanic spreading axes\_mechanical approach. *Tectonophysics* **346**: 223-246
- Garmann J (1989) Accumulations of melt at the base of young oceanic crust. *Nature* **340**: 628-632
- Garrido CJ, Kelemen PB, Hirth G (2001) Variation of cooling rate with depth in lower crust formed at an oceanic spreading ridge: Plagioclase crystal size distributions in gabbros from the Oman ophiolite. *Geochemistry Geophysics Geosystems* **2-10**: 1,041. doi: 10.1029/2000GC000136
- Gerbert-Gaillard L (2002) Caractérisation géochimique des péridotites de l'ophiolite d'Oman: processus magmatiques aux limites lithosphère-asthénosphère. *PhD memoir from Géosciences Montpellier, France* 241pp.
- Gerlach DC, Leeman WP, Avé Lallemand HG (1981) Petrology and geochemistry of plagiogranite in the Canyon Mountain ophiolite, Oregon. *Contribution to Mineralogy and Petrology* **72**: 82-92
- Ghazi AM, Hassanipak AA, Mahoney JJ, Duncan RA (2004) Geochemical characteristics, <sup>40</sup>Ar-<sup>39</sup>Ar ages and original tectonic setting of the Band-e-Zeyarat-Dar Anar ophiolite, Makran accretionary prism, S.E. Iran. *Tectonophysics* **393**: 175-196
- Ghiorso MS, Sack RO (1995) Chemical mass transfer in magmatic processes IV. A Revised and internally consistent thermodynamic model for the interpolation of liquid-solid equilibria in magmatic systems at elevated temperatures and pressures. *Contribution to Mineralogy and Petrology* **119**: 197-212
- Gillis KM (2002) The root zone of an ancient hydrothermal system exposed in the Troodos ophiolite, Cyprus. *The Journal of Geology* **110**: 57-74. doi:10.1086/324205
- Gillis KM (2008) The roof of an axial magma chamber: A hornfelsic heat exchanger. *Geology* **36-4**: 299-302. doi: 10.1130/G24590A.1
- Gillis KM, Coogan LA (2002) Anatectic migmatites from the roof of an ocean ridge magma chamber. *Journal of Petrology* **43-11**: 2,075-2,095. doi: 10.1093/petrology/43.11.2075
- Gillis KM, Roberts MD (1999) Cracking at the magma-hydrothermal transition: Evidence from the Troodos ophiolite, Cyprus. *Earth and Planetary Science Letters* **169**: 227-244. doi: 10.1016/S0012-821X(99)00087-4
- Gillis KM, Coogan LA, Chaussidon M (2003) Volatile element (B, Cl, F) behaviour in the roof of an axial magma chamber from the East Pacific Rise. *Earth and Planetary Science Letters* **213**: 447-462. doi: 10.1016/S0012-821X(03)00346-7
- Giordano D, Russell JK, Dingwell DB (2008) Viscosity of magmatic liquids: A model. *Earth and Planetary Science Letters* **271**: 123-134
- Godard M, Dautria JM, Perrin M (2003) Geochemical variability of the Oman ophiolite lavas: relationship with spatial distribution and paleomagnetic directions. *Geochemistry Geophysics Geosystems* **4-6**: 1-15
- Grove TL, Bryan WB (1983) Fractionation of pyroxene-phyric MORB at low pressure: an experimental study. *Contributions to Mineralogy and Petrology* **84**: 293-309
- Gudmundsson A (1990) Emplacement of dikes, sills and crustal magma chambers at divergent plate boundaries. *Tectonophysics* **176**: 257-275

- Hacker BR (1990) Amphibolite-facies to granulite-facies reactions in experimentally deformed, unpowdered amphibolite. *American Mineralogist* **75**: 1,349-1,361
- Haase KM, Stroncik NA, Hékinian R, Stoffers P (2005) Nb-depleted andesites from the Pacific-Antarctic Rise as analogs for early continental crust. *Geology* **33-12**: 921-924. doi: 10.1130/G21899.1
- Harding AJ, Orcutt JA, Kappus ME, Vera EE, Mutter JC, Buhl P, Detrick RS, Brocher TM (1989) Structure of young oceanic crust at 13°N on the East Pacific Rise from expanding spread profiles. *Journal of Geophysical Research* **94-B9**: 12,163-12,196. doi: 10.1029/JB094iB09p12163
- Helz RT (1973) Phase relations of basalt in their melting ranges at  $\text{PH}_2\text{O}=5$  kb as a function of oxygen fugacity. *Journal of Petrology* **14**: 249-302
- Henstock TJ, Woods AW, White RS (1993) The accretion of oceanic crust by episodic sill intrusion. *Journal of Geophysical Research* **98-B3**: 4,143-4,161
- Holland T, Blundy J (1994) Non-ideal interactions in calcic amphiboles and their bearing on amphibole-plagioclase thermometry. *Contributions to Mineralogy and Petrology* **116**: 433-447
- Holloway JR, Burnham CW (1972) Melting relations of basalt with equilibrium water pressure less than total pressure. *Journal of Petrology* **13**: 1-29
- Hooft EEE, Detrick RS, Kent GM (1997) Seismic structure and indicators of magma budget along the southern East Pacific Rise. *Journal of Geophysical Research* **102-B12**: 27,319-27,340. doi: 10.1029/97JB02349
- Hopson CA, Coleman RG, Gregory RT, Pallister JS, Bailey EH (1981) Geologic section through the Samail ophiolite and associated rocks along a Muscat-Ibra transect, Southeastern Oman mountains. *Journal of Geophysical Research* **86**: 2,527-2,544. doi: 10.1029/JB086iB04p02527
- Hussenoeder SA, Collins JA, Kent GM, Detrick RS, Harding AJ, Orcutt JA, Mutter JC, Buhl P (1996) Seismic analysis of the axial magma chamber reflector along the southern East Pacific Rise from conventional reflection profiling. *Journal of Geophysical Research* **101-B10**: 22,087-22,105. doi: 10.1029/96JB01907
- Irvine TN, Baragar WRA (1971) A guide to the chemical classification of the common volcanic rocks. *Canadian Journal of Earth Sciences* **8**: 532-548
- Johannes W, Koepke J (2001) Uncomplete reaction of plagioclase in experimental dehydration melting of amphibolite. *Australian Journal of Earth Sciences* **48**: 581-590
- Juster TC, Grove TL, Perfit MR (1989) Experimental Constraints on the Generation of FeTi Basalts, Andesites, and Rhyodacites at the Galapagos Spreading Center, 85W and 95W. *Journal of Geophysical Research* **94-B7**: 9,251-9,274
- Juteau T, Beurrier M, Dahl R, Nehlig P (1988) Segmentation at a fossil spreading center: The plutonic sequence of the Wadi Haymilyah area (Haylayn block, Sumail nappe, Oman). *Tectonophysics* **151**: 167-197. doi: 10.1016/0040-1951(88)90245-4
- Juteau T, Bideau D, Dauteuil O, Manac'h G, Naidoo DD, Nehlig P, Ondreas H, Tivey MA, Whipple KX, Delaney JR (1995) A Submersible Study in the Western Blanco Fracture Zone, N.E. Pacific: Structure and Evolution during the Last 1.6 Ma. *Marine Geophysical Researches* **17**: 399-430
- Kawamoto T (1996) Experimental constraints on differentiation and H<sub>2</sub>O abundance of calc-alkaline magmas. *Earth and Planetary Science Letters* **144**: 577-589
- Kelemen PB, Shimizu N, Salters VJM (1995) Extraction of midocean-ridge basalt from the upwelling mantle by focused flow of melt in dunite channels. *Nature* **375**: 747-753. doi:10.1038/375747a0
- Kelemen P, Koga K, Shimizu N (1997) Geochemistry of gabbro sills in the crust-mantle transition zone of the Oman ophiolite: implications for the origin of the oceanic lower crust. *Earth and Planetary Science Letters* **146**: 475-488
- Kelley DS, Baross JA, Delaney JR (2002) Volcanoes, fluids and life at mid-ocean ridge spreading centers. *Annual Reviews in Earth and Planetary Sciences* **30**: 385-491
- Kent GM, Harding AJ, and Orcutt JA (1990) Evidence for a smaller magma chamber beneath the East Pacific Rise at 9°30'N. *Nature* **344**: 650-653
- Kent GM, Singh SC, Harding AJ, Sinha MC, Orcutt JA, Barton PJ, White RS, Bazin S, Hobbs RW, Tong CH, Pye JW (2000) Evidence from three-dimensional seismic reflectivity images for enhanced melt supply beneath mid-ocean-ridge discontinuities. *Nature* **406-6,796**: 614-618

## References

- Kinzler RJ, Grove TL (1992) Primary Magmas of Mid-Ocean Ridge Basalts 1. Experiments and Methods. *Journal of Geophysical Research* **97-B5**: 6,885-6,906. doi: 10.1029/91JB02840
- Klein EM (2003) Geochemistry of the Igneous Ocean Crust. In *Treatise on Geochemistry*, (exec. eds. Turekian KK, Holland HD; vol. ed.: Rudnick R), Elsevier **3**: 433-463. doi: 10.1016/B0-08-043751-6/03030-9
- Klein EM, Langmuir CH (1987) Global correlations of ocean ridge basalt chemistry with axial depth and crustal thickness. *Journal of Geophysical Research* **92**: 8,089-8,115
- Klein EM, Langmuir CH, Staudigel H (1991) Geochemistry of basalts from the Southeast Indian Ridge, 115°E-138°E. *Journal of Geophysical Research* **96**: 2,089-2,107
- Klimm K, Holtz F, Johannes W, King PL (2003) Fractionation of metaluminous A-type granites: an experimental study of the Wangrah Suite, Lachlan Fold Belt, Australia. *Precambrian Research* **124**: 327-341
- Koepke J, Feig ST, Snow J, Freise M (2004) Petrogenesis of oceanic plagiogranites by partial melting of gabbros: an experimental study. *Contributions to Mineralogy and Petrology* **146**: 414-432
- Koepke J, Feig S, Snow J (2005a) Late stage magmatic evolution of oceanic gabbros as a result of hydrous partial melting: Evidence from the Ocean Drilling Program (ODP) Leg 153 drilling at the Mid-Atlantic Ridge. *Geochemistry Geophysics Geosystems* **6**: Q02001. doi: 10.1029/2004GC000805
- Koepke J, Feig ST, Snow J (2005b) Hydrous partial melting within the lower oceanic crust. *Terra Nova* **17**: 286-91. doi: 10.1111/j.1365-3121.2005.00613.x
- Koepke J, Berndt J, Feig ST, Holtz F (2007) The formation of SiO<sub>2</sub>-rich melts within the deep oceanic crust by hydrous partial melting of gabbros. *Contributions to Mineralogy and Petrology* **153**: 7-84. doi: 10.1007/s00410-006-0135-y
- Koepke J, Christie DM, Dziony W, Holtz F, Lattard D, Maclennan J, Park S, Scheibner B, Yamasaki T, Yamazaki S (2008) Petrography of the Dike/Gabbro Transition at IODP Site 1256 (Equatorial Pacific): The evolution of the Granoblastic Dikes. *Geochemistry Geophysics Geosystems* **9-7**: Q07O09. doi: 10.1029/2008GC001939
- Koepke J, Schoenborn S, Oelze M, Wittmann H, Feig ST, Hellebrand E, Boudier F, Schoenberg R (2009) Petrogenesis of crustal wehrlites in the Oman ophiolite: Experiments and natural rocks. *Geochemistry Geophysics Geosystems* **10-10**: Q10002. doi: 10.1029/2009GC002488
- Koepke J, Dziony W, France L, Gabbros from IODP Site 1256 (Equatorial Pacific): Insight into axial magma chamber processes at fast-spreading ocean ridges. *Submitted to Geochemistry Geophysics Geosystems* (Appendix A4)
- Koga KT, Kelemen PB, Shimizu N (2001) Petrogenesis of the crust-mantle transition zone and the origin of lower crustal wehrlite in the Oman ophiolite. *Geochemistry Geophysics Geosystems* **2**: 2000GC000132
- Korenaga J, Kelemen PB (1997) Origin of gabbro sills in the Moho transition zone of the Oman ophiolite: Implications for magma transport in the oceanic lower crust. *Journal of Geophysical Research* **102-B12**: 27,729-27,749
- Kress VC, Carmichael ISE (1991) The compressibility of silicate liquids containing Fe<sub>2</sub>O<sub>3</sub> and the effect of composition, temperature, oxygen fugacity and pressure on their redox states. *Contributions to Mineralogy and Petrology* **108**: 82-92
- Kvassnes AJS, Strand AH, Moen-Eikeland H, Pedersen RB (2004) The Lyngen Gabbro: the lower crust of an Ordovician Incipient Arc. *Contributions to Mineralogy and Petrology* **148**: 358-379
- Lagabriele Y, Cormier MH (1999) Formation of large summit troughs along the East Pacific Rise as collapse calderas: An evolutionary model. *Journal of Geophysical Research* **104-B6**: 12,971-12,988. doi: 10.1029/1999JB900015
- Lagabriele Y, Garel E, Dauteuil O, Cormier MH (2001) Extensional faulting and caldera collapse in the axial region of fast spreading ridges: Analog modeling. *Journal of Geophysical Research* **106-B2**: 2,005-2,015
- Lambart S, Laporte D, Schiano P (2009) An experimental study of focused magma transport and basalt-peridotite interactions beneath mid-ocean ridges: implications for the generation of primitive MORB compositions. *Contributions to Mineralogy and Petrology* **157**: 429-451

- Lamoureux G, Ildefonse B, Mainprice D (1999) Modelling the seismic properties of fast-spreading ridge crustal Low-Velocity Zones: insights from Oman gabbro textures. *Tectonophysics* **312**: 283-301
- Lange RL, Carmichael ISE (1990) Thermodynamic properties of silicate liquids with emphasis on density, thermal expansion and compressibility. *Reviews in Mineralogy and Geochemistry* **24-1**: 25-64
- Langmuir CH, Bender JF, Batiza R (1986) Petrologic and tectonic segmentation of the East Pacific Rise, 5°30'-14°30'N. *Nature* **322**: 422-426
- Liou JG (1971) Synthesis and stability relations of prehnite,  $\text{Ca}_2\text{Al}_2\text{Si}_3\text{O}_{10}(\text{OH})_2$ . *American Mineralogist* **56**: 507-531
- Lippard SJ, Shelton AW, Gass IG (1986) The ophiolite of Northern Oman. In: *Geological Society Memoir, 11*. Blackwell, Oxford 178pp.
- Lowell RP, Rona PA, Von Herzen RP (1995) Seafloor hydrothermal systems. *Journal of Geophysical Research* **100**: 327-352
- Luchitskaya MV, Morozov OL, Palandzhyan SA (2005) Plagiogranite magmatism in the Mesozoic island-arc structure of the Pekulney Ridge, Chukotka Peninsula, NE Russia. *Lithos* **79**: 251-269. doi: 10.1016/j.lithos.2004.04.056
- Lundgaard KL, Tegner C (2004) Partitioning of ferric and ferrous iron between plagioclase and silicate melt. *Contributions to Mineralogy and Petrology* **147**: 470-483
- Lundstrom CC, Shaw HF, Ryerson FJ, Williams Q, Gill J (1998) Crystal chemical control of clinopyroxene-melt partitioning in the Di-Ab-An system: Implications for elemental fractionations in the depleted mantle. *Geochimica et Cosmochimica Acta* **62-16**: 2,849-2,862. doi: 10.1016/S0016-7037(98)00197-5
- Macdonald KC, Fox PJ, Perram LJ, Eisen MF, Haymon RM, Miller SP, Carbotte SM, Cormier MH, Shor AN, (1988) A new view of the mid-ocean ridge from the behaviour of ridge-axis discontinuities. *Nature* **335-6,187**: 217-225
- MacLeod CJ, Rothery DA (1992) Ridge axial segmentation in the Oman ophiolite: Evidence from along-strike variations in the sheeted dyke complex. In *Ophiolites and Their Modern Analogues*, edited by Parson LM, Murton BJ, Browning P, *Geol. Soc. Spec. Publ.* **60**: 39-63. doi: 10.1144/GSL.SP.1992.060.01.03
- MacLeod CJ, Yaouancq G (2000) A fossil melt lens in the Oman ophiolite: Implications for magma chamber processes at fast spreading ridges. *Earth and Planetary Science Letters* **176**: 357-373. doi: 10.1016/S0012-821X(00)00020-0
- Malpas J (1979) Two contrasting trondhjemite associations from transported ophiolites in Western Newfoundland: Initial report. In: *Barker F (ed) Trondhjemites, dacites, and related rocks*. Elsevier, Amsterdam 465-487
- Manning CE, MacLeod CJ (1996) Fracture-controlled metamorphism of Hess Deep gabbros, Site 894: Constraints on the roots of mid-ocean-ridge hydrothermal systems at fast-spreading centers. In *Mével C, Gillis KM, Allan JF, Meyer PS (eds.), Proceedings of the Ocean Drilling Program, Scientific Results* **147**: 189-212
- Manning CE, Weston PE, Mahon KI (1996) Rapid high-temperature metamorphism of East Pacific Rise gabbros from Hess Deep. *Earth and Planetary Science Letters* **144**: 123-132
- Ménot RP (1987) Magmatismes paléozoïques et structuration carbonifère du massif de Belledonne, Alpes françaises. Contraintes nouvelles pour les schémas d'évolution de la chaîne varisque ouest-européenne. *PhD dissertation, University Lyon I, France*
- Merlet C (1994) An accurate computer correction program for quantitative electron probe microanalysis. *Mikrochimica Acta* **114-115**: 363-376. doi: 10.1007/BF01244563
- Mével C (1987) Evolution of oceanic gabbros from DSDP Leg 82: influence of the fluid phase on metamorphic crystallizations. *Earth and Planetary Science Letters* **83**: 67-79
- Mével C (1988) Metamorphism in ocean layer 3, Gorringer Bank, Eastern Atlantic. *Contributions to Mineralogy and Petrology* **100**: 496-509
- Mével C (2003) Serpentinization of abyssal peridotites at mid-ocean ridges. *C.R. Geosciences* **335**: 825-852

## References

- Michael PJ, Cornell WC (1998) Influence of spreading rate and magma supply on crystallization and assimilation beneath mid-ocean ridges: Evidence from chlorine and major element chemistry of mid-ocean ridge basalts. *Journal of Geophysical Research* **103**: 18,325-18,356
- Michael PJ, Schilling JG (1989) Chlorine in mid-ocean ridge magmas: evidence for assimilation of seawater-influenced components. *Geochimica et Cosmochimica Acta* **53**: 3,131-3,143
- Miyashiro A (1974) Volcanic rock series in island arcs and active continental margins. *American Journal of Science* **274**: 321-355
- Miyashita S, Adachi Y, Umino S (2003) Along-axis magmatic system in the northern Oman ophiolite: Implications of compositional variation of the sheeted dike complex. *Geochemistry Geophysics Geosystems* **4-9**: 8,617. doi: 10.1029/2001GC000235
- Morton JL, Sleep NH (1985) Seismic reflections from a Lau basin magma chamber. In: Scholl DW, Vallier TL (Editors), *Geology and offshore resources of Pacific island arcs-Tonga region. Circum-Pacific Council for Energy and Mineral Resources, Earth Science Series, Houston, Texas* 441-453
- Mutter JC, Carton H, Carbotte SM, Canales JP, Nedimovic MR, Newman KR, Marjanovic M, Xu M, Aghaei O, Stowe LC (2008) Searching for Changes in AMC Characteristics on the EPR Using Comparisons of Reflection Images Obtained in 1985 and 2008. *Eos Trans. AGU, Fall Meet. Suppl.* **89-53**: B21A-0319
- Natland JH, Dick HJB (1996) Melt migration through high-level gabbroic cumulates of the East Pacific Rise at Hess Deep: The origin of magma lenses and the deep crustal structure of fast-spreading ridges. In Mével C, Gillis KM, Allan JF, Meyer PS (Eds.), *Proc. ODP, Sci. Results, College Station, TX (Ocean Drilling Program)* **147**: 21-58. doi: 10.2973/odp.proc.sr.147.002.1996
- Nedimovic MR, Carbotte SM, Harding AJ, Detrick RS, Canales JP, Diebold JB, Kent GM, Tischer M, Babcock JM (2005) Frozen magma lenses below the oceanic crust. *Nature* **436**: 1,149-1,152
- Nicolas A. (1989) Structures of Ophiolites and Dynamics of Oceanic Lithosphere. *Kluwer, Boston* 367 pp.
- Nicolas A, Boudier F (1991) Rooting of the sheeted dike complex in the Oman ophiolite. In *Ophiolite Genesis and Evolution of the Oceanic Lithosphere*, edited by Peters T, Nicolas A, Coleman RG, *Kluwer Acad., Dordrecht, Netherlands* 39-54
- Nicolas A, Boudier F (1995) Mapping oceanic ridge segments in the Oman ophiolite. *Journal of Geophysical Research* **100-B4**: 6,179-6,197
- Nicolas A, Boudier F (2008) Large shear zones with no relative displacement. *Terra Nova* **20**: 200-205. doi: 10.1111/j.1365-3121.2008.00806.x
- Nicolas A, Mainprice D (2005) Burst of high-temperature seawater injection throughout accreting oceanic crust: A case study in Oman ophiolite. *Terra Nova* **17**: 326-330. doi: 10.1111/j.1365-3121.2005.00617.x
- Nicolas A, Ceuleneer G, Boudier F, Misseri M (1988a) Structural mapping in the Oman ophiolites: mantle diapirism along an oceanic ridge. *Tectonophysics* **151**: 27-56. doi: 10.1016/0040-1951(88)90239-9
- Nicolas A, Reuber I, Benn K (1988b) A new magma chamber model based on structural studies in the Oman ophiolite. *Tectonophysics* **151**: 87-105. doi:10.1016/0040-1951(88)90242-9
- Nicolas A, Boudier F, Ildefonse B, Ball E (2000) Accretion of Oman and United Arab Emirates ophiolite: Discussion of a new structural map. *Marine Geophysical Research* **21**: 147-179. doi: 10.1023/A:1026769727917
- Nicolas A, Mainprice D, Boudier F (2003) High-temperature seawater circulation throughout crust of oceanic ridges: A model derived from the Oman ophiolites. *Journal of Geophysical Research* **108-B8**: 2,371. doi: 10.1029/2002JB002094
- Nicolas A, Boudier F, Koepke J, France L, Ildefonse B, Mevel C (2008) Root zone of the sheeted dike complex in the Oman ophiolite. *Geochemistry Geophysics Geosystems* **9**: Q05001. doi: 10.1029/2007GC001918
- Nicolas A, Boudier F, France L (2009) Subsidence in magma chamber and the development of magmatic foliation in Oman ophiolite gabbros. *Earth and Planetary Science Letters* **284**: 76-87. doi: 10.1016/j.epsl.2009.04.012
- Niu Y, Gilmore T, Mackie S, Greig A, Bach W (2002) Mineral chemistry, whole-rock compositions, and petrogenesis of Leg 176 gabbros: data and discussion. In: Natland JH, Dick HJB, Miller DJ, Von Herzen RP (eds) *Proc ODP, Sci Results, Ocean Drilling Program, College Station, TX*, **176**: 1-60, [Online]

[http://www-odp.tamu.edu/publications/176\\_SR/VOLUME/CHAPTERS/SR176\\_08.PDF](http://www-odp.tamu.edu/publications/176_SR/VOLUME/CHAPTERS/SR176_08.PDF) [Cited 23-08-2003]

- Pallister JS, Hopson CA (1981) Samail Ophiolite Plutonic Suite: Field relations, phase variation, cryptic variation and layering, and a model of a spreading ridge magma chamber. *Journal of Geophysical Research* **86-B4**: 2,593-2,644. doi:10.1029/JB086iB04p02593
- Pallister JS, Knight RJ (1981) Rare-Earth Element Geochemistry of the Samail Ophiolite near Ibra, Oman. *Journal of Geophysical Research* **86-B4**: 2,673-2,697
- Pearce JA, Lippard SJ, Roberts S (1984) Characteristics and tectonic significance of supra-subduction zone ophiolites. In Kokelaar BP, Howells MF, eds. *Marginal basin geology: volcanic and associated sedimentary and tectonic processes in modern and ancient marginal basins*. Geol. Soc. Lond. Spec. Publ. **16**: 77-94
- Pearce NJG, Perkins WT, Westgate JA, Gorton MP, Jackson SE, Neal CR, Chenery SP (1997) A compilation of new and published major and trace element data for NIST SRM 610 and NIST SRM 612 glass reference materials. *Geostandard Newsletter* **21**: 115-144
- Patino Douce AE, Beard JS (1995) Dehydration-melting of biotite gneiss and quartz amphibolite from 3 to 15 kbar. *Journal of Petrology* **36**: 707-738
- Pedersen RB, Malpas J (1984) The origin of oceanic plagiogranites from the Karmoy ophiolite, Western Norway. *Contributions to Mineralogy and Petrology* **88**: 36-52
- Philpotts AR (1982) Compositions of immiscible liquids in volcanic rocks. *Contributions to Mineralogy and Petrology* **80**: 201-218
- Phipps Morgan J, Chen YJ (1993) The genesis of oceanic crust: Magma injection, hydrothermal circulation, and crustal flow. *Journal of Geophysical Research* **98**: 6,283-6,297
- Pollock ME, Klein EM, Karson JA, Coleman DS (2009) Compositions of dikes and lavas from the Pito Deep Rift: Implications for crustal accretion at superfast spreading centers. *Journal of Geophysical Research* **114**: B03,207. doi: 10.1029/2007JB005436
- Pouchou JL, Pichoir F (1991) Quantitative analysis of homogeneous or stratified microvolumes applying the model "PAP". In: Heinrich KFJ, Newbury DE (eds) *Electron probe quantification*. Plenum Press, New York 31-75
- Proureau G, Scaillet B, Pichavant M, Maury RC (1999) Fluid-present melting of ocean crust in subduction zones. *Geology* **27-12**: 1,111-1,114
- Purdy GM, Kong LSL, Christeson GL, Salomon SC (1992) Relationship between spreading rate and the seismic structure of mid-ocean ridges. *Nature* **355**: 815-817. doi: 10.1038/355815a0
- Quick JE, Denlinger RP (1993) Ductile deformation and the origin of layered gabbro in ophiolites. *Journal of Geophysical Research* **98**: 14,015-14,027
- Raitt RW (1963) The crystal rocks. In *The Sea*, edited by Hill MN, Wiley Interscience, New York **3**: 85-102
- Rannou E, Caroff M, Cordier C (2006) A geochemical approach to model periodically replenished magma chambers: Does oscillatory supply account for the magmatic evolution of EPR 17-19°S? *Geochimica et Cosmochimica Acta* **70**: 4,783-4,796. doi: 10.1016/j.gca.2006.07.007
- Rao DR, Rai H, Kumar JS (2004) Origin of oceanic plagiogranite in the Nidar ophiolitic sequence of eastern Ladakh, India. *Current Science* **87-7**: 999-1,005
- Rapp RP, Watson EB (1995) Dehydration melting of metabasalt at 8–32 kbar: implications for continental growth and crust-mantle recycling. *Journal of Petrology* **36**: 891-931
- Rapp RP, Watson EB, Miller CF (1991) Partial melting of amphibolite/eclogite and the origin of Archean trondhjemites and tonalites. *Precambrian Research* **51**: 1-25
- Reed WP (1992) Certificate of analysis, standard reference materials 610 611. (*National Institute of Standard and Technology*)
- Rochette P, Jenatton L, Dupuy C, Boudier F, Reuber I (1991) Diabase dikes emplacement in the Oman ophiolite: A magnetic fabric study with reference to geochemistry. In: *Ophiolite Genesis and Evolution of the Oceanic Lithosphere*, edited by Peters T, Nicolas A, Coleman RG, Kluwer Acad., Dordrecht, Netherlands 39-54

## References

- Roeder PL, Emslie RF (1970) Olivine–liquid equilibrium. *Contributions to Mineralogy and Petrology* **29**: 275-289
- Rollinson H (2009) New models for the genesis of plagiogranites in the Oman Ophiolite. *Lithos* **112**: 603-614. doi: 10.1016/j.lithos.2009.06.006
- Rothery DA (1983) The base of a sheeted dyke complex, Oman ophiolite: Implications for magma chambers at oceanic spreading axes. *Journal of the Geological Society, London* **140**: 287-296. doi: 10.1144/gsjgs.140.2.0287
- Rubin KH, Sinton JM (2007) Inferences on mid-ocean ridge thermal and magmatic structure from MORB compositions. *Earth and Planetary Science Letters* **260**: 257-276. doi: 10.1016/j.epsl.2007.05.035
- Rubin KH, Van des Zander I, Smith MC, Bergmanis EC (2005) Minimum speed limit for ocean ridge magmatism from  $^{210}\text{Pb}$ - $^{226}\text{Ra}$ - $^{230}\text{Th}$  disequilibria. *Nature* **437**. doi: 10.1038/nature03993
- Rushmer T (1991) Partial melting of two amphibolites: contrasting experimental results under fluid-absent conditions. *Contributions to Mineralogy and Petrology* **107**: 41-59
- Rushmer T (1993) Experimental high-pressure granulites: some applications to natural mafic xenolith suites and Archean granulite terranes. *Geology* **21**: 411-414
- Sato H (1978) Segregation vesicles and immiscible liquid droplets in ocean-floor basalt of Hole 396B, IPOD/DSDP Leg 46. In: Dimitriev L, Heirtzler J, et al (eds) *Initial reports of the Deep Sea Drilling Project, U.S. Government Printing Office, Washington* **46**: 283-291
- Sauerzapf U, Lattard D, Burchard M, Engelmann R (2008) The titanomagnetite-ilmenite equilibrium: New experimental data and thermo-oxybarometric application to the crystallization of basic to intermediate rocks. *Journal of Petrology* **49-6**: 1,161-1,185. doi:10.1093/petrology/egn021
- Scaillet B, Pichavant M, Roux J, Humbert G, Lefèvre A (1992) Improvements of the Shaw membrane technique for measurement and control of  $f\text{H}_2$  at high temperatures and pressures. *American Mineralogist* **77**: 647-655
- Selbekk RS, Furnes H, Pedersen RB, Skjerlie KP (1998) Contrasting tonalite genesis in the Lyngen magmatic complex, north Norwegian Caledonides. *Lithos* **42**: 243-268
- Sen C, Dunn T (1994) Dehydration melting of a basaltic composition amphibolite at 1.5 and 2.0 GPa: implications for the origin of adakites. *Contributions to Mineralogy and Petrology* **117**: 394-409
- Shastry A, Srivastava RK, Chandra R, Jenner GA (2001) Fe-Ti enriched mafic rocks from South Andaman ophiolite suite: implications of late stage liquid immiscibility. *Current Science* **80**: 453-454
- Shervais JW (1982) Ti-V plots and the petrogenesis of modern and ophiolitic lavas. *Earth and Planetary Science Letters* **59**: 101-118
- Shimizu N, Hart SR (1982) Application of the ion microprobe to geochemistry and cosmochemistry. *Annual Review of Earth and Planetary Sciences* **10**: 483-526
- Shor GG, Menard HW, Raitt RW (1970) Structure of the Pacific Basin. In *The Sea, edited by Maxwell AE, Wiley Interscience, New York* **4**: 3-27
- Singh SC, Kent GM, Collier JS, Harding AJ, Orcutt JA (1998) Melt to mush variations in crustal magma properties along the ridge crest at the southern East Pacific Rise. *Nature* **394-6696**: 874-878
- Singh SC, Harding AJ, Kent GM, Sinha MC, Combier V, Bazin S, Tong CH, Barton PJ, Hobbs RW, White RS, Orcutt JA (2006) Seismic reflection images of the Moho underlying melt sills at the East Pacific Rise. *Nature* **442**: 287-290
- Sinton JM, Detrick RS (1992) Mid-ocean ridge magma chambers. *Journal of Geophysical Research* **97**: 197-216. doi:10.1029/91JB02508
- Sinton JM, Smaglik SM, Mahoney JJ, Macdonald KC (1991) Magmatic processes at superfast spreading oceanic ridges: Glass compositional variations along the East Pacific Rise, 13°-23°S. *Journal of Geophysical Research* **96**: 6,133-6,155
- Sinton JM, Bergmanis E, Rubin KH, Batiza R, Gregg TKP, Grönvold K, Macdonald KC, White SM (2002) Volcanic eruptions on mid-ocean ridges: New evidence from the superfast spreading East Pacific Rise, 17°-19°S. *Journal of Geophysical Research* **107-B6**: 2,115. doi: 10.1029/2000JB000090



- Sleep NH (1975) Formation of oceanic crust: some thermal constraints, *Journal of Geophysical Research* **80-29**: 4,037-4,042. doi: 10.1029/JB080i029p04037
- Smewing JD (1981) Mixing Characteristics and Compositional Differences in Mantle-Derived Melts Beneath Spreading Axes: Evidence From Cyclically Layered Rocks in the Ophiolite of North Oman. *Journal of Geophysical Research* **86-B4**: 2,645-2,659
- Snyder D, Carmichael ISE, Wiebe RA (1993) Experimental study of liquid evolution in an Fe-rich, layered mafic intrusion: constraints of Fe-Ti oxide precipitation on the T-fO<sub>2</sub> and T-ρ paths of tholeiitic magmas. *Contributions to Mineralogy and Petrology* **113**: 73-86. doi: 10.1007/BF00320832
- Solomon SC, Toomey DR (1992) The structure of mid-ocean ridges. *Annual Review of Earth and Planetary Sciences* **20**: 329-364. doi: 10.1146/annurev.earth.20.050192.001553
- Soule SA, Fornari DJ, Perfit MR, Ridley WI, Reed MH, Cann JR (2006) Incorporation of seawater into mid-ocean ridge lava flows during emplacement. *Earth and Planetary Science Letters* **252**: 289-307
- Soule SA, Fornari DJ, Perfit MR, Rubin KH (2007) New insights into mid-ocean ridge volcanic processes from the 2005–2006 eruption of the East Pacific Rise, 9°46'N-9°56'N. *Geology* **35-12**: 1,079-1,082
- Spear FS, Markussen JC (1997) Mineral Zoning, P-T-X-M Phase Relations, and Metamorphic Evolution of some Adirondack Granulites, New York. *Journal of Petrology*. **38-6**: 757-783. doi: 10.1093/ptro/38.6.757
- Spray JG, Dunning GR (1991) A U/Pb age for the Shetland Islands oceanic fragment, Scottish Caledonides: evidence from anatectic plagiogranites in 'layer 3' shear zones. *Geological Magazine* **128**: 667-671
- Stakes DS, Taylor HP (2003) Magmatic, Metamorphic and Tectonic Processes in Ophiolite Genesis: Oxygen isotope and chemical studies on the origin of large plagiogranite bodies in northern Oman, and their relationship to the overlying massive sulphide deposits. *Geological Society, London, Special Publications* **218**: 315-351. doi: 10.1144/GSL.SP.2003.218.01.17
- Steinbeck J (1961) High Drama to Bold Thrust through Ocean Floor. Earth second layer is tapped in prelude to Mohole. *Life April*: 111-122
- Stolper E (1980) A phase diagram for mid-ocean ridge basalts: preliminary results and implications for petrogenesis. *Contributions to Mineralogy and Petrology* **74**, 13-27
- Teagle DAH, Alt JC, Umino S, Miyashita S, Banerjee NR, Wilson DS, and the Expedition 309/312 Scientists (2006) Superfast Spreading Rate Crust 2 and 3. *Proceedings of the Integrated Ocean Drilling Program* **309/312**. doi:10.2204/iodp.proc.309312.2006
- Thy P, Leshner CE, Mayfield JD (1999) Low-pressure melting studies of basalt and basaltic andesite from the southeast Greenland continental margin and the origin of dacites at site 917. In: *Larsen HC, Duncan RA, Allan JF, Brooks K (eds) Proceedings of the ODP, Science Research, Ocean Drilling Program, College Station* **163**: 95-112
- Tolstoy M, Waldhauser F, Bohnenstiehl DR, Weekly RT, Kim WY (2008) Seismic identification of along-axis hydrothermal flow on the East Pacific Rise. *Nature* **451**: 191-184. doi: 10.1038/nature06424
- Toomey DR, Purdy GM, Solomon SC (1989) Three-dimensional structure of the East Pacific Rise at 9°30'N. *Eos Trans. AGU* **70**: 1,317
- Toplis MJ (2005) The thermodynamics of iron and magnesium partitioning between olivine and liquid: criteria for assessing and predicting equilibrium in natural and experimental systems. *Contributions to Mineralogy and Petrology* **149**: 22-39
- Toplis MJ, Carroll MR (1995) An Experimental Study of the Influence of Oxygen Fugacity on Fe-Ti Oxide Stability, Phase Relations, and Mineral-Melt Equilibria in Ferro-Basaltic Systems. *Journal of Petrology* **36-5**: 1,137-1,170
- Toplis MJ, Libourel G, Carroll MR (1994) The role of phosphorus in crystallisation processes of basalt: An experimental study. *Geochimica et Cosmochimica Acta* **58-2**: 797-810. doi: 10.1016/0016-7037(94)90506-1
- Twinning K (1996) Origin of plagiogranites in the Troodos ophiolite, Cyprus. *The Ninth Keck Research Symposium in Geology* 245-248

## References

- Ulrich T, Borsien GR (1996) Fedoz metagabbros and Forno metabasalt (Val Malenco, N Italy): comparative petrographic and geochemical investigations. *Schweiz Miner Petrogr Mitt* **76**: 521-535
- Umino S, Miyashita S, Hotta F, Adachi Y (2003) Along-strike variation of the sheeted dike complex in the Oman Ophiolite: Insights into subaxial ridge segment structures and the magma plumbing system. *Geochemistry Geophysics Geosystems* **4-9**: 8,618. doi: 10.1029/2001GC000233
- VanTongeren JA, Kelemen PB, Hanghoj K (2008) Cooling rates in the lower crust of the Oman ophiolite: Ca in olivine, revisited. *Earth and Planetary Science Letters* **267-1-2**: 69-82. doi: 10.1016/j.epsl.2007.11.034
- Waldhauser F, Ellsworth WL (2000) A double-difference earthquake location algorithm: Method and application to the Northern Hayward Fault, California. *Bull. Seism. Soc. Am.* **90**: 1,353-1,368
- Warren CJ, Parrish RR, Waters DJ, Searle MP (2005) Dating the geologic history of Oman's Semail Ophiolite: insights from U–Pb geochronology. *Contributions to Mineralogy and Petrology* **150**: 403-422
- Warren CJ, Searle MP, Parrish RR, Waters DJ (2007) Reply to Comment by F. Boudier and A. Nicolas on “Dating the geologic history of Oman's Semail Ophiolite: insights from U–Pb geochronology” by C.J. Warren, R.R. Parrish, M.P. Searle and D.J. Waters. *Contributions to Mineralogy and Petrology* **154**: 115-118
- Webb SC (2008) Is There a Deep Hydrothermal Circulation at the EPR? *Eos Trans. AGU, Fall Meet. Suppl.* **89-53**: B21A-0327
- Wilke M, Behrens H (1999) The dependence of the partitioning of iron and europium between plagioclase and hydrous tonalitic melt on oxygen fugacity. *Contributions to Mineralogy and Petrology* **137**: 102-114
- Wilson DS, Teagle DAH, Alt JC, Banerjee NR, Umino S, Miyashita S, Acton GD, Anma R, Barr SR, Belghoul A, Carlut J, Christie DM, Coggon RM, Cooper KM, Cordier C, Crispini L, Durand SR, Einaudi F, Galli L, Gao Y, Geldmacher J, Gilbert LA, Hayman NW, Herrero-Bervera E, Hirano N, Holter S, Ingle S, Jiang S, Kalberkamp U, Kerneklian M, Koepke J, Laverne C, Vasquez HLL, Maclennan J, Morgan S, Neo N, Nichols HJ, Park SH, Reichow MK, Sakuyama T, Sano T, Sandwell R, Scheibner B, Smith-Duque CE, Swift SA, Tartarotti P, Tikku AA, Tominaga M, Veloso EA, Yamasaki T, Yamazaki S, Ziegler C (2006) Drilling to gabbro in intact ocean crust. *Science* **312**: 1,016-1,020. doi: 10.1126/science.1126090
- Wolf MB, Wyllie PJ (1994) Dehydration-melting of amphibolite at 10 kbar: the effects of temperature and time. *Contributions to Mineralogy and Petrology* **115**: 369-383
- Yamasaki T, Maeda J, Mizuta T (2006) Geochemical evidence in clinopyroxenes from gabbroic sequence for two distinct magmatisms in the Oman ophiolite. *Earth and Planetary Science Letters* **251**: 52-65. doi: 10.1016/j.epsl.2006.08.027